The role of clusterin in the amyloid cascade in human IPSC-derived neurons

Robbins, Jacqueline

Awarding institution:
King's College London

THE ROLE OF CLUSTERIN IN THE AMYLOID CASCADE IN HUMAN iPSC-DERIVED NEURONS

Thesis submitted for the degree of Doctor of Philosophy

Jacqueline Robbins

King's College London

2016

Abstract

Our understanding of the molecular processes underlying Alzheimer's disease (AD) is still limited, hindering the development of effective treatments and highlighting the need for human-specific models. The potential for human induced pluripotent stem cells (iPSCs) to provide a model for AD is an exciting advancement, and has great potential for investigating the mechanisms involved in neurodegeneration. Advances in identifying components of the amyloid cascade are progressing, including the role of the protein clusterin in mediating β-amyloid (Aβ) toxicity. Mutations in CLU and APOE, major genetic AD risk factors, are known to have important roles in Aβ processing. This thesis aims to characterise the molecular cascade initiated by Aβ previously identified in rodent neurons. Aβ-mediated toxicity will be studied in cortical neurons differentiated from wild type iPSCs and a clusterin-knockout cell line generated by precise genome editing. This thesis also presents the process of developing an APOE mutant iPSC line.

iPSCs from a healthy male with an APOE ε3/ε3 genotype were differentiated into cortical neurons and treated with $A\beta_{25-35}$ peptides and $A\beta_{1-42}$ oligomers. The downstream effects of Aβ exposure were measured using an automated imaging assay, optimised to identify changes in neuronal morphology. Western blotting and qPCR were used to assess changes in protein and gene expression. CRISPR/Cas9-mediated gene editing generated a CLU-knockout iPSC line. The morphological and transcriptomic effects of the CLU deletion were then investigated in differentiated neurons.

In wildtype cells imaging indicated that neuronal processes degenerate following Aβ treatment, in a dose dependent manner, and that intracellular levels of clusterin are increased following Aβ treatment, as occurs in rodent neurons. However, in CLU knockout neurons these morphological effects of Aβ neurotoxicity were absent, suggesting that clusterin is an important component of the amyloid cascade. Transcriptomic data from RNAseq were analysed to elucidate the pathways responsible for the altered response to Aβ in CLU knockout neurons.

An iPSC based isogenic model of AD has been established with different alleles of known risk genes. Determining the role of specific risk alleles on established measures of Aβ-neurotoxicity using a high throughput assay will be of great value to obtaining a better understanding of the underlying disease mechanisms and for the evaluation of compounds able to modulate these pathways.

Acknowledgements

Thesis acknowledgements can sometimes sound like the student is grateful to simply have survived the ordeal that the last few years was for them, so I would like to start by thanking my supervisors for making my PhD such a great experience. Jack Price, Simon Lovestone and Mene Pangalos created an interesting and exciting project, encouraged me to use innovative techniques and gave me excellent advice throughout my PhD. I've genuinely enjoyed every day of it – thank you for helping me grow into a good scientist.

I've also been lucky enough to work in multiple fantastic institutes. Jack's lab has been an ideal environment and the depth of knowledge contained within the group has been invaluable, so thanks to the whole team especially Leo Perfect, Graham Cocks, Aaron Jeffries, Paulina Nowosiad, Rosy D'Oyly Watkins and Matt Reid. Leo deserves special mention for his RNAseq wizardry and for teaching me so much about how to be a good researcher. The CBU at King's is the best environment I could have wished for, with so many intelligent, enthusiastic people with great ideas and I'd particularly like to thank Christos Michaelides, Tytus Murphy and Helen Brooks for their advice in the lab and even more importantly their galvanising friendships. Richard Killick at King's was fundamental to the project design and an inspiring scientist to work with. My time at AstraZeneca was a brilliant learning experience and hugely beneficial to my project. I couldn't have done any of this work without Marcello Maresca, Mohammad Bohlooly and Anders Lundin, who were incredible to work with and I miss immensely. During my time at Oxford many people have been very generous with their time: thanks to Daniel Ebner for welcoming me into the TDI and Elena Ribe and the whole of the Lovestone, Ebner and Cowley teams for their help. Mainly all of the people I've mentioned above made coming into the lab every day so much fun and I hope that I am able to work with everybody again in the future.

Lastly I'd like to thank Trevor Robbins, Barbara Sahakian, Miranda Robbins and Martin Ducker for always encouraging me, having all the answers and being the best support crew. Martin, you have always motivated me to be better both personally and professionally and your contagious enthusiasm and ambition is what brought me here today.

Table of Contents

Table of Figures

Table of Tables

Abbreviations

Aβ	Amyloid-beta
AD	Alzheimer's disease
APOE	Apolipoprotein E
APP	Amyloid precursor protein
AraC	Cytosine β-D-arabinofuranoside
BIN1	Bridging integrator 1
CAM	Calcein AM
cc3	Cleaved-caspase 3
CDK5	Cyclin-dependent kinase 5
ChAT	Choline acetyltransferase
CHO	Chinese hamster ovary
CR1	Complement receptor type 1
CRISPR	Clustered Regularly Interspaced Short Palindromic Repeats
CSF	Cerebral spinal fluid
DKK1	Dickkopf 1
DNA	Deoxyribonucleic acid
DS	Donkey serum
DSB	Double strand break
FACS	Fluorescence-activated cell sorting
fAD	Familial Alzheimer's disease
GSK3	Glycogen-synthase kinase 3
GWAS	Genome Wide Association Study
HDR	Homology directed repair
HEK	Human Embryonic Kidney
iPSCs	Induced pluripotent stem cells
JNK	c-Jun NH2-terminal kinase
LTD	Long term depression

LTP	Long term potentiation
MAPT	Microtubule-associated protein tau
MARK	Microtubule-associated regulatory kinase
NFT	Neurofibrillary tangle
NHEJ	Non-homologous end joining
PAM	Protospacer adjacent motif
PBMC	Peripheral blood mononuclear cell
PBS	Phosphate buffered saline
PCR	Polymerase chain reaction
PET	Positron Emission Tomography
PiB	Pittsburgh compound B
PICALM	Phosphatidylinositol-binding clathrin assembly protein
PSEN1	Presenilin 1
PSEN2	Presenilin 2
qPCR	Quantitative polymerase chain reaction
RNA	Ribonucleic acid
RT	Room temperature
sAD	Sporadic Alzheimer's disease
ssODN	Single-stranded oligodeoxynucleotide
TALEN	Transcriptor Activator-like Effector Nuclease
TBS	Tris-buffered saline
TPK1	Tau protein kinase 1
TREM2	triggering receptor expressed on myeloid cells 2
Wnt	Wingless-Int
ZFN	Zinc-Finger Nuclease

Chapter 1 Introduction

1.1 The pathogenesis of Alzheimer's disease

1.1.1 The burden of Alzheimer's disease

Alzheimer's disease (AD) is a neurodegenerative disorder characterised by steady cognitive decline, usually first noticed by memory impairment but later affecting all cognitive functions and eventually causing premature death (Mayeux & Stern, 2012). AD is the most common type of dementia, accounting for up to 80% of all cases and prevalence sharply increasing with age (Lobo et al., 2000). Dementia was estimated to affect 46.8 million people globally in 2015 with this number expected to double every 20 years, although the estimates have been rapidly increasing in recent reports. This enormous growth in prevalence is due to rapid population ageing, which is set to continue with numbers of older people forecast to increase by 56% in high income countries compared to 239% in low income countries. The cost of dementia is enormous due to the slow progression of the disease, and the families of patients must cover the majority of this cost. These projections will cripple global economies and are predicted to cost $1 trillion globally by 2018 (World Alzheimer Report, 2015). With these staggering statistics, dementia research and risk reduction is a serious global priority and new understanding about the disease is urgently needed. Improvements in the understanding and prevention of risk factors could help to curtail the AD epidemic, as is suggested by the drop in incidence in the UK over the last two decades (Matthews et al., 2016).

1.1.2 Molecular pathways in AD

Two major aims in the field of AD research today are the discovery of novel therapies based on understanding of molecular pathogenesis and the translation to clinic using improved clinical trials (Trojanowski et al., 2012). Alzheimer's disease is characterised by the presence of amyloid plaques and neurofibrillary tangles at autopsy. However, the debate as to which of these protein aggregations is the primary cause of the neurodegeneration is still intensely debated (Mann and Hardy, 2013). The most popular theory is the amyloid cascade hypothesis, stating that amyloid deposits are the earliest event and lead to the development of neurofibrillary tangles (Hardy and Allsop, 1991). Although we are starting to gain more insight into the specific mechanisms behind AD, developments have not been as fast as anticipated since the identification of β-amyloid (Aβ) in 1984.

1.1.3 Theories for AD pathogenesis

Amyloid cascade hypothesis

Since the 'amyloid cascade hypothesis' was proposed over 20 years ago by Hardy and Allsop (1991), a number of steps have been made in understanding the molecular pathogenesis of AD. The extracellular amyloid plaque and intracellular tau tangle pathologies that cause neuronal death were first described a century ago by Alois Alzheimer, and are still considered to be the most important factors in AD onset. The amyloid hypothesis proposes that accumulation of Aβ and/or a decrease in clearance of Aβ is the driving cause of a molecular cascade that results in tau phosphorylation and aggregation, neuronal dysfunction and cognitive symptoms that develop in patients with

AD. The amyloid pathology is caused by cleavage of the Amyloid Precursor Protein (APP) by α-secreatse, β-secretase and γ-secretase, as described in Figure 1, producing Aβ40 and Aβ42 fragments at the synapse. The 42 amino acid fragment is more prone to aggregation, resulting in oligomers and fibrils formation. Aggregates of insoluble Aβ form large amyloid plaques, however, the presence of amyloid-β-derived diffusible ligands and soluble toxic oligomers may be better correlated with symptoms (Haas and Selkoe, 2007; Karran et al., 2011).

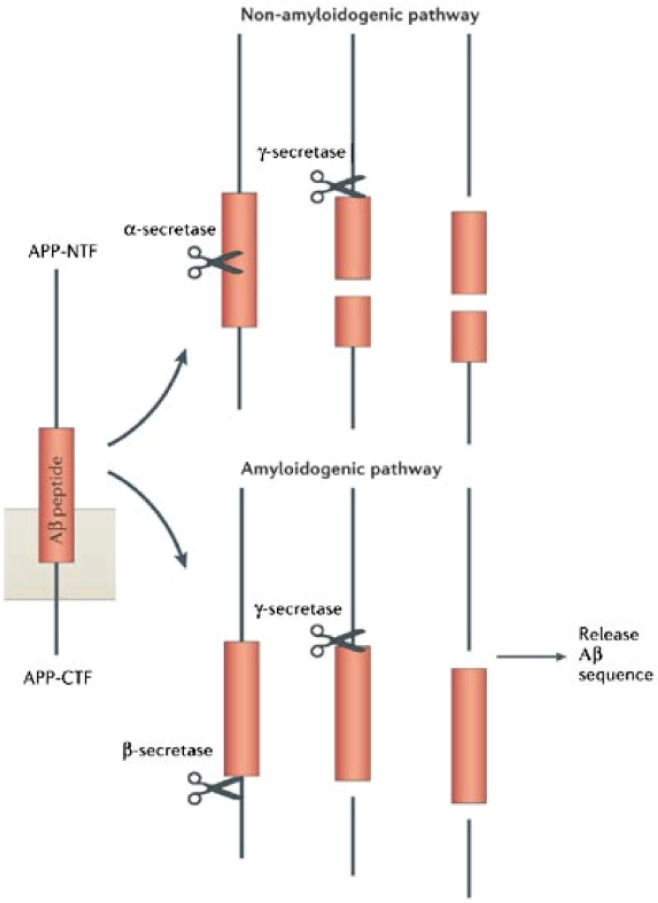

Figure 1. Amyloid precursor protein (APP) processing by several secretases. The non-amyloidogenic pathway involves cleavage by α- and γ-secretases and results in the release of several soluble APP fragments. The amyloidogenic pathway involves cleavage by β- and γ-secretases producing Aβ peptides. Diagram from Van Dam & De Deyn (2006).

The discovery of the autosomal dominant mutations in APP, presenilin 1 (PSEN1) and presenilin 2 (PSEN2), inspired the amyloid hypothesis (Kang et al., 1987; Sherrington et a., 1995). To date all known mutations that cause autosomal dominant AD increase the production or aggregation of amyloid. Protective mutations in the APP gene have also been discovered, such as the A673T coding mutation. This protects against AD and cognitive decline in elderly carriers and has also been found reduce the formation of amyloidogenic peptides by 40% in HEK293 cell cultures (Jonsson et al., 2012). Down's syndrome patients carry a third copy of chromosome 21, the chromosome with the APP gene, and have a high risk of developing Alzheimer's disease symptoms in adulthood, furthering support for APP disruption as the primary cause of AD (Gouras, 2001). Moreover, mutations in tau, although causing neurodegeneration, do not cause AD (Zahs and Ashe, 2013).

Tau hypothesis

The second key molecular feature of AD is the intracellular neurofibrillary tangles (NFTs) composed of abnormal accumulation of tau protein. These NFTs are large aggregates of tau that fill the cell body of the neuron, composed of paired helical filaments (twisted, double-helical ribbons) and straight filaments of protein (single, smaller abnormal filaments) (Crowther, 1991). The tau hypothesis for AD is supported by the finding that the number of neurofibrillary tangles in the cerebral cortex in histological studies of patients post mortem is associated with the severity of dementia (Wilcock and Esiri, 1982). Tau knockout models provide mechanistic support for the role of tau in AD, despite the phenotype being mild, as microtubule number and density appeared to be reduced in the cerebellum of MAPT−/− animals (Harada et al., 1994), and primary

hippocampal cultures from MAPT−/− mice show delayed maturation of hippocampal neurons (Dawson et al., 2001).

The phosphorylation of tau has been proposed as the major contributor to the protein aggregation. Glycogen synthase kinase 3 (GSK3), cyclin-dependent kinase 5 (Cdk5), c-Jun NH2-terminal kinase (JNK) and microtubule-associated regulatory kinase (MARK) have been identified as major tau kinases, and therefore their aberrant activity could be responsible for the tau dysfunction and downstream pathological events (Dolan and Johnson, 2010). The abnormal phosphorylation of microtubule-associated protein tau causes tau to dissociate from the microtubule, resulting in tau oligomerisation and tangle formation, which triggers the initiation of apoptotic processes in the cell (Gouras, 2001). In addition to phosphorylation, tau truncation could also cause pathogenic conformation changes in tau. Certain lengths of tau fragments have been found to have increased potential to aggregate, however the proteases that truncate tau are not yet known (Hanger and Wray, 2010).

Many researchers have favoured the tau hypothesis due to emerging findings that Aβ deposition is a nonspecific event, and therefore tau phosphorylation may be more closely tied with AD symptoms. In mature neurons tau is very important in axonal structure and transport through the regulation of microtubule stability. The microtubule assembling activity of tau is regulated by its degree of phosphorylation, and thereby tau in its hyperphosphorylated state (or after truncation) such as in Alzheimer's disease, polymerises into paired helical filaments admixed with straight filaments depressing the microtubule assembly promoting activity of tau (Iqbal et al., 2010). In addition to its role in microtubule dysfunction, tau has also been proposed to have a role in AD pathogenesis through stimulating the deleterious cycle leading to exacerbated neurodegeneration in the 'revitalised tau hypothesis' as proposed by Maccioni and colleagues (2010). Here,

damage signals including Aβ deposition, pathogenic iron overload and oxidative stress cause neurodegeneration and tau hyperphosphorylation. The dying neurons release the neurofibrillary tangles into the extracellular environment, activating microglia that produce proinflammatory cytokines, which cause damage to neurons. Moreover, the activation of microglia is also suggested to cause dysregulation of the tau kinases in turn, resulting in a neurotoxic positive feedback loop (Maccioni et al., 2010; Morales et al., 2010).

A pathological diagnosis of AD can be performed using the topographic staging of NFTs, starting in the entorhinal cortex and hippocampus then spreading to the associative isocortex (Braak and Braak, 1991; Braak et al., 1994). Tau propagation has recently been proposed from observations in AD models of tau being actively secreted and taken up by connected neurons, rather than an exclusively passive release of aggregated tau from dying neurons (Pooler et al., 2013). This phenomenon reaffirms the relevance of the tau hypothesis and offers novel therapeutic angles. Transgenic mice lines with mutant tau expressed in the medial entorhinal cortex (a region with early AD pathology) developed robust tau pathology in anatomically connected brain regions during aging in three independent studies (Harris et al., 2012; de Calignon et al., 2012; Liu et al., 2012).

Advances with Positron Emission Tomography (PET) imaging using the tau PET agent 18F-AV-1451 allow early stages of AD to be studied, and also differences in tau in PET scans of individuals with different amyloid plaque loads as measured by Pittsburgh compound B (PiB). Although high PiB PET can be found in cognitively normal older adults, levels of tau in the medial temporal lobe predicted episodic memory decline during aging (Schöll et al., 2016). This PET finding of tau associating with memory function in the cortex supports histology studies finding the extent of AD symptoms can be closely correlated with the anatomical extent and number of tangles in the cortex (Wilcock and Esiri, 1982; Ingelsson et al., 2004).

Cholinergic hypothesis

The cholinergic hypothesis stems from the observation that the degeneration of cholinergic neurons is an early hallmark of AD. In the 1970s AD investigations focused on finding an analogous cause and treatment for AD as had been established for Parkinson's disease with dopamine dysfunction. Neocortical deficits in the enzyme responsible for the synthesis of acetylcholine, choline acetyltransferase (ChAT), were discovered, along with reduced choline uptake and release (Francis et al., 1999). The development of acetylcholinesterase inhibitors were the first drug therapies with success in relieving AD symptoms (Bartus, 2000). Despite the cholinergic hypothesis no longer being considered sufficient to solely explain AD onset, treatments targeting the cholinergic system are the best options currently available for relief of symptoms and remain the only approved therapies (Bartus, 2000; Craig et al., 2011).

Alternative theories

A number of new theories have now been developed with recent advances in AD research. The major emerging theories include immune system dysfunction, vascular factors such as a compromised blood brain barrier, and dysregulated insulin metabolism (Armstrong, 2013). Evidence for immune system dysregulation comes from the activation of complement proteins, reactive microglia, and cytotoxic/suppressor T-cells as well as other signs of immune system dysfunction (McGeer et al., 1991). The relationships between microglial activation, complement activation and Aβ deposition are unclear but these processes may exacerbate one another. Moreover, TREM2 is an innate immune receptor expressed on the cell surface of microglia, macrophages, osteoclasts and

immature dendritic cells, recently identified to have rare variants with an associated AD risk similar to APOEε4 (Guerreriro et al., 2013; Jonsson et al., 2013).

The relationship between AD and comorbid diseases such as diabetes or cardiovascular diseases suggest insulin deficiency and insulin resistance, and vascular factors as important mediators of AD-type neurodegeneration (de la Monte and Wands, 2008). These different AD theories complement each other well due to their numerous shared molecular pathways, suggesting that the deconvolution of this heterogenous disease will require continued research into these genetic and environmental risk factors.

1.1.4 Evaluation of the theories for AD etiology

Single factor theories for the etiology of AD are now widely disregarded as research continues to reveal the complexity of this disease and there is evidence for the importance of many different pathogenic processes. Support for amyloid as an early causal factor remains strong, with many studies backing this as a leading pathogenic event (Gouras, 2001). Due to the complexity and heterogeneity of AD cases, multiple combinations of co-factors could provide a superior theory for AD. However, this still leaves space for an amyloid-initiated cascade hypothesis.

The major obstacle in verifying the amyloid cascade hypothesis is determining the linkage between this pathway initiated by amyloid and the cognitive and behavioural symptoms experienced by patients. Further research into the downstream events that lead to tau phosphorylation and neuronal death in AD models is needed to support the amyloid cascade hypothesis and develop effective therapeutics. The literature supporting an Aβ-driven neurotoxic pathway is broad and will be deconstructed in Chapter 1.2 by reviewing

the evidence from targeted experimentation on *in vivo* and *in vitro* systems, and then untargeted approaches that contribute to the pathway deconvolution.

1.2 Aβ-driven neurotoxic pathway

1.2.1 Aβ cascade

Evidence for an Aβ-driven cascade has been consolidated through studies in animals, cell models, post-mortem tissue, and more recently in large-scale genomic projects. This cascade is summarised in Figure 2. One of the major objections to the amyloid cascade hypothesis is the unsolved question of whether and how the deposition of Aβ leads to the formation of neurofibrillary tangles. The elucidation of the components of the cascade, including the events leading to tau accumulation, has been advanced through the studies discussed below.

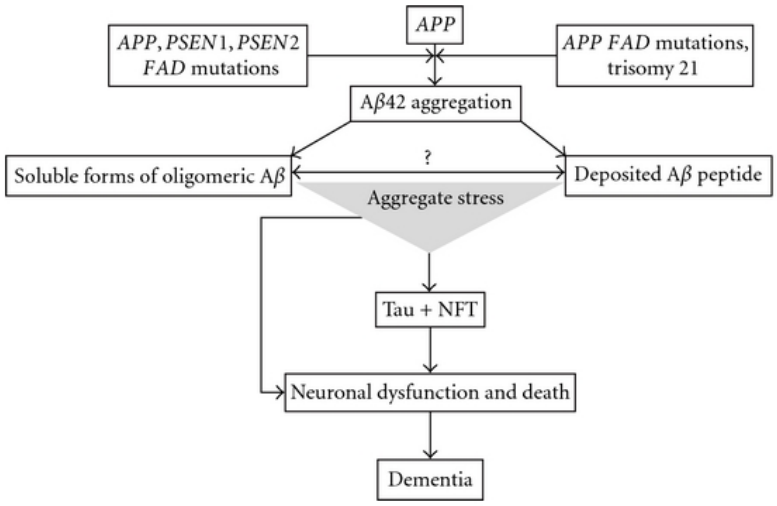

Figure 2. The amyloid cascade. This cascade is triggered by the misprocessing of APP and the accumulation of Aβ, and results in neurodegeneration and dementia symptoms (Reitz, 2012; with permission to reuse)

1.2.2 *In vivo* studies

The amyloid cascade hypothesis has been supported and disentangled by a number of important studies *in vivo*. The relationship between the plaque and tangle pathologies was first investigated in fAD cases. AD cases with PSEN1 mutations have been found, in addition to the established increased Aβ deposition, to have greater than 6-fold increase in tau-2-positive plaques than sporadic AD cases (Shepherd et al., 2004). Transgenic mouse models for AD have been incredibly useful for studying the link between Aβ and tau.

A variety of transgenic models have been employed, introducing human mutations of the APP and PSEN1 transgenes, or both. These models cause deposition of Aβ and neurodegeneration. The Tg2576 transgenic mouse model is a long established and favourite in AD *in vivo* research, with a double mutation in human APP, K670N and M671L (Swedish mutation). This mouse shows increased accumulation of Aβ and impairments in learning and memory by 10 months of age (Hsiao et al., 1996). Although there is no evidence of neurofibrillary tangles or neuronal loss (Irizarry et al., 1997), changes in synaptic plasticity are observed early with decreased long-term potentiation (LTP) by 5 months (Jacobsen et al., 2006).

Another commonly used model is the 3xTg mouse, a triple transgenic model of AD harbouring three mutant genes: beta-amyloid precursor protein (betaAPPSwe), presenilin-1 (PS1M146V), and MAPT-P301L (Oddo et al., 2003a). This mouse exhibits both Aβ and tau pathology regionally similar to AD, with Aβ deposits developing prior to tau positive lesions (Oddo et al., 2003b). Deficits in long-term synaptic plasticity, including LTP deficits, correlate with the accumulation of intraneuronal Aβ (Oddo et al., 2003a). Moreover, Aβ immunotherapy was found to reduce both extracellular and intracellular Aβ accumulations in 3xTg, and interestingly also lead to the clearance of early tau pathology, but not late hyperphosphorylated tau aggregates (Oddo et al., 2004). This

further supports the relationship between these two pathologies. Oddo and colleagues (2003a) also investigated the double-transgenic mouse (2×Tg) with PS1M146V and MAPT-P301L but lacking the human APP transgene. Notably, the 2×Tg mice do not develop any extracellular plaques or show LTP deficits. This highlights the importance of the role of APP in the AD pathogenesis.

In transgenic models the presence of an APP mutation, or in combination with PSEN1, can induce Aβ deposition. However, without the presence of tau transgenes in the form of a triple model there is no tau pathology necessary to replicate AD pathology. Further insights into the relationship between Aβ and tau have been provided by tau knockout transgenics, showing that animals lacking tau are protected from the synaptic and cognitive problems associated with Aβ overproduction.

Roberson and colleagues (2007) investigated the role of tau by reducing endogenous tau levels in mice with a double APP mutation (J20). Halving tau levels protected the neurons from dying prematurely and helped them resist the Aβ-induced cognitive impairment, whilst the Aβ levels remained unchanged. There is evidence for this neuroprotective effect acting through axonal transport (Vossel et al., 2010) spontaneous epileptiform activity (Roberson et al., 2011) and hippocampal long-term potentiation typically impaired by Aβ (Shipton et al., 2011), supporting the downstream role of tau in Aβ-mediated neurodegeneration.

1.2.3 *In vitro* studies

In vitro studies have been especially useful for complementing the *in vivo* work in studying Aβ toxicity and the downstream targets of Aβ. Simplistic *in vitro* models can be

used to model the effect of single factors in preventing or enhancing Aβ toxicity. Treating neuronal cultures with $A\beta_{1-42}$, the Aβ isoform most closely associated with AD pathogenesis (Yang et al., 1995), is a useful strategy for specifically investigating the consequence of the protein deposits and provides a general model for all AD, regardless of genetic background.

Busciglio and colleagues (1995) treated rat hippocampal and human cortical neuronal cultures with Aβ, Fibrillar forms of Aβ induced the phosphorylation of tau at Ser-202 and Ser-396/Ser-404, rendering it incapable of binding to microtubules. However, soluble Aβ and Aβ aggregates did not cause any change in tau phosphorylation. To determine the role of the tau kinase, tau protein kinase 1 (TPK1) in Aβ-toxicity, Takashima and colleagues (1993) treated rat hippocampal neurons with $A\beta_{25-35}$ or $A\beta_{1-43}$ and TPK1 induction was measured. Aβ treatment significantly increased TPK I activity, tau phosphorylation and neurotoxicity. Perez et al. (2004) also showed that cytotoxic $A\beta_{25-35}$ peptide could induce the aggregation of tau proteins. Interestingly, a tau peptide reduced Aβ aggregation in this in vitro model. Hence, aggregation of tau may be associated with disassembly of Aβ, which may help to explain how the relationship between Aβ and tau causes a lack of co-localisation between the pathologies in AD. Rapoport et al (2002) investigated the effect of fibrillar Aβ in tau-depleted hippocampal cultures. These cultures did not degenerate in the presence of fibrillar Aβ in contrast to wildtype neurons. These complementary studies confirm Aβ is neurotoxic and can induce changes in tau protein that may lead to the formation of NFTs and neurodegeneration. This demonstrates a mechanistic link between the Aβ and tau pathologies.

1.2.4 Genetic, transcriptomic, and proteomic studies of AD

In addition to the *in vivo* work using transgenics based on the early-onset genetic variants, genes identified from genetic studies in late-onset AD provide support for the amyloid cascade hypothesis. The apolipoprotein E (APOE) gene, which was identified as the first susceptibility gene for late-onset AD, is the major genetic risk factor (Corder et al., 1993). APOE is known to have a functional role in Aβ deposition and fibrillisation (Holtzman et al., 2000). Recent large-scale genome-wide association studies (GWAS) in European cohorts detected genetic variants associated with AD in 11 genes: complement component (3b/4b) receptor 1 (CR1), clusterin (CLU), bridging integrator 1 (BIN1), phosphatidylinositol-binding clathrin assembly protein (PICALM), ABCA7, CD33, CD2AP, EPHA1 and MS4A6A-MS4A4E (Harold et al., 2009; Lambert et al., 2009; Hollingworth et al., 2011). A meta-analysis study of the GWAS studies, comprising a total of 17008 AD cases and 37154 controls, identified 5 newly associated AD loci in addition to the previously established genes: HLA-DRB5–HLA-DRB1, PTK2B, SORL1, SLC24A4-RIN3 and DSG2 (Lambert et al., 2013). Whole genome sequencing approaches have resulted in the identification of AD risk mutations, such as the TREM2 variant R47H. This mutation was discovered to have an AD risk odds ratio of 2.92 in an Icelandic population of 2261, and was confirmed to have an sporadic AD (sAD) association through a meta analysis (Jonsson et al., 2013; Guerreiro et al., 2013).

Despite more functional experimentation being needed on these genes, CR1, CLU, BIN1 and PICALM are all known to have a function in Aβ processing in AD, supporting the amyloid cascade hypothesis (Reitz et al., 2012). More recently, gene expression profiling has been used to identify the downstream effects of pathogenic AD mutations. For example, Beglopoulos et al. (2004) used microarray in PSEN1 knockout mice and found upregulation of inflammatory pathways, including increased complement component C1q in the hippocampus. In human tissue, Colangelo et al. (2002) microarrayed hippocampal

CA1 regions from six individuals with sAD and found increased expression of the APP gene along with increases in pro-apoptotic and pro-inflammatory genes. These studies support Aβ as a central player in AD pathogenesis and reveal genes that may be important in mediating the deposition of Aβ and NFTs. It is now important to determine the specific role that dysregulation of these genes plays in the development and progression of AD in order to develop relevant targets for therapeutic strategies.

1.2.5 Downstream Aβ targets

The *in vivo*, *in vitro* and genetic research supports the pathway linking Aβ and tau as an important part of the neurotoxic cascade. Our understanding of the molecular basis for the amyloid cascade hypothesis is evolving and determining the molecular events underlying the Aβ toxicity and tau dysfunction is now an important link to decipher.

Along with TPK1, GSK3 is the other major kinase in tau modifications leading to NFTs. GSK3 is a candidate for an important role in the Aβ-driven cascade, as it has been linked with memory impairment, tau hyperphosphorylation and plaque-associated microglial activation (Hooper et al., 2008). Its role in Aβ signaling may be relevant to all of these outcomes. GSK3 has been shown to be a tau kinase in neurons, and phosphorylates tau *in vitro* (Hanger et al., 1992; Lovestone et al., 1999). Furthermore, Aβ increases GSK3 activity, and in turn decreasing GSK3 activity reduces Aβ levels and Aβ-induced toxicity of neurons (Takashima et al., 1995; Sofola et al., 2010; Hernandez et al., 2010). Regulation of GSK3 activity is important in LTP and LTD, and hence could be a key mechanism underlying the cognitive deficits in AD (Hooper et al., 2007; Peineau et al., 2007; Giese, 2009).

The Wingless-Int (Wnt) signalling pathway is affected in neurodegenerative diseases, and is known to mediate Aβ toxicity (Boonen et al., 2009; Toledo et al., 2010). GSK3 activity is modulated by insulin and Wnt signalling, and in the absence of Wnt, β-catenin is phosphorylated by GSK3, thereby activating the Wnt/β-catenin pathway (Hooper et al., 2008; Inestrosa and Varela-Nallar, 2014). There is a strong relationship between AD and Wnt signaling pathway impairments, and the APOE ε4 risk allele has been proposed as an inhibitor of canonical Wnt signalling (Caruso et al., 2006).

Aβ also induces the expression of the Wnt antagonist, Dickkopf-related protein 1 (Dkk1), encoded by the gene DKK1. This is an important mediator of apoptosis, and not typically expressed in the healthy adult brain (Grotewold and Rüther, 2002; Diep et al., 2004). Interestingly, LRP5, the Dkk1 receptor, can also bind APOE (Kim et al., 1998). DKK1 is induced by p53 (Wang et al., 2000), preventing GSK3 inhibition by Wnt, and hence initiating tau phosphorylation and neuronal death. The induction of DKK1, and the consequent neurotoxicity, in this pathway is p53 dependent (Killick et al., 2014). DKK1 expression was found to be necessary for tau phosphorylation, as silencing DKK1 prevented GSK3 activation and tau phosphorylation in neurons treated with Aβ (Caricasole et al., 2004). Purro and colleagues (2012) found that Aβ oligomers induced Dkk1 expression in rodent hippocampal slices and caused synaptic disassembly. Dkk1 treatment decreased the number of synapses but did not cause cell toxicity. The accumulation of studies on Wnt in AD suggests that its role is in tau phosphorylation and synaptoxocity, events early in the pathogenesis and prior to neurodegeneration.

Aβ and Dkk1 have been found to induce a number of common genes, suggesting that Dkk1 is important in mediating the effects of Aβ on gene expression. These common genes are CCND1, EGR1, NAB2, KLF10 and FOS and may be important in the neurotoxic signaling pathway. Many of these genes are common to cellular apoptosis

pathways and so their specificity to an Aβ-Dkk1-mediated cascade needs further investigation. Interestingly, these target genes are not mediated by canonical Wnt signaling but by activation of the non-canonical Wnt pathway, the Wnt-planar cell polarity (PCP) pathway (Killick et al., 2014).

Clusterin is a likely mediator for Dkk1 activity in AD. In rodent primary neurons, clusterin knockdown reduced Aβ toxicity and DKK1 expression, and an increased intracellular to extracellular clusterin ratio led to DKK1 upregulation (Killick et al., 2014). The roles of clusterin (or apolipoprotein J) together with APOE in AD, and specifically in the amyloid cascade, will be discussed further in section 1.3.

1.3 Apolipoproteins in AD

1.3.1 Apolipoproteins in Aβ-regulation

Apolipoproteins are primarily involved in the transport of lipid and cholesterol within the central nervous system. A number of apolipoproteins have been found to be associated with AD, particularly APOE, clusterin (CLU, APOJ) and APOA-1 (Lewis et al., 2010). As described in section 1.2.4, large-scale, genetic studies have consistently found APOE and CLU as important genes in late-onset AD. In AlzGene's ranking of the most strongly associated genes from meta analyses APOE is ranked first and CLU is third most significant (BIN1 is second) (AlzGene, 2011). There is growing support for the role of these genes in AD, and their mode of interaction with Aβ, although the pathways through which APOE and CLU mediate Aβ pathology are still unclear.

1.3.2 Apolipoprotein E

The APOE protein is involved in cholesterol transport and lipid homeostasis, through mediating lipid transport from one cell type to another. The APOE ε4 genotype is associated with hyperlipidaemia and hypercholesterolemia, which lead to atherosclerosis, coronary heart disease and stroke (Liu et al., 2013). In the central nervous system APOE is mainly produced by astrocytes, and transports cholesterol to neurons. The ε4 allele of the APOE gene is the greatest risk factor for sporadic AD (Zahs and Ashe, 2013). Individuals with one copy of the ε4 allele are three times more likely to develop AD than individuals with the most common genotype, two copies of the ε3 allele. Individuals with two ε4 alleles are up to 15 times more likely to develop AD. The ε2 allele is protective (Corder et al., 1993).

How the different APOE proteins mediate their effects in AD is not definitively known, but there are many studies demonstrating a role for APOE in Aβ metabolism. APOE is co-deposited in senile plaques in the brains of AD patients (Namba et al., 1991), and is thought to increase Aβ aggregation and ε4 allele has been found to correlate with higher plaque density in the cortex in patients with AD (Beffert and Poirier, 1996). This study also found similar correlations for NFTs with the APOE ε4 allele in the frontal and fusiform cortex. The clearance of Aβ is proposed as an important role for APOE in Aβ processing. APOE can sequester Aβ and modulate Aβ clearance through endocytosis or transport across the blood brain barrier. Beffert and colleagues (1999) have demonstrated the binding of APOE to Aβ in vitro with isoform-specific differences, although replications of the isoform differences have had mixed results (Kim et al., 2009). Transgenic mice with APP and APOE mutations have shown that the clearance of Aβ was dependent upon the APOE allele, with the efficiency of Aβ clearance poorest for the ε4 allele (Castellano et al., 2011).

APOE is produced primarily by astrocytes and microglia in the brain and its role in AD may stretch far beyond Aβ metabolism (Liu et al., 2013). Another likely role is in inflammation: APOE co-localises with microglia and APOE isoforms could differentially regulate the immune response. The ε4 allele may exacerbate AD pathology as APOE ε4 transgenic mice have been shown to exhibit a greater inflammatory response (Lynch et al., 2003).

APOE may also have a coordinated action with other apolipoproteins such as clusterin (White et al., 2001). DeMattos et al. (2004) used transgenic APP mice bred with APOE knockouts and CLU knockouts to investigate the Aβ pathology in the absence of APOE, CLU and both genes. The APP mice with the double knockout (APOE-/- and CLU-/-) had both earlier and greater Aβ deposition than the other transgenics, with increased soluble Aβ in the cerebral spinal fluid (CSF) and brain prior to deposition. In the APOE-/- and the CLU-/- mice there was significantly reduced Aβ deposition. These results suggest a cooperative regulation of Aβ by APOE and clusterin, and a role for these proteins outside of Aβ fibril formation in AD.

1.3.3 Clusterin

Clusterin is the other apolipoprotein produced in the brain (May and Finch, 1992). The important role of clusterin in mediating Aβ toxicity is starting to be elucidated, and, similarly to APOE, its influences in AD have been found to stretch beyond the amyloid cascade pathway. Clusterin has many functions in normal physiology resulting in an array of aliases: apolipoprotein J (ApoJ), sulfated glycoprotein-2 (SGP-2), secreted glycoprotein gp80, complement-associated protein SP-40,40, complement lysis inhibitor (CLI), and testosterone-repressed prostate message 2 (TRPM-2) (Nuutinen et al., 2009).

Clusterin was first thought to have an involvement in AD in 1990, when hippocampal samples from AD patients were found to have increased clusterin protein levels (May et al., 1990).

Outside of the brain, elevated levels of clusterin have been identified in the brain, blood, and CSF of individuals with AD or increased amyloid aggregates in the brain (Lidström et al., 1998; Nilselid et al., 2006). Clusterin in plasma has been associated with disease severity, progression and Aβ levels in AD patients (Thambisetty et al., 2010). Desikan et al. (2014) found CSF clusterin to be associated with atrophy in the entorhinal cortex (EC), reported as one of the first sites of AD pathology in the brain, in cognitively normal individuals and those with mild cognitive impairment. CSF phosphorylated tau was not associated with EC atrophy, which may support increased clusterin levels as an early event in AD progression.

Clusterin has been functionally linked with AD pathology through a number of mechanisms. It is a chaperone glycoprotein composed of an α and β subunit. The protein has 3 molten globule domains, intrinsic disordered regions, which can stabilize stressed proteins such as Aβ peptides. This binding is important in preventing the fibrillisation of Aβ peptides and in the clearance (Nuutinen et al., 2009). Ghiso and colleagues (1993) found that clusterin in the CSF bound to synthetic Aβ peptides, and were then able to retrieve soluble Aβ from the CSF using a clusterin antibody. Narayan and colleagues (2011) established that clusterin sequesters small $A\beta_{1\text{-}40}$ oligomers, thereby influencing the aggregation, and disaggregation, of $A\beta_{1\text{-}40}$ preventing neurotoxic amyloid fibril formation.

Furthermore, clusterin is involved in many Aβ-independent mechanisms in AD. As an apolipoprotein it has important roles in lipid transport in the brain. It is involved in the transport of cholesterol, which has known effects on AD susceptibility, along with its

predecessor apolipoprotein APOE (Yu and Tan, 2012). Clusterin may also influence AD pathology through activation of neuroinflammation pathways, such as via the activation of microglia (Xie et al., 2005). Complement has an important role in neuroinflammation, and clusterin is a known inhibitor of this, proposing another role for clusterin in immune dysregulation in AD (Kirszbaum et al., 1992). Clusterin might also be involved in the activation of microglia and recently has been shown to bind to the TREM2 receptor on microglia (Yeh et al., 2016).

Research on CLU knockout transgenic mice has helped to determine the role of clusterin in AD development. The normal phenotype of CLU knockout mice suggests that other molecules may successfully compensate for its absence, and APOE has been proposed in this role (Morgan and Carrasquillo, 2013). DeMattos and colleagues (2002) bred APP transgenic mice with CLU knockout mice to investigate how Aβ pathology was altered. The CLU knockout mice had significantly less fibrillar Aβ, although an unchanged overall level of total Aβ. The CLU knockout mice also had fewer dystrophic neurites, suggesting that amyloid deposition without clusterin presence is less toxic, perhaps due to increased fibrillisation. CLU knockout mice have also been useful in studying inflammatory response in brain injury. Following middle cerebral artery occlusion, wildtype mice had prolonged upregulated clusterin expression, whereas CLU knockout mice had increased reactive astrocytes and poor remodelling of the region (Imhof et al., 2006). These studies in CLU knockout mice have increased our understanding of the role of the gene in Aβ pathology and other AD-relevant pathologies.

Whether clusterin has a neurotoxic or neuroprotective role in AD continues to elude scientists. Similarly in other fields, including cancer, it has been referred to as an ‘enigmatic protein’. Its differing biological actions may be explained by the production of different protein products from the CLU gene. The secreted form of CLU (sCLU) is the

better understood form, but CLU localized to the nucleus, nCLU, has also been identified. The localization of the protein may determine its role: sCLU may be involved in neuroprotective functions such as amyloid clearance, whereas nCLU retained inside the cell may have an apoptotic role (Bettuzzi & Rizzi, 2009). The major roles of clusterin in AD are described in Figure 3.

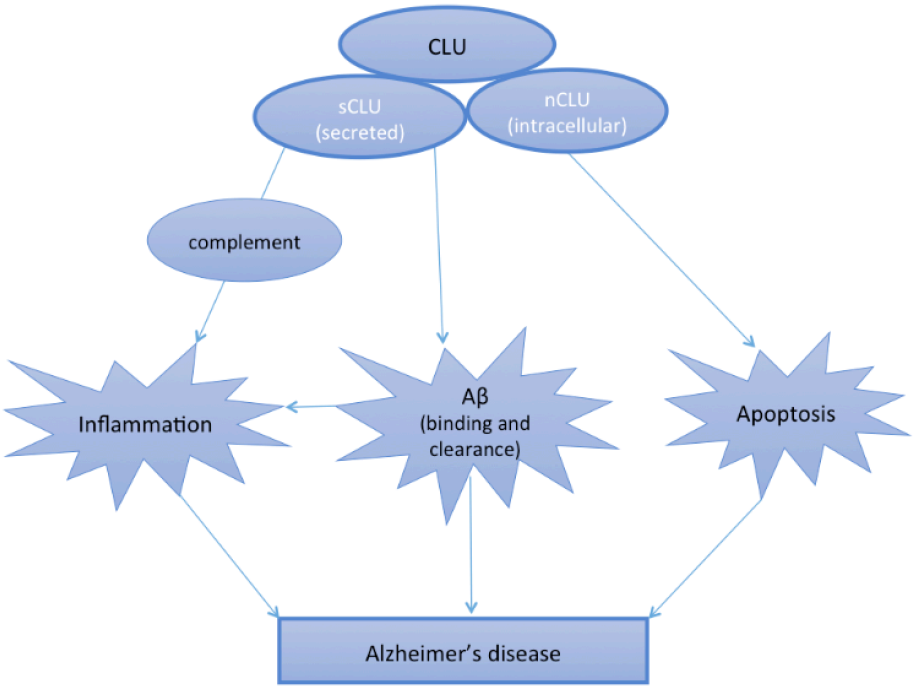

Figure 3. Actions of clusterin in the AD brain. Secreted CLU (sCLU) has been identified in neuroinflammation and Aβ processing, and nuclear clusterin (nCLU) is involved in apoptosis (Wu et al., 2012; Yu and Tan, 2012; Nuutinen et al., 2009; Bettuzzi & Rizzi, 2009).

More recently genome wide association studies (GWAS) for sporadic AD have flagged clusterin as a major hit, with the finding of the single nucleotide polymorphism (SNP) rs11136000 (Harold et al., 2009; Lambert et al., 2009), with rs11136000(T) conferring a slightly decreased risk for AD with an odds ratio of 0.84 compared to (C) (Carrasquillo et al., 2010). Mutations in this gene may explain 9% of AD attributable risk (Bertram et al.,

2007). Two AD-associated SNPs, rs9331888 and rs11136000, are associated with decreased levels of clusterin in plasma (Schürmann et al., 2011; Xing et al., 2012). Links between the risk allele of rs11136000 and white matter integrity in several brain regions of healthy adults have also been identified (Braskie et al., 2011). A functional link between the polymorphisms and AD is still unclear and new studies investigating the mechanistic action of clusterin in AD are revealing the multiple functions of this protein. Whether this protein has a protective or pathogenic role in AD remains uncertain.

Findings from Bettens and colleagues (2015) provide an important breakthrough in linking the CLU polymorphisms to mechanisms. Rare patient mutations in the β-chain of CLU, where previously observed SNPs were clustered, reduce the normal clusterin secretion from the cell and alter the subcellular localization of the protein. Higher amounts of clusterin were identified in the endoplasmic reticulum (ER) and corresponding lower levels in the Golgi apparatus, resulting in clusterin degradation prior to trafficking out of the cell. This was studied using HeLa and HEK293 cells transiently overexpressing wildtype or mutated CLU, although these results were only found for 2 of the 10 rare patient mutations: p.R338W and p.I360N (Bettens et al., 2015).

Supporting the localization of clusterin as a key part of its role in AD, treating cells with Aβ peptides causes an increase in intracellular clusterin in neurons, and a decrease in clusterin in the cell culture medium. However, cell stressors other than Aβ had little effect on clusterin levels. Decreasing clusterin expression protects neurons from Aβ-induced toxicity, and moreover prevents the increased DKK1 expression caused by Aβ-treatment of cells (Killick et al., 2014). This study proposes an interesting pathway to link the activity of clusterin and Aβ with the Wnt signalling and tau phosphorylation downstream. Further elucidation of this pathway will be important in understanding the cellular mechanisms in AD and identifying potential targets for therapeutics.

A summary of how clusterin and Dkk1 cause Aβ-toxicity through this non-canonical Wnt signaling in neuronal cells is summarized in Figure 4. The roles of the Aβ and Dkk1 induced genes in AD will be important to study to find out how they exert their effect, and it will also be useful to know the specificity of their activation and whether this is limited to Aβ and Dkk1.

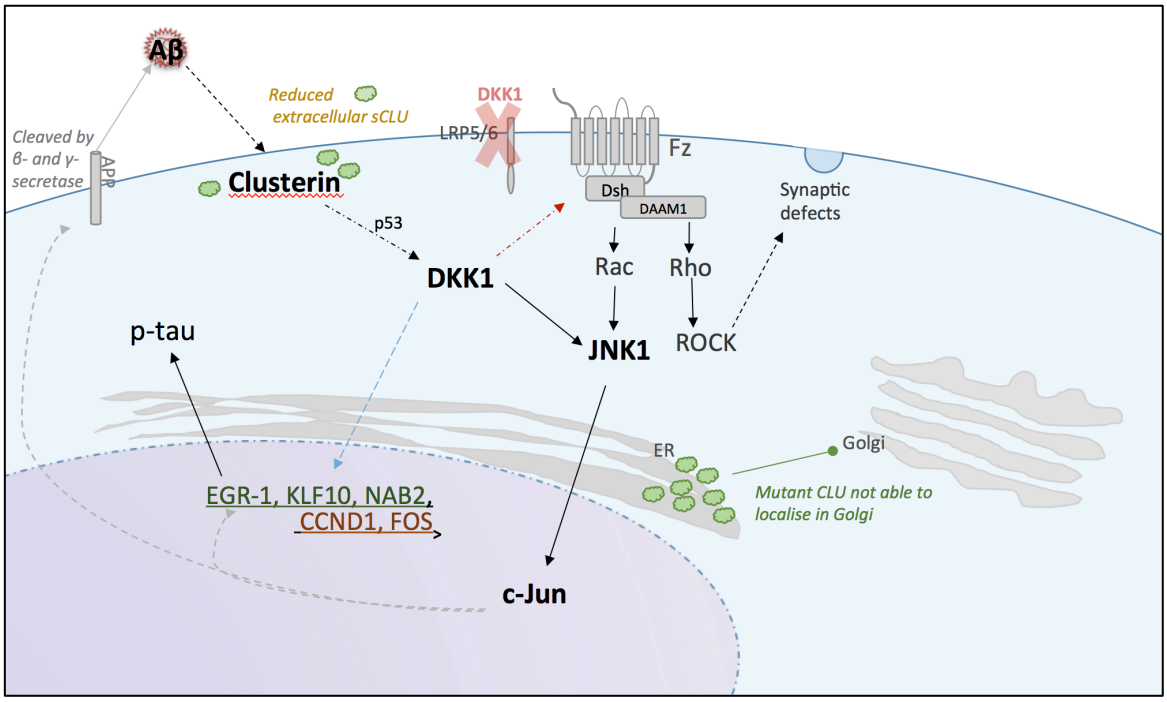

Figure 4. Aβ-toxicity in neuronal cells via clusterin and Dkk1. $A\beta_{1-42}$ presence causes increased intracellular clusterin levels due to reduced clusterin secretion, which may be exacerbated by AD-associated clusterin mutations (Bettens et al., 2015). Clusterin induces DKK1 through p53. Canonical Wnt signalling is inhibited by upregulated DKK1, allowing Fz receptor to drive the Wnt-PCP pathway (Killick et al., 2014).

This pathway has now been identified in rodent cell cultures and human post mortem tissue, lending support to the amyloid hypothesis of AD, and elucidating novel signaling

genes involved in this pathway. It is now important to confirm the pathway elucidated in rodent cells, as summarised in Figure 5, occurs in human cells exposed to Aβ.

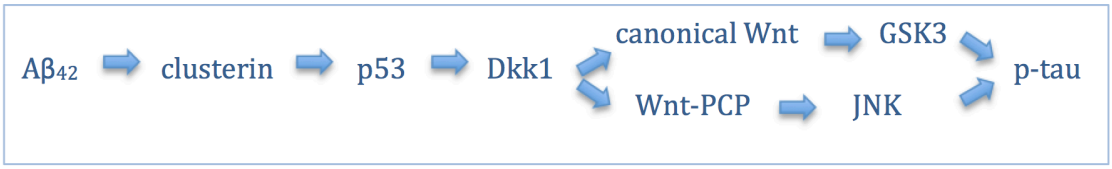

Figure 5. Important proteins in the pathological cascade in AD. Aβ initiates a pathogenic pathway resulting in the phosphorylation of tau. This is mediated by an increase in clusterin, which is proposed to activate DKK1 via p53. There is support for both the canonical Wnt and the non-canonical PCP pathway in this pathological cascade (Killick et al., 2014).

1.4 Modelling AD with induced pluripotent stem cells

1.4.1 Animal models vs. human models

AD is an age-related disorder that is characterised by cognitive decline alongside amyloid and tau pathology. Although many animals show age-related cognitive deficits, there are few 'natural' animal models of AD that also show the pathology. The transgenic mouse models for AD have been useful for studying specific genes and the development of pathologies. Limitations to rodent AD models include human and rodent species disparities such as brain to body mass ratio and neuronal cell types (Shi et al., 2012a). Rodents have a smaller proportion of white matter, which is an important difference with disease modelling (Fisher et al., 2009). A difference in some of the normal cellular processes between humans and smaller mammals also makes disease modelling in animals difficult, such as differences in immunity (Mestas and Hughes, 2004). This is true in AD, and the relevance of findings in cellular pathways in animal models cannot be

proved directly relevant to the human disease. Since the complex genetics of such diseases cannot be reproduced the relevance of most animal studies are limited to monogenic forms of the disease, which are causal of less than 5% of all AD cases. Failed translation of therapeutics from preclinical to clinical trials has made the development of a new system for testing drugs a priority for novel therapeutic strategies.

Post mortem tissue and immortalised cell lines offer opportunities for studying the AD process in human tissue. Samples from brain regions donated by AD patients are the best way to study pathological features of the disease, but is largely limited to looking at the end stage of the disease, with it being impossible to access the brains of patients at earlier stages. Human cell lines are useful for confirming molecular pathways in an *in vitro* human system, but unfortunately immortalised human cell lines tend to have chromosomal abnormalities causing different innate properties (Bray et al., 2012). These do not accurately represent the intracellular environment that human neurons in the brains of AD patients are exposed to, and therefore neurons derived from human iPSCs provide a great opportunity.

1.4.2 Potential for human iPSC models in AD

The development of induced pluripotent stem cells (iPSCs) was a revolutionary publication by Takahashi and Yamanaka, winning Yamanaka the Nobel Prize in Medicine. They demonstrated that adult somatic cells could be restored to a pluripotent state through the exogenous expression of four transcription factors: Oct4, Sox2, Klf4, and c-Myc. These iPSCs express markers exclusive to embryonic stem cells, mimic their morphology and growth properties, and can be differentiated into any specified cell type when in the presence of the molecular signals that would typically be present during

development (Takahashi and Yamanaka, 2006). The opportunity for human patient-specific iPSCs models of disease have already become apparent with iPSC-derived cell studies producing insights into mechanisms and evaluation of pre-clinical drugs (Bellin et al., 2012, Mertens et al., 2013, Ross & Akimov, 2014).

The complex genetics of AD is still a major obstacle in successfully modelling the disease and it will be critical to determine the pathogenic mechanisms in human neurons. The development of human iPSC technology has offered a new method for studying human cells without the use of embryos. There are now numerous protocols for converting different cell types into stem cells, including relatively non-invasive cell types such as keratinocytes or blood cells (Takahashi et al., 2007). iPSC cells can be passaged a large number of times with no impact on genomic integrity and can be differentiated into any cell type (in theory) (Musunuru, 2013). Efficient protocols for cortical neurons based on developmental neurobiology studies are now well established and can produce neuronal cells with functional excitatory synapses. This offers a great opportunity to develop live patient-specific models for disease *in vitro* (Shi et al., 2012a; Espuny-Camacho et al., 2013). The excitement caused by this technological development is demonstrated by the rapid uptake of this model system by the research community, with the number of journal articles on Alzheimer's disease and iPSCs growing steadily and the number of citations now over 2000 for all articles combined (Figure 6).

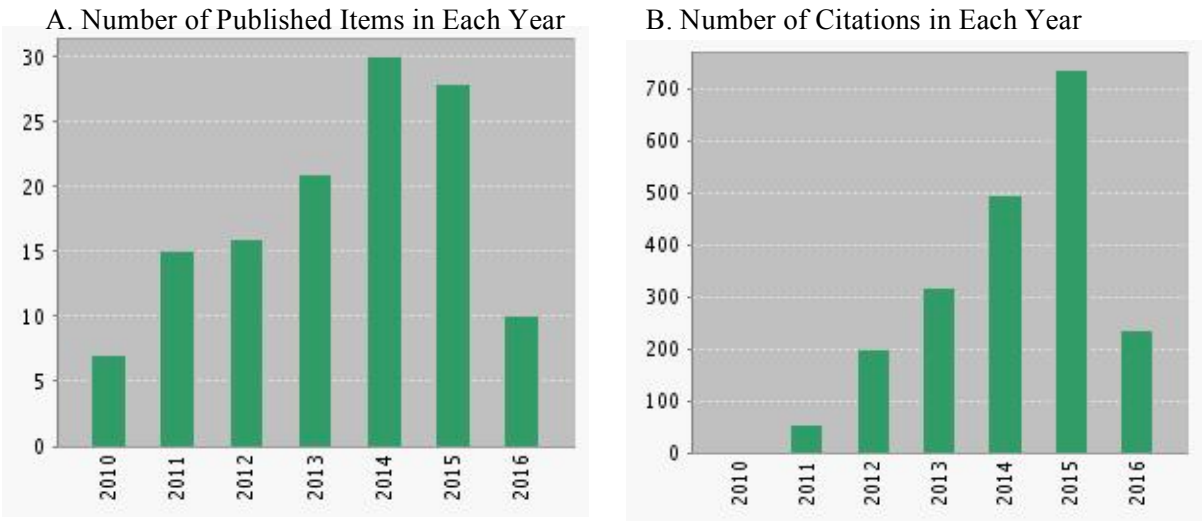

Figure 6. The increase in journal articles on Alzheimer's disease using iPSCs. Generated from Web of Science citation report using search term 'alzheimer's induced pluripotent stem cell'. A. Number of published articles by year. B. Number of citations of all articles per year. (Web of Science search performed 03/05/16.)

The first phenotypes in neurons from familial (fAD) patient iPSCs have been published, showing increased $A\beta_{42}$ secretions compared to cells from healthy controls (Yagi et al., 2011; Israel et al., 2012). Yagi and colleagues (2011) were the first study to demonstrate that increased $A\beta_{42}$ is secreted by neurons derived from patients with an fAD mutation in a period of weeks *in vitro*, whereas Aβ misprocessing in humans can start years after birth. This has been replicated by Israel et al. (2012) and Shi et al. (2012b). Shi and colleagues (2012b) also found abnormal tau phosphorylation and localisation in Down's Syndrome patients with an increased expression of the APP gene on chromosome 21. Additionally cell death was increased in these cell cultures compared to controls. However, variability between patient lines has also been found, which suggests difficulty in drawing conclusions about cellular processes in AD from a small number of iPSC lines. Israel and colleagues (2012) did not find higher levels of $A\beta_{42}$ in the neurons derived from one of the sAD patients, and Kondo and colleagues (2013) found differences between intracellular and extracellular $A\beta_{42}$ levels in patients with different

APP mutations and sAD patient lines. This highlights difficulties in modelling the more complex processes in sAD with an *in vitro* neuronal model.

Neurons derived from iPSCs are now being utilised for drug screens to test for chemical compounds that may prevent Aβ toxicity of neurons (Yahata et al., 2011; Xu et al., 2013). Gamma secretase inhibitors were found to modulate the increased $A\beta_{42}$ found in fAD patients, and hence it may be beneficial to test the efficacy of compounds at reversing Aβ and tau-mediated toxicity in human neurons before clinical trials (Yagi et al., 2011). Mertens et al. (2013) tested NSAID-based γ-secretase modulators in iPSC-derived neurons from fAD patients, which had previously lowered Aβ levels in various model systems but had translated poorly into human clinical trials. Results showed no change of these drugs on Aβ, suggesting resistance of human neurons to NSAID-based γ-secretase modulation. Xu and colleagues (2013) developed a high throughput screen for iPSC-derived neurons, and screened a chemical library containing several hundred compounds. Their Aβ toxicity screen discovered several small molecules that significantly blocked the toxic effects of $A\beta_{1–42}$. These studies highlight the potential for iPSC models of AD as a tool for screening therapeutic compounds and developing a platform for drug development.

Novel, 3D culture systems have also been established for AD, which may support a more realistic network of cell types, including GABAergic, glutamatergic, and dopaminergic neurons, astrocytes, and oligodendrocytes. Choi et al. (2014) reported extracellular deposition of Aβ, including Aβ plaques, and aggregates of phosphorylated tau in the cell bodies of neurons differentiated from fAD iPSC lines. The 3D culture system may be important in observing this AD pathology, as 2D iPSC-derived models have not reported plaque pathology.

These studies highlight the exciting developments in modelling disease pathogenesis with patient-derived iPSCs, and the potential to use these models in early toxicity and efficacy compound screening. Moreover, the advancement of this technology coincides brilliantly with rapid progress in genetic techniques such as precise genome engineering and transcriptomic and proteomic analysis. The complement of these techniques could allow for human cells to model known pathogenic mutations *in vitro*, which could then be functionally validated and downstream targets could be confirmed. In the future these models could give rise to new preclinical model for drug discovery and even personalised therapeutics based on individuals genetics.

1.4.3 Limitations of iPSCs

There are currently some limitations to the iPSC technology that have resulted in the principle of using iPSCs for modelling disease coming under criticism. One major concern is the heterogeneity of iPSC lines due to variation in the genetic background of individuals, but also the result of factors such as random viral integration and incomplete silencing of reprogramming factors (Marchetto and Gage, 2012). Non-integrating methods have omitted these reprogramming issues, but somatic mutation and CNVs acquired during reprogramming still need to be accounted for. Due to large variability between individuals, the number of patient and control lines that should be generated to produce a significant effect when studying a clinical phenotype is still debated. For example, Kondo and colleagues (2013) found different phenotypes amongst cell lines from 4 AD patients (2 sAD, 2 fAD). Hence a large number of cell lines may be needed to detect subtle disease-related pathologies.

Another difficulty in modelling Alzheimer's disease is the best approach to use in terms of familial and sporadic forms of the disease. There are many advantages of using cells from fAD patients, in which a single mutation can cause a phenotype. However, due to the low percentage of AD patients with a familial mutation, cells from sporadic patients may be more relevant to advancing the understanding of AD development. However, lines from sAD patients may have incredibly different cellular phenotypes, or no obvious phenotype, especially in an in vivo model predominantly with one cell type. A more general model for AD may be to treat wildtype neurons with Aβ, as done in Aβ toxicity screening by Xu and colleagues (2013), and in many primary culture studies (Killick et al., 2014).

Another interesting consideration is the age of iPSC-derived neurons, since age is the major risk factor for AD. Studies indicate that during reprogramming to an embryo-like iPSC state the original age of the somatic cells is lost (Lapasset et al., 2011, Meissner et al., 2008). The reprogramming phase resets many known key ageing hallmarks, including: extension of telomere length, restoration of mitochondrial function and reduced oxidative stress (Rohani et al., 2014). Mertens et al. (2015) generated iPSCs and neurons from fibroblasts derived from donors aged 0 to 89 years, finding that these cells did not retain ageing-associated molecular signatures, including nuclear transport receptor RanBP17 levels and nucleocytoplasmic compartmentalisation. However, the neurons they made directly from fibroblasts, induced neurons (iNs), preserved these signatures. Therefore, iNs may be a useful technique in the future for modelling AD, and other diseases where ageing is an important risk factor, *in vitro,* although currently the increased time and labour costs required to make a similar number of cells do not make them a viable alternative to iPSC-derived neurons.

1.5 Genome engineering in *in vitro* models

The development of advanced techniques for engineering the genome could rapidly increase our understanding of the genetic contribution of specific alleles to disease processes. Studies comparing iPSCs from patients with a defined mutation to controls have not been able to account for differences in genetic background and epigenetic states of the iPSC lines. Precise genome editing allows for the specific effects of a mutation or gene to be studied in a cell line and the isogenic control. Correcting a single mutation or creating one removes all other variables, such as genetic alterations from reprogramming or irregularities with the epigenetic memory of an iPSC line (Musunuru, 2013).

1.5.1 Precise genome engineering

There are different approaches one can take to genetically modify stem cells in order to produce a human cell model of disease. Previously RNA interference (RNAi) has typically been used to investigate gene function as it is quick, inexpensive and can be used on high throughput platforms (Agrawal et al., 2003). RNAi is a process where small RNA molecules are used to inhibit gene expression (McManus and Sharp, 2002). However, RNAi does not always offer complete knockdown of a gene, and additionally knockdown is temporary and the effectiveness varies between genes (Holmes et al., 2010). RNAi may also have unpredictable off-target effects, which have ultimately impeded researchers' ability to unequivocally link phenotype to genotype in RNAi experiments (Gaj et al., 2013).

Over the past decade, the field of precise genome editing has gradually emerged whereby researchers can manipulate almost any gene in various cell types and organisms through cleavage of DNA in a site-specific manner. This ability to make precise changes in the

genome to engineer biological systems has enormous potential to interrogate genetic contribution to disease. There are currently three main technologies used: Zinc-Finger Nucleases (ZFNs), Transcriptor Activator-like Effector Nucleases (TALENs) and the Clustered Regularly Interspaced Short Palindromic Repeats (CRISPR)-cas nuclease system.

ZFNs and TALENs use a strategy of a DNA-binding domain, to specifically recognise the gene of interest. This is combined with a DNA-cleavage (FokI) domain to induce a double-strand break (DSB). The FokI cleavage domain must dimerise in order to cleave the target DNA, and so a pair of DNA-binding domains must be used. Although ZFNs and TALENs have proved effective for genetic manipulation, a new ZFN or TALEN protein must be generated for each DNA target site, which can have huge cost implications (Gaj et al., 2013).

1.5.2 CRISPR/Cas9

The CRISPR/Cas system is the new player in genome-editing technology, and was first discovered in bacteria. The CRISPR sequences were found to function as a defence mechanism to identify and inactivate foreign DNA (viral or plasmid) (Sander and Joung, 2014, Wiedenheft et al., 2012). The Cas endonuclease is guided by small RNAs to induce a DSB. It achieves this through its two active domains, RuvC and HNH, which cleave the complementary strand and non-complementary strand respectively (Gasiunas et al., 2012; Jinek et al., 2012; Nishimasu et al., 2014). The CRISPR/cas system identifies a 20 nucleotide targeting sequence corresponding to the CRISPR sequence to guide cas9 to a specific target locus (shown in Figure 7). The CRISPR/cas system is therefore markedly

easier to design, highly specific, efficient and a much cheaper method for genome engineering.

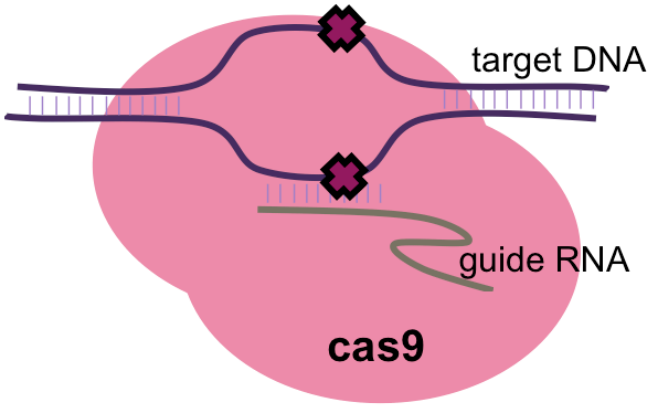

Figure 7. Action of CRISPR/Cas9 with guide RNA targeting DNA site. The guide RNA is expressed with the CRISPR associated endonuclease, and directs it to the target DNA site. The cas9 will then cause a double strand break of the DNA.

There are three distinct bacterial CRISPR systems: type I, II and III. Type II is the basis for current genome engineering technology (Sander and Joung, 2014). In bacteria, the endogenous CRISPR/Cas system targets foreign DNA with a short, complementary single-stranded (ss)-RNA (CRISPR RNA (crRNA)) duplexed with trans-activating crRNA (tracrRNA), that directs the CRISPR associated endonuclease (cas9) to the target DNA sequence (Horvath and Barrangou, 2010; Wiedenheft et al., 2012). The DNA target sequence can be on a plasmid or integrated into the bacterial genome. Mali and colleagues (2013) demonstrated that expression of crRNA-tracrRNA fusion transcript, termed 'guide RNAs' (gRNAs) from human U6 polymerase III promoter, allowed cas9 to cleave sequences of interest. In human cells, expression of a human codon-optimised Cas9 protein with an appropriate nuclear localisation signal is required, while U6 promoter naturally drives the transcription of small RNAs (Makinen et al., 2006).

Utilising CRISPR/Cas9 in mammalian cells is now a routine procedure. gRNAs that match the DNA sequence of interest are designed for each targetable site. The gRNA is expressed intracellularly with a cas9 nuclease and directs cas9 to the target sequence where it unwinds and cleaves double-stranded DNA (Cho et al., 2013). If the DNA target is not unique and appears in multiple locations, all of these will be targeted by the cas9 nuclease for cleavage (Cong et al., 2013, Cho et al., 2013). There are some restrictions specific to the CRISPR system. Potential target sequences must have a specific sequence on the 3' end (the protospacer adjacent motif, PAM). The Type II CRISPR system is currently limited to target sequences that are G-N_{12-20}-GG, where NGG represents the PAM (Sander and Joung, 2014, Wiedenheft et al., 2012, Jiang et al., 2013). This can create difficulties for correcting mutations on SNPs, where the target area is restricted.

1.5.3 DNA repair following a double-strand break

Together the two active domains on cas9, RuvC and HNH domain, cause a DSB in genomic DNA at a specific locus (Jinek et al., 2012; Nishimasu et al., 2014). Depending on the aim of the genome editing either the NHEJ or HDR pathway can be encouraged (as summarised by Figure 8).

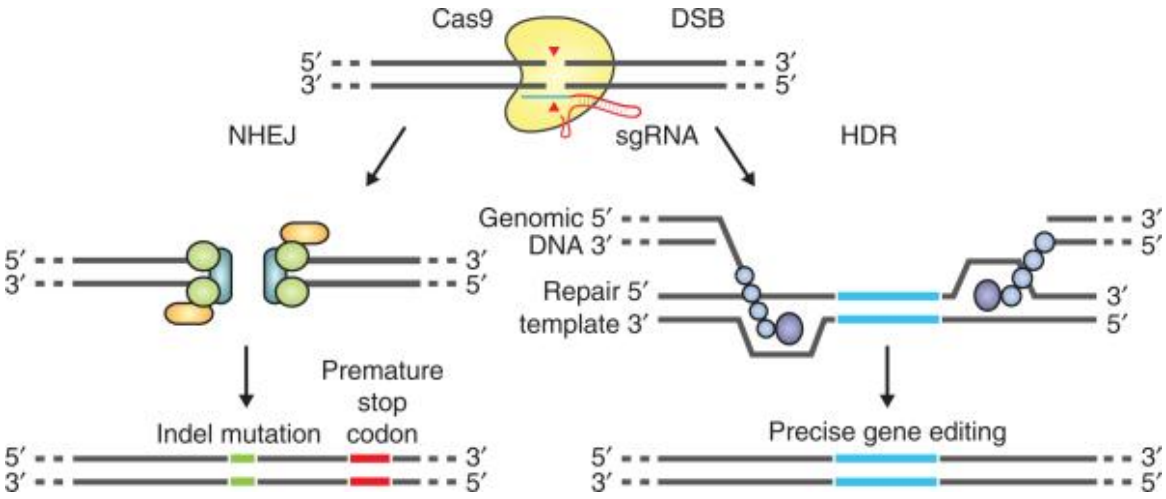

Figure 8. DNA repair following a double-strand break (DSB). The endonuclease cas9 cleaves both strands of the target DNA, creating a DSB. A DSB can be repaired by one of two pathways; non-homologous end joining (NHEJ) or homology-directed repair (HDR) (taken from Ran, 2013, with permission).

Following damage to the DNA, and without an available donor template, DSBs are repaired by NHEJ. The pathway is referred to as "non-homologous" as DNA homology is not required to join the ends of the DNA. NHEJ is error prone and can result in the loss or gain of nucleotide number, with the end-joining product often including nucleotide insertion mutations or missing nucleotides causing deletions (indels) (Valerie and Povirk, 2003). NHEJ can therefore cause maximum disruption, which can be employed as a strategy to generate a gene knockout by indel formation. This strategy is only successful if the indel produces a frame shift mutation, which often generates a premature stop codon (Perez et al., 2008). Therefore the best strategy is to target an exon closest to the N terminus of the gene, as this will cause maximum disruption to its transcription.

HDR is a high fidelity pathway that depends on a repair template. In general, HDR is less error-prone than NHEJ but typically occurs at much lower rates. However, introducing a repair template after the DSB can enhance this pathway. This can be in the form of a targeting construct, composed of homology arms flanking the target sequence, or a single-

strand DNA oligonucleotide, with the latter providing a potential method for making single nucleotide mutations (Ran et al., 2013).

HDR will be utilised in this project by the design of both a short DNA repair template with homology to the sequence and a larger targeting construct. For the CLU knockout project a targeting construct with antibiotic resistance will allow for selection of mutated cells, and a genetic scar will not be an issue. For the APOE knockin, scarless genetic modification is the priority, and a short (<150bp) single-stranded oligodeoxynucleotide (ssODN; or single-stranded oligo donor) will be designed with the point mutation included.

1.6 Aims and Objectives

The aim of this PhD is to characterise the molecular cascade initiated by Aβ in human neurons. Specifically, Aβ has been found to initiate a neurotoxic pathway via clusterin/p53/Dkk1/wnt-PCP-JNK signalling in rodent cells (Killick et al., 2014), which is now important to test in human cells.

The objectives will include measuring Aβ-toxicity in human cortical neurons differentiated from iPSCs through the development of a robust high throughput assay. First neurons differentiated from iPSCs will be treated with synthetic amyloid preparations ($A\beta_{25-35}$ and $A\beta_{1-42}$) and an imaging assay to measure toxicity will be established. Following this the roles of genes downstream of Aβ in the amyloid cascade, CLU, DKK1 and EGR1 will be investigated to determine if their expression is increased with Aβ exposure as hypothesised from animal studies. We hypothesise that clusterin levels will be increased in human neurons following exposure to Aβ, as in rodent cultures.

If this pathway is relevant in a human *in vitro* system CRISPR/Cas9 technology will be utilised to interrogate the role of clusterin and APOE in Aβ-toxicity. A CLU knockout iPSC line will be generated as well as an APOE ε4/ε4 line from the healthy APOE ε3/ε3 line. To determine the roles of these genes in Aβ-toxicity the genome edited lines and the isogenic controls will be used for targeted investigation of the Aβ-CLU-driven pathway, as well as investigating alternative important pathways using Transcriptomic approaches. Determining the role of these genes on established measures of Aβ-neurotoxicity will be of great value to obtaining a better understanding of the underlying disease mechanisms in AD.

Chapter 2 Aβ toxicity in human neurons

2.1 Introduction

2.1.1 Amyloid toxicity

Amyloid plaques were first sequenced by Glenner and Wong in 1984, yet our precise understanding of the neurotoxic action of Aβ is still far from clear. Excessive Aβ is known to be an early event in AD pathology, initiating a complex cascade resulting in synaptic disruption, glial activation and tau hyperphosphorylation. According to the amyloid cascade hypothesis this pathway results in neuronal loss causing dysregulated neurotransmitter signalling and cognitive decline (Hardy and Selkoe, 2002).

Neurotoxicity of Aβ has been investigated in rodent studies using LTP as a measure of neuronal function. These found that both natural human Aβ and synthetic Aβ oligomers reduced LTP, impacting signalling and synaptic plasticity (Walsh et al., 2002; Shankar et al., 2008; Lambert et al., 1998). The synaptotoxicity of Aβ has also now been confirmed in a human neuronal model by Nieweg at al. (2015). In this study Aβ from Chinese hamster ovary (CHO) cells that stably expressed mutant human APP was added for 8 days to iPSC-derived neurons purified by FACS. Decreased vesicle cycling dye, FM4-64, and synaptic vGlut1 staining demonstrated a reduction in synaptic vesicles and glutamatergic synapse function, although no significant cell death was detected.

2.1.2 Amyloid species

Aβ is generated by cleavage of APP via the 'amyloidogenic pathway'. The protein is cleaved sequentially by β–secretase and γ-secretase. The γ-secretase complex cleavage

site is variable and can occur after 38, 40 and 42 amino acids, resulting in Aβ variants of differing lengths (Haas and Selkoe, 2007). 1-40 is the major species and is less prone to aggregation than 1-42. Aβ can self-associate to form aggregates ranging from dimers through to fibrils (Haass, 2004).

The type of Aβ responsible for neurotoxicity is still an unresolved question, with no clear link between a specific form of Aβ and synapse loss (Shankar et al., 2007). A study by Tsai et al. (2004) found that neurons passing through large plaques of fibrillar Aβ in AD brains showed spine loss and neurite breakage. However, it is difficult to differentiate the assumed toxicity of these fibrils from the toxicity of the smaller oligomers that likely surround these aggregates.

Although it was originally presumed that the insoluble amyloid plaque cores were the toxic element, evidence has been building that the soluble forms of Aβ are necessary for toxicity (Haas and Selkoe, 2007). This shift in focus from fibrils to oligomers is supported by the work of Shankar and colleagues (2007; 2008), which suggests that it is Aβ dimers and trimers, but not monomers, which result in synaptotoxicity. The amyloid plaque cores from the same brains did not affect spine density in rodent neurons unless they were solubilized, indicating that plaques have low toxicity and it is the sequestered soluble, low-n oligomers of human Aβ that cause neurodegeneration.

Due to difficulties in isolating naturally occurring Aβ species, many studies focus on synthetic Aβ. Yanker et al. (1990) investigated overlapping peptides spanning the entire Aβ protein sequence and found that only the 25-35 fragment had the same effect on toxicity at 20μM as the 1-40 polypeptide. Therefore the 25-35 fragment is thought to be the functional region of the peptide, necessary for the neurotoxic effects of the β-amyloid protein.

2.1.3 Cell types and Aβ-toxicity

Glial cells are thought to have an important role in modulating the Aβ-neurotoxicity in AD. The severity of glial activation correlates with the extent of brain atrophy and cognitive decline and Aβ can be cleared from the brain through uptake and phagocytosis by cells such as microglia, astrocytes, and macrophages (Cagnin et al., 2001; Parachikova et al., 2007; Ries and Sastre, 2016).

Activated microglia and reactive astrocytes cause neuroinflammation, and have been found to exacerbate Aβ-induced neuronal loss. Garwood et al. (2011) demonstrated accelerated Aβ-neurotoxicity in mixed (4% GFAP-positive cells) compared to pure neuronal cultures when treated with 10μM soluble Aβ oligomers. However, Noble and colleagues (2009) found a decrease in cell survival in neuronal cultures in the same 48hr $A\beta_{1-42}$ treatment, and so the necessity of astrocytes for *in vitro* Aβ-toxicity remains unclear. This is now supported by findings in human iPSC-derived neurons purified by FACS. iPSC-derived neurons exposed to Aβ for 8 days led to synaptotoxicity via a reduction in the number of vesicle clusters (Nieweg et al., 2015). A challenge for *in vitro* studies of Aβ-toxicity is accurately reflecting the cell types in the brain, and this may alter the degree of toxicity from that found *in vivo*.

2.1.4 Aims

The aim of this chapter was to establish a reproducible assay for measuring Aβ-toxicity, in order to confirm that Aβ is toxic to human neurons *in vitro* as has been established in rodent cultures (Killick et al., 2014), and. This was important to validate using the

synthetic $A\beta_{25-35}$ and $A\beta_{1-42}$ as this had not been established previously in human iPSC-derived cortical neurons. The importance of an assay to measure Aβ-toxicity in the neurons was three-fold. Firstly, it was utilised to characterise the Aβ preparations at the start of experiments. The potency of the Aβ preparation was measured against the established Aβ-toxicity curve. Secondly, the lowest concentration of Aβ that gives toxicity could be established. Thereby future experiments could be carried out using the most physiologically relevant concentration we found to be effective. Physiological concentrations of Aβ in the brains of AD patients are predicted to be low due to clearance mechanisms *in vivo,* although approximations of physiologically relevant concentrations are lacking. Up to 10mg of $A\beta_{42}$ has been reported in the brains of late AD patients, with approximately 25.5 ng per ml of Aβ42 in the interstitial fluid of the brain. Thirdly a reproducible, robust assay was necessary to develop for future compound screening purposes. Human neurons have become a useful tool for investigating disease mechanisms but there is also now great potential to use them in drug safety and efficacy screens. In this project the Aβ assay will be used to detect Aβ-induced neurodegeneration and the expression of downstream genes involved, such as clusterin can then be measured.

Studies in primary cultures have demonstrated that short Aβ exposure times at relatively high concentrations cause apoptotic neuronal cell death and increased caspase-3 cleaved tau phosphorylation (Noble et al., 2009; Garwood et al., 2011). Caspases have an important role in the apoptotic cascade and caspase 3 activation has been found to be necessary in Aβ-toxicity in AD (Mattson et al., 1998). Killick and colleagues (2014) counted intact nuclei and used the live cell stain Calcein AM to measure cell viability. Aβ has also been reported to induce synaptotoxicity before any neurodegeneration (Nieweg et al., 2015), and a more sensitive assay to detect this may be appropriate. Therefore,

intact nuclei, cleaved caspase 3 intensity and the length of neuronal processes were all investigated as potential imaging assays for measuring cell toxicity.

The secondary aim was to investigate whether Aβ-toxicity required the presence of non-neuronal cells. A study by Garwood and colleagues (2011) suggested that the presence of astrocytes were necessary for Aβ-neurotoxicity. Therefore it was important to determine whether the presence of non-neuronal cells in the cultures affected toxicity and whether Aβ-neurotoxicity could occur as a cell autonomous process. The primary rodent neuronal cultures used by Killick and colleagues contained a measurable percentage of glial cells, whereas iPSC-derived neuronal cultures of high neuronal purity may exhibit a different response to Aβ.

2.2 Methods

2.2.1 Neuronal differentiation

The protocol for neuronal differentiation was adapted from Chambers et al. (2009) and Shi et al. (2012a). iPSC colonies were between passage number 20 and 50 at start of neuralisation.

2.2.1.1 Cell culture reagents

Geltrex (Life Technologies, Paisley, UK; A1413302)

HBSS (Life Technologies, Paisley, UK; 14170146)

Versene (Lonza; BE17-711E)

E8 Medium (Life Technologies, Paisley, UK; A1517001)

ROCK inhibitors (Sigma Aldrich, Gillingham, UK; Y0503)

Accutase (Life Technologies, Paisley, UK; a1110501)

N2 Supplement (Life Technologies, Paisley, UK; 17502-048)

DMEM (Sigma Aldrich, Gillingham, UK; D6421)

B27 Supplement (Life Technologies, Paisley, UK; 17504-044)

Neurobasal Medium (Life Technologies, Paisley, UK; 21103-049)

Glutamax (Life Technologies, Paisley, UK; 35050-038)

SB431542 (Cambridge Bioscience; ZRD-SB-50)

Dorsomorphin (Sigma Aldrich, Gillingham, UK; P5499)

AA2P (Sigma Aldrich, Gillingham, UK; A4403)

Poly-l-ornithine hydrobromide reconstituted to 10mg/mL solution in dH_20 (Sigma Aldrich, Gillingham, UK; P3655)

Laminin (Sigma Aldrich, Gillingham, UK; L2020)

All reagents in this thesis were purchased from Life Technologies unless stated otherwise.

2.2.1.2 Cellular reprogramming

The iPSC lines used in this project were generated within the Price lab from human keratinocytes taken from hair samples of healthy adult males (Cocks et al, 2014). The cell line CTR M3 36S that was primarily used in this project was reprogrammed from keratinocyte culture by exogenous expression of four reprogramming factors, *OCT3*/*4*, *SOX2*, *cMYC*, *KLF4*, using Sendai virus vector (SeVdp-iPS) from Mahito Nakanishi Research Center for Stem Cell Engineering, National Institute of Advanced Industrial Science and Technology, Japan. CTR M1 04 and CTR M2 42 lines were reprogrammed using Lentivirus.

All experiments used iPSC line CTR M3 36S unless stated otherwise. Karyotyping showed this line to be normal (Figure 9)

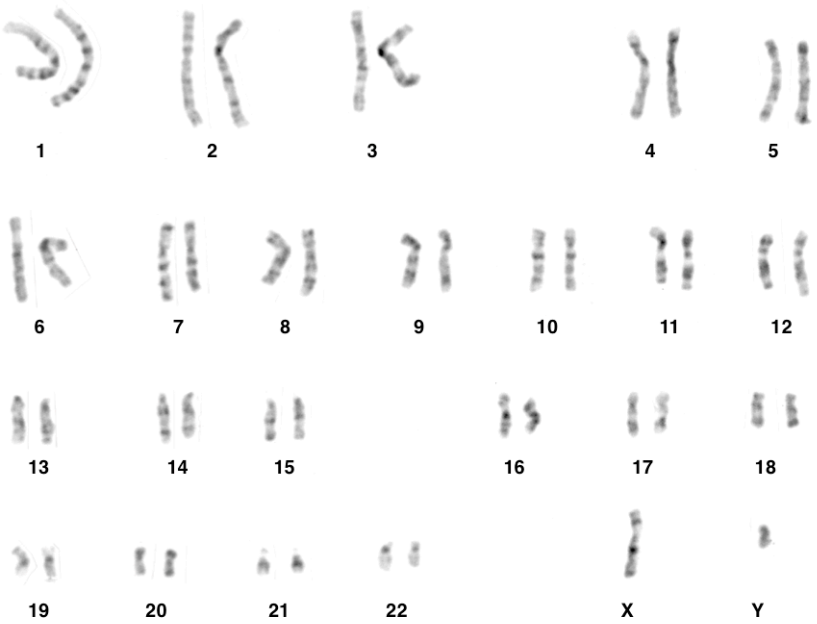

Figure 9. CTR M3 36S Karyotype 46,XY

2.2.1.3 Cell culture plate preparation

For iPSCs through to neural progenitors, cells were plated onto Geltrex-coated 6 well plates. Plates were prepared by diluting 1ml of Geltrex in 20ml of Dulbecco's Modified Eagle's Medium (DMEM). 1ml of Geltrex-DMEM solution was added to each well and plates were incubated at 37^0C for 1 hour prior to use. Geltrex was aspirated before cells were plated.

For differentiating neural progenitors into post-mitotic neurons, cells were plated onto poly-l-ornithine and laminin-coated Nunc cell culture dishes (ThermoFisher Scientific, Paisley, UK). Poly-l-ornithine stock was diluted 1:100 in H_20 and added to 96 well plates at 50µL/well for 2 hours incubation at 37^0C. Laminin (Sigma Aldrich, Gillingham, UK) was diluted into DMEM for a final concentration of 1µg/cm^2 in the wells. Plates were incubated overnight at 37^0C and laminin was aspirated before plating cells.

2.2.1.4 iPSC culture

Cells were maintained in Essential 8 (E8) medium in 6 well Nunc cell culture treated multidishes at 37^0C (5% O_2 5% CO_2). Differentiated regions of cells were removed from culture by scraping with a pipette tip and E8 medium was changed every day. iPSCs were passaged with 1ml/well Versene after 5 days or when the iPSC colonies were large and starting to merge. Cells were then replated into wells coated with Geltrex matrix at a 1:5 passage ratio in 2ml/well E8 medium. .

2.2.1.5 Neuralisation

For neuralisation, iPSCs were passaged after 5 days when approximately 70% confluent at a 2:1 split ensuring 100% confluency after 24 hours. For passaging 10μM of ROCK inhibitors (ROCKi) (Y-27632; Millipore) was added to each well 1 hour prior to passaging. iPSC colonies were cleaned with a pipette tip, and 1ml of Versene (EDTA) was added to each well. Cells were incubated at 37°C for 3-5 min until colonies started to detach. Versene was aspirated and replaced with 1ml/well E8 medium at room temperature (RT). A 5ml pipette was used to transfer all cells to a tube. Once transferred, there was twice the volume of suspension as geltrex-coated wells, and cells were transferred to new geltrex-coated wells without breaking the colonies up too much. Cells were incubated for 24 hours (37°C; 5% CO2; 5% O2) or until 100% confluent.

Once confluent, SMAD inhibitors Dorsomorphin (1μM) and SB431542 (10μM) (Sigma Aldrich, Gillingham, UK) were added to each well in 50% N2 medium (N2 supplement in DMEM/F12 medium) and 50% B27 medium (B27 supplement in neurobasal medium + 1% GlutaMAX), and cells were incubated at 37ºC (20% O_2; 5% CO_2). N2/B27 medium and SMAD inhibitors were replaced every day for 7 days.

On day 8 of neuralisation, once a uniform neuroepithelial layer had formed, cells were passaged 1:1. Wells were washed with cool (~10˚C) HBSS and passaged with Accutase. After 2 – 5 min incubation with Accutase the cell solution was diluted with an equal amount of DMEM and cells were lifted with a 1000μl pipette tip. Cells were lifted by pipetting gently up and down a maxiumum of 5 times to maintain cells as clusters and centrifuged at 900RPM for 5 min. Cells were resuspended in N2/B27 medium with 10μM of ROCKi and plated on Geltrex in N2/B27 medium with SMAD inhibitors. After 24 hours incubation (37°C; 5% CO_2; 20% O_2) the total volume of medium was replaced with 2ml/well N2:B27 (without SMAD inhibitors).

On day 13 cells were passaged as on day 8, replating 1:1 in N2/B27 medium +200 μM AA2P. Medium was replaced with fresh N2:B27 + 200μM AA2P every 24 hours until Day 16. Cells were passaged on Day 16 at 2:3 split and replated in N2/B27 + 10μM ROCKi +200μM AA2P. Cells were passaged day 19 at 1:2 split with replating in N2/B27 + 10μM ROCKi +200μM AA2P. Following 24hr incubation, media was removed and replaced with B27 + 10μM DAPT for 48 hours to push dividing cells into differentiation.

On day 21 neural progenitors were passaged at a lower density onto laminin (Sigma Aldrich, Gillingham, UK; 1μg/cm2) for terminal differentiation of neurons. Accutase was added to wells for 3 min and cells were removed from plates using a 1000μl pipette tip, pipetting several times to generate a homogenous, single-cell suspension. Cells were centrifuged at 1250RPM for 3 min and resuspended in 1ml B27 + 10μM DAPT + 200μM AA2P + 10μM ROCKi, pipetting gently 5 times before counting. Laminin was removed from plates and cells were seeded at 15000 cells/cm2 in B27 + 10μM DAPT + 200μM AA2P + 10μM ROCKi. After 48 hours incubation media was replaced with B27. Cells were maintained in B27 medium for up to 45 days with a half media change every 3 days.

Cells were treated with Aβ after 35 days of differentiation (unless stated otherwise) for up to 48 hours. For neurons treated with AraC, 5μM was added to the medium at day 25 and removed on day 28.

2.2.2 Neuronal characterisation

2.2.2.1 Immunocytochemistry

Cells were fixed with 4% paraformaldehyde (PFA) (made up with phosphate-buffered saline (PBS) from 16% PFA; Alfa Aesar) in PBS for 10 min. For neurons differentiated for 35 days or more PFA was made up to 8% and was added to the media in the wells at a final concentration of 4% for 15 min. Cells were washed and permeabilised with 0.1% Triton X-100 (ThermoFisher Scientific) in 1 x tris-buffered saline (TBS), incubated at RT for 10 min. Non-specific antibody binding was blocked by incubating cells in 4% normal donkey serum in 1 x TBS for 30 min at RT. Primary antibodies were then added and incubated overnight at 4°C. Cells were washed with TBS and incubated with AlexaFluor secondary antibodies at 1:1000 in TBS for 2 hours at RT. Cells were washed with TBS and incubated with 1mg/ml Hoechst 33342 (Sigma Aldrich, Gillingham, UK) at 1:2000 for 20 seconds. Cells were then washed and stored at 4°C in TBS for imaging with an automated microscope.

2.2.2.2 Neuronal markers

Neural stem cell differentiation markers were used to characterise the cells during the differentiation protocol. PAX6 and SOX2 antibodies (mouse 1:500; Life Technologies, Paisley, UK) were used to stain for neural progenitor cells. Anti-β-III tubulin (1:1000 mouse; BioLegend 801201) stained neuron-restricted progenitors and post-mitotic neurons. To investigate maturation rate day 45 neurons were stained with anti-synapsin (1:500 rabbit; Cell Signalling D12G5) to detect synapse formation (Figure 10) and anti-TBR1 (1:200 rabbit; Abcam ab31940) to confirm cortical specificity (Figure 11).

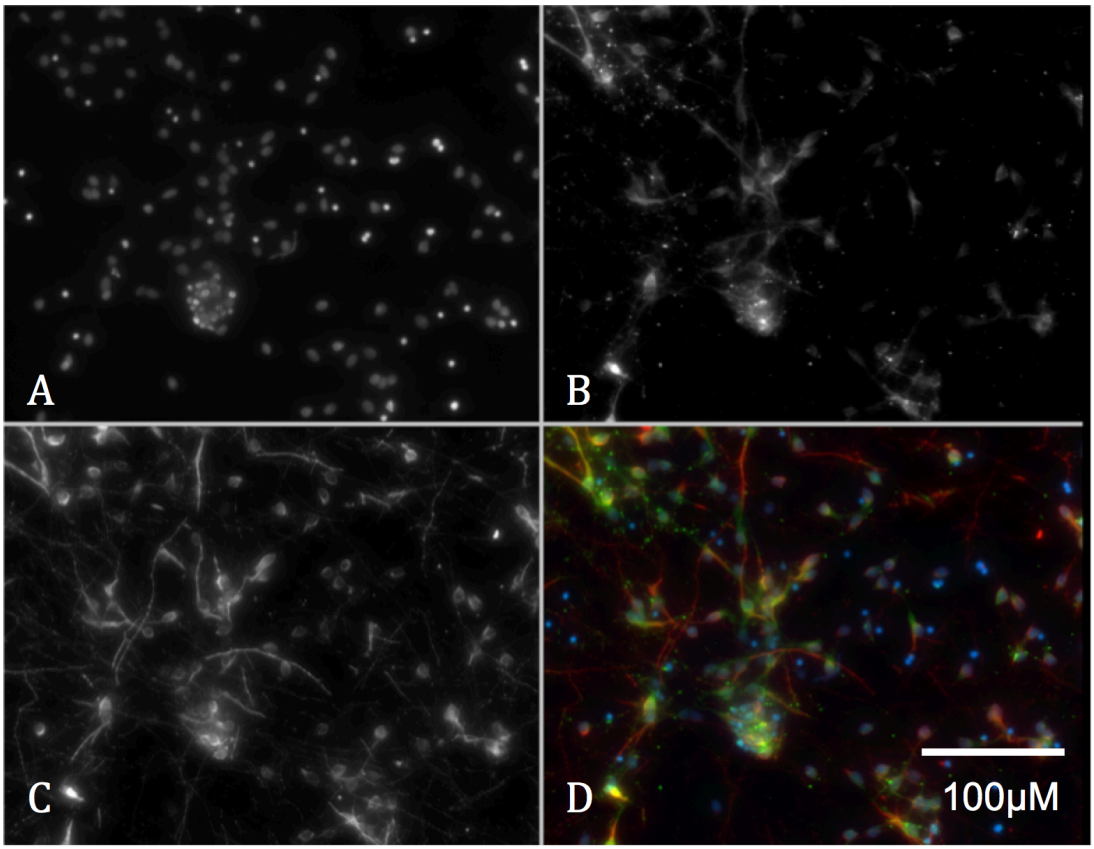

Figure 10. Synapsin and β-III tubulin in day 45 neurons. A. Hoechst (blue). B. Synapsin (green). C. β-III tubulin (red). D. merge of all channels.

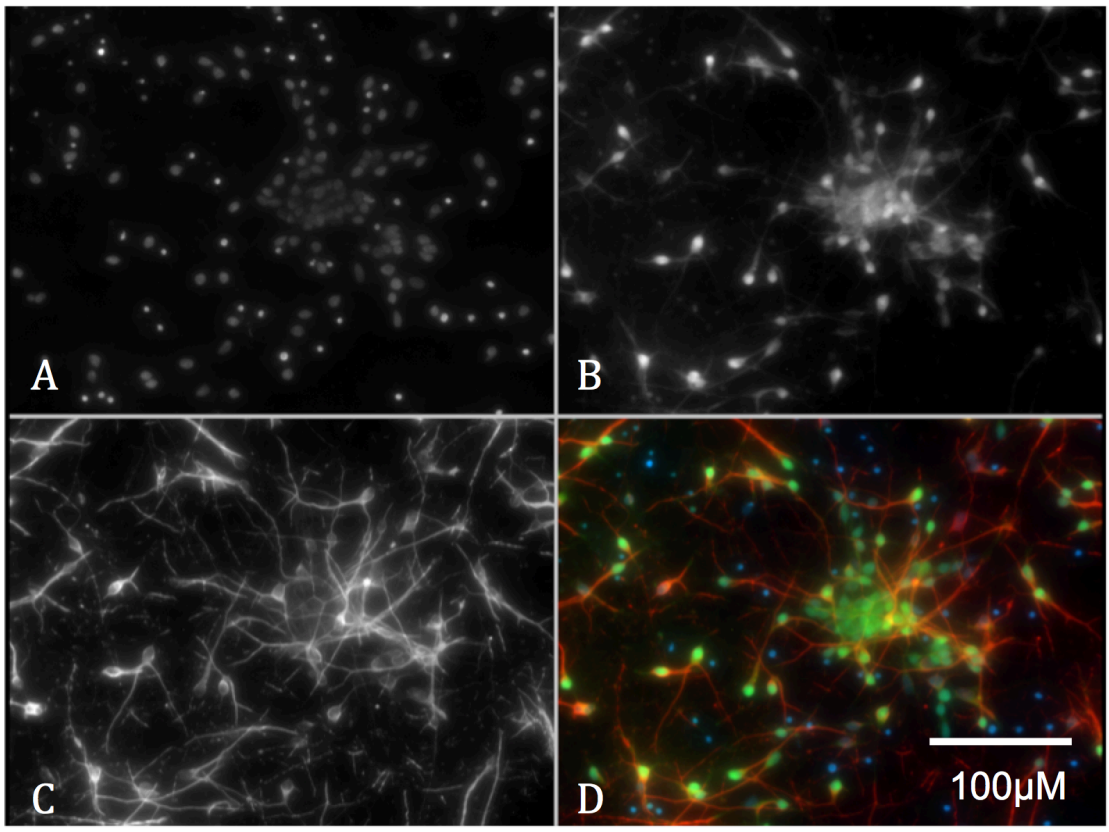

Figure 11. TBR1 and β-III tubulin in day 45 neurons. A. Hoechst (blue). B. TBR1 (green). C. β-III tubulin (red). D. merge of all channels.

2.2.2.3 Non-neuronal cell types

The presence of astrocytes in neuronal cultures follows the maturation of cortical neurons, with mature neurons generated in the second month, and astrocyte maturation occurring in the third month in iPSC neuronal differentiation protocols (Liu and Zhang, 2011). Understanding the percentage of cells that are non-neuronal is important when considering the results of assays. To study neuronal toxicity pathways, cultures with high purity are preferable, however, in the course of neurogenesis neural progenitors, neurons, astrocytes, and oligodendrocytes will all be generated sequentially.

To reduce the presence of non-neuronal cells in the cortical neuronal cultures, cytosine β-D-arabinofuranoside (AraC) was added to cultures 48 hours after terminal plating at 5μM (day 24 neurons). AraC interferes with DNA synthesis, disrupting cell divisions. Anti-vimentin (1:400 rabbit; Cell Signalling D21H3) was used to detect non-neuronal cells, as it is expressed in astrocytes and their precursors (Lin and Goldman, 2009), but absent from neurons. Neurons at 35 days would be too immature to express typical astroglial markers and so vimentin was used as a general marker for non-neuronal cells. Vimentin-positive cells as a proportion of total Hoechst-stained cells were counted using the ThermoFisher Scientific CellInsight Personal Image Cytometer with iDEV software. There was a non-significant reduction in the percentage of vimentin-positive cells at day 30 of differentiation in cultures treated with 5μM AraC compared to controls ($p=0.1057$; Figure 12A). This non-significant trend may be because of cell variability between differentiation experiments. The average vimentin-positive cells in cultures with 0μM AraC was 7.1%, compared to 2.1% in the 5μM AraC treated condition. The co-staining of vimentin with SOX2 (1:250 goat; Santa Cruz Biotechnology Y-17) suggests that the non-neuronal cells in the cultures are neuronal progenitor cells (Figure 12B).

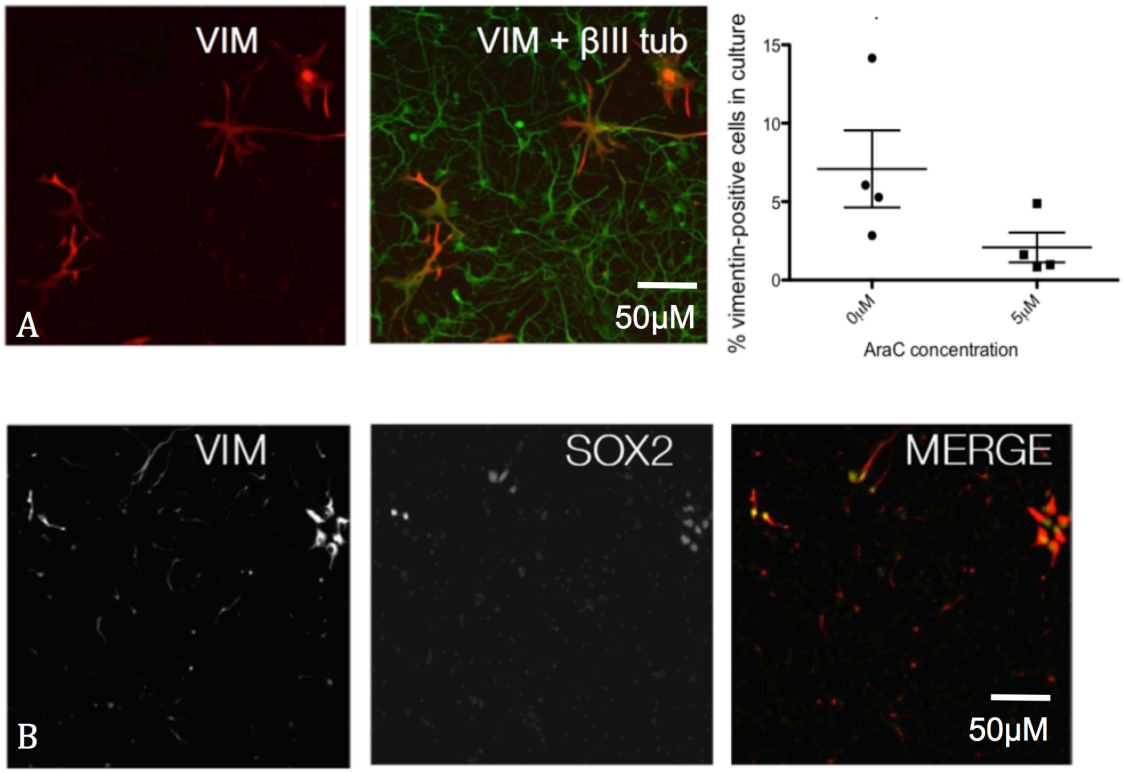

Figure 12. The percentage of non-neuronal cells in cortical neuronal cultures at day 30. A. Vimentin staining (red) of non-neuronal cells and β-III tubulin (green). A small proportion (<10%) of cells in the culture are vimentin positive at day 30. This was not significantly different when cultures were treated with 5μM AraC (n=4 differentiations). B. Vimentin (red) and SOX2 (green) staining shows that the majority of SOX2+ cells were also Vimentin+, indicating that non-neuronal cells are neuronal progenitor cells.

2.2.3 Aβ preparations

Amyloid β-Protein (25-35) trifluoroacetate salt (Bachem, H-1992) was solubilised in sterile water at 2mg/ml and incubated for 2 hours at 37 °C. For addition to wells 20μM $A\beta_{25\text{-}35}$ is equal to 21.2μg/ml, with the final dilution of 1:95 into media.

Amyloid β-Protein (35-25) trifluoroacetate salt (Bachem, H-2964) was used as the control peptide in experiments using $A\beta_{25-35}$ at a concentration of 20μM, and was prepared as $A\beta_{25-35}$.

$A\beta_{1-42}$ peptide was purchased from Dr. David Teplow (UCLA, California, USA) and was prepared by the Lovestone lab as described in Tizon et al. (2010). It was first resuspended in 100% 1,1,1,3,3,3 hexafluoro-2-propanol (HFIP) at a final concentration of 1 mM. The peptide was homogenised using a Teflon plugged Hamilton syringe and HFIP was evaporated in a SpeedVac. $A\beta_{1-42}$ stocks were frozen at -20 °C until 48 hours before treatment. $A\beta_{1-42}$ was resuspended in dimethylsulfoxide (DMSO) at 5μM and sonicated for 10 min. $A\beta_{1-42}$ oligomers were prepared by dilution in PBS to 400μM and 2% sodium dodecyl sulphate (SDS) in H_20 was added 1:10. After 24 hours incubation at 37 °C PBS was added to a final concentration of 100μM. $A\beta_{1-42}$ oligomers were incubated at 37 °C for 18 hours before adding to cell media at concentrations between 1μM and 10μM. Characterisation by ultracentrifugation was done for 10μM preparations (Figure 13). DMSO and SDS buffers were used as a control for $A\beta_{1-42}$ treatment at concentrations equal to in 10μM treatment.

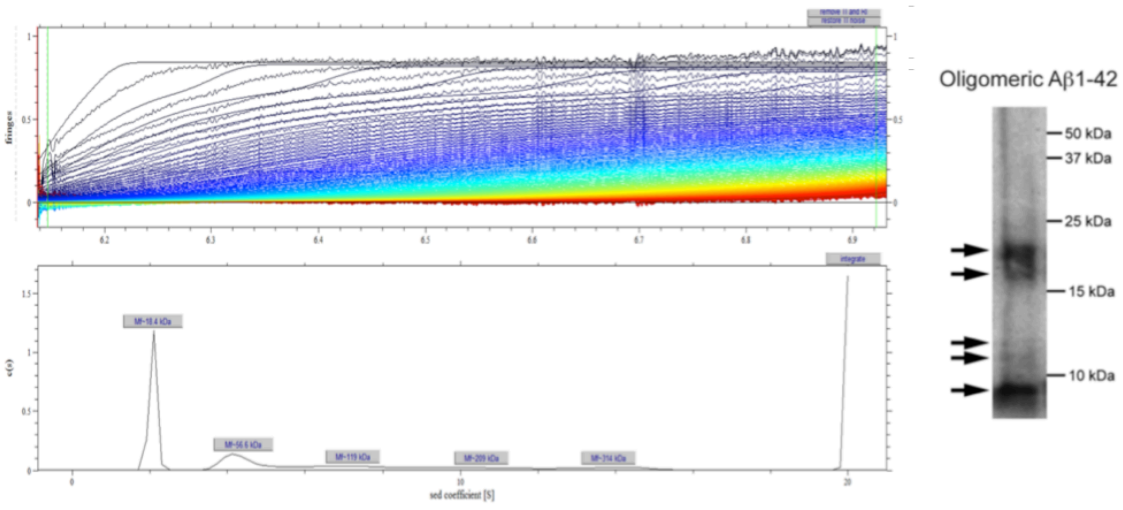

Figure 13. Characterisation of $A\beta_{1-42}$ oligomers with analytical ultracentrifugation. Ultracentrifugation shows most $A\beta_{1-42}$ in the sample to be a single size, 18.4kDa, which is confirmed by western blot.

2.2.4 Immunocytochemistry and live cell stain

After 48 hours of Aβ exposure cells were washed with PBS and fixed with 4% paraformaldehyde (made up with PBS from 16% PFA; Alfa Aesar) in PBS for 10 min. Cells were washed and permeabilised with 0.1% Triton X-100 (Fisher) in tris-buffered saline (TBS; Sigma Aldrich, Gillingham, UK) for 10 min. A 1 hour incubation with 5% donkey serum (DS; Sigma Aldrich, Gillingham, UK) in TBS was used for blocking. Cleaved caspase-3 (cc3) monoclonal primary antibody (1:500 rabbit; Cell Signalling Technology) was used for the Aβ toxicity assay at 1:500 in TBS with 1% DS overnight at 4°C. Cells were incubated with AlexaFluor 488 anti-rabbit secondary antibody at 1:500 in TBS for 2 hours at RT. Cells were washed with TBS and incubated with 1mg/ml Hoechst 33342 (Sigma Aldrich, Gillingham, UK) at 1:2000 for 20 seconds. Cells were then washed and stored at 4°C in TBS for imaging.

Imaging of live cells was done using Calcein Green AM (CAM; C34852) diluted in media at 10μg/ml, and membrane-permeable Hoechst at 1.6μg/ml. The working solution was then added to wells 1:10 and incubated at 37°C for 20 min to visualise the cell bodies and nuclei.

2.2.5 Imaging assay

ThermoFisher Scientific CellInsight Personal Image Cytometer with iDEV software was used to develop imaging assays. The Cell Health Profiling BioApplication was utilised for detecting intact nuclei and high intensity regions of apoptosis. Images were taken at 10x magnification.

The intact nuclei protocol for channel 1 (Hoechst 350nm) counted nuclei that were considered 'intact'. Nuclei undergoing apoptosis have distinct morphologies, including cell shrinkage and intense staining due to nuclear and cytoplasmic condensation (Elmore, 2007). The software counted all Hoechst-stained nuclei above 25µm in diameter and below a fixed intensity threshold. These were selected by setting the threshold at within 2 standard deviations of the mean of control wells across 3 plates. Nuclei outside of these parameters were considered to be undergoing apoptosis and disregarded. These same settings were applied to each well upon scanning of the plate, removing counting bias.

The apoptosis protocol for cc3 (488nm) selected a circular region of interest around all nuclei and then counted areas with an intensity in channel 2 over a determined value to detect high levels of apoptosis. The threshold set for positive staining must be higher than the highest value observed in the negative staining control.

The neurite length assay was developed from the Neuronal Profiling BioApplication in iDEV. Intact, Hoechst-stained nuclei were selected in channel 1 (350nm) and cell bodies stained with CAM were identified in channel 2 (488nm). Neurites protruding from cell bodies were then traced by the software and the average length across the well measured (Figure 14).

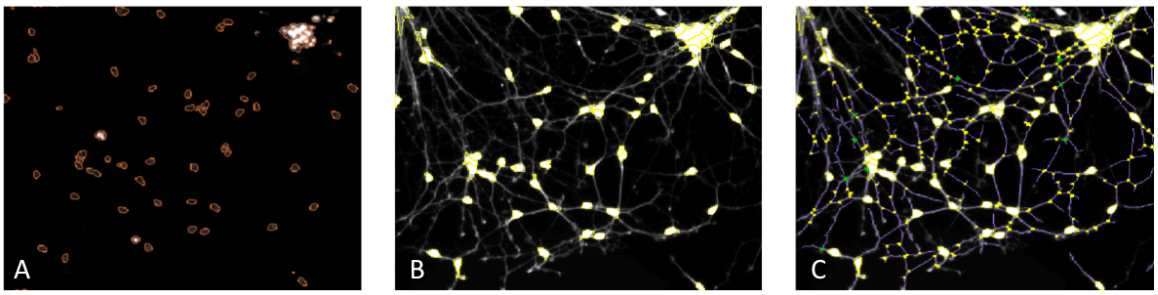

Figure 14. Neurite length assay. A. Nuclei stained with Hoechst are selected in channel 1. B. Cell bodies in channel 2 with nuclei in channel 1 are selected. C. Neuronal processes are traced and measured.

The assays using $A\beta_{1-42}$ were performed using Operetta High Content Imaging System with Harmony® Analysis Software. The neurite length assay in Harmony was developed based on the parameters of the CellInsight-iDEV protocol.

Statistical analysis was performed using GraphPad Prism. Two-tailed, un-paired t-tests were performed to test for differences between neurons treated with Aβ and controls, with significance at $p<0.05$. In figures $p<0.05$ (*), $p<0.01$ (**), $p<0.001$ (***), $p<0.0001$ (****). For all experiments n = 3 independent differentiation experiments, with each graphed concentration point the average of 5 technical replicates (wells in the same 96 wells plate), unless stated otherwise.

2.3 Results

2.3.1 Intact nuclei assay for Aβ-toxicity

The number of live cells present in cultures was employed to ascertain the toxicity of Aβ. Neurons were differentiated for 35 days, treated with $A\beta_{25-35}$ peptides for up to 48 hours, fixed and stained with Hoechst. Nuclei were counted as 'intact' if they were within 2 standard deviations of the mean of control, untreated wells for both nuclei area and average intensity. A 20μM treatment of $A\beta_{25-35}$ peptides for 48 hours resulted in a 19% reduction in intact nuclei number ($p=0.0085$) in neuronal cells from CTR M1 04 (Figure 15). However, shorter time treatments of $A\beta_{25-35}$ did not significantly reduce the number of healthy nuclei. 20μM is a high concentration of Aβ, and an assay that can measure toxic effects of Aβ at lower concentrations or time points would have more physiological relevance and be preferable for this project.

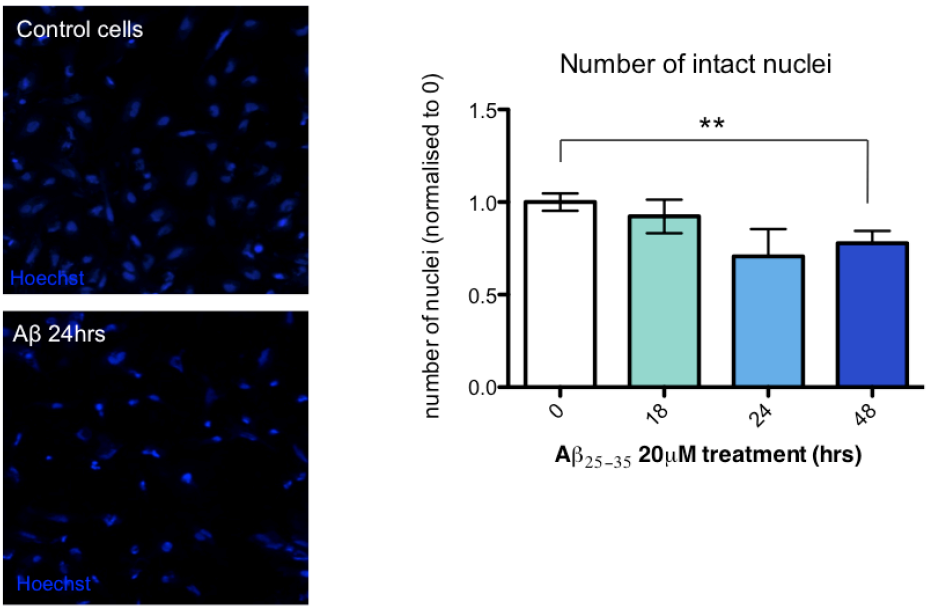

Figure 15. Aβ treatment decreases the number of intact nuclei at 48 hours. Neurons were treated with $A\beta_{25-35}$ or H_20 control and nuclei were stained with Hoechst in 4 independent experiments.

2.3.2 Apoptosis assay for Aβ-toxicity

Apoptosis in neuronal cultures was measured by immunocytochemistry using an antibody for cleaved-caspase 3 (cc3). Cultures were treated at 35 days of neuronal differentiation with $A\beta_{25-35}$ peptides. Intensity of cc3 staining showed significantly increased apoptosis in neuronal cultures treated with $A\beta_{25-35}$ for 24 and 48 hours compared to controls (Figure 16). Neurons treated for 48 hours with 20μM had the highest increase in cc3 intensity across wells, a 36.5% change ($p=0.0087$). 10μM Aβ treatment also caused an increase in cc3 intensity at 24 hours ($p= 0.0235$).

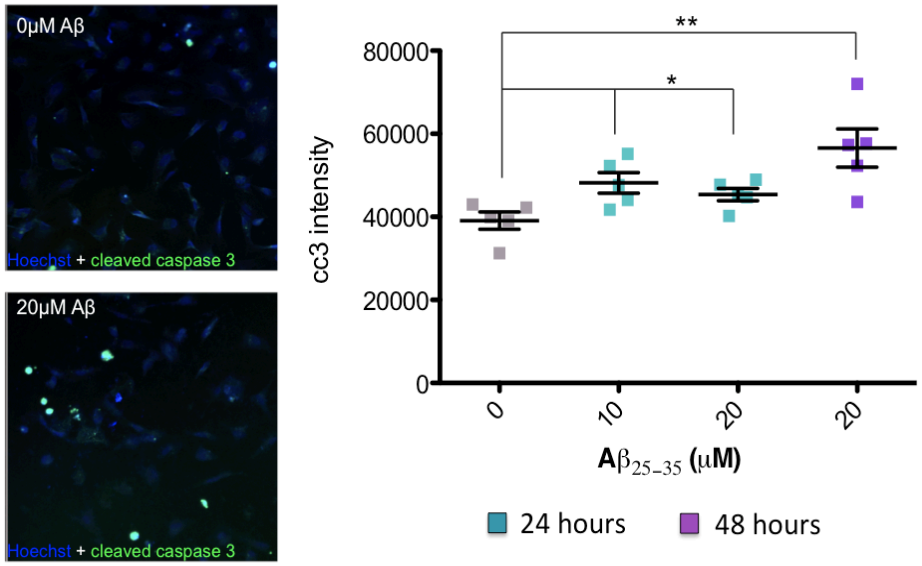

Figure 16. Aβ treatment increases apoptosis at 24 hours. Neurons were treated with $A\beta_{25-35}$ or H_20 control for 24 or 48 hours and cells were stained with cc3 antibody (1:500) prior to imaging with the Thermo CellInsight. Image panels show neurons stained with Hoechst and cc3, untreated and treated with 20μM for 48 hours.

2.3.3 Neurite length assay for Aβ-toxicity

The length of neuronal processes was measured as a readout of cell toxicity. Neurons were differentiated for 35 days and treated with $A\beta_{25-35}$ peptides for 6 or 48 hours. Neurons were incubated with the live cell stain Calcein AM (CAM) and Hoechst for imaging. A concentration curve was established for 6 hours of treatment and 48 hours of treatment (Figure 17). Length of the neurites was significantly reduced after 6 hours of Aβ treatment at 10μM and 20μM. Neurite length was significantly decreased above 10μM for neurons treated for 6 hours ($p=0.043$) and neurite length was significantly decreased above 5μM for neurons treated for 48 hours ($p=0.0163$).

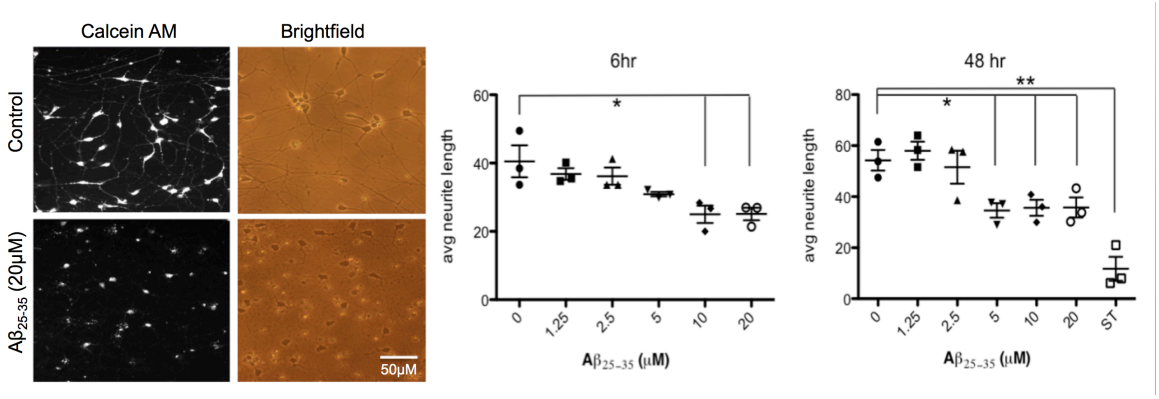

Figure 17. $A\beta_{25-35}$ treatment decreases length of neuronal processes. Neurons were treated for 6 or 48 hours with $A\beta_{25-35}$ concentrations up to 20μM, or control peptide $A\beta_{25-35}$ at 20μM (labelled 0μM), and stained with live cell dye CAM. Average neurite length was measured by the Thermo CellInsight. Image panel shows neurons untreated and treated with 20μM for 48 hours with live cell stain and in brightfield.

The neurite length assay offers a sensitive measure of toxicity in iPSC-derived neurons. The assay demonstrated that 5μM of $A\beta_{25-35}$ for 48 hours is a sufficient dose for a significant toxicity effect and therefore this concentration can be used in subsequent experiments. Moreover, the simplicity of this assay makes it useful for characterising the toxicity of Aβ preparations. A log curve for a 6 hour $A\beta_{25-35}$ treatment shows that the IC50 fell at 5μM (with a maximum effect at 20μM), suggesting that this dose may be useful for assessing compounds to reverse this toxicity in the future (Figure 18).

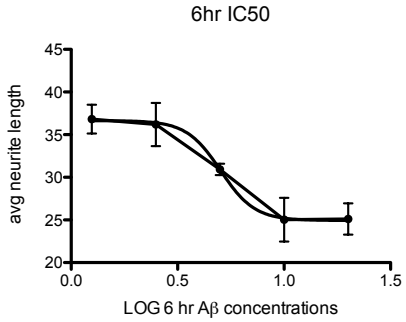

Figure 18. IC50 curve for 6 hour $A\beta_{25-35}$ treatment. Neurons were treated with $A\beta_{25-35}$ concentrations up to 20µM for 6 hours in 3 independent experiments and the length of the neuronal processes was measured by the Thermo CellInsight. LogIC50 = 0.70 (IC50 = 5.033µM).

The neurite length assay was verified with $A\beta_{1-42}$ oligomers to determine the corresponding minimum significant dose for toxicity in a 48 hour treatment. Neurons were differentiated for 35 days and treated with 0-20µM of $A\beta_{1-42}$ oligomers. After 48 hours incubation with Aβ neurons were stained with CAM and imaged. $A\beta_{1-42}$ oligomers were also shown to be toxic to neurons causing significantly reduced neurite length in the treated wells (Figure 19). $A\beta_{1-42}$ significantly reduced the length of the neurites at 1.25µM ($p=0.0020$). The robust readout for toxicity of the neurite length assay with $A\beta_{1-42}$ suggests that this assay can be used for characterising future $A\beta_{1-42}$ preparations and a 1.25µM dose can confidently be used to induce toxicity in the human iPSC-derived neurons.

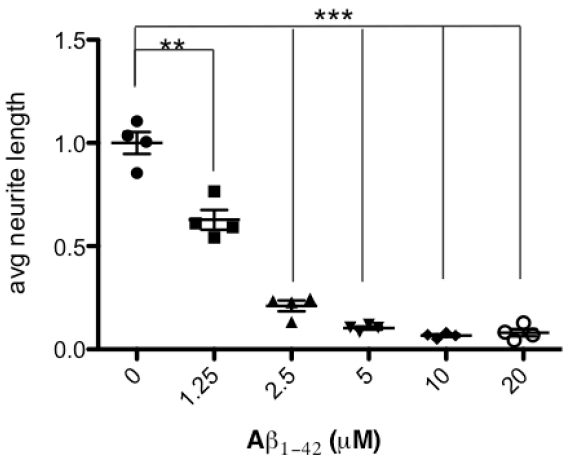

Figure 19. $A\beta_{1-42}$ treatment decreases length of neuronal processes. Neurons were treated with 0-20μM $A\beta_{1-42}$ for 48 hours or control DMSO and SDS equivalent to largest dose (labelled 0μM) and imaged with CAM live cell stain. Average neurite length was measured by Thermo Cell Insight machine.

2.3.4 Non-neuronal cells in Aβ-toxicity

The effect of non-neuronal cells on Aβ-toxicity was measured using the neurite length assay. Cultures were treated with 0 or 5μM of AraC, an inhibitor of proliferation. Figure 12 indicated that AraC did not significantly reduce the number of proliferating cells in the cultures. Moreover, an Aβ-concentration curve showed that there was no difference in the neurite length of cultures treated with AraC compared to those untreated (Figure 20). For both 0 and 5μM AraC conditions the neurite length was significantly reduced at 15 and 20μM of $A\beta_{25-35}$.

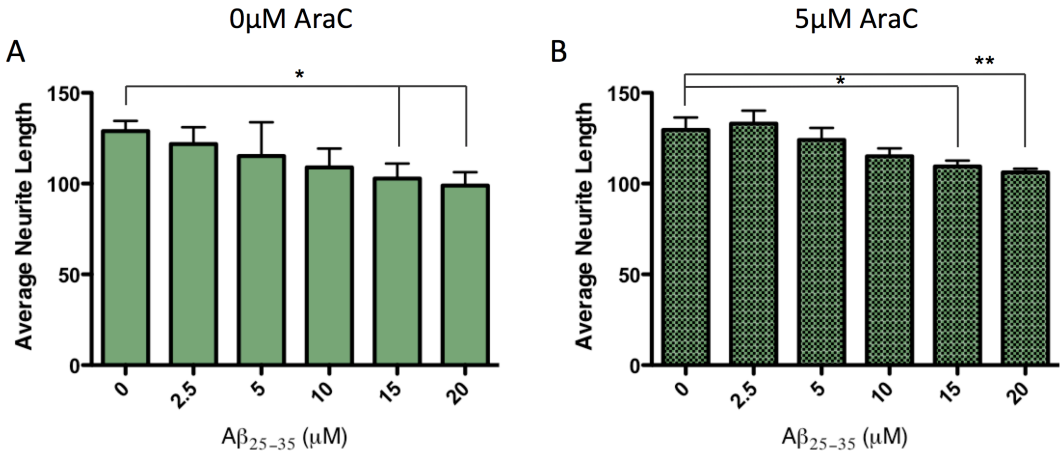

Figure 20. Neurite length is not affected by AraC treatment. A. Neuronal cultures were treated with A. 0μM or B. 5μM of AraC and cultures were treated with $A\beta_{25\text{-}35}$ peptides up to 20μM. Cells were stained with CAM and average neurite length was measured with the Thermo CellInsight.

2.4 Discussion

2.4.1 Aβ reduces neurite length

The Aβ-toxicity shown in rodent cultures in vitro was replicated in human neurons using both $A\beta_{25\text{-}35}$ and $A\beta_{1\text{-}42}$. A key aim for this study was to develop an assay to sensitively and robustly measure Aβ-toxicity in human neurons. The most appropriate candidate assay for measuring Aβ-toxicity was the assay for neurite length. Neuronal processes are reduced prior to apoptosis and cell death, making this a good early and reversible measure of Aβ-toxicity. For a 48hour treatment a decrease in neurite length could be detected at 5μM for $A\beta_{25\text{-}35}$ and 1.25μM for $A\beta_{1\text{-}42}$. These established doses could be used for studying genes involved in Aβ-toxicity in this model human *in vitro* system.

Previous studies show synapse disruption following acute Aβ exposure. The iPSC-derived neurons in this study were 35 days old and so did not yet have functional synapses. The decrease in neurite length is likely to be a good intermediary measure between initial synapse dysregulation and apoptosis. The loss of neuronal connections rather than the decrease in overall cell number measured in the neurite length assay is representative of the synaptic perturbations caused by Aβ with no overall neurodegeneration described in AD patients and animal models. The synaptotoxicity is likely to be a primary event of Aβ oligomers, rather than a later, secondary event caused by neurodegeneration (Mucke and Selkoe, 2012; Shankar et al., 2007). This makes the combination of the iPSC-derived neurons with the neurite length assay a good model for studying the earliest events in AD and the molecular activities that initiate them. The neurite length assay does not require cell death, which makes it a useful tool for screening compounds that can halt or reverse Aβ-toxicity in the future.

An established physiologically relevant concentration of Aβ has not been agreed upon due to differences between individuals, brain regions, and the intrinsic clearance mechanisms *in vivo*. Näslund and colleagues (2000) investigated levels of $A\beta_{1-40}$ and $A\beta_{1-42}$ in the cortex of post-mortem AD brains and estimated amyloid load at 1-3μM. Therefore the 1.25μM for $A\beta_{1-42}$ and corresponding toxicity of 5μM of $A\beta_{25-35}$ established in the neurite length assay can be considered in the physiologically relevant range.

2.4.2 Non-neuronal cells do not affect Aβ-toxicity

This study suggests that the non-neuronal cells present in the cortical cultures did not have a significant impact on the neurotoxic effects of Aβ, as measured by a decrease in neurite length. Non-neuronal cells were not significantly reduced in AraC treated

cultures, which may have been a result of original numbers of these cells in the cultures being low. Aβ-toxicity in neuronal cultures treated with AraC did not have altered toxicity to cells without AraC exposure.

These results may suggest that glial cells are not necessary for Aβ-toxicity, since a neurodegeneration effect can be measured in a high-purity neuronal population. Higher numbers of non-neuronal cells in cultures could potentially alter the speed or magnitude of toxicity, and further experiments in more mature cultures with higher populations of non-neuronal cells would be required to investigate this. AraC allowed the reduction of vimentin-positive cells to 2% in this system, at least two fold lower than other studies that reported Aβ-toxicity in mixed cultures ranging from glia contribution of 4% in mouse primary cultures (Garwood et al., 2011) to 63% in neuroglia cultures from the NT2.D1 cell line (Tarczyluk et al., 2015). Estimates for the proportion of astrocytes as a total of all cells in the brain varies widely. Human iPSC models with a higher number of astrocytes will be able to more accurately model the AD brain, whereas the high purity neuronal model in this project is a good system to identify neuronal-specific effects of Aβ.

Chapter 3 Investigating clusterin-mediated AB-toxicity

3.1 Introduction

3.1.1 Clusterin-mediated Aβ-toxicity

A number of genes have been discovered as important in mediating tau phosphorylation and neuronal death downstream of Aβ deposition. The proteins clusterin and Dkk1 have been found to have a role in this Aβ-driven cascade in amyloid transgenic mouse models of AD (DeMattos et al., 2002; Rosi et al., 2010; Purro et al., 2012). In primary cultures, treatment of neurons with Aβ peptides caused an increase in intracellular clusterin, and a decrease in clusterin in the extracellular media. However, cell stressors other than Aβ had little effect on clusterin levels. Decreasing clusterin expression using siRNA protected neurons from Aβ-induced toxicity, and prevented the increased DKK1 expression caused by Aβ-treatment of cells. Aβ and Dkk1 have been found to induce a number of common genes, including EGR1, suggesting that Dkk1 is important in mediating the effects of Aβ on gene expression. The increased clusterin and Dkk1 levels may be an important mechanism in the Aβ cascade through the regulation of the Wnt signalling pathway (Killick et al., 2014).

3.1.2 Aims

The aim of the work described in this chapter was to investigate whether Aβ exposure caused changes in the protein levels and gene expression of the main targets of the proposed Aβ cascade pathway: CLU, DKK1 and EGR1. These genes have been identified

as important genes in the amyloid cascade in rodent primary cell cultures by Killick and colleagues (2014) and it is important to repeat these investigations in human neurons to verify whether this pathway could be a potential target for therapeutic strategies in AD.

Human iPSC-derived neurons were treated with Aβ peptides and the protein and gene expression levels of the genes of interest were measured. Based on the results in primary cultures, Aβ exposure was predicted to cause an increase in intracellular clusterin, paired with a decrease in extracellular clusterin levels, and an increase in Dkk1 protein levels. Elevated expression of CLU, DKK1 and EGR1 genes were expected in the Aβ-treated iPSC-derived neuronal cultures.

3.2 Methods

3.2.1 Cell lysates

Neurons were differentiated for 35 days in 6 well plates at 20,000 cells/cm^2 as described in Chapter 2.1.5. $A\beta_{25-35}$ peptides at a concentration of 20μM were added to neurons up to 48 hours prior to cell lysis. For protein samples all media was removed from wells and plates were put on ice. 200μl of 4x Laemmli Sample buffer was added to each well and cells were scraped and transferred to an eppendorf tube. Samples were vortexed, boiled at 95°C for 5 mins and centrifuged at 10,000RPM for 1 minute. Supernatant was transferred to new tubes for storage at -20°C.

Samples of cell culture media from the same wells were also collected and stored at -20°C. These were then mixed 1:1 with 4x Laemmli Sample buffer, boiled at 95°C for 5 mins and centrifuged at 10,000RPM for 1 minute prior to loading in the gel lanes.

Samples for qPCR were collected in TRIzol Reagent. All media was removed from wells and 3 wells were pooled per sample (approximately 2.5µg RNA total). 350µl TRIzol was added to each well. Cells were scraped and 1ml of TRIzol was transferred to an eppendorf, pipetting up and down 5 times to increase homogenisation of sample. TRIzol samples were left to stand for 1 minute and then stored at -80°C until RNA extraction (Section 3.2.3.1).

3.2.2 Western Blotting

3.2.2.1 Electrophoresis and protein transfer

Equal volumes of laemmli-protein samples from Section 3.2.1 were loaded into NuPAGE® Novex® 4-12% Bis-Tris gels at 25µl each per well (50µl for media samples) with 5µl Novex® Sharp Pre-stained protein ladder. Gel electrophoresis was run with Bolt MES running buffer at 200V for 30 min at RT or until the protein migration front reached the bottom of the gel. The protein was transferred to a nitrocellulose membrane by dry electroblotting using the iBlot® 2 Gel Transfer Device, Life Technologies, with transfer at 20V for 7 min.

3.2.2.2 Protein detection

The membrane was blocked with 5% skimmed milk in TBS for 1 hour prior to incubation in TBS-Tx with 1% skimmed milk and the primary antibody (anti-clusterin, 1:1000 (Santa Cruz); Dkk1, 1:1000 (Abcam)). The membrane was incubated overnight at 4˚C. 3 x 10 minute washes with TBS-Tx solution were performed and the membrane was stained

with the secondary antibody (AlexaFluor800 donkey anti-mouse / AlexaFluor680 donkey anti-rabbit, 1:5000 dilution) in TBS-Tx with 1% skimmed milk for 2hours. Membranes were washed with 3 x TBS-Tx prior to imaging.

To ensure even loading of the samples, the same membrane was probed with α-tubulin antibody (rat; Abcam) or β-actin (mouse; Abcam) at a 1:10 000 dilution overnight at 4˚C. Membranes were probed with AlexaFluor680 donkey anti-rat or AlexaFluor800 donkey anti-mouse secondary antibody at 1:50 000 dilution for 1 hour before imaging. Protein detection was performed using Li-Cor Odyssey infrared imaging system, Cambridge, UK.

3.2.2.3 Protein quantification

Protein quantification was carried out using ImageJ software. The expression of the protein of interest was calculated by measuring the integrated density for each band and normalising against α-tubulin to account for varying protein loads between samples. Two-tailed, independent t-tests were performed in Prism 6 to test for differences between neurons treated with Aβ and controls, with significance determined as $p<0.05$ (*), $p<0.01$ (**), $p<0.001$ (***), $p<0.0001$ (****).

3.2.3 Quantitative real-time Polymerase Chain Reaction (qPCR)

3.2.3.1 RNA extraction and clean-up

TRIzol samples were thawed at RT for 5 min. Samples were washed with chloroform at a 5:1 ratio (200µl) and inverted 10 times. Tubes were incubated at RT for 3 min where the

layers started to separate out with a RNA layer on the top. After centrifugation at 10,000 RPM for 5 min at 4°C, the aqueous top layer was transferred into a new eppendorf tube, isopropanol was added at 2:1 ratio to chloroform (500 µl) and mixed by inversion 10 times. Tubes were incubated for 15 min at RT whilst isopropanol precipitated out nucleic acids. Samples were centrifuged at 13,000 RPM for 15 min at 4°C. Isopropanol was discarded leaving pellet at the bottom, which was then washed in 80% ethanol and spun down at 13,000 RPM for 5 min at 4°C before air drying pellet until it turns clear (10-15 min). The pellet was re-suspended by gentle flick-mix in 100µl molecular grade, RNAse-free H_20 (Sigma Aldrich, Gillingham, UK) and left on ice for 15 min before adding 10µl of 3M Sodium Acetate (R1181, ThermoFisher Scientific, Paisley, UK) and 300µl of 100% ethanol. RNA was incubated at -80°C for 30 min or overnight. Samples were thawed and spun down at 13,000 RPM for 15 min at 4°C. The ethanol was poured off and RNA was washed with 500µl 80% ethanol and centrifuged at 13,000 RPM for 5 min at 4°C. RNA pellet was air dried, resuspended in 30µl of H_20 and left on ice for 15 min. RNA was stored at -80°C.

3.2.3.2 Quantification of RNA concentration and purity

The concentration and purity of extracted nucleic acids was measured using the NanoDrop™ 1000 spectrophotometer (ThermoFisher Scientific, Paisley, UK). The 260/280 and 260/230 absorbance ratios were used to assess the purity of RNA. A ratio of ≥2.0 for 260/280 and 260/230 was considered pure for RNA. If a sample did not meet these standards, the sample was re-precipitated in 3M Sodium Acetate as described in Section 4.3.2.1 and clean-up was repeated.

3.2.3.3 DNAse treatment of RNA

To remove residual genomic DNA contamination, all RNA samples were treated with TURBO DNA-*free*™ (AM1907). 2µg of extracted RNA was combined with 1µl of TURBO DNase, 2.5µl of TURBO DNase Buffer and made up to 25µl with nuclease-free H_20. The sample was incubated for 50 min at 37°C. The DNase was subsequently inactivated by incubation with 6µl of DNase Inactivation Reagent at RT for 5 min, vortexing every 30 seconds. The sample was then centrifuged at 13,000 RPM for 90 seconds and the supernatant was transferred to a new eppendorf tube and stored at -80°C.

To verify complete removal of genomic DNA, 1µl of DNase treated RNA was saved for use as template for qPCR using a GAPDH primer pair. The RNA samples were run alongside a no-template negative control and only samples without amplification were reverse transcribed.

3.2.3.4 Reverse transcription

Complimentary DNA (cDNA) was synthesised using SuperScript® III Reverse Transcriptase (18080-044). 250ng of random hexamers (N8080127) and 1mM dNTP mix (R0191, ThermoFisher Scientific, Paisley, UK) was added to 1µg of DNase-treated RNA, and made up to 13µl with nuclease-free H_20 (Sigma Aldrich, Gillingham, UK). The mix was incubated at 65°C for 5 min to denature RNA secondary structure and then incubated on ice for 1 minute. The mix was made up to 20µl with 1x First Strand Buffer (Life Technologies, Paisley, UK), 5mM Dithithretiol (18080-044), 40 units RNaseOUT™ (10777), 200 units SuperScript® III Reverse Transcriptase (Life Technologies, Paisley, UK) and 3µl of nuclease-free H_20. Samples were incubated in a PCR machine on an RT

protocol: 25ºC for 5 min, 50ºC for 1 hour (optimal temperature for Superscript® III), 55ºC for 30 min (removal of any secondary structures) and 70ºC for 15 min (termination of the reaction). Samples were diluted in 100µl nuclease-free H_20 for qPCR.

3.2.3.5 Primer design

PCR primer pairs were designed to amplify an amplicon of approximately 100 base pairs. DNA sequences for genes of interest were obtained from the University of California, Santa Cruz, genome browser (http://genome.ucsc.edu) and primers designed using Integrated DNA Technology (IDT) software (http://www.idtdna.com/primerquest/home/index). GC content was kept between 40% and 60% and primers were designed with an annealing temperature between 55ºC and 65ºC with only 1ºC between the pair. They were designed to have minimal self-complementarity and no complementarity to the other primer and were tested for single-peak melt curves using uMelt software (https://www.dna.utah.edu/umelt/umelt.html). qPCR primers were designed to span large exon boundaries to prevent the amplification of any residual genomic DNA. GAPDH primer pair used to test for genomic DNA contamination did not span exon-boundaries.

Oligonucleotides were synthesised by IDT. They were re-suspended in nuclease-free H_20 to a stock concentration of 100 µM and used at a working concentration of 2 µM.

3.2.3.6 qPCR protocol

White-welled qPCR plates (AB-0900/W, ThermoFisher) were exposed to UV for 10-20 min in the UV Stratalinker 1800 (Stratagene) to crosslink DNA prior to plating, in order to damage possible contaminant DNA and prevent its amplification during PCR. The reaction comprised of 33ng template nucleic acid (4 µl), 10µl 2x SYBR® Green PCR Master Mix, 0.2 µM primer mix (3µl), and nuclease-free H_20 to make a total reaction volume of 20µl. All PCR reactions were carried out with one negative control for each primer pair, where H_20 was used as the template. qPCR reactions were carried out on a Chromo4™ Real-Time PCR detector (Bio-Rad, Bath, UK) using the following parameters:

	45 cycles		
Initial denaturation	Denaturation	Annealing	Extension
95ºC for 15 min	95ºC for 30 seconds	60ºC for 30 seconds	72ºC for 30 seconds

Fluorescence was recorded at the end of each cycle. A melt curve was carried out from 60ºC-95ºC with a 10 second hold and a plate read at every 1ºC increment. Each reaction was carried out with a technical replicate and with 3 biological replicates.

3.2.3.7 Primer testing

Agarose gel electrophoresis (Section 3.2.4) was used to test the integrity of extracted nucleic acids as well as to assess the level and specificity of PCR amplification by designed primers. To test primers qPCR was run with both cDNA and H_20. Only primers with bands specifically for cDNA were used in qPCR. Reference genes were selected from Vandesompele et al. (2002) and de Jonge et al. (2007) and HPRT1, RPL27 and RPL30 were selected for efficiency and specificity as house keepers that should be stable in neuronal samples. All primer sequences used in the results of this chapter are shown in Table 1.

Table 1. qPCR primer sequences for target genes and housekeeper genes

Target gene	**Forward (5' to 3')**	**Reverse (5' to 3')**
CLU	CAGCCCTTCCTTGAGATGATAC	GGAACAGTCCACAGACAAGAT
DKK1	CGCGCCGGGAATCCTGTACC	CGCACGGGTACGGCTGGTAG
EGR1	GCCAGTATAGGTGATGGGGG	ACCTGACCGCAGAGTCTTTTC
GAPDH	GTGACCACTGGCATTCATTTG	TCCTCCCTCTTCCGAGATTT
HPRT1	TGACACTGGCAAAACAATGCA	GGTCCTTTTCACCAGCAAGCT
RPL27	ATCGCCAAGAGATCAAAGATAA	TCTGAAGACATCCTTATTGACG
RPL30	ACAGCATGCGGAAAATACTAC	AAAGGAAAATTTTGCAGGTTT

3.2.4 Agarose gel electrophoresis

Agarose gels were made by melting agarose (A9539, Sigma Aldrich, Gillingham, UK) into 1x tris-acetate-EDTA (TAE) buffer. A 1.5% concentration of agarose gel was made to resolve amplicons of around 100bp. After cooling, ethidium bromide (1% solution in water, 111615, MerckMillipore) was added at 1µl/100 ml of TAE and the gel was left to set in a mould. Samples were mixed with 1x DNA Loading Dye (R0611, ThermoFisher Scientific, Paisley, UK) before being loaded into the wells and were run alongside an appropriate sized DNA ladder (100bp). Electrophoresis was carried out at 100V for approximately 20 min or until desired separation was achieved. Gels were analysed by ultra violet trans-illumination using the BioSpectrumAC Imaging System (UVP) and imaged using the Vision Works LS software (UVP).

3.2.4.1 qPCR analysis

qPCR data files were opened in Opticon Monitor™ (Bio-Rad), where the threshold was selected and melting profiles were assessed. The Pfaffl mathematical model for relative transcript quantification was used for data analysis using cycle threshold (CT) values and efficiency values (Pfaffl, 2001):

$$\text{Ratio} = \frac{(E_{target})^{\Delta CT_{target}\,(control - sample)}}{(E_{ref})^{\Delta CT_{ref}\,(control - sample)}}$$

In the Pfaffl formula ΔCT_{target} = target gene cycle threshold, ΔCT_{ref} = mean of reference gene CTs, and E = PCR efficiency. This method enables relative quantification of a target gene in comparison to an endogenous standard, the housekeeper genes and a control reference sample. Statistical analysis was carried out in Prism 6. The Kolmogorov-Smirnov test was used to test data sets for normality. Comparisons of relative expression using the Pfaffl method in Aβ-treated cells compared to controls were performed using unpaired, two-tailed t-tests with 95% confidence intervals.

3.3 Results

3.3.1 Intracellular clusterin levels

Neurons exposed to a 48hour $A\beta_{25-35}$ treatment had increased levels of intracellular clusterin compared to untreated neurons as measured by western blotting (Figure 21). Clusterin inside the cell was higher in neurons treated with Aβ in 4 independent experiments (each 1 well from 4 independent differentiations) when normalized against α-tubulin levels to account for differences in protein load ($p = 0.0158$). The increased intracellular clusterin may be a result of increased clusterin expression or a reduction in secretion or degradation of the protein.

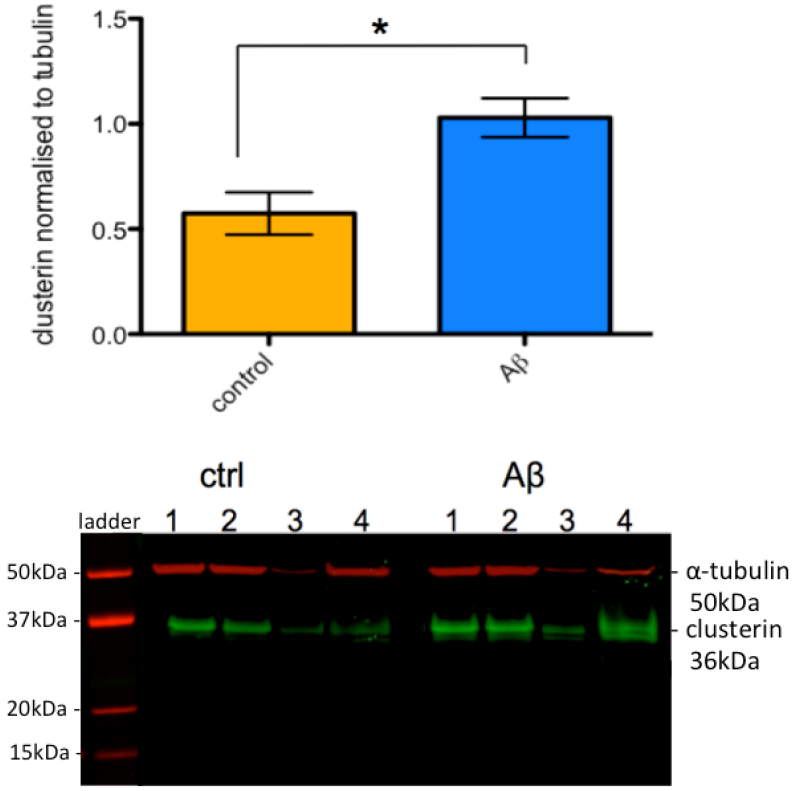

Figure 21. Intracellular clusterin levels are higher in Aβ-treated neurons. Neurons from 4 wells from 4 independent differentiations were treated with 20uM $A\beta_{25-35}$ or the control $A\beta_{35-25}$ for 48 hours and protein levels were measured by western blotting. Clusterin levels normalised to tubulin are shown with SEM and unpaired t-tests were performed.

3.3.2 Extracellular clusterin levels

Cultures exposed to $A\beta_{25-35}$ for 48 hours did not have significantly reduced levels of clusterin protein in the cell culture medium (Figure 22). Western blotting of media from 4 wells of neurons from different differentiation experiments that were treated with $A\beta_{25-35}$ or control scrambled peptide for 48 hours did not have different sized protein bands when stained with clusterin antibody. Since extracellular clusterin levels were not significantly affected by Aβ exposure, decreased clusterin secretion by the cells was not the major contributing factor to the increased amounts of the protein intracellularly.

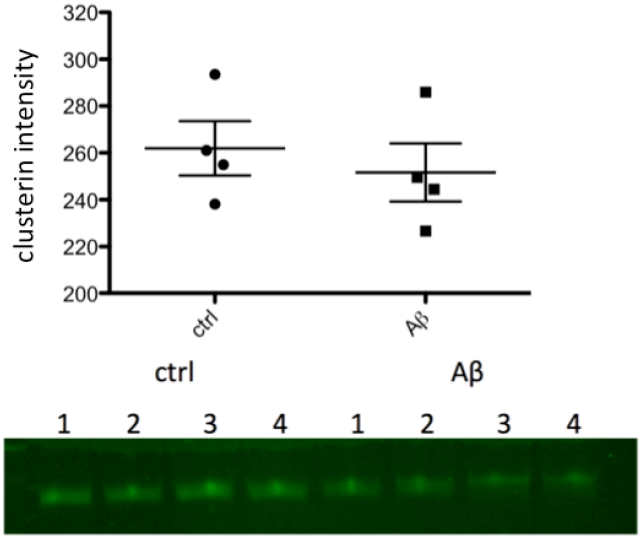

Figure 22. Extracellular clusterin levels are unchanged by Aβ exposure. Medium from 4 biological replicates of neurons treated with 20uM $A\beta_{25-35}$ and untreated neurons were immunoblotted for clusterin and intensity of bands was measured.

3.3.3 Intracellular Dkk1 levels

Dkk1 protein levels were measured by western blotting of neuronal samples from cultures treated with $A\beta_{25-35}$ for 48 hours and untreated neurons. Intracellular Dkk1 levels were not different in Aβ-treated cells compared to controls (Figure 23).

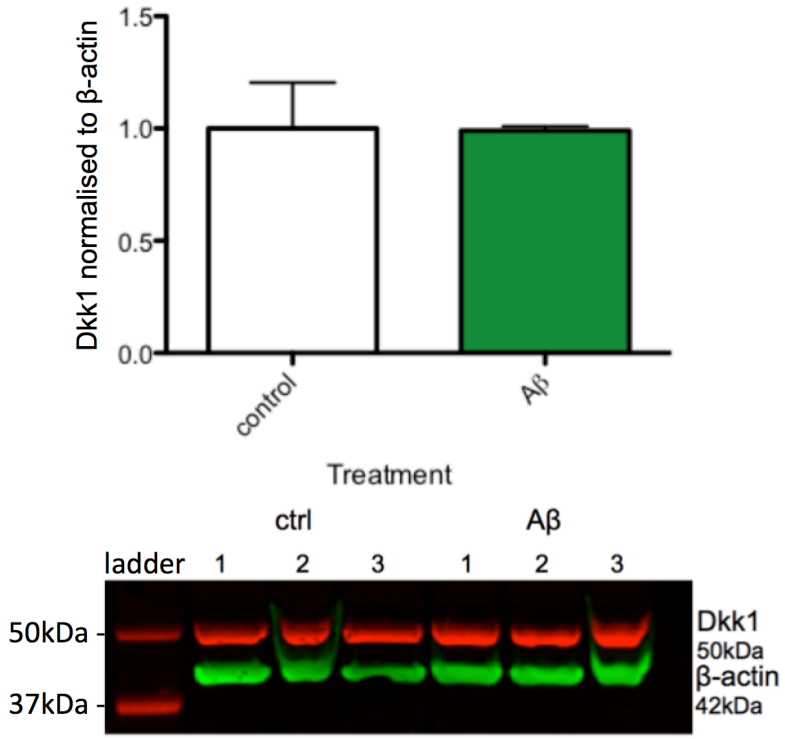

Figure 23. Intracellular Dkk1 levels are not affected by Aβ exposure. Western blots for Dkk1 (red) of neurons treated with 20uM $A\beta_{25-35}$ and untreated controls were normalised to β-actin levels (green). Neuronal cultures from three independent differentiations were treated with $A\beta_{25-35}$ or untreated and Dkk1 levels were normalised to β-actin, and unaired t-tests were performed.

3.3.4 Aβ-induced genes

The expression of CLU, DKK1 and EGR1 was investigated in neurons treated with 20uM $A\beta_{25-35}$ for up to 48 hours. RNA was extracted after 0, 2, 4, 8 or 48 hours of Aβ-treatment for qPCR and expression levels were normalised to 3 housekeeper genes. CLU expression was significantly increased after 48 hours of Aβ exposure (Figure 24A). Earlier time points did not show any change in CLU expression. DKK1 expression was not affected by Aβ-treatment (Figure 24B). EGR1 expression significantly increased at all tested time points, from 2 hours of Aβ exposure through to 48 hours (Figure 24C). The highest

increase in EGR1 expression was a 4.5-fold change (±SEM) after 8 hours of Aβ compared to 0 hour control neurons.

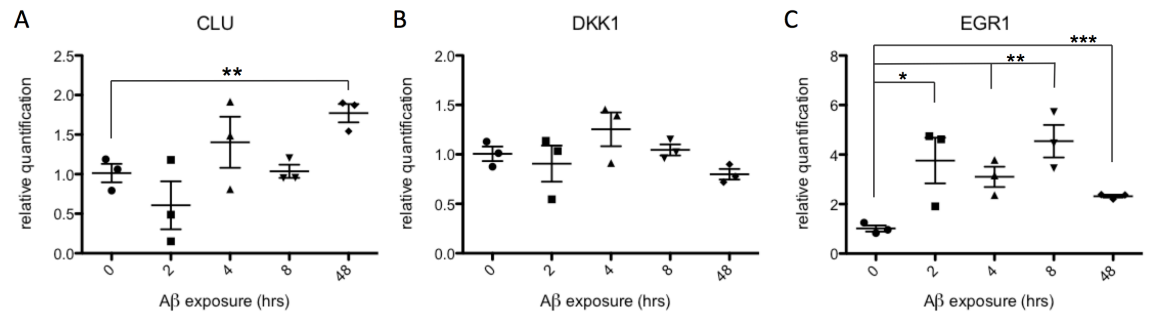

Figure 24. Changes in CLU, DKK1 and EGR1 gene expression in Aβ-treated neurons. Neurons from three independent differentiations were treated with 20uM $A\beta_{25-35}$ for up to 48 hours and expression of genes was quantified relative to housekeeper genes. The relative gene expression levels are graphed normalised to the control 0 hour treatment ±SEM, and unpaired t-tests were performed for all 4 time points.

3.4 Discussion

3.4.1 Intracellular clusterin levels are higher in Aβ-treated neurons

Results from western blotting show the intracellular clusterin protein levels are increased in neurons following a 48 hour Aβ exposure. This confirms the result found in rodent neurons. However, unlike in the rodent neurons, the extracellular levels of clusterin were not decreased, suggesting that the mechanism for this intracellular increase in the protein may differ. Variability between cell culture plates may have been the contributing factor in this result. A paired experiment to look at extracellular clusterin in the media before and after Aβ treatment in the same well (rather than un-paired wells) may result in an

effect when experimental differences between different neuronal differentiations are removed.

Increased clusterin expression was seen by qPCR after 48 hours of Aβ treatment, a result not found by Killick and colleagues (2014) in rodent cells. This increased gene expression may be the cause of the increased protein inside the human neurons, rather than the decreased protein secretion. An experiment to investigate whether the cells have increased uptake of clusterin would be important in elucidating the cause of increased intracellular clusterin. Increased intracellular clusterin is thought to be an important process in the cellular pathology of AD, with important roles in Aβ toxicity, clearance and cell apoptosis (Bettuzzi & Rizzi, 2009; Killick et al., 2014; Bettens et al., 2015).

3.4.2 Intracellular Dkk1 levels are not affected by Aβ exposure

Protein levels and gene expression for DKK1 were not significantly affected by Aβ treatment of the neurons. This differs from the study in rodent cells where DKK1 was found to increase after 20uM $A\beta_{25-35}$ treatment. DKK1 expression levels are very low at baseline, with cycle threshold values over 30, which could make changes in the gene expression or protein level hard to detect. It may also be interesting to experiment more at lower time points. In the rodent culture studies, the increase in DKK1 expression was found at three hours after Aβ-exposure (Killick et al., 2014), and the greatest change in expression in the iPSC-derived neuron results was at the four-hour time point. Repeating these experiments at early time points with larger sample sizes may be beneficial in confirming the roles of these genes. However, this experiment suggests that Aβ-toxicity in human neurons could be acting through a DKK1-independent pathway.

3.4.3 EGR1 expression is increased in Aβ-treated neurons

Killick et al. (2014) found EGR1 is activated by both Aβ and DKK1 and mediates Aβ-toxicity. In human neurons EGR1 expression is also increased by Aβ presence. EGR1 was significantly increased from 2 hours after Aβ exposure and remained increased for 48 hours. EGR1 has been found to have target genes related to synaptic plasticity, protein transport and Aβ processing and therefore could have multiple roles in the Aβ-driven cascade (Koldamova et al., 2014).

3.4.4 Conclusions

Treatment of cells with Aβ caused an increase in intracellular clusterin, as expected based on primary cell culture experiments. Expression levels of CLU were increased with Aβ treatment. Although rodent cells did not show increased CLU expression in response to Aβ, the rodent cells did not respond to Aβ when treated with CLU siRNA to knockdown the gene, suggesting that altered CLU expression may cause the increased intracellular levels in both *in vitro* systems. The extracellular levels of clusterin were unchanged in the iPSC-derived neurons. Whether the uptake of clusterin was altered in response to Aβ would need to be investigated to elucidate the cause of altered clusterin levels.

EGR1 expression was also increased following Aβ exposure. Gene expression levels of DKK1 were not increased. This result was not expected, and may be a result of the very low expression of DKK1 in neuronal cells or the low sample size. The results in this chapter confirm clusterin is activated by Aβ, as supported by studies in rodent models (Killick et al., 2014; Bettens et al., 2015).

Chapter 4 Generation of iPSC lines by CRISPR/Cas9 genome editing

4.1 Introduction

4.1.1 Human cell models of disease

Human cell lines able to model the genetics of disease will offer new possibilities for studying AD. With novel gene editing techniques relevant mutations can now be permanently introduced into human stem cell-based models. Introducing disease-relevant mutations into human cells can test the precise function of genes in disease mechanisms, and links between SNPs identified by GWAS and gene functionality.

Before the advent of precise genome editing it was not possible to propose a stable genetic strategy for dissecting out the clusterin-mediated Aβ toxicity. CRISPR/Cas9 technology allows for Aβ-toxicity to be studied in human neurons expressing clusterin and knockout cells. Deletion of CLU from iPSCs will help resolve the gaps in understanding of how clusterin functions in cells in AD. In this chapter CRISPR/Cas9 technology is used to selectively knock out CLU expression from iPSCs. The APOE gene is also known to have an important role as a major Aβ binding protein, amongst its many other roles including lipid transport, glucose metabolism, and neuroinflammation. A human *in vitro* model to investigate whether APOE isoforms differentially regulate Aβ-toxicity would be useful in determining its mechanisms of action. The design and attempted development of an APOE ε4 homozygous line from the APOE ε3 homozygous iPSC line is also described.

4.1.1.1 CRISPR/Cas9

The CRISPR/Cas9 system was first discovered in bacteria as a defence mechanism to identify and destroy foreign DNA (Sander and Joung, 2014). Cas9 can be directed to almost any target of interest in immediate vicinity of the PAM sequence by design of the 20 base pair guide RNA. In the CRISPR-Cas system derived from Streptococcus pyogenes, used in this project, the target DNA must immediately precede a 5′-NGG PAM. Cas9 produces a DSB, and the locus typically undergoes one of two major pathways for DNA damage repair: NHEJ or HDR. The advantage of CRISPR/Cas9 system over other genome editing strategies includes the ease of customisation of constructs, high targeting efficiency and the ability to facilitate multiplex genome editing (Ran et al., 2013). The CRISPR/Cas9 system will be utilised to specifically disrupt the CLU and APOE genes in an iPSC system, aiding us to study their function and ultimately the molecular pathogenesis of AD.

4.1.2 Aims

The aim of this chapter was to generate iPSC lines to aid investigation into how AD-relevant mutations differentially regulate Aβ processing by human neurons. The first iPSC line developed was a CLU knockout line.

A SNP associated with the clusterin gene has been identified as a major genetic risk factor for AD by GWAS (Harold et al., 2009; Lambert et al., 2009). The T allele of the rs11136000 SNP in the clusterin sequence has been found to be somewhat protective, with rs11136000(T) carriers having a decreased risk for AD with an odds ratio of 0.84 (Carrasquillo et al., 2010). However, the CLU SNP rs111360000 is intronic and has high

linkage disequilibrium, and an exact point mutation causing a functional effect was unknown at the time of this project. Therefore, a CLU knockout cell line was proposed.

The SNPExpress online database allowed for the interrogation of the effects of transcript level expression of the CLU SNP in two different human tissues: brain and peripheral blood mononuclear cells (PBMCs). This revealed that in brain tissue the clusterin risk allele C (C = 2) has lower CLU expression than the T allele (1), whereas there is no differential expression in the blood between alleles (Figure 25). Therefore, a CLU knockout cell line compared to a wildtype cell line could provide results relevant to the differential expression of rs111360000 AD SNP when studying neuronal cells, supporting the generation of a knockout iPSC line.

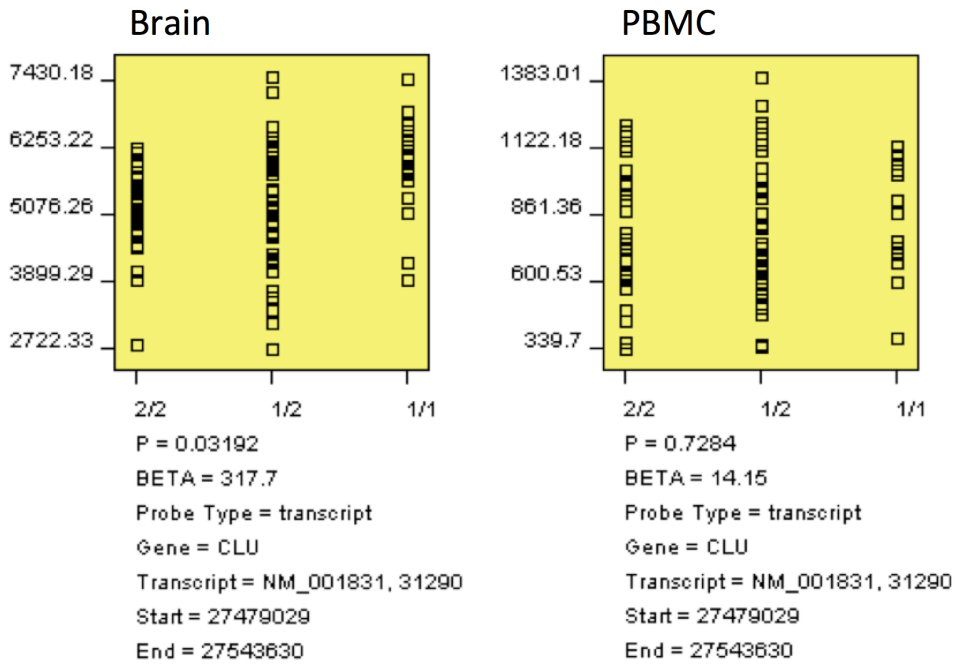

Figure 25. CLU expression differs between genotypes at rs111360000 in brain cells but not in blood cells (PBMC). Figures from SNPExpress show that in the brain the risk allele 2 (C) has lower CLU expression than the allele 1 (T). There is no difference in expression in the blood. (Data from SNPExpress online database.)

To develop the knockout cell line a CRISPR/Cas9 construct was transfected into healthy iPSC cells with a targeting construct to introduce a stop codon, and neomycin and GFP markers into the CLU gene in chromosome 8.

The second line planned was an APOE knockin line. All control iPSC lines were APOE ε3/ε3, and to create the ε4/ε4 genotype homozygous T was edited to homozygous C at the rs429358 SNP in APOE (ATGGAGGACGTGT to ATGGAGGACGTGC). A CRISPR/Cas9 construct was transfected into healthy iPSC cells with either a donor oligonucleotide or a targeting construct to introduce the mutation through HDR.

4.2 Methods

4.2.1 Sequencing of iPSC lines

Sequencing was performed on control iPSC lines to confirm the CLU and APOE genotypes. Primers were designed to amplify the regions around the SNPs and were diluted to 2μM. The region was amplified by PCR reaction with Taq polymerase as in Table 2.

Table 2. Reagents for sequencing PCR

Reagent	Volume	Final concentration
Primer sol. (2µM)	2	200nM
PCR Buffer (10x)	2	1X
$MgCl_2$	1.2	2nM
dNTPs	0.2	200µM
Taq polymerase	0.1	1 unit
DMSO	2	5%
H_20	11.5	n/a
DNA	1	n/a

The PCR reaction was run as described in Section 3.2.3.6, with annealing temperature 60°C:

Hold	33 cycles			Hold
Initial denaturation	Denaturation	Annealing	Extension	Extension
95ºC for 15 mins	95ºC for 30s	60ºC for 30s	72ºC for 30s	72ºC for 10 mins

The PCR product was run on an agarose gel as described in Section 3.2.4 to check if the PCR worked due to the difficulty of amplifying the G-C rich region in APOE.

Clean-up of the PCR product was done using the 'SAP/EXO' method using Shrimp Alkaline Phosphotase (SAP) to remove leftover dNTPs and Exonuclease I (EXO) to remove remaining primers. Into each well of PCR product 1µl of Rapid Alkaline phosphatase, 0.2µl of Exonuclease I and 1.3µl of H_20 were added. Samples were incubated at 37˚C for 30 min and then 95˚C for 5 min.

Sanger sequencing was performed using the BigDye Terminator v1.1 Cycle Sequencing kit. 0.5µl of BigDye, 2µl of 5x buffer and 2µl of either the forward or reverse primer was added to 1µl of PCR template and made up to 10µl with H_20. The reaction was run on a Step sequencing protocol:

Hold	Hold	Hold	33 cycles		
37ºC, 15 mins	80ºC, 2 mins	96ºC, 1 min	96ºC, 10s	50ºC, 5s	60ºC, 75s

20µl of sequencing reaction was precipitated by adding 5µl of cold 125mM EDTA and 60µl of 100% ethanol. Samples were incubated at RT for 15 min in the dark and centrifuged at 4000g for 30 min at 4°C. Plates were inverted to remove ethanol and 60µl 70% ethanol was added to samples. The plate was spun at 1650g for 15 min. The plate was inverted again and 20µl H_20 was added to each well for sequence analysis on a Beckman Coulter CEQ 800 Genetic Analysis System (Beckman Instruments, CA,USA).

Sequence assembly was performed using Codon Code Aligner software (CodonCode Corporation) and SNPs were investigated using dbSNP (NCBI) https://www.ncbi.nlm.nih.gov/projects/SNP/.

4.2.2 Preparation of gRNA expression construct

4.2.2.1 CRISPR design

For knockout design exon 3 of the CLU gene was selected for gRNA design as it was the exon closest to the N terminus of the gene that was present in all isoforms of CLU. For knockin the sequence around the SNP of interest was copied. The genomic DNA sequences were inputted to online CRISPR design tools www.e-crisp.org and www.crispr.mit.edu. This selected suitable target sites starting with a PAM (‘NGG) sequence, necessary for CRISPR/Cas9 recognition, and with low probability of off-target action. Oligonucleotides (oligos) for insertion into Aar1 site by removing PAM and adding ACC(G) to 5’ end of forward oligo, and CAAA to 5’ reverse strand oligo. Oligos are summarized in Table 3 and were made by IDT.

Table 3. CRISPR and ssODN sequences tested for efficiency

Oligo name	Oligo sequence F	Oligo sequence R
APOE cr1	accGcggacatggaggacgtgtg	Aaaccacacgtcctccatgtccg
APOE cr2	accGgacatggaggacgtgtg	Aaaccacacgtcctccatgtc
APOE cr3	accGgacgtgtgcggccgcc	Aaacggcggccgcacacgtc
APOE ssODN F	gcaggcccggctgggcgcggacatggaggatgtgcgcggccgcctggtgcagtaccgcg gcgagg	
APOE ssODN R	cctcgccgcggtactgcaccaggcggccgcgcacatcctccatgtccgcgcccagccggg cctgc	
APOE ssODN L*	Ctgtccaaggagctgcaggcggcgcaggcccggctgggcgcggacatggaggacgtgc gcgggcgcctggtgcagtaccgcggcgaggtgcaggccatgctcggccagagcaccgagg ag	
CLU cr1	accGaagactctgctgctgtttg	Aaaccaaacagcagcagagtctt
CLU cr3	accGacgtacttacttccctgat	Aaacatcagggaagtaagtacgt
CLU cr4	accGaaattcaaaatgctgtcaa	Aaacttgacagcattttgaattt

*=from Gonzalez et al. (2014)

Single-stranded oligodeoxynucleotide (ssODN) sequences of 65-120 base pairs with homology arms were designed for insertion with HDR to introduce the point mutation for APOE (Table 3). This was designed to introduce the T to C change at rs429358 and also an extra mutation near the SNP for selection using a restriction enzyme assay (demonstrated in Figure 26). A Fok1 site was introduced and the validity of this mutation was checked using insilicase.co.uk web software.

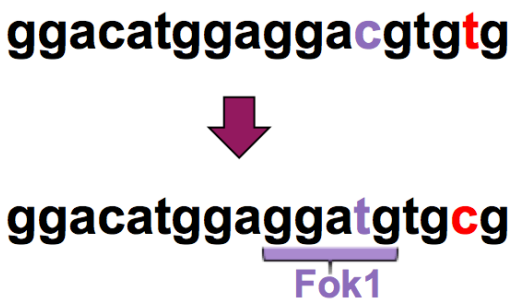

Figure 26. APOE sequence change at rs429358from ε3 to ε4 by ssODN. To introduce the necessary mutation at the SNP site a ssODN containing a base change T to C and additionally a C to T change to introduce a Fok1 site was utilised. The Fok1 site could be used for checking the introduction of the the ssODN using a restriction enzyme assay.

A targeting construct was designed for both the CLU and APOE mutations. The CLU targeting constructed included neomycin selection and GFP selection cassette. The APOE targeting constructed contained blasticidin selection, as well as loxP or gRNA sequences for excision of the targeting construct as despite being at the end of the gene it may interfere with the gene expression (Figure 27).

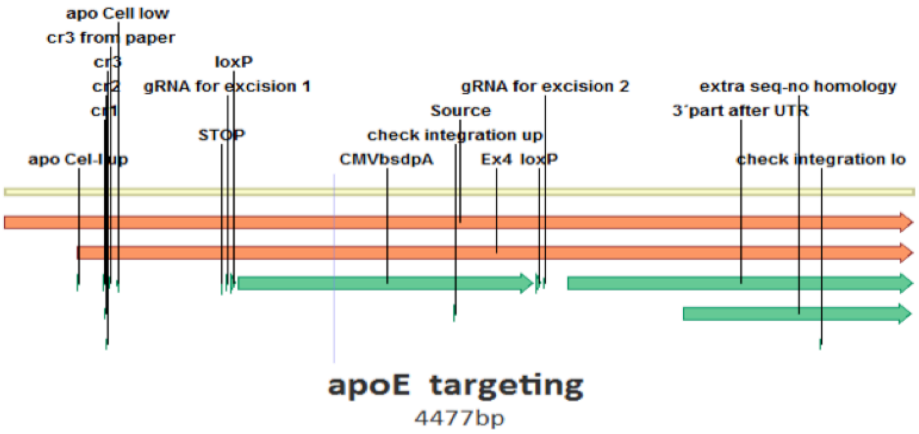

Figure 27. APOE targeting construct (Vector NTI). The targeting construct contained homology arms to the APOE gene and a bsd cassette to allow for selection of the mutation by antibiotics. There was also a gRNA for excision of the targeting construct at a later point if it resulted in changing the gene expression more than desired.

4.2.2.2 Cloning of oligo inserts into cas9 plasmid

Oligos were diluted to 100µM. F+R CRISPR oligos were annealed with T4 Ligase buffer and incubated at 95°C for 1 minute:

Reagent	**Volume**
Forward gRNA	1µl (100µM)
Reverse gRNA	1µl (100µM)
Ligase buffer	2µl
H_20	16µl

Annealed oligos were left to cool to RT and then diluted 1:200 with ddH_20.

The cas9 plasmids used in this project were generated by AstraZeneca and contained a promoter sequence of either EF1α or CMV. All plasmids contained a kanamycin resistance cassette. Plasmids contained either a GFP selection cassette or puromycin selection driven by the EF1α or CMV promoter. The EF1α cas9 GFP plasmid is shown in Figure 28. Plasmids were designed using Vector NTI software (Life Technologies, Paisley, UK).

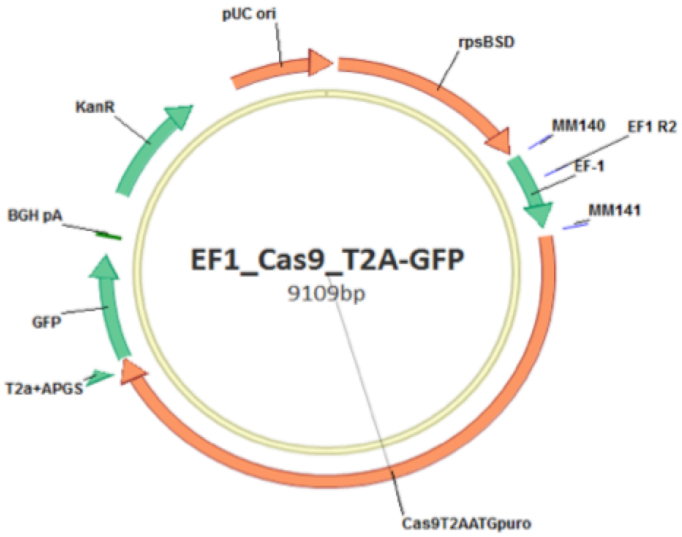

Figure 28. EF1α cas9 plasmid map from Vector NTI software. Cas9 plasmid contains EF1α promoter, kanamycin, and GFP cassette.

The cas9 plasmid was digested with Aar1 to allow for insertion of gRNA.

Reagent	**Volume**
pDNA	4µl (2µg)
Aar1 enzyme	0.5µl (2units/µg)
Oligo for Aar1	0.8µl
Buffer Aar1	4µl
H_20	30.7µl

A 40µl total volume was incubated at 37°C for 2 hours and the digest was run on a 0.8% agarose gel. The band at 8.5kbp was cut out under trans UV and prep UV illumination on the BioSpectrumAC Imaging System. Agarose was dissolved and DNA was isolated using Qiagen Gel Extraction kit according to manufacturer's instructions. Oligos were ligated with 20ng cas9 GFP plasmid DNA (pDNA) using 10x ligation buffer and T4 ligase enzyme and incubating at 16°C for 2 hours.

The plasmids produced that were used in the iPSC transfections were EF1α-cas9-CLUcr3-GFP, EF1α-cas9-CLUcr4-GFP and CMV-cas9-APOEcr2-puro.

4.2.3 Transformation of CRISPR/Cas9 construct into competent cells

3ul of ligated cas9 plasmid was added to 20µl of competent bacteria (NEB, C3109) and incubated on ice for 30 min. Cells were heat shocked at 42°C for 1 minute and incubated on ice for a further 1 minute. 300µl Luria Broth (LB) was added and bacteria were shaken at 37°C for 1 hour. 75µl of bacteria culture was transferred to LB plates with kanamycin selection (50 µg/ml) and incubated at 37°C overnight.

Clones were inoculated by adding individual bacterial colonies to LB with 50µg/ml kanamycin and incubated at 37°C overnight with agitation. DNA was extracted from bacterial cells by miniprep with Qiagen QIAprep Miniprep kit following manufacturers protocol (Appendix 1). pDNA was resuspended in 50µl H_20 and stored at -20°C.

4.2.4 Sequencing of plasmid

PCR product was prepared with 100ng DNA, 5uM of primer sequencing from the U6 promoter and BigDye sequencing kit as described in 5.2.1. Sequencing product was precipitated and run on Applied Biosystems sequencer. Sequences were checked against the U6 sequence with the 20bp gRNA sequence using NCBI's online Basic Local Alignment Search Tool (BLAST) https://blast.ncbi.nlm.nih.gov/Blast.cgi.

4.2.5 Functional testing of gRNAs in HEK293 cells

4.2.5.1 Maxipreps of CRISPR plasmid

Plasmids were transformed into competent cells and cultured in 200ml LB with 50µg/ml kanamycin. Quantities of DNA for transfection optimization were prepared by maxiprep using Qiagen Endo-free Plasmid Maxi Kit.

4.2.5.2 Cell culture

HEK293 cells (Sigma-Aldrich) for functional validation of CRISPRs were maintained in DMEM with 10% heat-inactivated fetal bovine serum (FBS) at 37°C, 5% CO_2, 5% O_2, and passaged with TrypLE when >80% confluent.

4.2.5.3 Transfection of HEK 293 cells

HEK 293 cells were plated into 12 well plates at 200,000 cells/well in DMEM the day prior to transfection with FuGENE (Promega). When cells were approximately 80% confluent they were transfected with 1.1ug DNA in 3.3ul FuGENE reagent (as suggested by FuGENE HD Protocol Database). After 24 hours incubation at 37°C GFP expression was checked under fluorescence microscope. Three days after transfection cultured HEK cells were lysed and DNA was purified using the Puregene Cell Kit (Qiagen) according to manufacturers instructions.

4.2.5.4 Testing cleavage efficiency of CRISPR sequences

The surveyor nuclease assay is used to assess the cutting of the plasmid in cultured cells. The surveyor nuclease is a member of the CEL-nuclease family (Yang et al., 2000). This group of nucleases recognise and cleave many different types of mismatches that have occurred due to the presence of SNPs and from small insertions or deletions (Pimkin et al., 2007). The sample DNA is amplified by PCR in the region where the mutation is expected to be and the PCR product is heated at high temperature to denature and separate the DNA strands. The strands are then cooled gradually and allowed to re-anneal. During this process, if there are mutations present in the DNA, homoduplexes and heteroduplexes will form and there will be mismatches at the point of the mutation when the DNA strands re-anneal with a non-mutated DNA strand (Shi et al., 2006, Pilato et al., 2012). The surveyor nuclease recognises and cleaves the DNA at the sites of the mismatched base pairs

A CEL-I assay was performed using *Surveyor® Mutation Detection Kit* (Transgenomic, 703060) with primers designed to be approximately 250 base pairs around mutation sites.

APOE Cel-I primers:

F tcggaactggaggaacaact R ggcgcttctgcaggtcatc

CLU Cel-I primers:

F ccttgacagcccctgaact R gttgctgagcagtgtcttgc

A 20µl PCR reaction of the genomic DNA was run with the forward and reverse primers and 10x Phusion Flash master mix with annealing temperature of 60°C for CLU sequences and 64°C for APOE sequences. 1µl of SURVEYOR nuclease and 1µl of Enhancer was added to 10µl of PCR reaction to cut mismatch sites in the heteroduplex when incubated at 42°C for 40 min. Fragments were analysed by mixing with TBE sample buffer and running on 10% TBE gel at 240v for 24 min. The gel was stained with ethidium bromide in TAE for 30 min and bands were imaged with UV. The presence of smaller bands smaller bands indicated points within the PCR product where it was cleaved by the surveyor nuclease and therefore a mutation was present.

4.2.5.5 Fok1 assay

The donor ssODN oligo with the APOE mutation was designed to include another single point mutation 3 nucleotides after the mutation at rs429358 to introduce a Fok1 cleavage site, without altering the amino acid sequence. This restriction enzyme could then be used to quickly assay whether the ssODN had been incorporated into the DNA.

100ng of genomic DNA was amplified by PCR (annealing temperature 64°C) with Phusion Flash master mix using 0.5µM of primers to amplify the mutations site. PCR product was purified with Qiagen PCR purification kit. 0.5µl of Fok1 enzyme (New England Bioscience, MA, USA) and 2µl of Buffer 4 was added to 30µl of PCR product and incubated at 37°C for 2 hours. Digested product was run with sample buffer on a 10% TBE gel to detect any small size constructs cut by the restriction enzyme.

4.2.6 Co-transfection of gRNA plasmid with HDR template

4.2.6.1 Transfection of iPSCs

iPSCs were maintained in E8 media on geltrex-coated 6 well NUNC plates at 37°C, 5% CO_2, 5% O_2 as described in Methods Section 2.1.1.4. Validated constructs were introduced into iPSC DNA by AMAXA or Lipofectamine transfection systems. All reagents Life Technologies.

4.2.6.2 AMAXA transfection

3 hours prior to transfection cells were treated with 10μM ROCKi added directly to media. 24 well plates were prepared with geltrex for 1 hour as described in Section 2.1.1.3. AMAXA Human Stem Cell Nucleofector (Lonza) kit 1 was used for nucleofection of iPSCs.

Cells were dissociated into single cells with Trypl and counted before centrifugation at 200g for 5 min. Cells were resuspended at 1.6 x 10^6 cells/ml (800 000 cells / nucleofection cuvette) in Human Stem Cell Nucleofector Solution 1 with 2μg of cas9 pDNA and 2μg targeting construct or 2μl of 100μM repair oligo. Cells were nucleofected with AMAXA programme A-013 and diluted in 500μl E8 + 10μM RI. Cells were transferred to 1 well of a 24 well plate containing warm E8 + RI and incubated at 37°C. E8 media was replaced after 24 hours and cells were imaged with IncuCyte Live Cell Analysis System (Essen Bioscience).

4.2.6.3 Reverse Lipofectamine transfection

Two hours prior to passaging 24 well plates were coated with 1μg/cm^2 Laminin521 (Biolamina, Sweden) in PBS (with calcium and magnesium) (Life Technologies), and 10μM RI was added to iPSC media. After 1 hour DNA was prepared and added to laminin matrix in this 'reverse' transfection protocol. 500ng cas9 + 1μg GFP targeting construct was added to 100μl of Opti-MEM. 1μl of Plus reagent from Lipofectamine LTX kit was added to the diluted DNA and incubated for 5 min at RT. 1.5μl of Lipofecatamine LTX Reagent was added, mixed by pipetting, and added to Laminin 521 matrix in the wells. Plates were incubated for 1 hour further and cells were passaged using Trypl and

plated in E8 + RI at 300,000 cells per well on top of the matrix (without removing PBS). Media was changed after 24 hours.

4.2.6.4 Selection and clonal isolation

Two days after transfection cells were 80% confluent and selection of mutated cells was begun. Cells were passaged as single cells using Trypl and each well was replated into a 1μg/cm^2 Laminin521-coated 10cm^2 Nunc dish to keep cell density low.

For cells transfected with CLU targeting construct 150μg/ml of Geneticin was added to E8 media to select for Neomycin. For cells transfected with APOE plasmid 250ng/ml of puromycin was used to select for transfected cells. Geneticin remained in the media throughout clonal isolation; puromycin was removed after 2 days. After approximately 1 week colonies had grown from cells and were passaged into 24 well plates using Cloning cylinders (Sigma Aldrich, Gillingham, UK) with Versene. Clonal populations were then expanded to 1 well of a 6 well plate, upon which the cells were passaged with Versene and half were lysed for analysis with Cell Lysis solution (Qiagen) and half were frozen with 10% DMSO in E8 medium.

4.2.6.5 Screening for mutations

The CLU knockout cells were screened by PCR. Genomic DNA was extracted using the Gentra Puregene Cell Kit (Qiagen) according to manufacturer's protocol (described in

Appendix 1). Primers were designed across 300 base pairs at both the 5' and 3' end in the neomycin of the targeting construct. A PCR of the genomic DNA was run with the primers and Phusion Flash master mix with annealing temperature of 58°C and an extension time of 30 seconds due to the large size of the PCR product. The PCR product was run on a 1% agarose gel with ethidium bromide and imaged (as described in Section 3.2.4).

Clones that showed a 300 bp band in the gel were then sequenced and also confirmed with a Cel-I assay. Sequencing was run with primers across the CRISPR/Cas9 cutting site and compared to the original sequence using NCBI's online Basic Local Alignment Search Tool. The Cel-I assay was performed as before except 5µl CLU PCR product was mixed with 5µl wildtype PCR product.

The APOE knockin cells transfected with ssODN were screened for the mutation using droplet digital PCR (ddPCR). A probe for the mutant sequence (FAM labeled) and a reference with the wild type sequence (HEX labeled) were designed spanning 16 base pairs across the site of the point mutation. A gBlock (a double-stranded, sequence-verified genomic block) was designed for the mutant DNA to act as a positive control (IDT), and wildtype gDNA was used as the negative control. A PCR reaction mix of 1µl gDNA, 1µl reference primers/probe, 1µl mutant primers/probe, 10µl ddPCR supermix (no dUTPs, BioRad) and H_20 to 20 µl was used. Before running the PCR the sample was made into droplets in the BioRad Droplet Generator by combining the 20µl sample mix with 70µl of droplet reader oil from the ddPCR kit (BioRad). Droplets were analysed by The QX200 Droplet Digital PCR system.

APOE knockin cells transfected with the APOE targeting construct were screened by PCR as with CLU clones.

4.2.7 Whole genome sequencing

Sequencing of CLU knockout clonal iPSC line was performed by Cergentis (Utrecht, The Netherlands) using their Targeted Locus Amplification (TLA) technology. TLA Technology enables hypothesis-neutral complete sequencing of any genomic locus, allowing identification of all genetic variation in loci of interest. To determine if the targeting construct had integrated two primer sets were used: one present on the endogenous locus and in the homology arms, and one located in the GFP sequence of the targeting construct. PCR products were purified and library prepped using the Illumina NexteraXT protocol and sequenced on an Illumina Miseq sequencer.

Primer set 1 (primers in endogenous locus):

Rev 5' GTTTCTGCAGGATCATTGTT Fwd 5' GAGCAGAATTAGCTACCCTG

Primer set 2 (primers in targeting construct):

Rev 5' TGAAGTTCATCTGCACCAC Fwd 5' GAACTTGTGGCCGTTTAC

4.3 Results

4.3.1 Sequencing APOE and CLU in iPSC line

To determine the genotype of the control iPSC lines, CTR M1 04, CTR M2 42 and CTR M3 36S regions around APOE SNPs rs7412 and rs429358, and CLU SNP rs111360000 were sequenced. Control lines all had the C allele for rs11136000 (Figure 29). All iPSC lines had the T allele at rs429358 (Figure 30) and the C allele at rs7412 (Figure 31), making the lines all homozygous APOE ε3/ε3. CTR M3 36S was used as the principal line for the CRISPR genome editing as it was the only line generated using integration-free virus vectors.

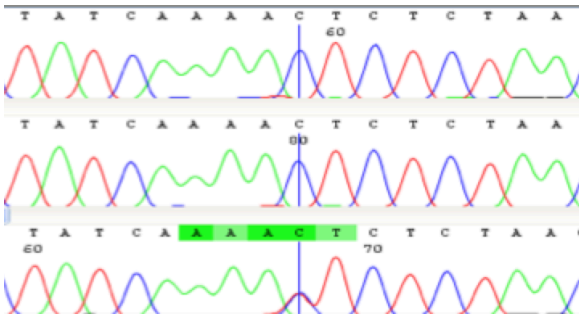

Figure 29. All 3 iPSC lines were CLU rs11136000(C). Sequencing shows the same genotype for this CLU region in all lines.

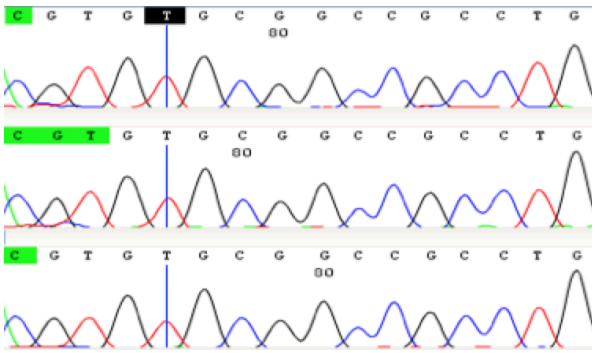

Figure 30. All 3 iPSC lines were rs429358(T). Sequencing shows the same genotype for APOE rs429358 region in all lines, which means none of the cell lines had an APOE ε4 allele.

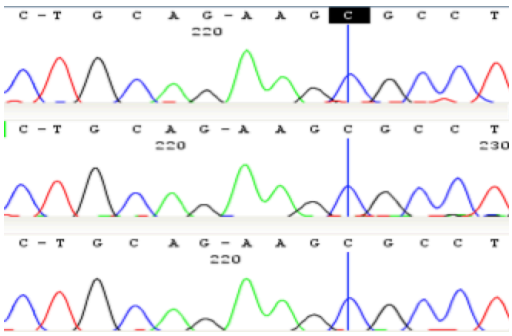

Figure 31. All 3 iPSC lines were rs7412(C). This shared sequence across this region means that none of the cell lines had an ε2 allele in the APOE gene.

4.3.2 Cas9 construct activity in mammalian cells

The Cel-I assay was performed on gDNA from cells transfected by cas9 constructs. Cas9 expressed with a CLU CRISPR or an APOE CRISPR was transfected into HEK293 cells and the gDNA was collected after 48 hours for analysis by the surveyor nuclease assay. The cas9 constructs were EF1α-cas9-CLUcr3-GFP, EF1α-cas9-CLUcr4-GFP and CMV-cas9-APOEcr2-puro. Small PCR fragments of approximately 100bp showed that the cas9 was active in a high number of cells and caused a cut to the specific region it was

targeting (Figure 32). There was no band to suggest cutting by the CMV-cas9-APOE-puro plasmid in iPSCs, which could be due to poor transfection efficiency or reduced CMV promoter activity in iPSCs.

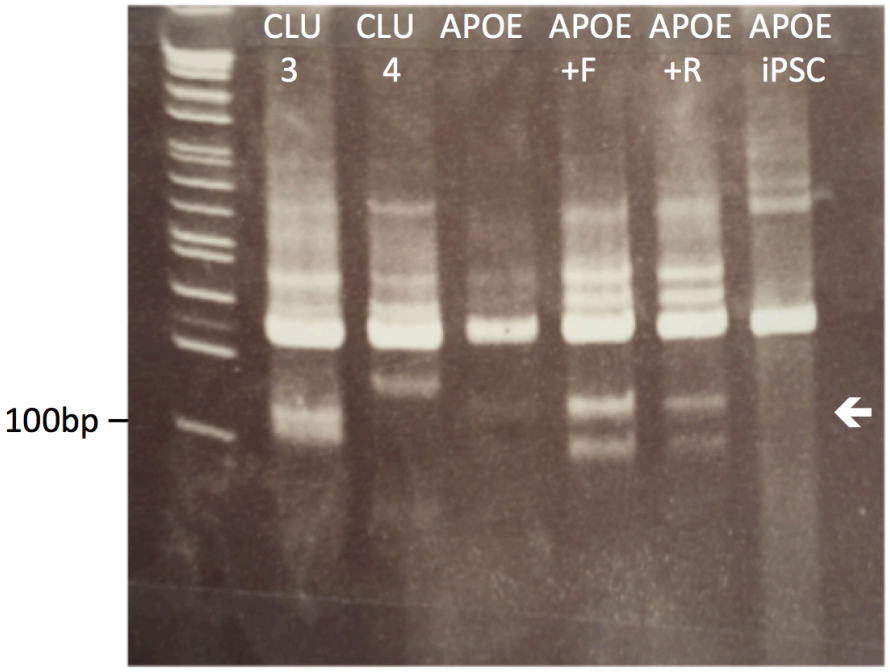

Figure 32. Small bands (in line with arrow) showed cutting activity by CLU cas9 and APOE cas9 constructs in HEK293 cells. From left to right lanes show 1kb ladder, CLU-gRNA3 cas9, CLU-gRNA4 cas9, APOE cas9, APOE cas9 + APOE ssODN F, APOE cas9 + APOE ssODN R, APOE cas9 in iPSCs.

Since iPSC transfections with EF1α-cas9-CLU3-GFP were positive, the APOE gRNA was recloned into and EF1α-cas9-GFP and EF1α-cas9-puro plasmids. The EF1α-cas9-APOEcr2-puro plasmid was successfully cloned and was tested for cutting efficiency in iPSCs using the Cel-I assay (Figure 33). The same construct transfected into HEK cells

was used as the positive control. The higher proportion of gDNA with cutting by cas9 in HEK cells was due to higher transfection efficiency compared to iPSCs.

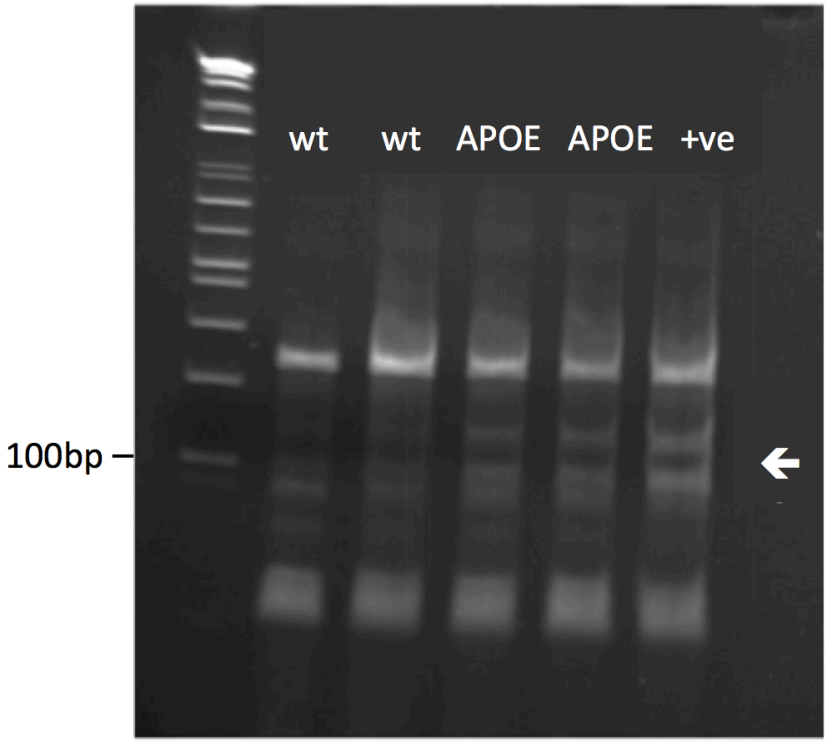

Figure 33. APOE cas9 construct efficiently cut DNA in iPSCs (cuts shown by arrow). From left to right: 1kb ladder, 'wt' negative controls with no transfection, 'APO' EF1α-cas9-APOE-puro transfected iPSCs, and '+ve' EF1α-cas9-APOE-puro transfected HEK cells.

4.3.3 AMAXA vs lipofectamine for iPSC transfection

Transfection of iPSCs with CRISPR/Cas9 GFP constructs was performed with different methods including AMAXA electroporation and Lipofectamine lipofection, and the number of GFP cells was analysed with the IncuCyte Live Cell Analysis System (Essen Bioscience). AMAXA electroporation had high transfection efficiency for iPSC

transfection (Figure 34A), with 20% of cells GFP-positive. The reverse Lipofectamine method had a lower number of GFP-positive cells (16%) (Figure 34B). However, it had higher cell survival 48 hours after transfection compared to electroporation.

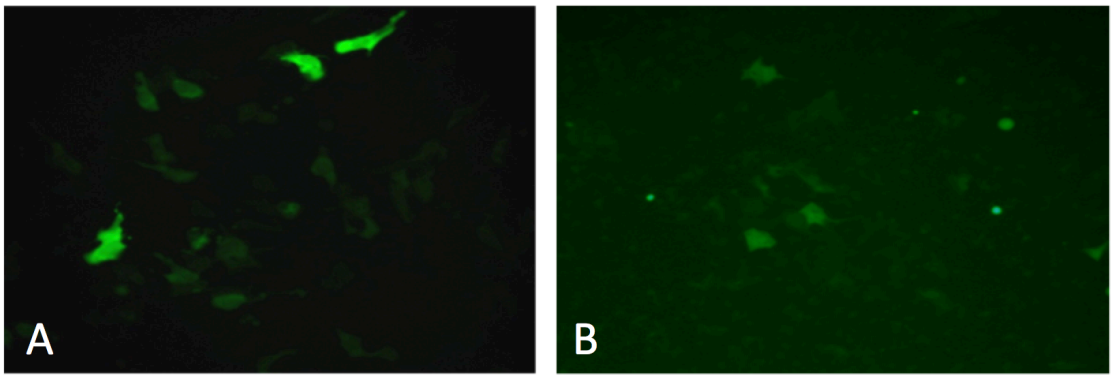

Figure 34. Transfections of cas9 plasmids into iPSCs with electroporation and lipofection methods. A. AMAXA transfection of EF1α-cas9-CLU3-GFP after 48 hours. B. Lipofectamine transfection of EF1α-cas9-CLU3-GFP after 48 hours. Representative images from 4 wells of a single plate.

To test the difference between the efficiency of the CMV and EF1α promoters in iPSCs, cells were transfected with the CMV-cas9-APOE-GFP construct or the EF1α-cas9-APOE-GFP plasmid using AMAXA. The EF1α plasmid had higher GFP expression than the CMV plasmid 48 hours after transfection, with 12% of cells expressing GFP compared to 3% respectively (Figure 35), confirming the EF1α promoter plasmids had better expression in iPSCs.

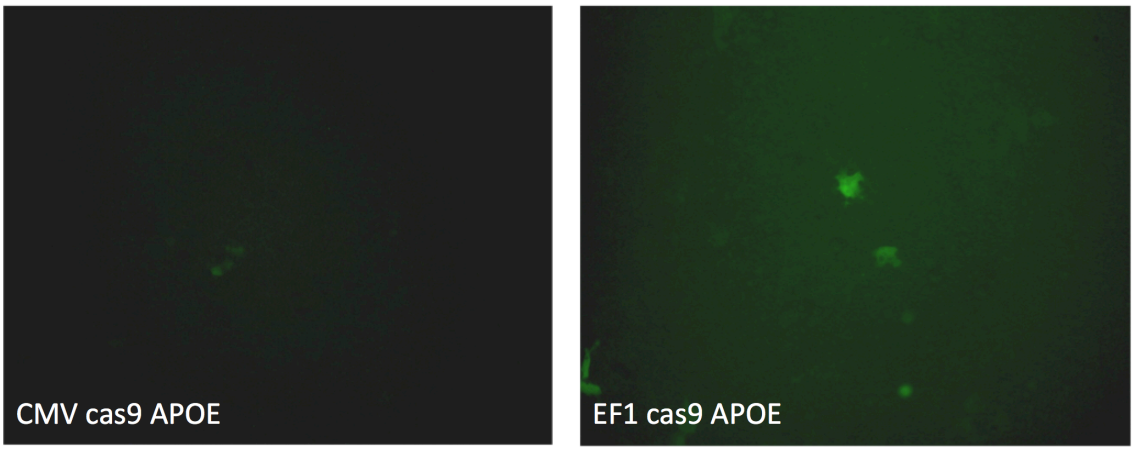

Figure 35. Transfections of CMV-cas9 vs. EF1α-cas9 plasmids into iPSCs. Transfection of the two plasmids by AMAXA shows increased expression by EF1α-cas9 compared to CMV-cas9 after 48 hours. Representative images from 3 wells of a single plate.

4.3.4 CLU targeting construct insertion

Clonal iPSC populations that had been selected by neomycin were assessed for the integration of the CLU targeting construct by PCR. The targeting construct inserted into exon 3 (Figure 36A) had primers designed for the 3' end of the construct (demonstrated by Figure 36B) and the 5' end. For both primer pairs one primer was in exon 3 and the other primer was in the targeting construct, thereby only cell populations with the targeting construct present in the correct location were amplified by PCR. Figure 37 shows clones 3 and 4 both had the targeting construct integrated at the 5' and the 3' end. Therefore these clones were expanded and clone 3 was sent for whole genome sequencing due to its higher quality in terms of iPSC growth rate and colony morphology. Clones 1 and 2 did not show bands for both the 3' and 5' end of the targeting construct.

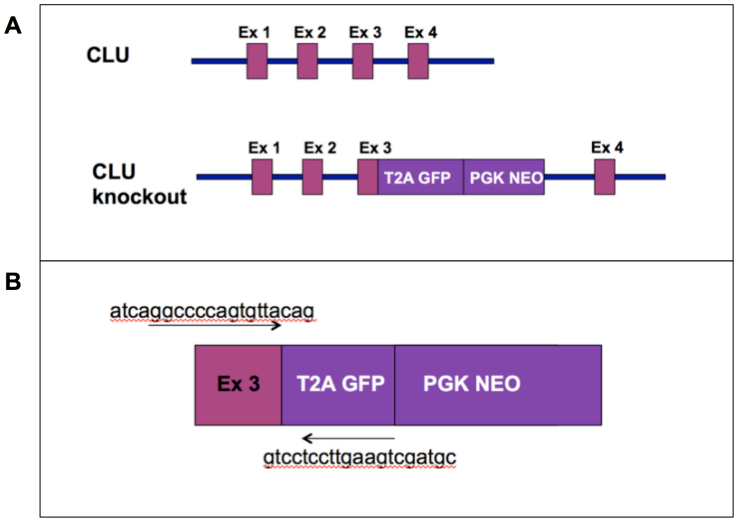

Figure 36. Schematic showing strategy for detecting integration of CLU targeting construct in exon 3 by PCR. A. CLU targeting construct integrates into exon 3 by HDR with homology arms. B. Primer pairs with one primer in the endogenous sequence and one primer in the targeting construct.

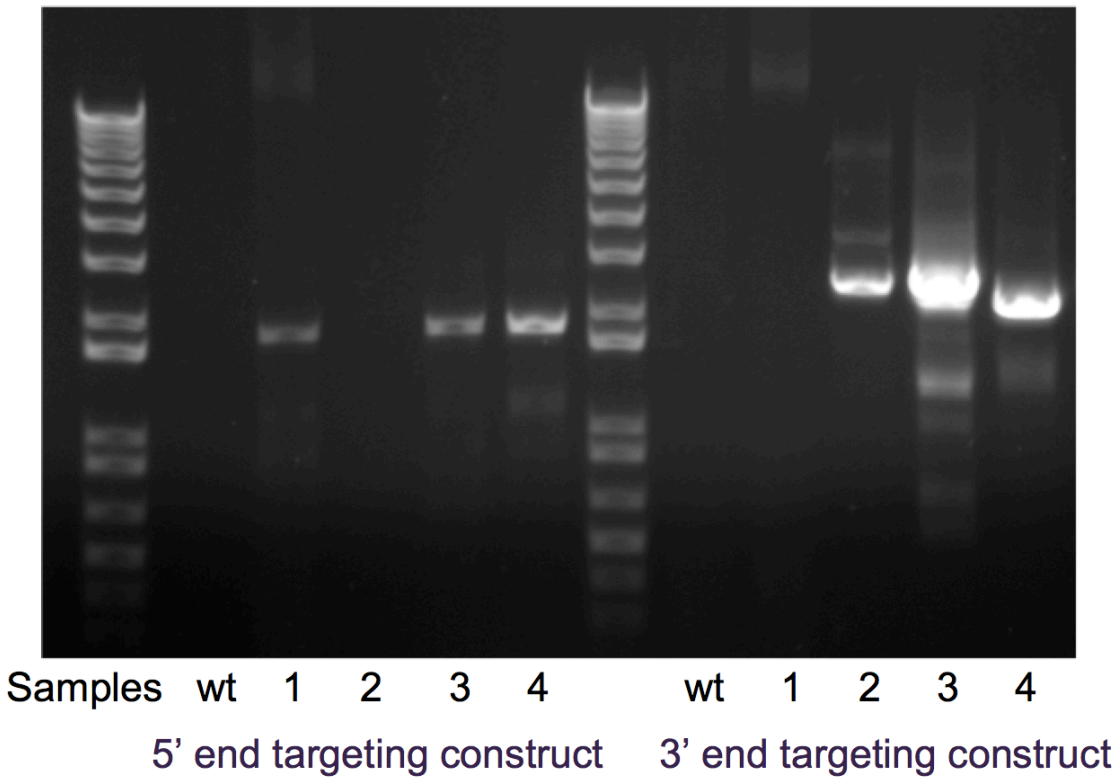

Figure 37. Sequencing PCR for CLU targeting construct in iPSC clones. A PCR across the targeting construct and the insertion site was performed to test for the mutation of CLU. PCR product was present where the clusterin gene sequence met the targeting construct at both the 5’ and the 3’ end of the construct in both iPSC clone 3 and 4.

4.3.5 Genome sequencing for CLU knockout

Whole genome sequencing was carried out by Cergentis (Utrecht, The Netherlands) using TLA to confirm that the CLU gene had been knocked out of the iPSC line and to check whether there was any off target activity that may affect other genes. There was a single identified integration site on Chromosome 8 and no off target integrations were found. Only one TLA peak was seen, located at the expected position in the CLU gene on chromosome 8 (Figure 38).

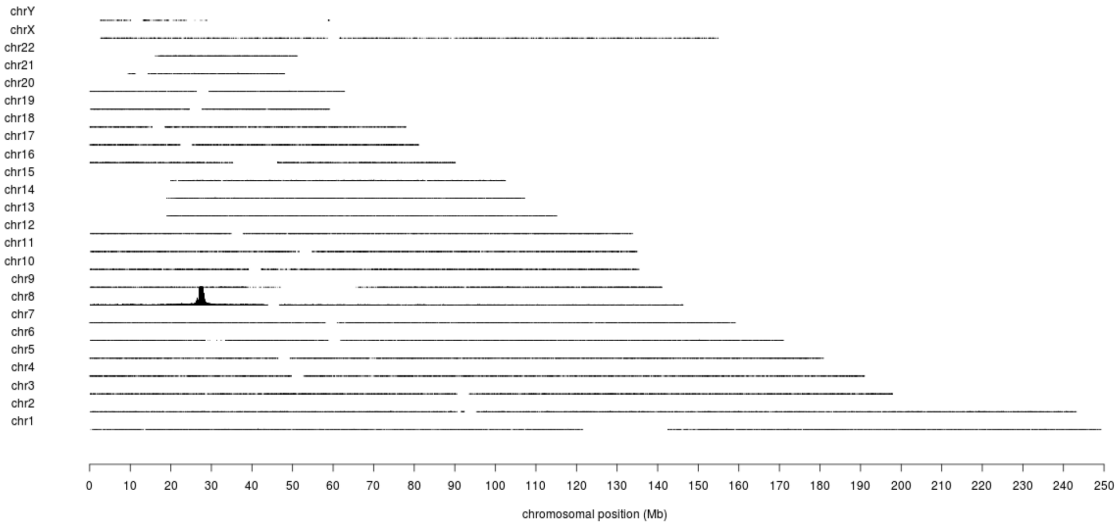

Figure 38. Targeting construct integration in chromosome 8. Whole genome coverage plot of generated data generated with the transgene specific primer pair (primer set 2). Peak in chromosome 8 at the site of the CLU gene indicates that the targeting construct has integrated at the correct site, with no off target integrations.

A coverage profile generated for the area surrounding the integration site on chromosome 8 showed no evidence for large deletions or any other rearrangements of chromosome 8 (Figure 39).

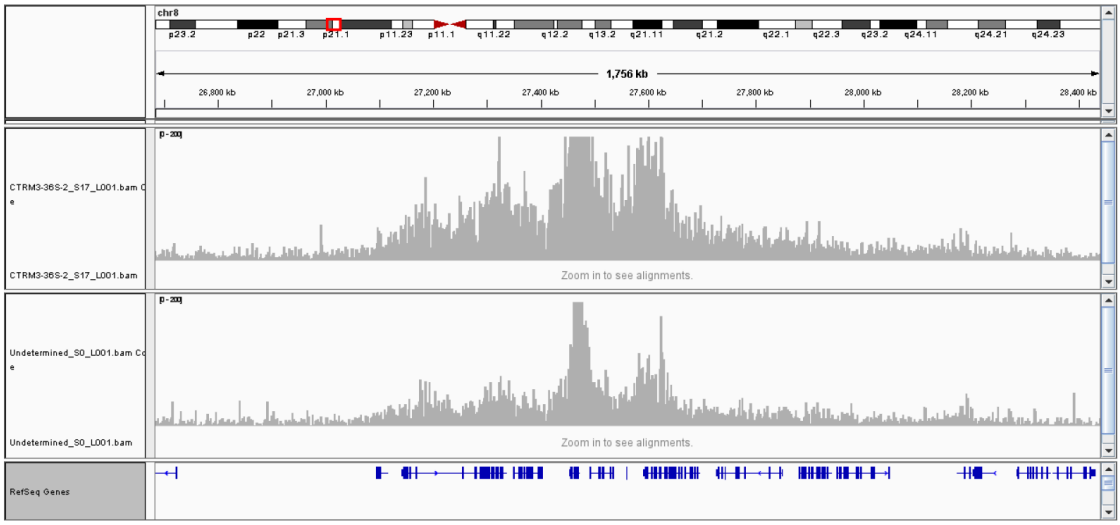

Figure 39. No large deletions or other rearrangements were detected surrounding the integration site. Coverage profile surrounding transgene integration site.

The sequence information generated on the position of the integration site (in between the two arms of homology) distinguished three types of reads at this site (Figure 40). Firstly there were reads from the integration (INT), which were expected to be found in the case of a clean integration. These were reads that represent the sequence from the end of the homology arms, running into the insert present in the construct.

Secondly there were reads containing a deletion (DEL) spanning from position 27,466,579 to 27,466,589 (within the CRISPR site). One end of the deletion, position 27,466,579 lies outside of the arms of homology and is not present in the targeting construct. This demonstrates that the deletion is located in a different allele than the construct integration. This deletion produced a frame-shift in the CLU gene and introduced an early stop codon.

Finally, primer set 1, which amplified both from the endogenous locus and from the targeting construct, found reads from the wild type allele (WT), fully aligning to the

genome sequence at this position. The number of wild type reads was significantly lower than the insertion and deletion reads. The wild type constitutes ~ 1% of the reads. This low amount of wild type reads may come from a small number of wild type or heterozygous cells present in the sample.

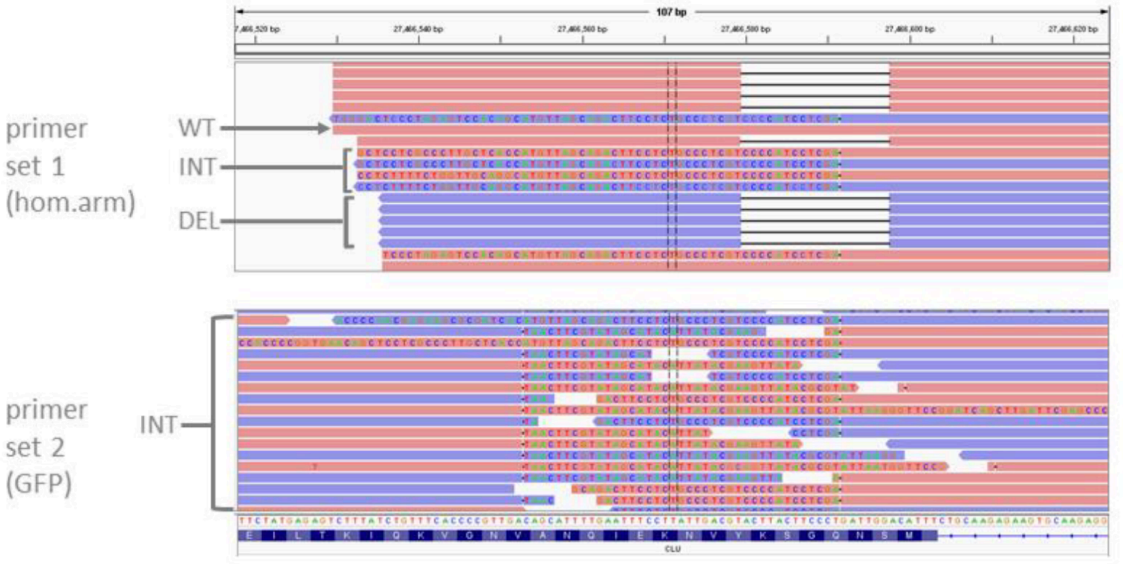

Figure 40. Plot of sequence information generated on the position of the integration site shows reads generated with primer pair 1 and 2. WT = Wild type sequence, INT = expected integration, DEL = deletion. Primer set 1 reads inside one of the homology arms detecting INT, DEL and WT. Primer set 2 reads INT. (Plot from Integrative Genomics Viewer.)

4.3.6 CLU knockout neurons differentiate normally

Wildtype and CLU knockout iPSCs were differentiated in parallel for 35 days to compare morphological characteristics. CLU knockout neurons differentiated comparably to

wildtype neurons (Figure 41), suggesting that CLU does not irrevocably interfere with the differentiation process and that this iPSC line will be a useful tool for neuronal studies.

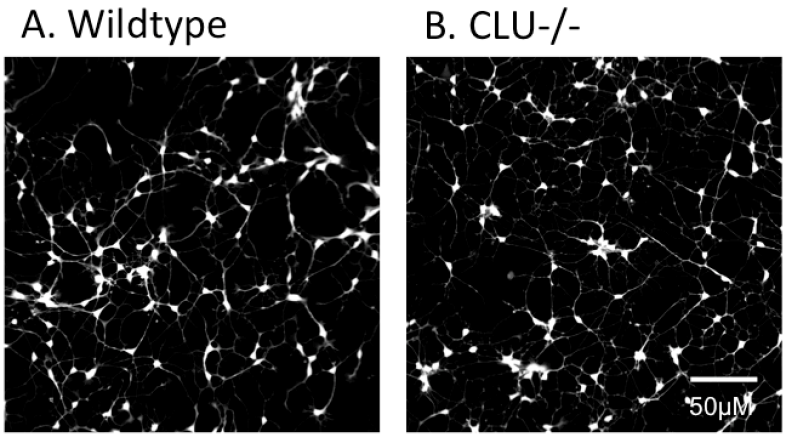

Figure 41. CLU-/- iPSCs differentiate into morphologically mature neurons. A. Wildtype neurons at day 35 of differentiation stained with βIII tubulin. B. CLU-/- neurons at day 35 of differentiation stained with βIII tubulin.

4.3.7 ddPCR for APOE ε4 knockin mutation detection

ddPCR measured the exact number of sequences with either the wt (ε3) sequence or the mutant (ε4) sequence. The probes detected some mutant DNA in APOE clones 1 – 11, with an especially high proportion of mutant DNA in APOE clone 7 (Figure 42). However, the presence of mutant events in the negative control suggested the mutant probe may not be exclusively targeting mutant ε4 sequences. This was confirmed by sequencing the clones, which did not show any non-ε3 sequence in any clones.

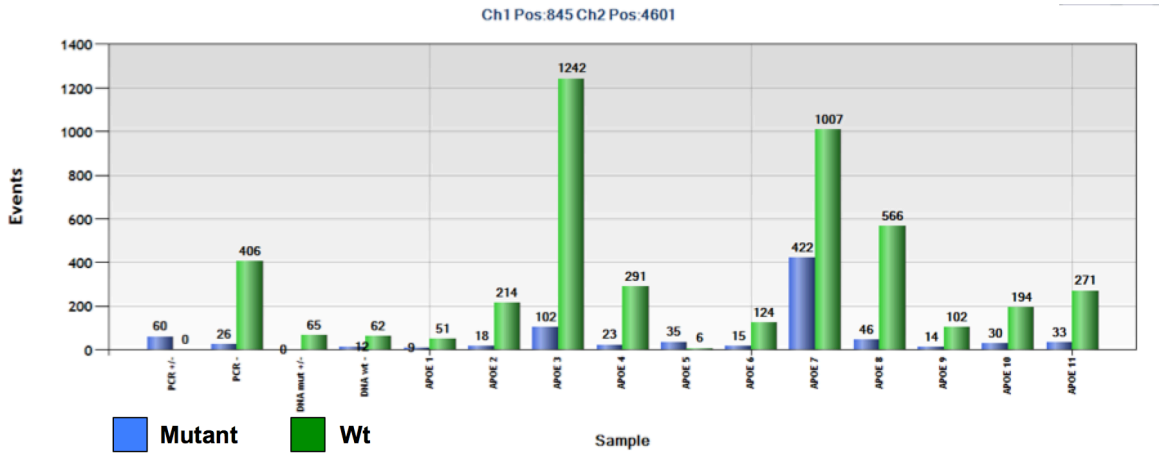

Figure 42. APOE mutation events measured by Droplet Digital PCR (ddPCR). Mutant (blue) and wt (green) events as measured by the probes in cultures transfected with EF1-cas9-APOE-puro together with an ssODN for the APOE mutation.

4.3.8 APOE targeting construct insertion

Difficulties with ssODN insertion, selection of positive clones and effective mutation detection were all issues with the APOE knockin cell line, and it was attempted to overcome these by designing a targeting construct with blasticidin selection. Clones were expanded with 3µg/ml and surviving colonies were screened by PCR using a primer set spanning the endogenous locus and the targeting construct. PCRs for this region showed some extra bands, but all surviving clonal colonies showed bands suggesting the APOE targeting construct was integrated (Figure 43). However, sequencing did not show integration of the targeting construct and all APOE clones were found to be ε3 homozygous.

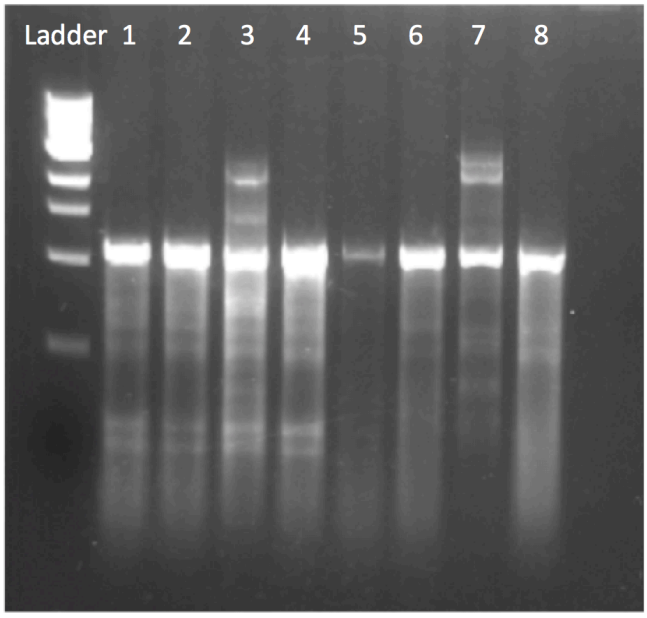

Figure 43. Sequencing PCR for APOE targeting construct in iPSC clones. A PCR across the targeting construct and the insertion site was performed to test for the APOE knockin in 8 iPSC clones expanded to 1 well of a 12 well plate. All gDNA samples had a band present indicating integration of targeting construct.

4.4 Discussion

4.4.1 'Reverse Lipofectamine' is a successful transfection strategy for iPSCs

Transfection of iPSCs is a capricious practice with typically low efficiency rates (Chatterjee et al., 2011). Transfections with cas9 DNA are especially difficult due to the large size of the plasmid. Lipofection performed by plating the cells onto matrix containing the DNA-Lipofectamine complex was found to be the most successful technique for transfecting iPSCs in terms of both cas9 efficiency and cell survival. iPSCs responded particularly well to this reverse transfection system as the usual passage did not need to be altered, unlike other systems that require cells to be resuspended in special solutions. This technique also worked better than the standard Lipofectamine system,

which showed no success in iPSC line CTR M3 36S. The process of passaging the cells may have been key as the cells would be lipofected at a higher rate during cell division. This transfection system may be useful for future CRISPR/Cas9 experiments in iPSCs.

4.4.2 The CLU construct integrated in the targeted position in one allele

The CLU targeting construct sequence has integrated in the targeted position but only in one allele. No large structural rearrangements are apparent at this allele. At the other allele a deletion is present in the CLU gene from position 27,466,579 to 27,466,589 at chromosome 8. This 10 base pair deletion causes a frame shift and introduces an early stop codon. Therefore, sequencing confirms this cell line to be a CLU knockout. This iPSC line will be useful in future experiments investigating the role of CLU in neuronal response to Aβ. Generation of the CLU knockout iPSC line with CRISPR/Cas9 is especially advantageous as it provides a perfect isogenic control for all experiments, and differences in response to Aβ can be limited to the role of clusterin.

4.4.3 APOE SNP rs429358 is a difficult mutation to target

Many problems were encountered with the APOE knockin project. Only one of the designed APOE CRISPR sequences (APOE cr2) efficiently cut the DNA at the targeted site. Testing the published constructs from Gonzalez et al. (2014) did not improve efficiency in our iPSCs either. Due to the GC-rich nature of the gene and the need to target the precise location of the SNP there were few CRISPR sequences available from the CRISPR design web programs. The original CMV cas9 plasmid the APOE CRISPRs

were cloned into was not effective in iPSCs, and it was necessary to reclone the APOE cr2 into a cas9 plasmid with the EF1α promoter.

Additionally, the region is difficult to PCR due to the high GC content. This made it difficult to sequence the region to detect whether the mutation had been inserted. A lot of optimisation was needed in terms of amplifying primers, PCR temperature and PCR mixes to successfully PCR the region to detect whether gDNA was wildtype or mutant or whether the targeting construct had been inserted. Gonzalez and colleagues (2014) report successfully editing iPSCs from ε3 to ε4, however their longer ssODN of 120 base pairs was no more effective than the standard 65 base pair ssODNs in CTR M3 36S. Moreover, their CRISPR sequences were not approved by the CRISPR design web programs due to the high potential for off target mutations in these sequences.

A potential issue with the design of the targeting construct for APOE was the blasticidin selection. The targeting construct should have made it easy to select for cells with mutation introduced, even if these were a very low proportion of cells. However, unlike with geneticin for selection of the targeting construct very few cells survived blasticidin selection, and the cells that did were later found to be wildtype.

A novel technique called base editing may be a promising future strategy for the APOE mutation. In the absence of efficient HR and donor oligonucleotides, Komor and colleagues (2016) have described a way to make specific base changes without double-strand breaks, making the technology very specific and footprintless. By expressing the cytidine deaminase enzyme with the CRISPR guide the enzyme will induce a C - T change at the site it is directed to. Therefore, this process could be ideal for editing an APOE ε4/ε4 line into an APOE ε3/ε3 by making the C-T substitution.

4.4.4 ssODNs are not an effective approach for HDR in iPSCs

Introducing the mutation via an ssODN was not effective for the APOE rs429358 SNP. The probability of an ssODN insertion is low due to a number of factors. Firstly iPSCs have low transfection efficiency and a very high rate of repair. This reduces the time window for HDR by the ssODN and could perhaps be improved by small molecules that modulate DNA repair such as NU7026, an inhibitor of the DNA-dependent protein kinase that could work by reducing NHEJ (Maresca et al., 2013). Also with mutation insertion by ssODN it is important to not introduce any other mutations that may alter the gene function, and so it is not possible to use methods that may increase cas9 activity, such as using two CRISPR/Cas9 constructs.

Cas9 plasmids with either GFP or puromycin selection were used for inducing a DSB at the mutation site. FACS for GFP did not result in pluripotent cultures following sorting and the transient puromycin did not give enough time to gently select individual, transfected cells with antibiotic without wildtype cells surviving in and often taking over cultures. Therefore a clonal population from a cell with an ssODN inserted was very improbable without selection. ddPCR was a good strategy that could work with pools of transfected iPSCs to increase mutated cells by sib-selection prior to making cell populations clonal, as demonstrated by Miyaoka and colleagues (2014). However, this did not help in the APOE project possibly due to nonspecific binding of the mutant and wt probes. Therefore, using a targeting construct with selection and then removing it after by loxP or gRNA excision sites may be the best strategy for timely CRISPR/Cas9 knockin generation.

4.4.5 Conclusions

A novel CLU knockout iPSC line has been successfully generated using CRISPR/Cas9 genome editing. This is an incredibly useful genetic tool for disease modelling in iPSC systems and the CLU knockout cell line can now be used to study the role of this gene in Aβ- driven neurodegeneration. The aim to create an APOE ε4/ε4 line from the original CTR M3 36S line with APOE ε3/ε3 line was not successful. A number of different strategies were tested to improve the mutation integration and screening of the SNP but in conclusion the APOE gene is a difficult one to target. As the CRISPR/Cas9 technology continues to develop at a rapid pace it will become easier to target certain regions and CRISPR will become a standard tool in the disassembly of disease pathways. The novel base editing technology exemplifies this, and may be a successful tool in creating isogenic APOE lines.

Chapter 5 Phenotyping of CLU knockout neurons

5.1 Introduction

5.1.1 *In vitro* studies of clusterin and Aβ-toxicity

Following the finding in human neurons in this project and in rodent neurons previously by Killick et al. (2014) that neurons treated with Aβ have increased clusterin levels, it is now important to investigate the pathways through which clusterin mediates Aβ-toxicity in neurons. The study by Killick et al. (2014) in primary neuronal cultures suggests that CLU knockdown neruons, show a reduced response to Aβ. In this study neurons were treated with the siRNA to CLU overnight and then treated with 20μM $A\beta_{25-35}$ for 24 hours. Cell survival was reduced to 60% in $A\beta_{25-35}$ treated cells, as measured by nuclear morphology, whereas in cells treated with siRNA to CLU and $A\beta_{25-35}$ cell survival was not decreased (Killick et al., 2014). It will be important to test whether CLU absence blocks Aβ-toxicity in human neurons, and determine whether CLU mediates the Aβ-toxicity through the same pathway in a human iPSC-derived model.

5.1.2 Transcriptomics

In addition to hypothesis-driven techniques to study the effects of CLU on Aβ-toxicity, hypothesis-free, whole genome interrogation offers a great opportunity to discover the broader effects of CLU in response to Aβ. Genome-wide expression analysis using next generation sequencing (RNAseq) provides in-depth molecular profiling of biological processes, and has allowed multiple genes and pathways in pathological conditions to be

elucidated. RNAseq allows novel, unpredicted genes/exons and splice isoforms, fusion transcripts and allele-specific expression to be identified, which may be relevant to neurodegenerative disease (Costa et al., 2013). Human neurons from gene-edited iPSCs provide an ideal system for RNAseq as background differences in transcription factors, DNA methylation, and chromatin modifiers between individuals are removed, and these are important factors in many disorders (Lin et al., 2011).

5.1.3 Aims

The aims of this chapter are to determine whether there is a phenotype of the CLU-/- neurons in response to Aβ. Neurons will be differentiated from CTR M3 36S (wildtype) and CTR M3 36S CLU-/- and treated with $A\beta_{1-42}$ and $A\beta_{25-35}$ for 48 hours. Results from Killick and colleagues (2014) and from this project suggest that CLU-/- neurons may be protected from Aβ treatment. The Aβ-concentration curve from the neurite length assay will be repeated in CLU-/- neurons to determine if the Aβ-concentration curve is shifted, and a higher concentration of Aβ is required to cause significant death to the neuronal processes.

RNAseq will be used to investigate the molecular pathways involved in this toxicity. Based on data presented in Chapter 4, EGR1 may be involved in this pathway and it would be hypothesised that following Aβ treatment CLU-/- neurons would not have increased expression of EGR1. RNAseq will also be used to look at other genes involved in this pathway, such as DKK1, and other AD-relevant pathways will be investigated. Due to the wide effects of CLU and Aβ other pathways may also be disturbed. The RNAseq result will also make it possible to compare untreated CLU-/- to isogenic wildtype, to investigate whether there are any major differences between the cell lines.

5.2 Methods

5.2.1 Neuronal cultures

Neurons derived from wildtype CTR M3 36S and the CT3 M3 36S CLU-/- line were passaged for terminal plating at day 22 and left to differentiate in B27 medium until day 35 as described in Chapter 2.2.1. Neurons were plated in 6 well plates for RNA extraction (250 000 cells/well) or in 96 well plates (5000 cells per well) for imaging. A 50% media change was performed every 3 days until Aβ treatment on day 35.

5.2.2 Imaging assay

$A\beta_{1-42}$ was added to 96 well plates for 48 hours at concentrations from 1μM up to 20μM, and was prepared as described in Chapter 2.2.4. CAM live cell dye and Hoechst nuclear stain was then added to the media and cells were imaged as described in 2.2.5. The neurite length assay was used as an assay to measure toxicity of Aβ.

5.2.3 RNA sequencing

5.2.3.1 Selection, preparation and quantification of samples

$A\beta_{1-42}$ was added to wt and CLU-/- neurons in 6 well plates for 48 hours at concentration 1μM, which was previously established in Chapter 2.3.3 to be the lowest dose to cause a significant decease in neurite length. Lysates were collected from Aβ-treated cells and untreated controls, with 3 biological replicates per group, in Trizol for RNA extraction as described in Section 3.2.1.

RNA was extracted as described in Section 3.2.3.1 and RNA clean-up was done by RNeasy kit (Qiagen) according to manufacturer's instructions. DNase treatment removed any residual gDNA as described in Section 3.2.3.3. RNA was quantified using a NanoDrop™ and RNA quality was confirmed using the Agilent 2100 Bioanalyzer system. Only samples with a RNA Integrity Number (RIN) of >9 were used for RNAseq.

5.2.3.2 Library preparation and RNA sequencing

Library preparation and RNAseq was done by Wellcome Trust Centre for Human Genetics, University of Oxford. RNA samples were first run on a tape-station for quality control. TruSeq RNA Library Preparation Kit (Illumina) was used and mRNA was enriched by polyA selection. RNAseq was run on the Illumina HiSeq 4000 with 10 samples per lane, approximately 24 million 75bp paired-end reads per sample.

5.2.3.3 Processing and analysis of data

Preprocessing was performed using the software tool Trimmomatic to quality trim the reads and remove adapters (Bolger et al., 2014; usadellab.org). Tophat2 was used with default settings to align the reads (Kim et al., 2013; http://ccb.jhu.edu/software/tophat) to the human genome references assembly (build GRCH38.p5). Transcript assembly and differential gene and transcript expression analysis was then performed using Cufflinks and Cuffdiff (Trapnell et al., 2012; http://cufflinks.cbcb.umd.edu/). The Cuffdiff output was then visualised using the R project package CummeRbund

(http://compbio.mit.edu/cummeRbund), designed to simplify the analysis and exploration of Cuffdiff differential expression analysis data.

5.2.3.4 Pathway analysis

Gene set enrichment and gene ontology analysis was carried out using the R package Generally Applicable Gene-set Enrichment (GAGE) (Luo et al., 2009; http://sysbio.engin.umich.edu/~luow/downloads.php) and pathways were visualised with the R package Pathview (Luo et al., 2009). The recommended RNAseq workflow was followed for these two packages. The Krypto Encyclopaedia of Genes and Genomes (KEGG) was used for pathway analysis, a collection of manually drawn pathway maps covering current knowledge on the molecular interactions and reaction networks for the main biological functions including human diseases. Gene ontology (GO) analysis was also carried out for 'Biological Process' and 'Molecular Function' terms. Mapping transcriptomic data to KEGG pathway maps and GO terms allowed for biological interpretation of system-level functions.

For all genes and gene set analyses (GSAs), the p-value (after multiple testing correction by Benjamini and Hochberg procedure), q-value (a false discovery rate (FDR) based on an adjustment of the p-value using the Benjamini and Hochberg procedure) and the gene count were calculated by the R programmes.

5.3 Results

5.3.1 Neurite length assay for wildtype vs. CLU knockout neurons

To study whether the CLU-/- neurons had an altered response to Aβ compared to wildtype neurons, the neurite length assay was used as previously shown in Section 2.2.5. Figure 44 shows a difference in the Aβ assay in CLU-/- neurons and wildtype neurons. Wildtype cells were responsive to Aβ exposure at low doses, with a significant decrease in neurite length from 1μM $A\beta_{1\text{-}42}$. In comparison, CLU-/- neurons showed no significant response to $A\beta_{1\text{-}42}$ treatment at concentrations up to 3μM.

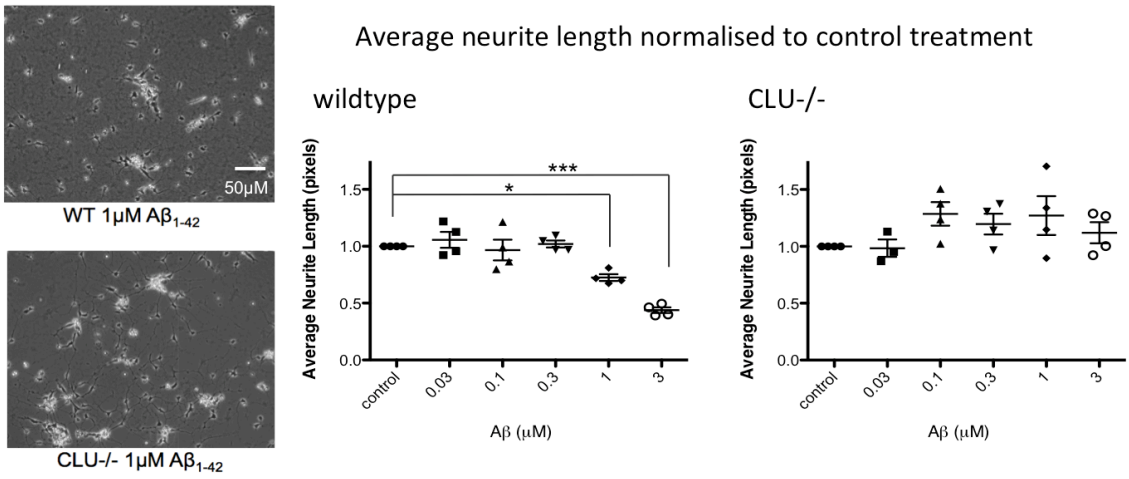

Figure 44. Neurite length is decreased in response to $A\beta_{1\text{-}42}$ in wildtype neurons but not in CLU-/- neurons. The neurite length assay measured length of neuronal processes in wt vs. CLU-/- neurons from 4 independent differentiations treated with $A\beta_{1\text{-}42}$ for 48 hours (or control buffers DMSO and SDS). Neurite length was significantly decreased in wt neurons at concentrations of 1μM and higher. Neurite length in CLU-/- neurons was not significantly decreased at any treatment concentration up to 3μM.

5.3.2 RNAseq analysis of wildtype vs. CLU knockout neurons

RNAseq was employed to investigate the pathways involved in Aβ toxicity that were not activated in CLU knockout neurons. RNA was harvested from cultures treated with 1μM $A\beta_{1-42}$ (the lowest dose found to cause toxicity in Section 2.3.3) and untreated from both wildtype and CLU-/- neurons. Gene Seta Analysis (GSA) was performed by GAGE and differentially expressed genes were identified and grouped to determine significantly up- and down-regulated KEGG pathways, biological processes and molecular functions were obtained for the 4 comparisons:

1. wildtype untreated neurons vs. CLU knockout untreated (WT0 vs. CLU0),
2. wildtype untreated neurons vs. wildtype 48hr Aβ-treated neurons (WT0 vs. WT48),
3. CLU knockout untreated vs. CLU knockout 48hr Aβ-treated (CLU0 vs. CLU48),
4. wildtype 48hr Aβ-treated neurons vs. CLU knockout 48hr Aβ-treated (WT48 vs. CLU48).

All significant KEGG pathways, molecular functions and biological processes are included in Appendix 2 (maximum 30), with the p-value, q-value, and the gene count.

5.3.2.1 Overall gene expression in the four conditions

The heatmap in Figure 45 visualises the expression of the entire significantly differentially expressed gene set at once by plotting the fragments per kilobase of exon per million reads mapped (FPKM) expression values. Figure 45 shows that the greatest difference in gene expression was between the wildtype and the CLU-/- lines, and not between the Aβ-treated and untreated groups. This is also shown simplistically in the

dendogram in Figure 46. The graph shows the closest relationships in gene expression were between the treatment conditions WT0 and WT48 samples and between the CLU0 and CLU48 samples, rather than between the cell lines WT0 and CLU0 and the WT48 and CLU48. The three biological replicates were very similar and have been grouped in all further analyses (see Appendix 3 for the dendogram of all samples).

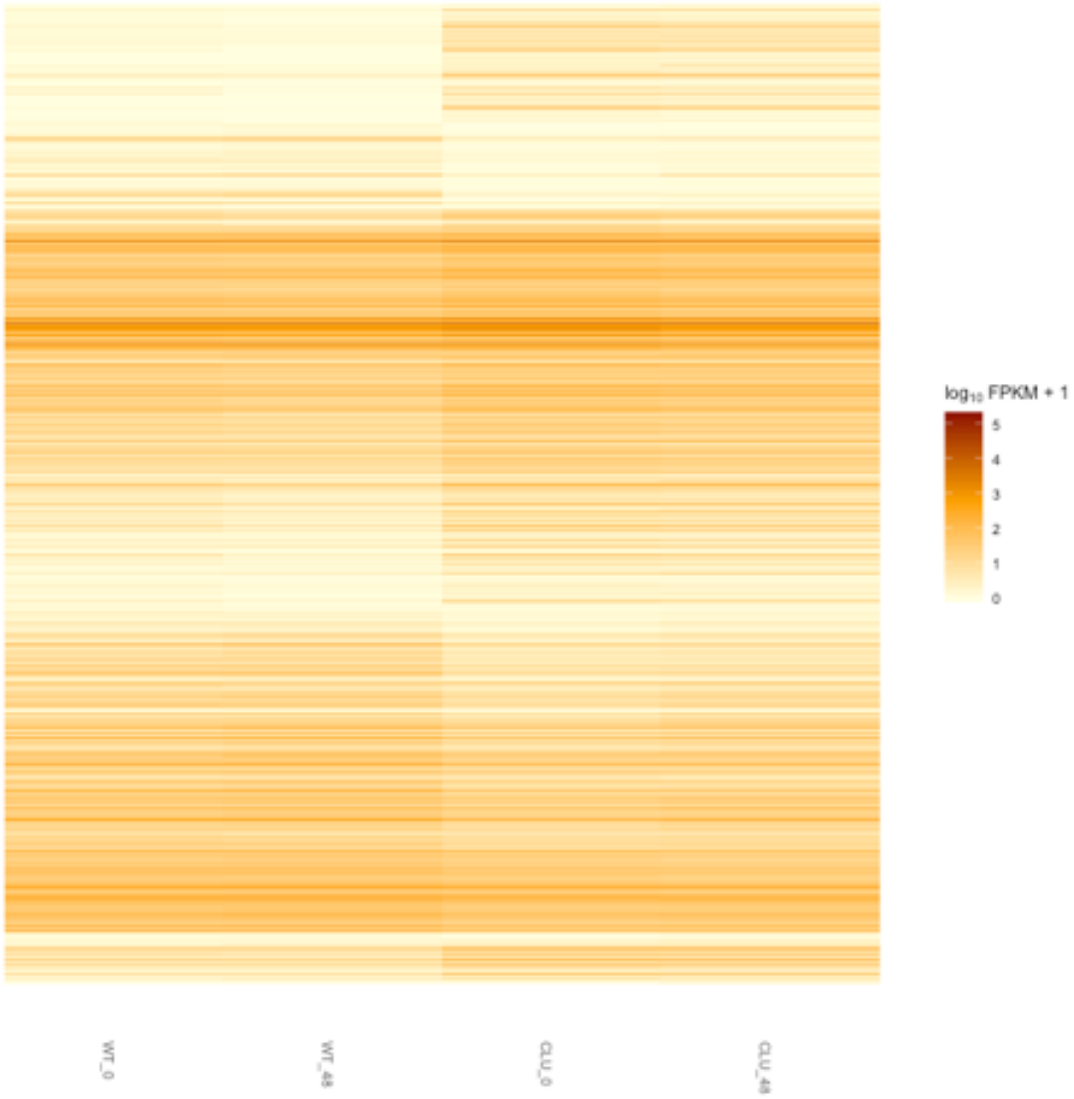

Figure 45. A heatmap of FPKM expression values in the 4 conditions. The gene set level visualisation across the whole genome is shown for all four conditions, WT and CLU-/-, treated and untreated.

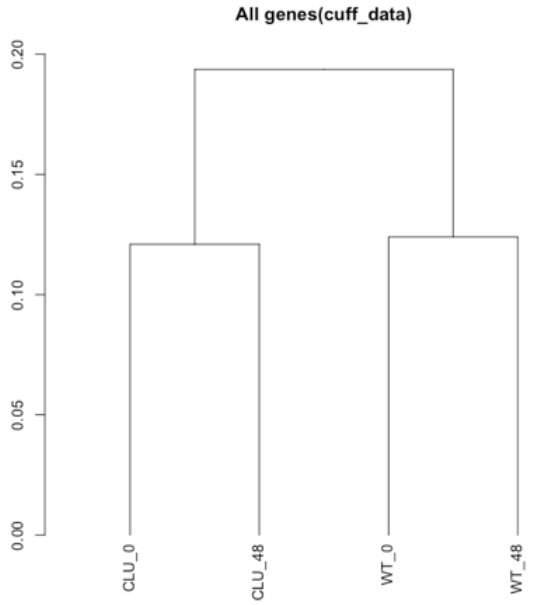

Figure 46. A dendrogram of the relationship between conditions based on the expression of all measured genes. The closest relationships are between CLU0 and CLU48 and also between WT0 and WT48.

The volcano plot in Figure 47 shows the relationship between fold-change and significance in each analysis. The y-axis shows the statistical significance (p-value after multiple corrections). The x-axis shows fold change out from the centre, with the greatest downregulated genes furthest on the left and the greatest upregulated genes furthest on the right. There are significant changes in gene expression for all group comparisons, with the least changes in WT0 vs. WT48 and CLU0 vs. CLU48, as indicated previously by Figures 45 and 46.

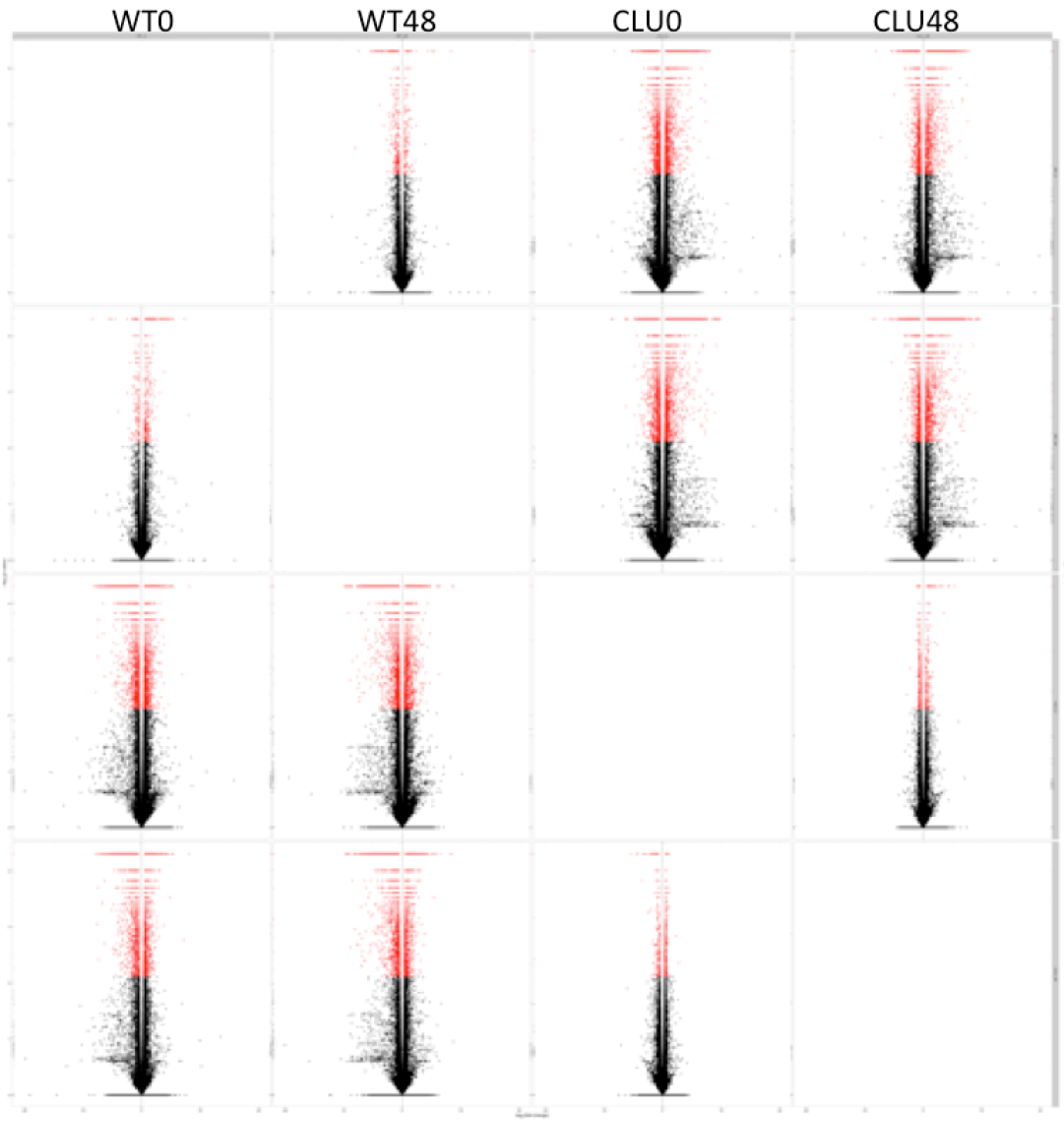

Figure 47. Volcano plot for fold change of all genes against p-value for all comparisons. X-axis shows log2(fold change), Y-axis shows − log10(p value). Red = significant (accounting for multiple correction analysis), black = non-significant.

5.3.2.2 Wildtype untreated vs. CLU-/- untreated

KEGG Pathways

Wildtype untreated neurons (WT0) were compared to CLU knockout untreated (CLU0) neurons to determine the extent of the difference in gene expression between the two cell lines. Genes were gathered into KEGG pathways and the top 5 significantly upregulated pathways are ranked in Table 4 (a full list of significantly enriched KEGG pathways is in Appendix 1).

Table 4. The top 5 pathways upregulated in WT0 vs. CLU0 KEGG analysis

Rank	Pathway	p-value
1	Focal adhesion	4.43E-22
2	ECM-receptor interaction	3.28E-12
3	P53 signalling pathway	2.78E-05
4	Lysosome	3.37E-11
5	Endocytosis	8.80E-11

Focal adhesion is the most significantly upregulated pathway in CLU0 compared to WT0 (p=4.43E-22). This pathway is involved in the regulation of the actin cytoskeleton, Wnt signalling and the MAPK signalling pathway (shown in Figure 48), all relevant pathways in AD pathogenesis. P53 is the 3rd most significant pathway (p=2.78E-05). This is shown in Figure 49, with the genes upregulated in CLU0 in red and downregulated in green. Through p53, apoptosis pathways are activated via upregulation of caspase 3.

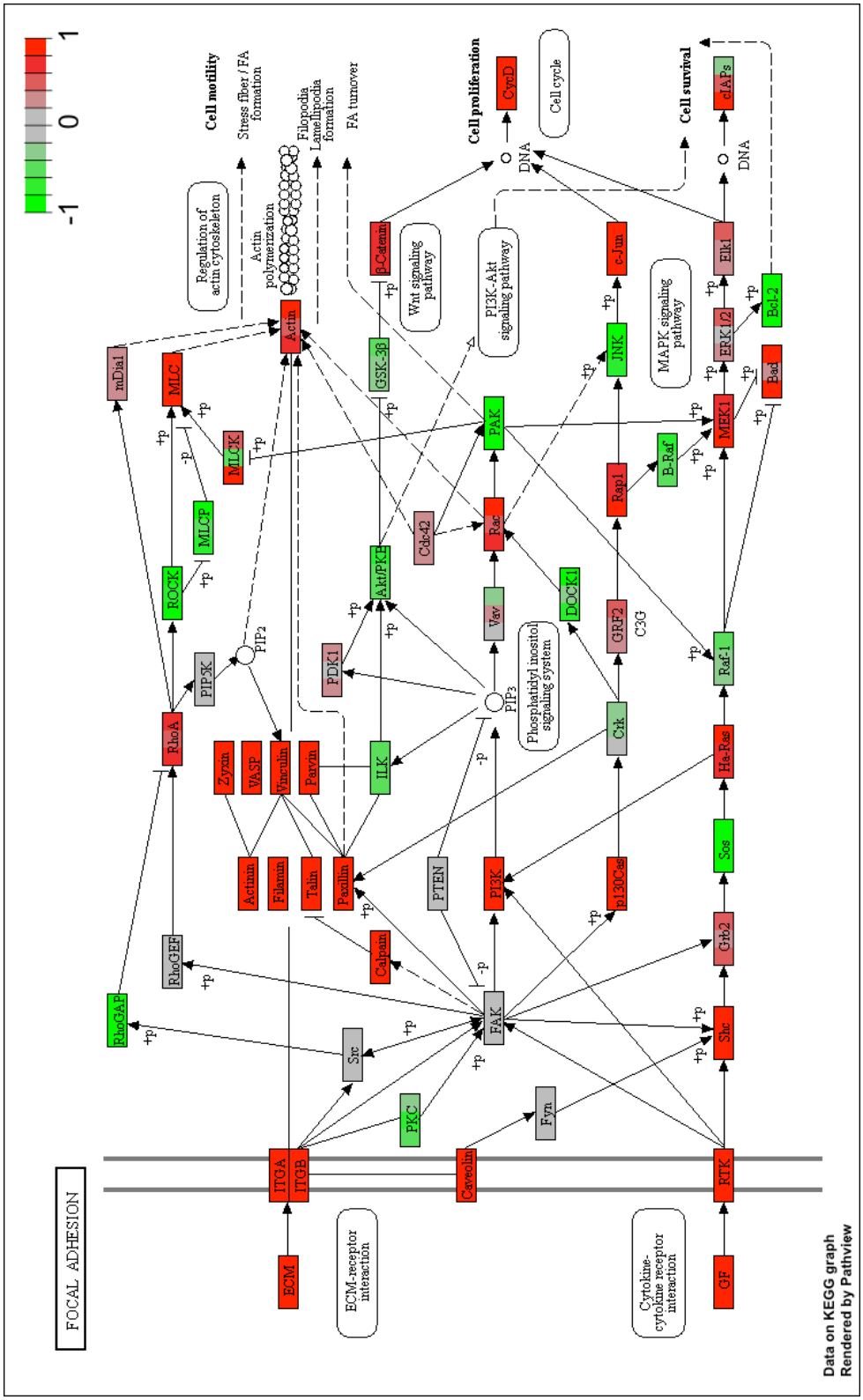

Figure 48. Focal adhesion was the most upregulated KEGG pathway in CLU0 compared to WT0. The scale bar shows upregulated genes (closer to 1) are labelled in red and downregulated genes (closer to -1) are labelled in green.

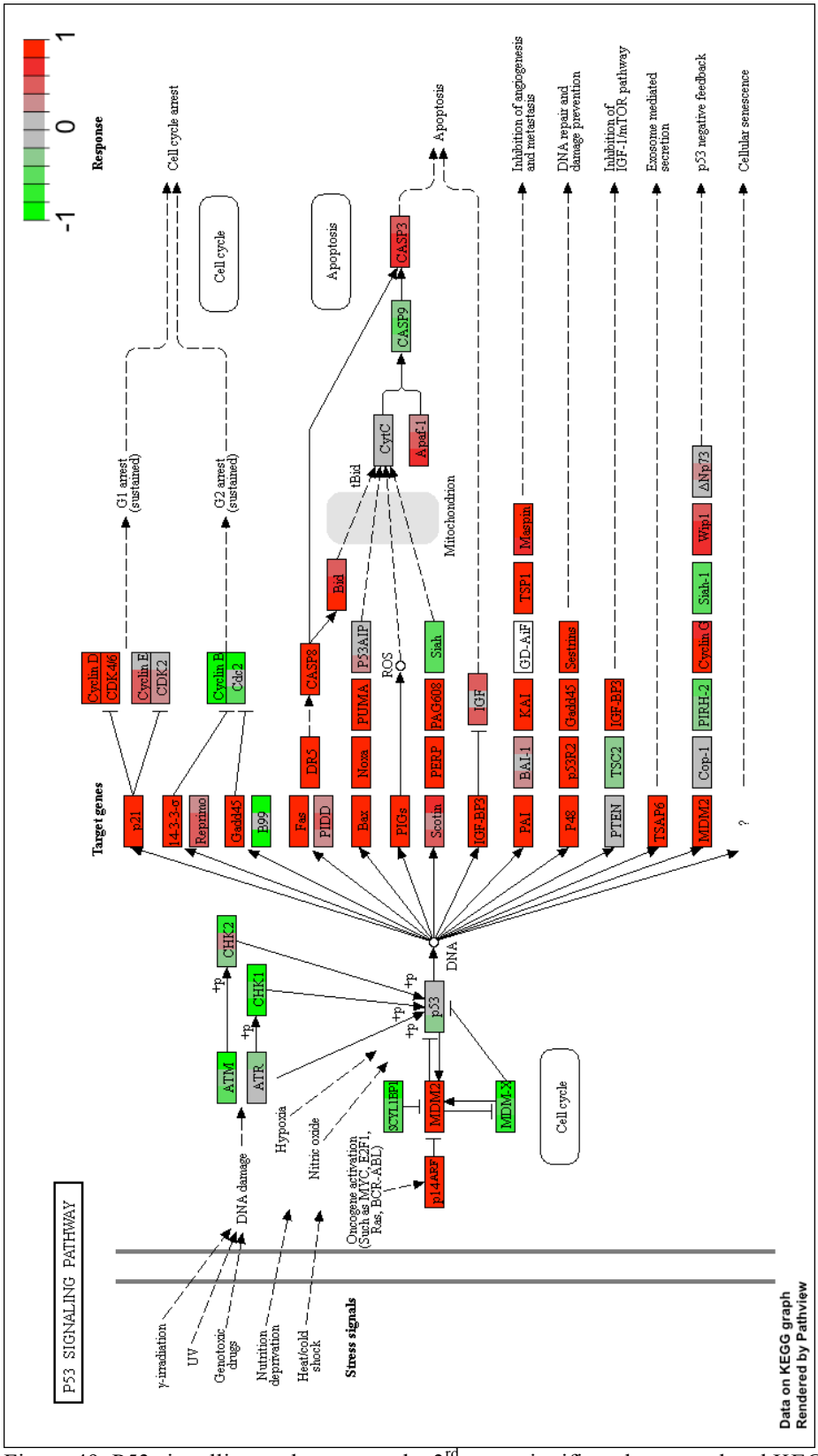

Figure 49. P53 signalling pathway was the 3rd most significantly upregulated KEGG pathway in CLU0 compared to WT0. The scale bar shows upregulated genes (closer to 1) are labelled in red and downregulated genes (closer to -1) are labelled in green.

Other significantly upregulated KEGG pathways of particular interest between CLU-/- untreated and wt untreated are apoptosis (the 9th ranked pathway, p=2.22E-08), the complement and coagulation pathway (11th top ranked, p=4.75E-08), regulation of the actin cytoskeleton (13th top ranked, p=7.17E-07) and the Wnt signalling pathway (65th ranked, p=0.0320), although there are many other pathways relevant to AD pathogenesis too (full list of significant KEGG pathways in Appendix 2). The apoptosis pathway is shown in Figure 50, with upregulated genes in red. The complement pathway is shown in Figure 51. The clusterin gene is known to be associated with both of these pathways (Bettuzzi and Pucci, 2009).

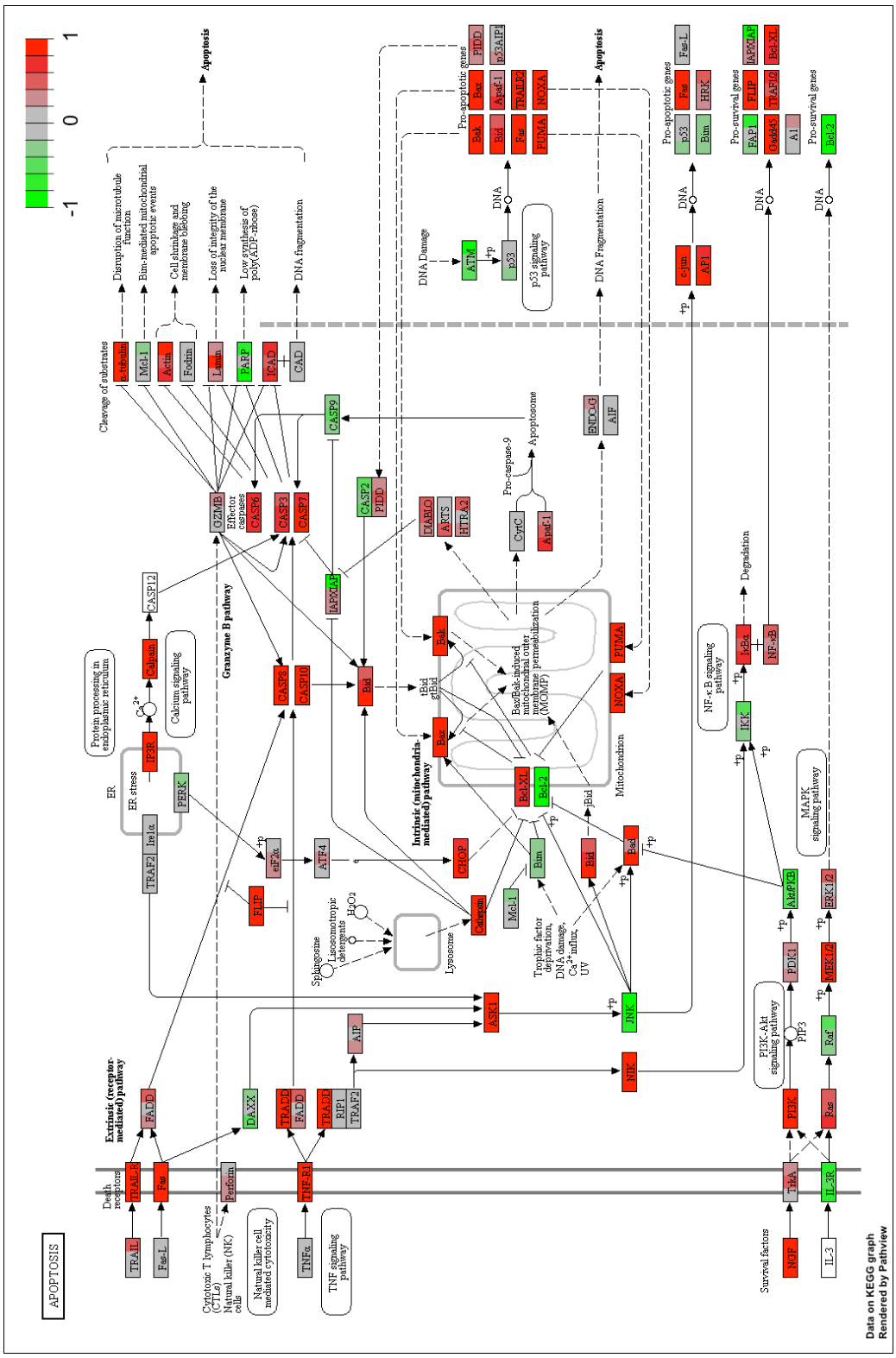

Figure 50. The apoptosis pathway was significantly upregulated in CLU0 compared to WT0. The scale bar shows upregulated genes (closer to 1) are labelled in red and downregulated genes (closer to -1) are labelled in green.

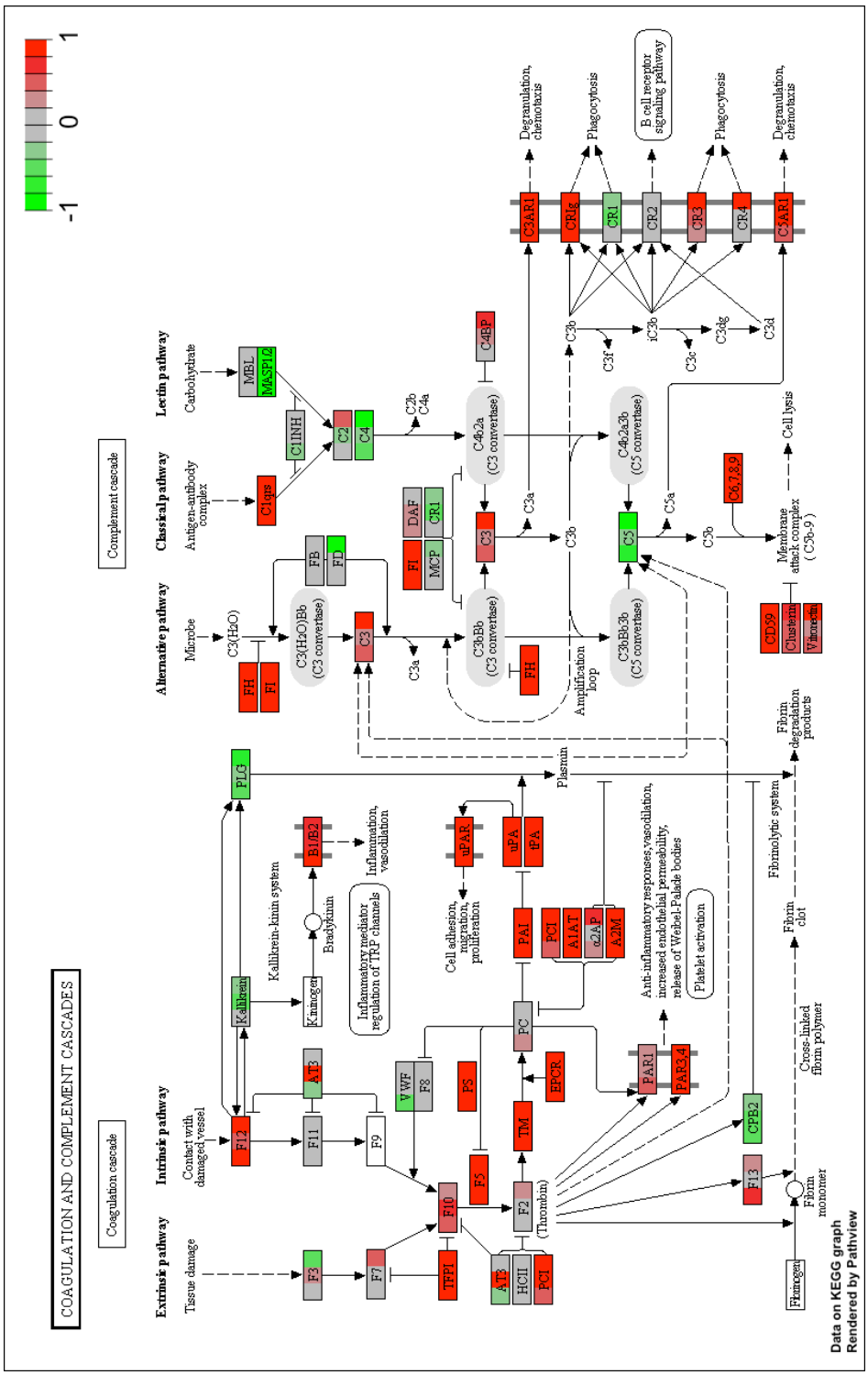

Figure 51. The complement and coagulation pathway was significantly upregulated in CLU0 compared to WT0. The scale bar shows upregulated genes (closer to 1) are labelled in red and downregulated genes (closer to -1) are labelled in green.

The 5 most significantly downregulated pathways in WT0 vs. CLU0 are presented in Table 5.

Table 5. The top 5 pathways downregulated in WT0 vs. CLU0 KEGG analysis

Rank	Pathway	p-value
1	Spliceosome	3.61E-10
2	RNA transport	1.34E-06
3	mRNA surveillance pathway	6.04E-06
4	Notch signaling pathway	0.000611989
5	DNA replication	0.000707827

Disease Pathways

The top disease-KEGG pathways from the WT0 vs. CLU0 comparison are summarised in Table 6. The top pathways are all diseases with literature to support clusterin as an important candidate gene (Betuzzi and Pucci, 2009). The Alzheimer's disease pathway was significantly upregulated in the CLU-/- untreated neurons. The genes regulating this are shown in the KEGG pathway in Figure 52, with the genes upregulated in CLU0 in red and downregulated in green. Genes APP, BACE and APOE are included in the upregulated genes in untreated CLU-/- neurons compared to untreated wildtype. However, the inclusion of Alzheimer's in the KEGG disease pathway list may be due to CLU having a major role in AD in the literature, and hence always flagging up this pathways where this gene is altered.

Table 6. The top 6 disease pathways upregulated in WT0 vs. CLU0 KEGG analysis

Rank	Pathway	p-value
1	Amoebiasis	2.67E-16
2	Rheumatoid arthritis	3.35E-12
3	Pathways in cancer	3.95E-09
4	Hypertrophic cardiomyopathy (HCM)	1.02E-07
5	Dilated cardiomyopathy	1.39E-07
6	Alzheimer's disease	1.59E-07

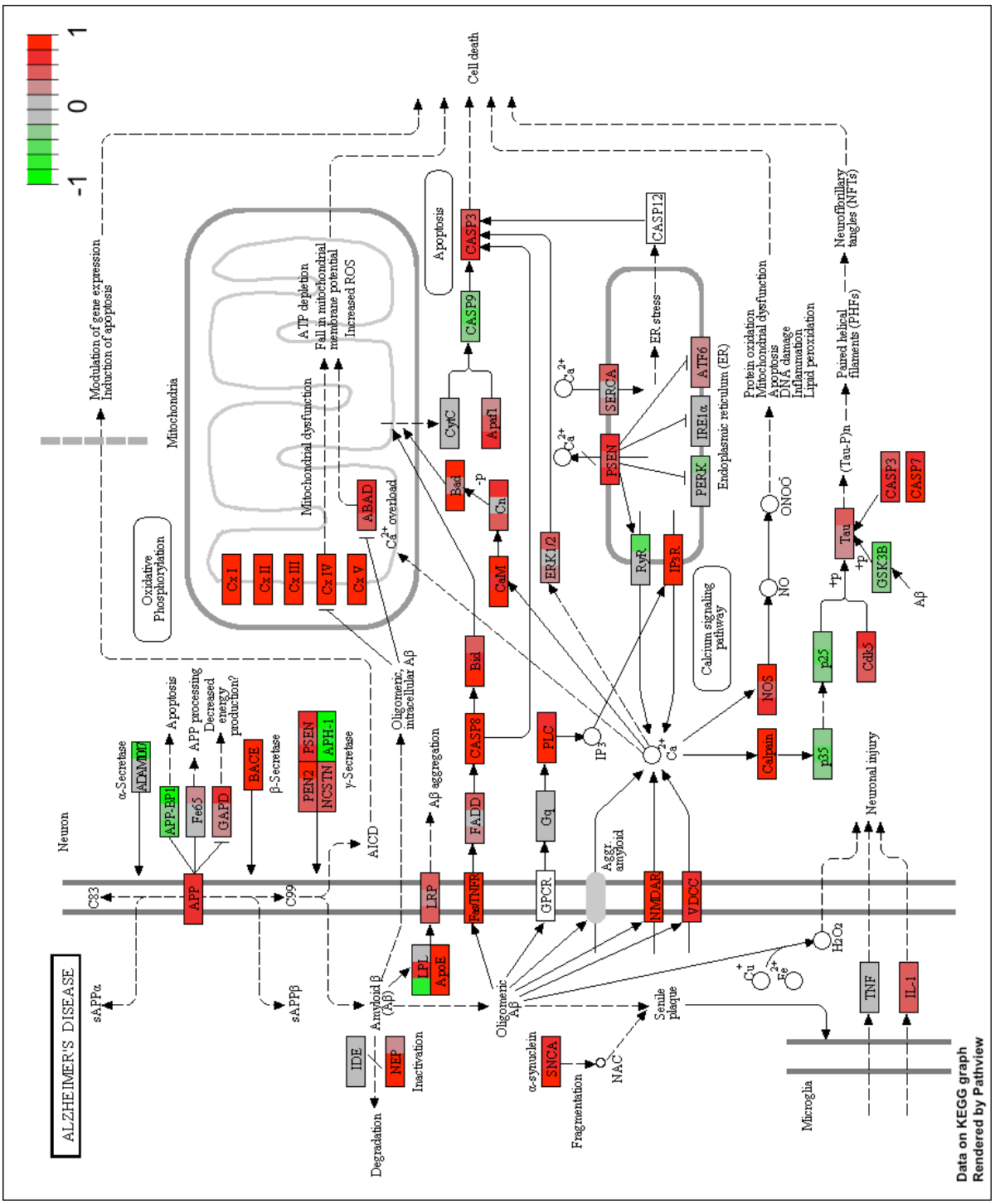

Figure 52. The Alzheimer's disease pathway is significantly upregulated in CLU0 compared to WT0 cells. The scale bar shows upregulated genes (closer to 1) are labelled in red and downregulated genes (closer to -1) are labelled in green.

Molecular functions

The molecular functions GO terms were also investigated in the WT0 vs. CLU0 analysis. The top molecular functions upregulated in CLU knockout cells compared to wildtype are shown in Table 7 and the top molecular functions downregulated are shown in Table 8.

Table 7. The top 5 molecular functions upregulated in WT0 vs. CLU0 analysis

Rank	Pathway	p-value
1	cytokine receptor binding	2.61E-15
2	growth factor binding	3.18E-15
3	cytokine activity	1.48E-14
4	carbohydrate derivative binding	2.12E-14
5	glycosaminoglycan binding	8.95E-14

Table 8. The top 5 molecular functions downregulated in WT0 vs. CLU0 analysis

Rank	Pathway	p-value
1	helicase activity	3.01E-11
2	DNA-dependent ATPase activity	2.77E-09
3	histone binding	4.23E-09
4	chromatin binding	7.73E-09
5	microtubule motor activity	8.30E-08

5.3.2.3 Wildtype untreated vs. wildtype Aβ-treated

Disease Pathways

The WT0 and WT48 comparison had only one disease pathway that was significantly upregulated in the KEGG analysis, which was Systemic lupus erythematosus (p= 0.00605). The top downregulated disease pathways for WT0 vs. WT48 are show in Table 9. These overlap closely with the upregulated disease pathways in the WT0 vs. CLU0 analysis (4/5 shared top 5 pathways). Pathways in cancer was not in the most significant 5 in the WT0 vs. WT48 analysis (as in WT0 vs. CLU0) but was the 12th highest ranked (p= 0.0275). Alzheimer's disease was 15th ranked but was not significantly downregulated in this analysis (p=0.0682).

Table 9. The top 5 disease pathways downregulated in WT0 vs. WT48 analysis

Rank	Pathway	p-value
1	Amoebiasis	3.98E-05
2	Hypertrophic cardiomyopathy (HCM)	0.001573365
3	Dilated cardiomyopathy	0.003850099
4	Rheumatoid arthritis	0.003870673
5	Bacterial invasion of epithelial cells	0.007491901

KEGG pathways

Only 8 KEGG pathways were significantly upregulated for the WT0 vs. WT48 analysis. The top 5 upregulated pathways are shown in Table 10. Table 11 shows the 5 top downregulated pathways in WT48 compared to WT0. Many of the top pathways in WT0 vs. CLU0 are also present in the top 5 pathways for WT0 vs. WT48.

Focal adhesion was the top upregulated pathway for WT0 vs. CLU0 and was the top downregulated pathway for WT0 vs. WT48. The focal adhesion pathway is shown in Figure 53. The top 3 downregulated pathways in WT0 vs. WT48 are all closely interacting pathways: focal adhesion, extracellular matrix (ECM)-receptor interaction and regulation of actin cytoskeleton.

Table 10. The top 5 KEGG upregulated pathways in WT0 vs. WT48 analysis

Rank	Pathway	p-value
1	Ubiquitin mediated proteolysis	0.002678677
2	RNA degradation	0.008252567
3	Cell cycle	0.011126756
4	Progesterone-mediated oocyte maturation	0.011938069
5	Notch signaling pathway	0.012883576

Table 11. The top 5 KEGG downregulated pathways in WT0 vs. WT48 analysis

Rank	Pathway	p-value
1	Focal adhesion	1.03E-08
2	ECM-receptor interaction	1.12E-06
3	Regulation of actin cytoskeleton	0.000284818
4	Hematopoietic cell lineage	0.000292085
5	Protein digestion and absorption	0.000816688

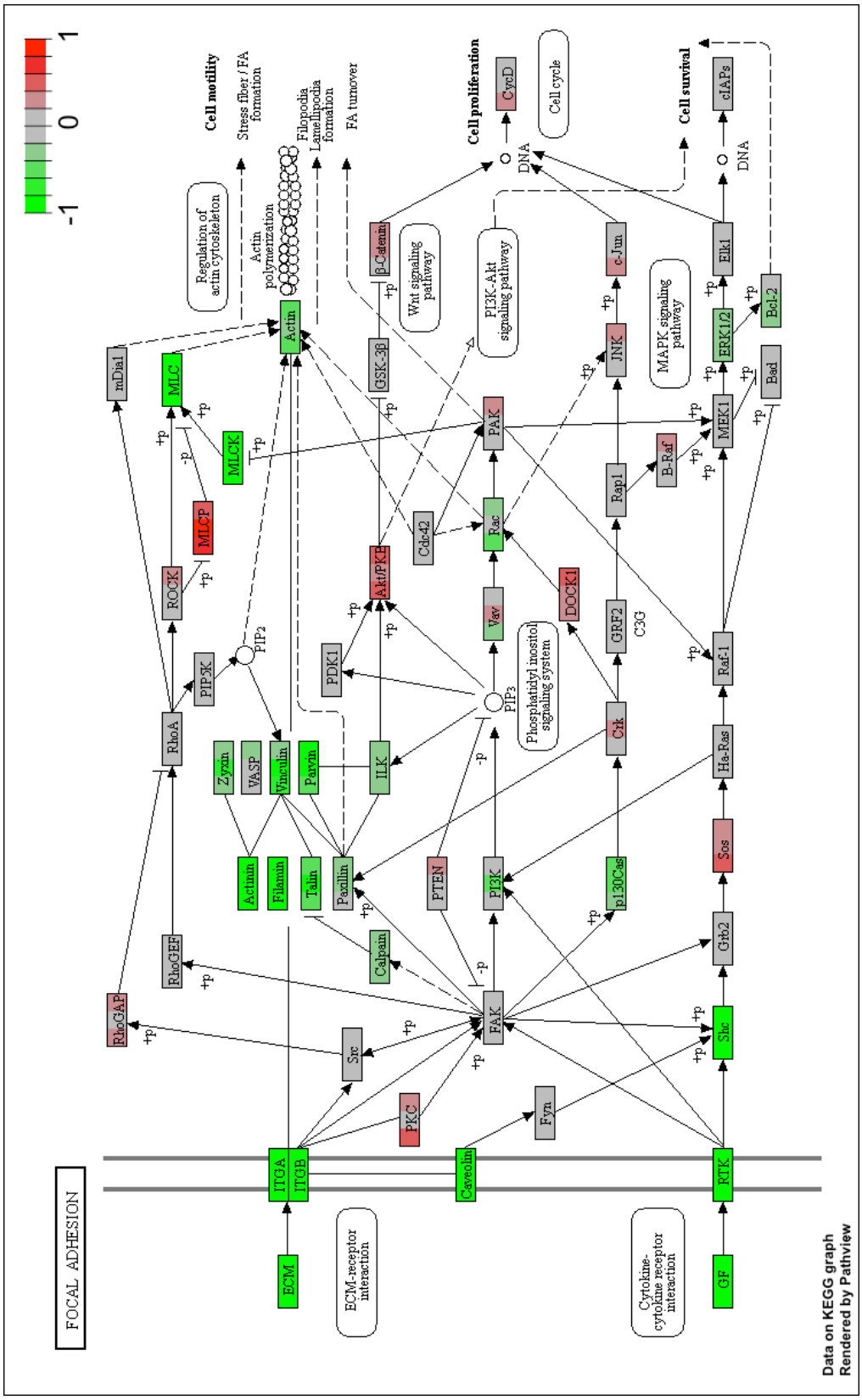

Figure 53. Focal adhesion pathway is downregulated in WT48 compared to WT0. Upregulated genes are highlighted red, downregulated genes are highlighted green.

Molecular functions

The top upregulated and downregulated molecular functions in Aβ-treated WT cells compared to the untreated WT cells are dominated by cytoskeletal structural and functional related processes, rather than relating directly to cell death processes. These are shown in Table 12 and 13.

Table 12. The top 5 upregulated molecular functions in WT0 vs. WT48 analysis

Rank	Pathway	p-value
1	chromatin binding	4.98E-06
2	microtubule motor activity	0.000173093
3	DNA-dependent ATPase activity	0.000449071
4	microtubule binding	0.000292085
5	ubiquitin-protein ligase activity	0.002079373

Table 13. The top 5 downregulated molecular functions in WT0 vs. WT48 analysis

Rank	Pathway	p-value
1	extracellular matrix structural constituent	5.46E-06
2	actin binding	5.95E-06
3	integrin binding	4.03E-05
4	actin filament binding	5.56E-05
5	ADP binding	9.95E-05

5.3.2.4 CLU-/- untreated vs. CLU-/- Aβ-treated

Disease Pathways

The disease pathways downregulated in the CLU0 vs. CLU48 analysis were dominated by neurodegenerative diseases. Alzheimer's disease is the 3rd most significant pathway downregulated (Figure 51). The downregulation of neurodegeneration pathways in CLU-/- cells following the addition of Aβ to cultures differs from wildtype cells. The list of the top 5 significantly downregulated disease pathways in the CLU-/- Aβ-treated samples compared to the untreated samples is summarised in Table 14.

The inclusion of Alzheimer's disease in the KEGG disease pathway list may be attributed to CLU being published in a large quantity of AD studies, and therefore any analysis involving clusterin could tag an AD pathway. However, the inclusion of the other neurodegenerative disease pathways, Parkinson's disease (Figure 52) and Huntington's disease (Figure 53), suggests that this is not the cause, and common neurodegenerative pathways, such as mitochondrial dysfunction and apoptosis are significantly dysregulated in the CLU48 condition.

No disease pathways were significantly upregulated in the CLU0 vs. CLU48 analysis.

Table 14. The top 5 disease pathways downregulated in CLU0 vs. CLU48 analysis

Rank	Pathway	p-value
1	Parkinson's disease	5.85E-11
2	Huntington's disease	1.10E-08
3	Alzheimer's disease	5.84E-07
4	Pathogenic Escherichia coli infection	0.000526046
5	Rheumatoid arthritis	0.002484202

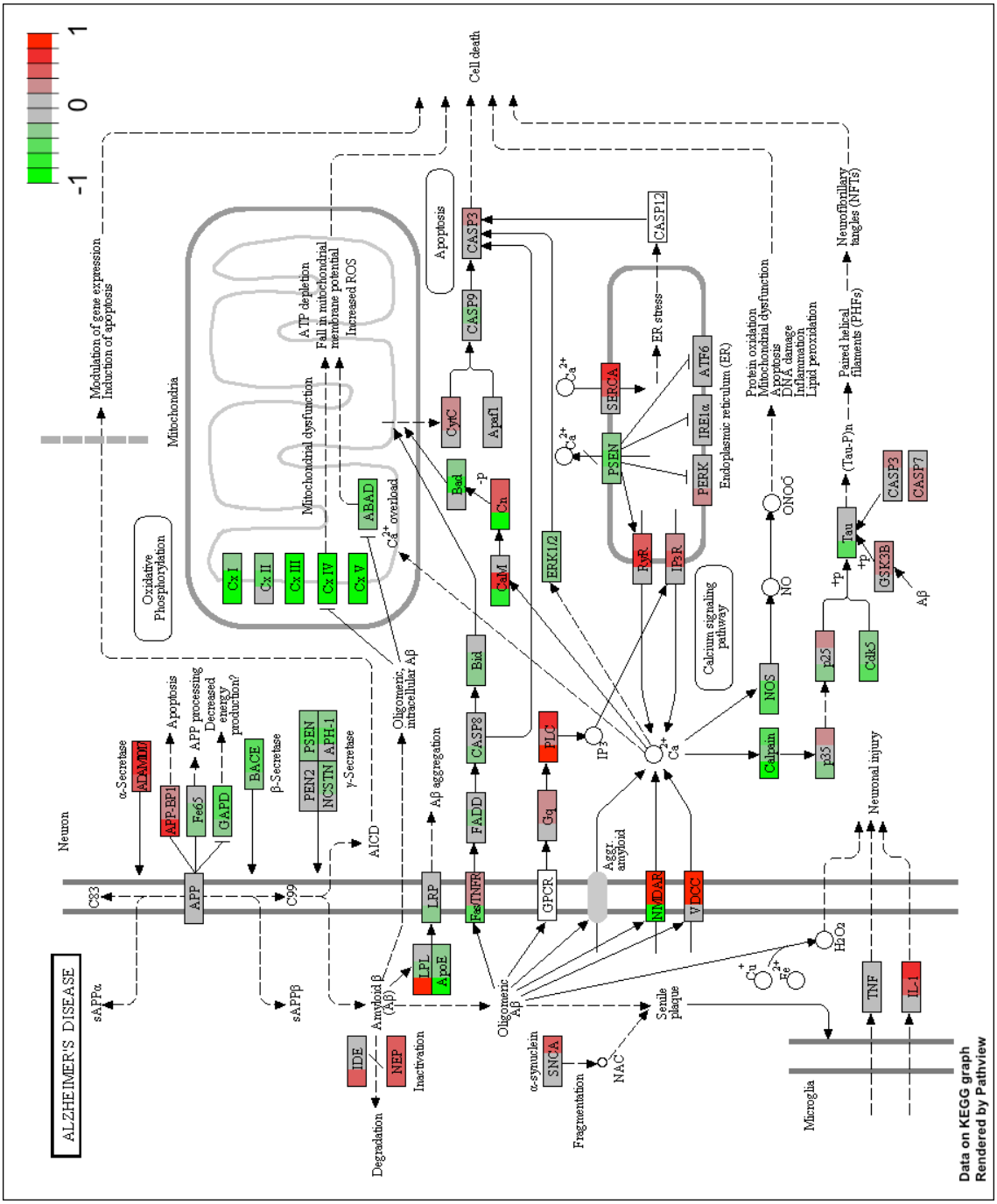

Figure 54. The Alzheimer's disease pathway is significantly downregulated in CLU0 compared to CLU48 cells. The scale bar shows upregulated genes (closer to 1) are labelled in red and downregulated genes (closer to -1) are labelled in green.

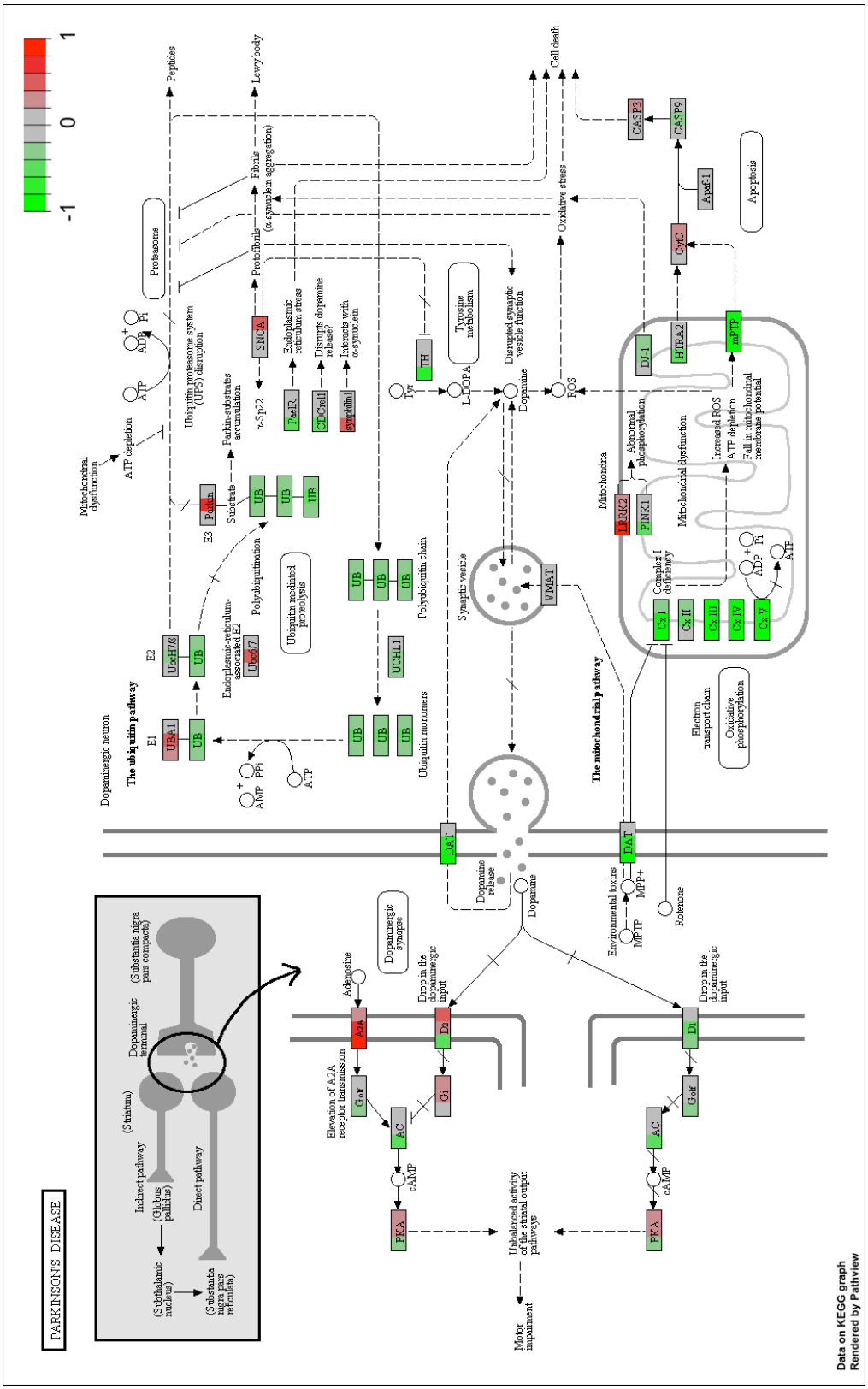

Figure 55. The Parkinson's disease pathway is significantly downregulated in CLU0 compared to CLU48 cells. The scale bar shows upregulated genes (closer to 1) are labelled in red and downregulated genes (closer to -1) are labelled in green.

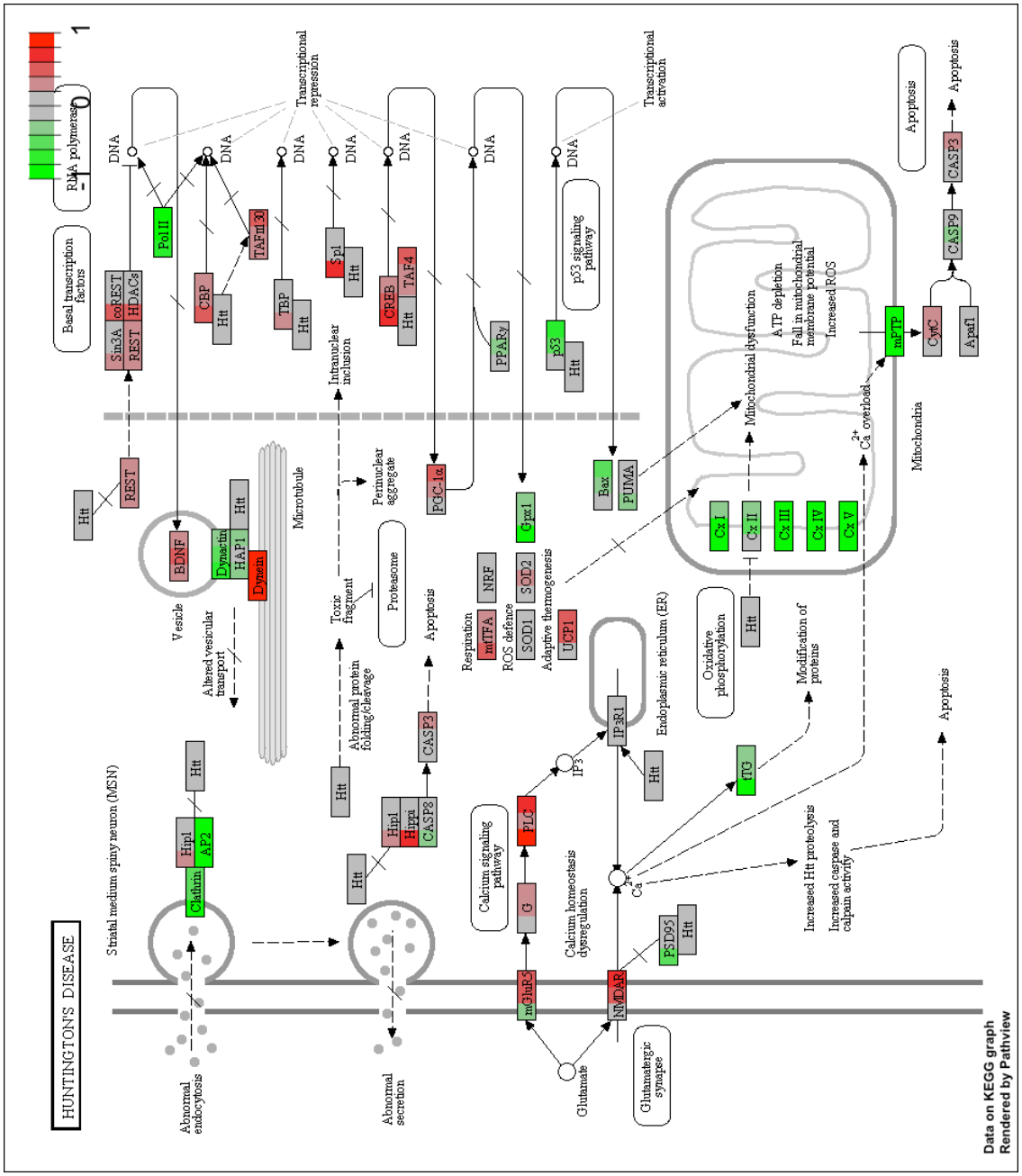

Figure 56. The Huntington's disease pathway is significantly downregulated in CLU0 compared to CLU48 cells. The scale bar shows upregulated genes (closer to 1) are labelled in red and downregulated genes (closer to -1) are labelled in green.

KEGG pathways

The only upregulated KEGG pathway for this analysis was the taste transduction pathway (p=0.0366). There 5 most significantly downregulated pathways in CLU48 compared to CLU0 are presented in Table 15.

Table 15. The top 5 downregulated KEGG pathways in CLU0 vs. CLU48 analysis

Rank	Pathway	p-value
1	Ribosome	1.19E-26
2	Oxidative phosphorylation	1.24E-11
3	Lysosome	2.16E-07
4	Phagosome	6.55E-06
5	Endocytosis	6.48E-05

5.3.2.5 Aβ-DKK1-EGR1 pathway analysis

DKK1 expression by FPKM in the 4 conditions is shown in Figure 57. DKK1 expression was not changed following Aβ treatment in either wildtype neurons or CLU knockout neurons. DKK1 expression was significantly higher in CLU knockout neurons compared to wildtype neurons. However, the expression of the gene is low in all samples. Other DKK genes, DKK2 and DKK3, also have increased expression in CLU-/- neurons (Figure 58). DKK2 expression is 20 times greater in CLU-/- neurons (baseline FPKM average=1) and DKK3 is 4 times greater in CLU-/- cells (baseline FPKM average=10). DKK4 expression levels are unchanged between conditions, and expression of the gene is very low in all conditions.

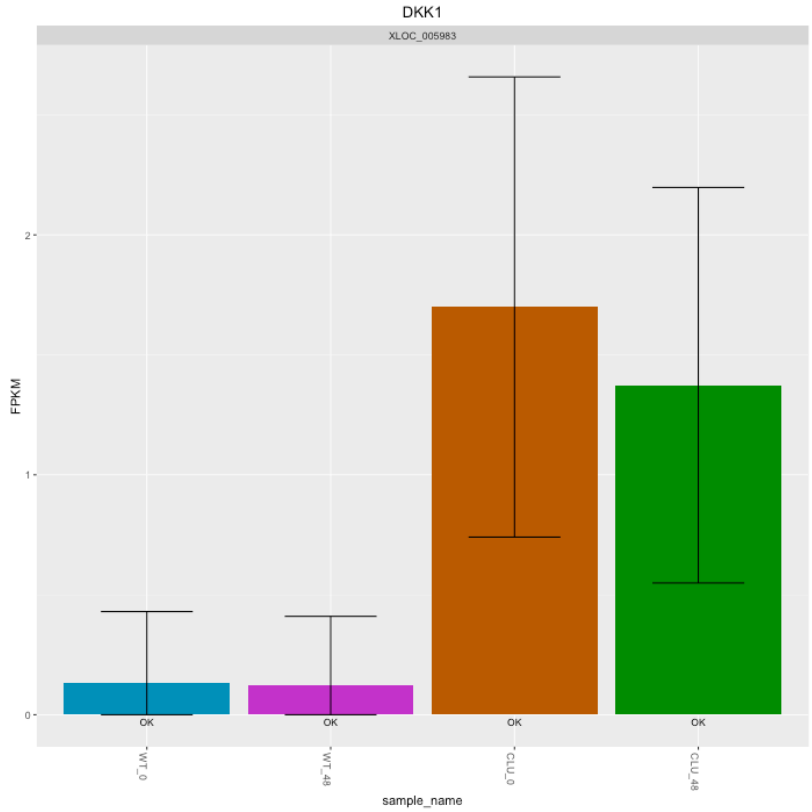

Figure 57. DKK1 expression in the 4 neuronal conditions. DKK1 expression is significantly increased in CLU-/- neurons.

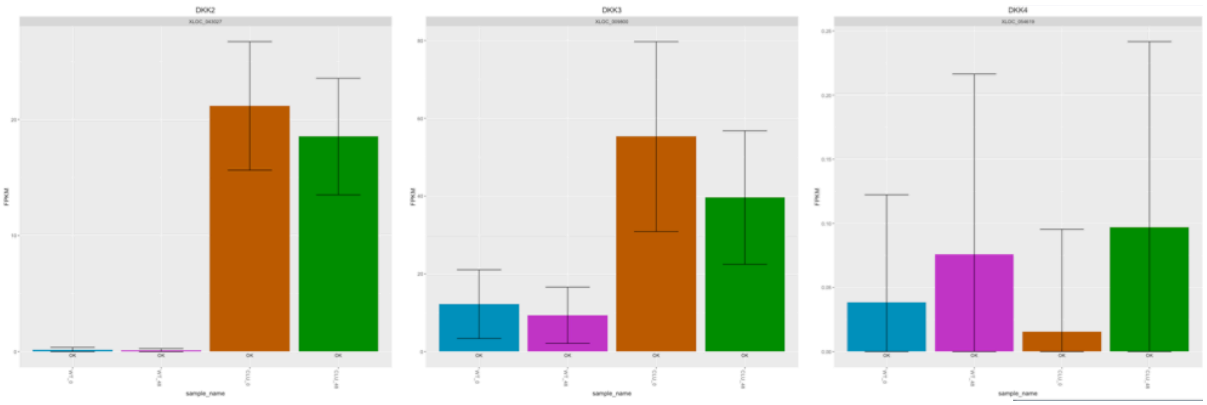

Figure 58. DKK2, DKK3 and DKK4 expression, respectively, in the 4 neuronal conditions. DKK2 and DKK3 expression is significantly higher in CLU-/- neurons.

EGR1 expression is significantly decreased in Aβ-treated wildtype neurons compared to untreated (p=5.00E-05). This differs from qPCR results in chapter 4.3.4. EGR1 in CLU0 samples is also significantly decreased compared to WT0. The expression levels of EGR1 by FPKM are shown in Figure 59.

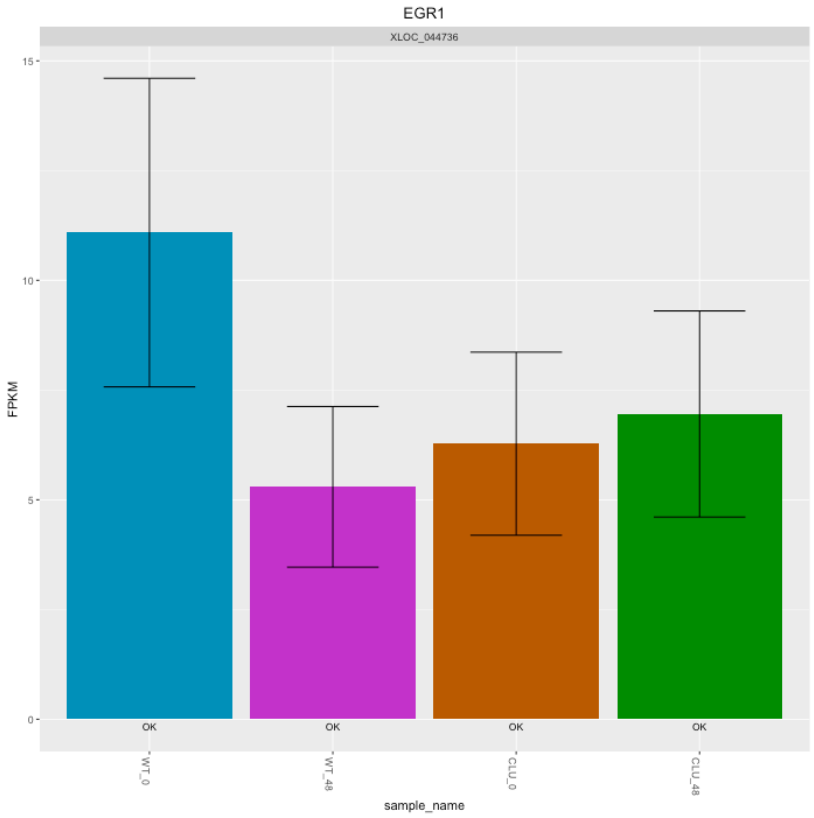

Figure 59. EGR1 expression in the 4 neuronal conditions.

KLF10 is another target gene of Aβ and DKK1, along with EGR1 in the Killick et al. study (2014). EGR1 is significantly upregulated in CLU-/- neurons compared to wildtype neurons (p= 5.00E-05), as shown in Figure 60. However, the expression of KLF10 is not significantly changed with Aβ exposure.

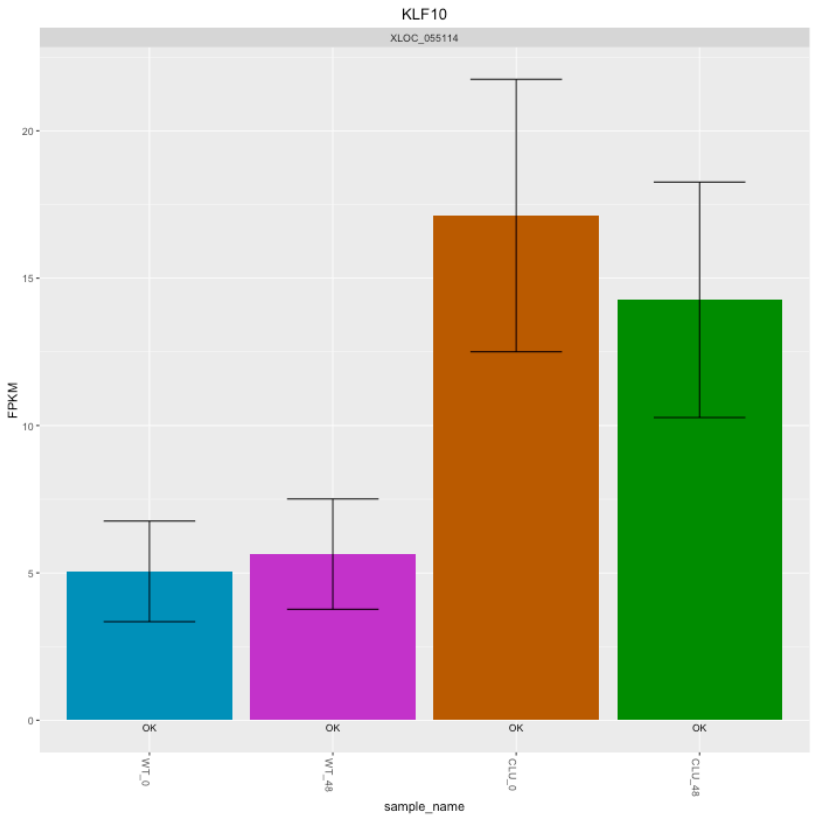

Figure 60. KLF10 expression in the 4 neuronal conditions.

APOE expression is increased in the CLU-/- neurons compared to the wildtype. The APOE gene is presented in Figure 61 with its neighbouring genes (APOC1, CTB, TOMM40), which Cufflinks grouped together as one transcript despite the signal coming predominantly from the APOE gene. FPKM expression was high for these genes, increasing from 42 for WT0 to 140 for CLU0.

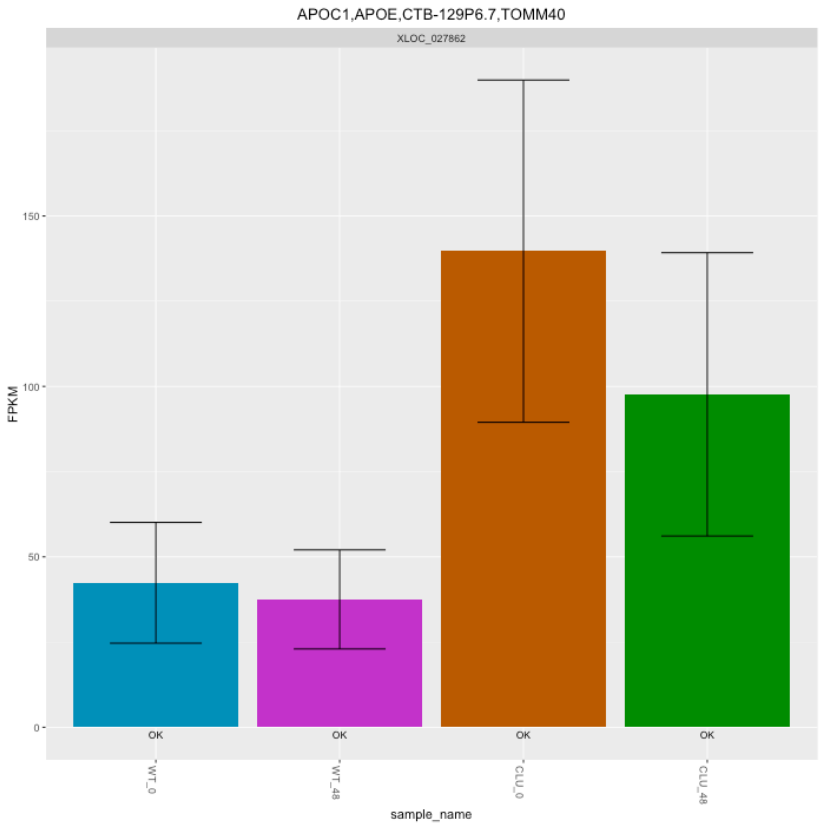

Figure 61. APOE expression in the 4 neuronal conditions.

5.3.2.6 Aβ target genes in wildtype vs. CLU-/- neurons

The large disparity in gene expression between the two cell lines made it difficult to reliably investigate Aβ-specific changes in gene expression in the CLU-/- line compared to in the wildtype line. Gene expression changes in individual Aβ target genes in the wildtype line in WT0 vs. WT48, were compared to the CLU knockout line in CLU0 vs. CLU48. Significant Aβ-mediated gene changes that were also found in the CLU-/- neurons could then be attributed to Aβ rather than purely cell line differences. Aβ target genes were selected from earlier WT0 vs. WT48 analysis and also identified from published genetic studies (Aydin et al. 2011; Reitz, 2012).

Very few target genes selected from the published literature were found to be significantly up- or down-regulated in WT0 vs. WT48. The genes that were significant were epidermal growth factor (EGF), EGF-receptor (EGFR), Notch1 and Notch3. When combining these and the significant genes identified from the earlier WT0 vs. WT48 analysis (in 5.3.2.3) none of the potential Aβ target genes significantly altered in the Aβ-treated wildtype line were significantly altered in the CLU-/- line. EGFR is shown in Figure 59 as an example. EGFR is significantly downregulated in WT0 vs. WT48 (p= 0.0038); however, its expression is not significantly changed in CLU0 vs. CLU48. The largest change is still between the wildtype line and the CLU line (p= 0.00005).

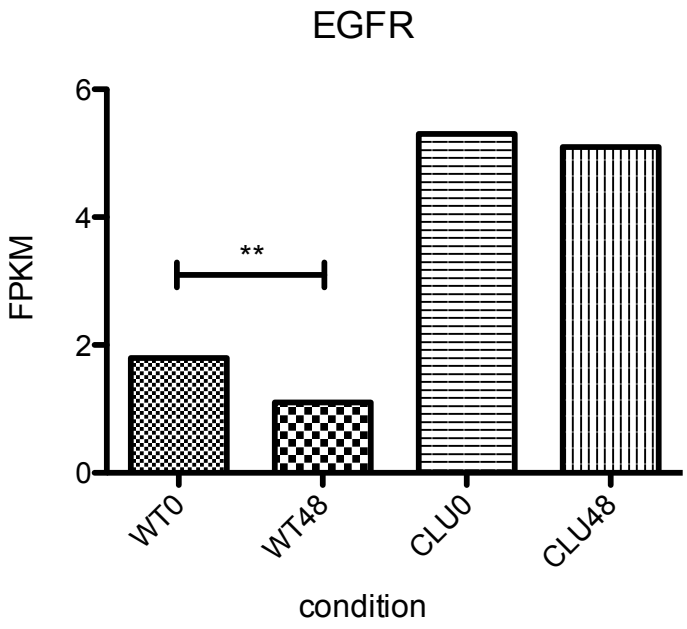

Figure 62. EGFR is significantly altered in response to Aβ in wildtype neurons but not in CLU-/- neurons. Gene expression is shown as FPKM.

AD relevant genes that were differentially expressed in the CLU knockout line compared to the wildtype include APP, PSEN2, MAP2, SORL1, and PICALM.

5.4 Discussion

5.4.1 CLU knockout neurons are not vulnerable to Aβ insult

CLU knockout neurons did not have significantly reduced neurite length in the imaging assay developed to measure Aβ toxicity in the neurons. Wildtype neurons had reduced neurite length as the neuronal processes started to die, but this was not found in the CLU knockout neurons. This reduced sensitivity to Aβ insult and shift in the Aβ-toxicity curve for this assay fitted our hypothesis and confirmed findings from a CLU knockdown in rodent cultures (Killick et al., 2014).

5.4.2 CLU knockout neurons have a different transcriptomic profile from wildtype

The CLU knockout neurons were found to have different gene expression to the wildtype neurons. This is interesting as the brains of CLU-/- mice seem to develop and age normally (deMattos et al., 2002). The heat map shows that the wildtype profile and the CLU-/- profile have a large number of differences. There are a number of genes that are altered in CLU knockout transgenics and in AD patients, however, due to the vast number of genes with altered regulation in the CLU-/- neuronal cells it is hard to be confident that significant changes in these are a specific result of the lack of clusterin production. For example, Plexin A4 has been associated with CLU and proposed as a CLU receptor (Kang et al., 2016). Related plexin genes are altered in WT0 vs. CLU0 analysis, but this could be due to changes in the cell line during genome editing rather than exclusively a result of the CLU gene.

Moreover, the difference between the two cell lines was far greater than the differences in gene expression between the treatment conditions (48 hours of Aβ-treatment compared to untreated). This made analysis of the wildtype Aβ-treated cells vs. the CLU-/- Aβ-treated cells problematic, as most differences would be driven by cell line differences, rather than by the Aβ. Therefore the difference between genes activated in Aβ-treated CLU-/- compared to WT cannot be reliably dissected. Since our programme could not perform analyses between two analyses (ie. (WT0 vs.WT48) vs. (CLU0 vs.CLU48)), Aβ target genes from the literature were compared between WT0 vs. WT48 and CLU0 vs. CLU48 to determine if the genes responded the same to the Aβ treatment in both lines. All of the genes responded differently to Aβ in wildtype neurons compared to CLU knockout neurons. This suggests that it is possible to dissect changes in gene expression in response to Aβ in the CLU-/- line by comparing it to wildtype, but the high background level of gene expression changes in CLU knockout cells must be considered.

In extensions to this study additional CLU-/- clones may help to elucidate exactly the role of clusterin in Aβ-mediated neurodegeneration. Moreover, a wildtype line that had been through the gene editing process, either unsuccessfully or with a non-targeting cas9, may act as a superior isogenic control. Alternatively, a higher dose of Aβ may be necessary to determine an effect of treatment above the background gene expression level differences between the cell lines.

5.4.3 Differentially expressed pathways in CLU knockout neurons

A number of AD-relevant pathways were significantly altered in CLU knockout neurons compared to wildtype. The top upregulated pathway in the CLU knockout untreated cells was focal adhesion, which is involved in regulation of the actin cytoskeleton, Wnt

signalling and MAPK signalling. In the Wnt pathway downstream of this GSK3 and JNK are both downregulated, suggesting alterations to both canonical and non-canonical PCP pathways. The p53 signalling pathway is the 3rd most significantly upregulated KEGG pathway. Interestingly this pathway has been proposed to regulate clusterin and Dkk1 downstream of Aβ (Killick et al., 2014; Purro et al., 2014).

The presence of the complement pathway in the list of most significantly upregulated KEGG pathways is especially noteworthy. CLU and CR1, the complement receptor, have been major hits in GWAS of AD, suggesting a role for the complement system in the etiology of AD (Crehan et al., 2012). It is particularly intriguing that the complement system is differentially regulated in untreated cells, and the complement pathway interaction with clusterin occurs here in the absence of pathology.

A final pathway also worthy of singling out is the endocytosis pathway. This was the 5th most significantly upregulated pathway in the CLU knockout neurons, and endocytosis has been identified as a key pathway from meta analyses of the AD GWAS, along with immunity and lipid processing (Hollingworth et al., 2011; Lambert et al., 2013). Excitingly, all of these processes are key to the CLU knockout analyses and the known roles of CLU *in vivo*.

5.4.4 Alzheimer's disease KEGG disease pathway was not significantly upregulated in Aβ-treated wildtype neurons compared to untreated

The Alzheimer's disease pathway was not upregulated in wildtype cells treated with Aβ. This may be attributable to the non-specific effects of Aβ, and toxic action of the oligomers could have been through a number of pathways and functions. It may also be

possible that the type of Aβ used in this experiment was not relevant to the AD pathway mapped by the KEGG analysis. This result may also be due to the cells. Despite 35-day-old neurons being morphologically mature they may not yet behave as functional neurons and this may result in other non-neurological disease pathways coming up in the analysis as more significant than AD. Moreover, normal AD pathway processes involve non-neuronal cell types that would not have been present in the *in vitro* model.

5.4.5 Alzheimer's disease KEGG disease pathway is significantly downregulated in Aβ-treated CLU-/- neurons compared to untreated

Alzheimer's disease, Parkinson's disease and Huntington's disease were the three most significantly downregulated disease pathways in Aβ-treated CLU-/- neurons compared to untreated CLU-/- neurons. The lack of clusterin protein could be relevant to this finding. The presence of Aβ, which would normally result in an increase of the pathological processes being triggered in the cells, instead results in downregulation of these neurodegeneration pathways. There may be specific genes in the pathway that are not activated due to the loss of CLU expression. From the pathway analysis it could be suggested that the altered apoptotic response of the CLU-/- cell line is involved, or that the changes in cytoskeletal and microtubule functioning that occurred in the wildtype neurons but not in the CLU-/- are relevant to the downregulation of neurodegenerative disease pathways.

The dysregulation in the Alzheimer's disease pathway could be a result of CLU dysfunction flagging up this pathway, as it is a dominant gene in AD literature. However, the inclusion of the other neurodegeneration pathways in the top 3 downregulated disease pathways suggests that this is not the cause, and there are common neurodegeneration

genes downregulated in Aβ-treated CLU-/- neurons compared to untreated CLU-/- neurons. The KEGG diagrams show genes involved with mitochondrial dysfunction to be significantly downregulated, which seem to be dampening the apoptosis pathway. Genes involved in these processes may be interesting for future analyses in identifying the lack of Aβ toxicity in the CLU knockout neurons.

5.4.6 Significant KEGG pathways and molecular functions in Aβ-treated neurons

Many of the significant changes in gene expression in the RNAseq analysis relate to the cytoskeleton and microtubule function. Aβ-treated wildtype neurons vs. untreated had microtubule or actin function as most significant molecular functions and cytoskeleton in the most significant KEGG pathways. These pathways also appeared in the analysis of the untreated CLU knockout cells. Focal adhesion was the most upregulated KEGG pathway in WT0 vs. CLU0 and the greatest downregulated pathway in WT0 vs. WT48. Focal adhesion activates MAPK, Wnt signalling and actin cytoskeleton regulation pathways. MAPK pathways have been found in other studies to be involved in the pathophysiology and pathogenesis of AD through the extracellular signal-regulated kinase (ERK), c-Jun N-terminal kinase (JNK) and p38 pathways (Zhu et al., 2002). Wnt signalling has also been found to have roles in AD through the canonical/β-catenin and non-canonical/PCP pathways (Inestrosa and Varela-Nallar, 2014). The role of CLU in disrupting these processes may help to explain the differences in Aβ-toxicity between the two cell lines.

The dysregulated microtubule function could be exerting its effect through tau or as a result of tau phosphorylation. It will be important to understand if these pathway changes are specific to Aβ and clusterin or whether this is a non-specific effect of

neurodegeneration and detachment from laminin matrix. A control toxic agent to add to the cells would be a good control to include.

Many of the molecular functions and pathways generated by the analyses as highly significant are unrelated to neuronal cells. It would be interesting to know if this is an iPSC issue due to immaturity of the neurons. Comparing the RNAseq results to untreated and Aβ-treated primary neurons may help to understand whether these pathways are due to the neurons not being functionally mature or due to other cell types present in the cultures. Many genes play different roles depending on the developmental stage of the cells, such as the Wnt signalling pathway (Inestrosa and Varela-Nallar, 2014), and so immature neurons may be confounding the data and masking AD-relevant gene expression changes. It would also be interesting to compare the CLU knockout line and the isogenic control to an iPSC line derived from an AD genetic background. This could reveal if the Aβ treatment is activating other non-AD specific pathways, which would not be activated in iPSC-derived neurons overproducing Aβ.

5.4.7 The Aβ-DKK1-EGR1 pathway does not show the expected gene expression changes

DKK1, EGR1, KLF10 and APOE are not significantly upregulated in Aβ-treated cells compared to untreated. However, there are significant changes in the gene expression levels in CLU knockout cells, suggesting that clusterin production and intracellular levels could be regulating these genes. The large differences in gene expression in the CLU-/- line and the wildtype line meant that it was problematic to draw conclusions as to the change in these genes in Aβ-treated CLU-/- cells compared to Aβ-treated wildtype cells.

Other genes related to the amyloid cascade are altered in Aβ-treated wildtype cells. These include genes in the notch family, EGF and EGFR. The gene expression of these genes were unchanged in Aβ-treated CLU knockout cells, and so could be proposed as important in regulating the Aβ-toxicity in the iPSC-derived neurons that is not present in the CLU knockout.

5.4.8 Limitations of the transcriptomics study

There are a few factors that may be confounding the RNAseq results in this project. Aβ target genes proposed from the literature and genes in the KEGG disease pathways are identified from *in vivo* models or tissue containing multiple cell types. Therefore, focusing on genes established from these systems may not be relevant to a pure neuronal *in vitro* model. For example, it is suggested in CLU knockout mice that the location of amyloid deposition is altered, accounting for the altered phenotype. The CLU gene has wide ranging functions and therefore the effect of the knockout in an *in vitro* system with one predominant cell type is difficult to predict. Also the effects of genome editing on the cell line is hard to determine. The isogenic line should be the perfect control for the CRISPR-edited CLU knockout, but from the vast differences observed between the cell lines it may be possible that there are more differences than just the one gene. The development of a control with a synonymous mutation engineered may be beneficial, so that both lines share a genome editing history, as the process of cloning could potentially introduce uncontrolled variance in genomic expression.

Batch effects have been reported to create complications in the analysis of high throughput genomic data, and batch effects can correlate with an outcome of interest and lead to misconstrued conclusions (Leek et al., 2010). The wildtype and CLU knockout neuronal samples for RNAseq were cultured at two independent times. This was not predicted to cause problems as the iPSC lines are two distinct lines, but it is possible that minor changes in laboratory conditions and reagent lots could have created uncontrolled variables in the data. Ideally all cultures for experiments should be differentiated in parallel, to minimise all variances outside of intrinsic differences between iPSC lines.

5.4.9 Conclusions

There is a phenotype in the CLU-/- neurons when treated with Aβ. As hypothesised, the CLU knockout neurons are less sensitive to Aβ, and do not show Aβ-toxicity in the neurite length assay.

Potential Aβ-related genetic phenotypes from the RNAseq data include some previously proposed Aβ target genes from the literature, including Notch and EGFR. These were significantly altered in wildtype neurons treated with Aβ and may be interesting to investigate further and confirm with qPCR. These genes were unaltered in CLU-/- neurons when treated with Aβ. The changes in the actin cytoskeleton pathway may also be important, as many genes and pathways related to this were altered in the different conditions. In future work using these neurons features relating to the cytoskeleton may be utilised as a useful molecular phenotype in Aβ studies.

The CLU knockout neurons also show changes in gene expression compared to wildtype neurons independent from Aβ treatment. This could be due to the knockout of CLU or as a result of the stressful gene editing process undergone by the cell line. The p53 and apoptosis pathways were significantly upregulated in CLU knockout neurons compared to wildtype but were not significantly changed in other analyses. Therefore the pro-apoptotic genes downstream of p53 may be useful phenotypic markers for future investigations using CLU-/- cells. The CLU receptor LRP2 was also significantly downregulated in CLU-/- cells and could be utilised as a readout of CLU expression. A number of disease pathways were highlighted in this analysis, as could be expected due to the wide-ranging roles of clusterin in different tissues, and so the CLU-/- iPSCs could be useful for studying a range of diseases.

Chapter 6 Discussion

6.1 Summary of key findings

6.1.1 Aβ reduces neurite length in iPSC-derived neurons

The development of an automated, imaging assay to measure the lengths of neuronal processes demonstrated that Aβ was toxic to human iPSC-derived neurons. Significant decrease in the length of neurites was measured at 5μM and higher with $A\beta_{25-35}$, and 1.25μM and higher with $A\beta_{1-42}$.

Due to the lengthy differentiation protocols for iPSC-derived cortical neuronal cultures compared to cells typically used for high throughput assays, many standard cell toxicity assays were not successful. The neurite length assay was established as a reproducible assay for detecting toxicity of Aβ at reasonable concentrations, which could be scaled up for screening purposes at a later stage. Many *in vitro* studies investigate the effect of Aβ at supraphysiological doses; however, a key aim in this study was to determine the lowest dose to produce a measurable toxic effect in human neurons. The benefit of measuring neurite length is that it is an earlier toxicity measure than overall cell number, and so in future compound screening a reverse of the effect should be measurable.

6.1.2 Clusterin protein levels are significantly increased in Aβ-treated neurons

Investigation of protein levels and gene expression levels found that clusterin was increased in response to $A\beta_{25-35}$. This result replicates the finding in rodent neurons by Killick et al. (2014). However, the DKK1 levels were not changed in human neurons, as previously found in rodent cells by Killick and colleagues. This may be due to differences in the model or in the human pathway and further investigation could help to deconvolute this. The upregulation of DKK1 in the CLU knockout neurons could point towards a compensatory action by this gene.

6.1.3 Aβ does not cause degeneration of CLU knockout neurons

The CLU knockout neurons were protected against Aβ-driven neurodegeneration. This result was found in rodent cultures when CLU was knocked down by siRNA (Killick et al., 2014). They found that the percentage of cells surviving in the CLU knockdown cultures treated with 20μM $A\beta_{25-35}$ was not significantly different from untreated controls. In the human iPSC-derived neurons the average length of the neuronal processes was not reduced in the CLU knockout cells treated with $A\beta_{1-42,}$ but wildtype cells had significantly reduced neuronal processes from 2.5μM $A\beta_{1-42}$ treatment up to 20μM.

The transcriptomics data highlighted a number of interesting pathways that could be involved in the differing responses of the wildtype and the CLU knockout line. Many of the pathways differentially expressed between the CLU knockout and wildtype neurons are related to cytoskeletal disruption. Importantly, these pathways were altered in the untreated CLU knockout compared to wildtype, and in the Aβ-treated wildtype compared to untreated, however, these pathways were not differentially expressed in the Aβ-treated

CLU knockout line. This may contribute to explaining the lack of Aβ-toxicity in these cells. Cytoskeletal pathology has been associated with AD in numerous studies, including in response to abnormal APP metabolism (Lantos et al., 1992). This cytoskeletal pathology in AD is largely though to be linked to phosphorylation and accumulation of the microtubule-associated protein, tau (Carter et al., 1996). Investigation of how Aβ affects cytoskeletal proteins, such as those involved in microtubule binding and actin binding, may reveal more information about the Aβ-toxicity pathway and whether CLU affects these pathways at the protein level.

The CLU complement and coagulation pathway was significantly upregulated in the CLU knockout cells compared to wildtype. Clusterin is an inhibitor of the complement pathway, and CLU and CR1, the receptor for complement fragments C3b and C4b, are major identified risk genes for the development of sporadic AD by GWAS (Crehan et al., 2012). The upregulation of complement in the CLU knockout neurons *in vitro* without Aβ treatment or glial cells present confirms the relationship between clusterin and complement, and this will be an interesting pathway to investigate further using the CLU knockout iPSC line.

6.2 Future experiments

The rapid advancements in the technologies utilised for this project opens up many opportunities to advance this project. Firstly, with the ongoing development of novel protocols for prodcing different neuronal cell lineages it is now possible to start establishing co-culture models. Protocols for astrocytes and microglia have progressed, although unfortunately this process is not straightforward (Liu and Zhang, 2011; Serio et al., 2013; Shaltoulki et al., 2013; Yanagimachi et al., 2013; Ohgidani et al., 2014).

Differentiating iPSCs into multiple cell types could produce a more accurate model of the cortical environment. Clusterin and APOE are predominantly synthesised and secreted by astrocytes in the brain (Xu et al., 2006), and therefore these astrocyte cultures and mixed neuronal cultures could transform our understanding of the roles of these proteins in AD. Mixed neuronal cultures will provide more physiologically relevant models for Aβ-driven neurodegeneration, and the action of clusterin in this process.

The development of the CLU knockout iPSC line is exciting and could be useful for future work. Immediately, the pathways that have emerged from the transcriptomics analysis could be interrogated further, through imaging assays and immunoblotting to measure specific proteins. It would be interesting to culture the neurons for longer to perform electrophysiology experiments on this line, with Aβ-treatment and untreated cultures, to determine how the functionality of the neurons is altered in wildtype vs. CLU knockout. Library screening could also be performed to investigate different responses in the CLU knockout line. Further analysis of the gene regulatory networks to determine the transcriptional and posttranscriptional regulatory relationships governing the identified pathways may enhance our understanding of the role of CLU in Aβ-toxicity.

New findings on the CLU SNP have been published since the outset of this project. Bettens and colleagues (2015) identified novel rare coding CLU mutations and established the functionality. Therefore, CRISPR/Cas9-edited iPSC lines could be established with these mutations, to determine how they affect clusterin function in human neurons, and their role in Aβ-toxicity.

The construction of an APOE line was problematic, but it would be a valuable line to work on in the future. Novel base editing techniques may overcome problems with editing at this SNP site, creating an APOE ε3 iPSC line from an ε4 homozygous line. It would be fascinating to study Aβ-toxicity in cells carrying this mutation, and to

investigate whether transcriptomics would reveal similarly differentially regulated pathways. It would also be ideal to have an iPSC line with both CLU and APOE mutations. De Mattos et al. (2004) found a cooperative action of APOE and CLU on Aβ in their double knockout transgenic mouse, and the transcriptomics data from this project suggests a compensatory function of APOE in the CLU knockout neurons. Investigating Aβ-toxicity in these different genetic permutations would contribute to a clarifying the influence of these proteins on Aβ.

6.3 Limitations

6.3.1 Limitations with the iPSC model

One feature of iPSC models, which is in some respects desirable but also a limitation is the homogeneity of the cultures. Neurons differentiated for 35 days were highly pure neuronal cultures. Increased culture time produces a significant percentage of astrocytic cells in culture (Liu and Zhang, 2011). However, the aim of developing an imaging assay that could be applicable to high throughput screening limited the neuronal cultures to 35 days. This model system demonstrated Aβ-toxicity in the cultures, but may not reflect the Aβ-driven pathways measured in *in vivo* studies. For example, clusterin is primarily expressed by astrocytes in the brain, and it is possible that certain downstream pathways such as the Dkk1-Wnt–PCP–JNK pathway may be predominantly active in cultures with a significant proportion of glial cells. This could also be taken into consideration in the RNAseq analysis, where the typical 'Alzheimer's disease pathway' genes from the analysis programme are taken from tissue with a number of different interacting cell types, and therefore the pathways in a purely neuronal system may differ. It may be interesting to investigate single cells, with FACs sorting or single cell RNAseq,

to interrogate whether the different cells in these cultures express different responses to Aβ.

6.3.2 Issues with the Aβ preparations

Many issues regularly occur with $A\beta_{1-42}$ preparations, which make them variable between batches and experiments, and can result in unimpaired neuronal function and morphology (Fa et al., 2010; Stine et al., 2003). In this project $A\beta_{25-35}$ was the main source used, which due to it's lower propensity to aggregate and its simpler preparation procedure offered much more reliable results. However, although this peptide has been reported as the cytotoxic fragment of the amyloid protein (Yanker et al., 1990), it is not typically produced by APP and so $A\beta_{1-42}$ is the preferred length in terms of physiological relevance. Improved characterisation could help standardise the amyloid preparations, such as routine dynamic light scattering (DLS) or native mass spectrometry (MS). However, during this project the neurite length assay was used to characterise the toxicity of amyloid preparations prior to molecular or genetic investigations. Differences in Aβ aggregation between experiments could therefore not be fully controlled.

6.3.3 Limitations of CRISPR/Cas9 in an iPSC system

CRISPR/Cas9 is an exciting tool to manipulate iPSC genotype, however, it is also a difficult technique in stem cells. Stem cells have a rapid repair mechanism, making transfection difficult, and therefore without a selection cassette to detect cells with the mutation these cells are difficult to identify. Additionally, iPSCs are not suited to clonal survival and culture. These issues can largely explain the lack of success in the knockin

project. Advances in CRISPR/Cas9 function, molecules to promote HDR, and culture systems and matrices to support single cell culture will all improve the success of genome editing projects in iPSCs.

Another interesting consideration is whether CRISPR/Cas9 is "footprintless" in iPSCs. The wide range of functions CLU is involved in could explain the different transcriptomic signature in the CLU knockout compared to the wildtype line. Moreover, the relevance of many of the pathways generated by the analysis makes this a reasonable inference. However, the opportunity to study a cell line that has undergone the CRISPR/Cas9 gene editing process but without any mutation introduced would be beneficial in confirming this. It is possible that the stress of transfection and selection on the line during genome editing has lasting epigenetic effects.

6.4 Potential applications of the cellular model

The cell model in this project has potential for further dissection of the amyloid cascade hypothesis. This study demonstrated the responsiveness of human iPSC-derived neurons to Aβ, and confirmed a reliable, automated assay for measuring this. The sensitivity of the assay at lower Aβ concentrations suggests its utility for compound screening, as reduced neurite length is a measure of early toxicity with the potential for regeneration. The novel CLU knockout iPSC line may be useful for further studies in AD, as well as other disease areas.

6.5 Conclusions

The aims of this thesis were to determine if Aβ oligomers were toxic to iPSC-derived neurons, develop a method to reliably measure neuronal toxicity, and improve the understanding of the molecular mechanisms mediating this toxicity. The human neurons degenerated in response to Aβ oligomers and the development of a novel CLU knockout cell line revealed that neurons lacking clusterin were resistant to Aβ. This confirms the role of clusterin in Aβ-mediated neurodegeneration. The mechanism of clusterin in Aβ-toxicity in human neuronal cultures is not yet determined, and this project has proposed many pathways that may be important. Investigation of the APOE gene, cytoskeletal dysfunction, mitochondrial dysfunction and the complement pathway may lead to a superior understanding of the role of clusterin in AD pathogenesis. These pathways were largely already implicated in the function of clusterin in AD, validating the integration of human iPSC-derived neurons in AD research.

References

Agrawal, N., Dasaradhi, P. V., Mohmmed, A., Malhotra, P., Bhatnagar, R. K. and Mukherjee, S. K. (2003) 'RNA interference: biology, mechanism, and applications', *Microbiol Mol Biol Rev,* 67(4), 657-85.

Armstrong, R. A. (2013) 'What causes Alzheimer's disease?', *Folia Neuropathol,* 51(3), 169-88.

Bartus, R. T. (2000) 'On neurodegenerative diseases, models, and treatment strategies: lessons learned and lessons forgotten a generation following the cholinergic hypothesis', *Exp Neurol,* 163(2), 495-529.

Beffert, U., Aumont, N., Dea, D., Lussier-Cacan, S., Davignon, J. and Poirier, J. (1999) 'Apolipoprotein E isoform-specific reduction of extracellular amyloid in neuronal cultures', *Molecular Brain Research,* 68(1–2), 181-185.

Beffert, U. and Poirier, J. (1996) 'Apolipoprotein E, Plaques, Tangles and Cholinergic Dysfunction in Alzheimer's Diseasea', *Annals of the New York Academy of Sciences,* 777(1), 166-174.

Beglopoulos, V., Sun, X., Saura, C. A., Lemere, C. A., Kim, R. D. and Shen, J. (2004) 'Reduced beta-amyloid production and increased inflammatory responses in presenilin conditional knock-out mice', *J Biol Chem,* 279(45), 46907-14.

Bellin, M., Marchetto, M. C., Gage, F. H. and Mummery, C. L. (2012) 'Induced pluripotent stem cells: the new patient?', *Nat Rev Mol Cell Biol,* 13(11), 713-26.

Bettens, K., Vermeulen, S., Van Cauwenberghe, C., Heeman, B., Asselbergh, B., Robberecht, C., Engelborghs, S., Vandenbulcke, M., Vandenberghe, R., De Deyn, P. P., Cruts, M., Van Broeckhoven, C. and Sleegers, K. (2015) 'Reduced secreted clusterin as a mechanism for Alzheimer-associated CLU mutations', *Molecular Neurodegeneration,* 10(1), 1-12.

Bettuzzi, S. and Rizzi, F. (2009) 'Chapter 5: Nuclear CLU (nCLU) and the fate of the cell' in Bettuzzi, S. and Pucci, S. 'Clusterin, Advances in Cancer Research*' Adv Cancer*

Res, 104, 59-88.

Bolger, A. M., Lohse, M. and Usadel, B. (2014) 'Trimmomatic: a flexible trimmer for Illumina sequence data', *Bioinformatics,* 30(15), 2114-20.

Boonen, R. A., van Tijn, P. and Zivkovic, D. (2009) 'Wnt signaling in Alzheimer's disease: up or down, that is the question', *Ageing Res Rev,* 8(2), 71-82.

Braak, H. & Braak, E. 1991, "Neuropathological stageing of Alzheimer-related changes", *Acta Neuropathologica,* vol. 82, no. 4, pp. 239-259.

Braak, H., Braak, E. & Strothjohann, M. 1994, "Abnormally phosphorylated tau protein related to the formation of neurofibrillary tangles and neuropil threads in the cerebral cortex of sheep and goat", *Neuroscience letters,* vol. 171, no. 1-2, pp. 1-4.

Braidy, N., Poljak, A., Jayasena, T., Mansour, H., Inestrosa, N. C. and Sachdev, P. S. (2015) 'Accelerating Alzheimer's research through 'natural' animal models', *Curr Opin Psychiatry,* 28(2), 155-64.

Braskie, M. N., Jahanshad, N., Stein, J. L., Barysheva, M., McMahon, K. L., de Zubicaray, G. I., Martin, N. G., Wright, M. J., Ringman, J. M., Toga, A. W. and Thompson, P. M. (2011) 'Common Alzheimer's Disease Risk Variant Within the CLU Gene Affects White Matter Microstructure in Young Adults', *The Journal of Neuroscience,* 31(18), 6764-6770.

Bray, N. J., Kapur, S. and Price, J. (2012) 'Investigating schizophrenia in a “dish”: possibilities, potential and limitations', *World Psychiatry,* 11(3), 153-155.

Busciglio, J., Lorenzo, A., Yeh, J. and Yankner, B. A. (1995) 'beta-amyloid fibrils induce tau phosphorylation and loss of microtubule binding', *Neuron,* 14(4), 879-88.

Cagnin, A., Myers, R., Gunn, R.N., Lawrence, A.D., Stevens, T., Kreutzberg, G.W., Jones, T. & Banati, R.B. 2001, "In vivo visualization of activated glia by [11C] (R)-PK11195-PET following herpes encephalitis reveals projected neuronal damage beyond the primary focal lesion", *Brain : a journal of neurology,* vol. 124, no. Pt 10, pp. 2014-2027.

Carrasquillo, M. M., Belbin, O., Hunter, T. A., Ma, L., Bisceglio, G. D., Zou, F., Crook, J. E., Pankratz, V. S., Dickson, D. W., Graff-Radford, N. R., Petersen, R. C., Morgan, K. and Younkin, S. G. (2010) 'Replication of CLU, CR1, and PICALM associations with alzheimer disease', *Arch Neurol,* 67(8), 961-4.

Caruso, A., Motolese, M., Iacovelli, L., Caraci, F., Copani, A., Nicoletti, F., Terstappen, G. C., Gaviraghi, G. and Caricasole, A. (2006) 'Inhibition of the canonical Wnt signaling pathway by apolipoprotein E4 in PC12 cells', *J Neurochem,* 98(2), 364-71.

Castellano, J. M., Kim, J., Stewart, F. R., Jiang, H., DeMattos, R. B., Patterson, B. W., Fagan, A. M., Morris, J. C., Mawuenyega, K. G., Cruchaga, C., Goate, A. M., Bales, K. R., Paul, S. M., Bateman, R. J. and Holtzman, D. M. (2011) 'Human apoE isoforms differentially regulate brain amyloid-beta peptide clearance', *Sci Transl Med,* 3(89), 89ra57.

Cho, S. W., Kim, S., Kim, J. M. and Kim, J. S. (2013) 'Targeted genome engineering in human cells with the Cas9 RNA-guided endonuclease', *Nat Biotechnol,* 31(3), 230-2.

Choi, S.H., Kim, Y.H., Hebisch, M., Sliwinski, C., Lee, S., D'Avanzo, C., Chen, H., Hooli, B., Asselin, C., Muffat, J., Klee, J.B., Zhang, C., Wainger, B.J., Peitz, M., Kovacs, D.M., Woolf, C.J., Wagner, S.L., Tanzi, R.E. & Kim, D.Y. 2014, "A three-dimensional human neural cell culture model of Alzheimer's disease", *Nature,* vol. 515, no. 7526, pp. 274-278.

Cocks, G., Curran, S., Gami, P., Uwanogho, D., Jeffries, A. R., Kathuria, A., Lucchesi, W., Wood, V., Dixon, R., Ogilvie, C., Steckler, T. and Price, J. (2014) 'The utility of patient specific induced pluripotent stem cells for the modelling of Autistic Spectrum Disorders', *Psychopharmacology,* 231(6), 1079-1088.

Colangelo, V., Schurr, J., Ball, M. J., Pelaez, R. P., Bazan, N. G. and Lukiw, W. J. (2002) 'Gene expression profiling of 12633 genes in Alzheimer hippocampal CA1: transcription and neurotrophic factor down-regulation and up-regulation of apoptotic and pro-inflammatory signaling', *J Neurosci Res,* 70(3), 462-73.

Cong, L., Ran, F. A., Cox, D., Lin, S., Barretto, R., Habib, N., Hsu, P. D., Wu, X., Jiang, W., Marraffini, L. A. and Zhang, F. (2013) 'Multiplex genome engineering using

CRISPR/Cas systems', *Science,* 339(6121), 819-23.

Corder, E. H., Saunders, A. M., Strittmatter, W. J., Schmechel, D. E., Gaskell, P. C., Small, G. W., Roses, A. D., Haines, J. L. and Pericak-Vance, M. A. (1993) 'Gene dose of apolipoprotein E type 4 allele and the risk of Alzheimer's disease in late onset families', *Science,* 261(5123), 921-3.

Costa, V., Aprile, M., Esposito, R. and Ciccodicola, A. (2013) 'RNA-Seq and human complex diseases: recent accomplishments and future perspectives', *Eur J Hum Genet,* 21(2), 134-42.

Craig, L. A., Hong, N. S. and McDonald, R. J. (2011) 'Revisiting the cholinergic hypothesis in the development of Alzheimer's disease', *Neurosci Biobehav Rev,* 35(6), 1397-409.

Crehan, H., Holton, P., Wray, S., Pocock, J., Guerreiro, R. and Hardy, J. (2012) 'Complement receptor 1 (CR1) and Alzheimer's disease', *Immunobiology,* 217(2), 244-250.

Crowther, R. A. (1991) 'Straight and paired helical filaments in Alzheimer disease have a common structural unit.' *Proceedings of the National Academy of Sciences* 88(6), 2288-2292

Dawson, H.N., Ferreira, A., Eyster, M.V., Ghoshal, N., Binder, L.I. & Vitek, M.P. 2001, "Inhibition of neuronal maturation in primary hippocampal neurons from tau deficient mice", *Journal of cell science,* vol. 114, no. Pt 6, pp. 1179-1187.

de Calignon, A., Polydoro, M., Suarez-Calvet, M., William, C., Adamowicz, D. H., Kopeikina, K. J., Pitstick, R., Sahara, N., Ashe, K. H., Carlson, G. A., Spires-Jones, T. L. and Hyman, B. T. (2012) 'Propagation of tau pathology in a model of early Alzheimer's disease', *Neuron,* 73(4), 685-97.

de la Monte, S. M. and Wands, J. R. (2008) 'Alzheimer's disease is type 3 diabetes-evidence reviewed', *J Diabetes Sci Technol,* 2(6), 1101-13.

DeMattos, R. B., Cirrito, J. R., Parsadanian, M., May, P. C., O'Dell, M. A., Taylor, J. W., Harmony, J. A., Aronow, B. J., Bales, K. R., Paul, S. M. and Holtzman, D. M.

(2004) 'ApoE and clusterin cooperatively suppress Abeta levels and deposition: evidence that ApoE regulates extracellular Abeta metabolism in vivo', *Neuron,* 41(2), 193-202.

DeMattos, R. B., O'Dell, M. A., Parsadanian, M., Taylor, J. W., Judith, A. K. H., Bales, K. R., Paul, S. M., Aronow, B. J. and Holtzman, D. M. (2002) 'Clusterin Promotes Amyloid Plaque Formation and is Critical for Neuritic Toxicity in a Mouse Model of Alzheimer's Disease', *Proceedings of the National Academy of Sciences of the United States of America,* 99(16), 10843-10848.

Dolan, P. J. and Johnson, G. V. W. (2010) 'The role of tau kinases in Alzheimer's disease', *Current opinion in drug discovery & development,* 13(5), 595-603.

Elmore, S. (2007) 'Apoptosis: A Review of Programmed Cell Death', *Toxicologic pathology,* 35(4), 495-516.

Fa, M., Orozco, I. J., Francis, Y. I., Saeed, F., Gong, Y. and Arancio, O. (2010) 'Preparation of Oligomeric β-amyloid(1-42) and Induction of Synaptic Plasticity Impairment on Hippocampal Slices', *Journal of Visualized Experiments : JoVE,* (41), 1884.

Fisher, M., Feuerstein, G., Howells, D. W., Hurn, P. D., Kent, T. A., Savitz, S. I. and Lo, E. H. (2009) 'Update of the Stroke Therapy Academic Industry Roundtable Preclinical Recommendations', *Stroke; a journal of cerebral circulation,* 40(6), 2244-2250.

Francis, P. T., Palmer, A. M., Snape, M. and Wilcock, G. K. (1999) 'The cholinergic hypothesis of Alzheimer's disease: a review of progress', *Journal of Neurology, Neurosurgery & Psychiatry,* 66(2), 137-147.

Gaj, T., Gersbach, C. A. and Barbas, C. F., 3rd (2013) 'ZFN, TALEN, and CRISPR/Cas-based methods for genome engineering', *Trends Biotechnol,* 31(7), 397-405.

Garwood, C. J., Pooler, A. M., Atherton, J., Hanger, D. P. and Noble, W. (2011) 'Astrocytes are important mediators of Abeta-induced neurotoxicity and tau phosphorylation in primary culture', *Cell Death Dis,* 2, e167.

Gasiunas, G., Barrangou, R., Horvath, P. and Siksnys, V. (2012) 'Cas9-crRNA ribonucleoprotein complex mediates specific DNA cleavage for adaptive immunity in bacteria', *Proc Natl Acad Sci U S A,* 109(39), E2579-86.

Ghiso, J., Matsubara, E., Koudinov, A., Choi-Miura, N. H., Tomita, M., Wisniewski, T. and Frangione, B. (1993) 'The cerebrospinal-fluid soluble form of Alzheimer's amyloid beta is complexed to SP-40,40 (apolipoprotein J), an inhibitor of the complement membrane-attack complex', *Biochemical Journal,* 293(Pt 1), 27-30.

Giese, K. P. (2009) 'GSK-3: a key player in neurodegeneration and memory', *IUBMB Life,* 61(5), 516-21.

Gouras, G. K. (2001) 'Current theories for the molecular and cellular pathogenesis of Alzheimers disease' in *Expert Rev Mol Med*, England: 1-11.

Grotewold, L. and Ruther, U. (2002) 'The Wnt antagonist Dickkopf-1 is regulated by Bmp signaling and c-Jun and modulates programmed cell death', *Embo j,* 21(5), 966-75.

Guerreiro, R., Wojtas, A., Bras, J., Carrasquillo, M., Rogaeva, E., Majounie, E., Cruchaga, C., Sassi, C., Kauwe, J.S., Younkin, S., Hazrati, L., Collinge, J., Pocock, J., Lashley, T., Williams, J., Lambert, J.C., Amouyel, P., Goate, A., Rademakers, R., Morgan, K., Powell, J., St George-Hyslop, P., Singleton, A., Hardy, J. & Alzheimer Genetic Analysis Group 2013, "TREM2 variants in Alzheimer's disease", *The New England journal of medicine,* 368(2), 117-127.

Haass, C. and Selkoe, D. J. (2007) 'Soluble protein oligomers in neurodegeneration: lessons from the Alzheimer's amyloid beta-peptide', *Nat Rev Mol Cell Biol,* 8(2), 101-12.

Hanger, D. P., Hughes, K., Woodgett, J. R., Brion, J. P. and Anderton, B. H. (1992) 'Glycogen synthase kinase-3 induces Alzheimer's disease-like phosphorylation of tau: generation of paired helical filament epitopes and neuronal localisation of the kinase', *Neurosci Lett,* 147(1), 58-62.

Hanger, D. P. and Wray, S. (2010) 'Tau cleavage and tau aggregation in neurodegenerative disease', *Biochem Soc Trans,* 38(4), 1016-20.

Harada, A., Oguchi, K., Okabe, S., Kuno, J., Terada, S., Ohshima, T., Sato-Yoshitake, R., Takei, Y., Noda, T. & Hirokawa, N. 1994, "Altered microtubule organization in small-calibre axons of mice lacking tau protein", *Nature,* vol. 369, no. 6480, pp. 488-491.

Hardy, J. and Allsop, D. (1991) 'Amyloid deposition as the central event in the aetiology of Alzheimer's disease', *Trends Pharmacol Sci,* 12(10), 383-8.

Hardy, J. and Selkoe, D. J. (2002) 'The amyloid hypothesis of Alzheimer's disease: progress and problems on the road to therapeutics', *Science,* 297(5580), 353-6.

Harold, D., Abraham, R., Hollingworth, P., Sims, R., Gerrish, A., Hamshere, M. L., Pahwa, J. S., Moskvina, V., Dowzell, K., Williams, A., Jones, N., Thomas, C., Stretton, A., Morgan, A. R., Lovestone, S., Powell, J., Proitsi, P., Lupton, M. K., Brayne, C., Rubinsztein, D. C., Gill, M., Lawlor, B., Lynch, A., Morgan, K., Brown, K. S., Passmore, P. A., Craig, D., McGuinness, B., Todd, S., Holmes, C., Mann, D., Smith, A. D., Love, S., Kehoe, P. G., Hardy, J., Mead, S., Fox, N., Rossor, M., Collinge, J., Maier, W., Jessen, F., Schurmann, B., Heun, R., van den Bussche, H., Heuser, I., Kornhuber, J., Wiltfang, J., Dichgans, M., Frolich, L., Hampel, H., Hull, M., Rujescu, D., Goate, A. M., Kauwe, J. S., Cruchaga, C., Nowotny, P., Morris, J. C., Mayo, K., Sleegers, K., Bettens, K., Engelborghs, S., De Deyn, P. P., Van Broeckhoven, C., Livingston, G., Bass, N. J., Gurling, H., McQuillin, A., Gwilliam, R., Deloukas, P., Al-Chalabi, A., Shaw, C. E., Tsolaki, M., Singleton, A. B., Guerreiro, R., Muhleisen, T. W., Nothen, M. M., Moebus, S., Jockel, K. H., Klopp, N., Wichmann, H. E., Carrasquillo, M. M., Pankratz, V. S., Younkin, S. G., Holmans, P. A., O'Donovan, M., Owen, M. J. and Williams, J. (2009) 'Genome-wide association study identifies variants at CLU and PICALM associated with Alzheimer's disease', *Nat Genet,* 41(10), 1088-93.

Harris, J. A., Koyama, A., Maeda, S., Ho, K., Devidze, N., Dubal, D. B., Yu, G. Q., Masliah, E. and Mucke, L. (2012) 'Human P301L-mutant tau expression in mouse entorhinal-hippocampal network causes tau aggregation and presynaptic pathology but no cognitive deficits', *PLoS One,* 7(9), e45881.

Heredia, L., Lin, R., Vigo, F. S., Kedikian, G., Busciglio, J. and Lorenzo, A. (2004) 'Deposition of amyloid fibrils promotes cell-surface accumulation of amyloid beta precursor protein', *Neurobiol Dis,* 16(3), 617-29.

Hernandez, F., Gomez de Barreda, E., Fuster-Matanzo, A., Lucas, J. J. and Avila, J. (2010) 'GSK3: a possible link between beta amyloid peptide and tau protein', *Exp Neurol,*

223(2), 322-5.

Hollingworth, P., Harold, D., Sims, R., Gerrish, A., Lambert, J.-C., Carrasquillo, M. M., Abraham, R., Hamshere, M. L., Pahwa, J. S., Moskvina, V., Dowzell, K., Jones, N., Stretton, A., Thomas, C., Richards, A., Ivanov, D., Widdowson, C., Chapman, J., Lovestone, S., Powell, J., Proitsi, P., Lupton, M. K., Brayne, C., Rubinsztein, D. C., Gill, M., Lawlor, B., Lynch, A., Brown, K. S., Passmore, P. A., Craig, D., McGuinness, B., Todd, S., Holmes, C., Mann, D., Smith, A. D., Beaumont, H., Warden, D., Wilcock, G., Love, S., Kehoe, P. G., Hooper, N. M., Vardy, E. R. L. C., Hardy, J., Mead, S., Fox, N. C., Rossor, M., Collinge, J., Maier, W., Jessen, F., Schürmann, B., Rüther, E., Heun, R., Kölsch, H., van den Bussche, H., Heuser, I., Kornhuber, J., Wiltfang, J., Dichgans, M., Frölich, L., Hampel, H., Hüll, M., Gallacher, J., Rujescu, D., Giegling, I., Goate, A. M., Kauwe, J. S. K., Cruchaga, C., Nowotny, P., Morris, J. C., Mayo, K., Sleegers, K., Bettens, K., Engelborghs, S., De Deyn, P. P., Van Broeckhoven, C., Livingston, G., Bass, N. J., Gurling, H., McQuillin, A., Gwilliam, R., Deloukas, P., Al-Chalabi, A., Shaw, C. E., Tsolaki, M., Singleton, A. B., Guerreiro, R., Mühleisen, T. W., Nöthen, M. M., Moebus, S., Jöckel, K.-H., Klopp, N., Wichmann, H. E., Pankratz, V. S., Sando, S. B., Aasly, J. O., Barcikowska, M., Wszolek, Z. K., Dickson, D. W., Graff-Radford, N. R., Petersen, R. C., et al. (2011) 'Common variants in ABCA7, MS4A6A/MS4A4E, EPHA1, CD33 and CD2AP are associated with Alzheimer's disease', *Nature genetics,* 43(5), 429-435.

Holmes, E. C. (2010) 'The RNA virus quasispecies: fact or fiction?', *J Mol Biol,* 400(3), 271-3.

Holtzman, D. M., Bales, K. R., Tenkova, T., Fagan, A. M., Parsadanian, M., Sartorius, L. J., Mackey, B., Olney, J., McKeel, D., Wozniak, D. and Paul, S. M. (2000) 'Apolipoprotein E isoform-dependent amyloid deposition and neuritic degeneration in a mouse model of Alzheimer's disease', *Proc Natl Acad Sci U S A,* 97(6), 2892-7.

Hooper, C., Killick, R. and Lovestone, S. (2008) 'The GSK3 hypothesis of Alzheimer's disease', *Journal of Neurochemistry,* 104(6), 1433-1439.

Hooper, C., Markevich, V., Plattner, F., Killick, R., Schofield, E., Engel, T., Hernandez, F., Anderton, B., Rosenblum, K., Bliss, T., Cooke, S. F., Avila, J., Lucas, J. J., Giese, K. P., Stephenson, J. and Lovestone, S. (2007) 'Glycogen synthase kinase-3 inhibition is integral to long-term potentiation', *Eur J Neurosci,* 25(1), 81-6.

Horvath, P. and Barrangou, R. (2010) 'CRISPR/Cas, the immune system of bacteria and archaea', *Science,* 327(5962), 167-70.

Hsia, A. Y., Masliah, E., McConlogue, L., Yu, G.-Q., Tatsuno, G., Hu, K., Kholodenko, D., Malenka, R. C., Nicoll, R. A. and Mucke, L. (1999) 'Plaque-independent disruption of neural circuits in Alzheimer's disease mouse models', *Proceedings of the National Academy of Sciences,* 96(6), 3228-3233.

Hsiao, K., Chapman, P., Nilsen, S., Eckman, C., Harigaya, Y., Younkin, S., Yang, F. and Cole, G. (1996) 'Correlative memory deficits, Abeta elevation, and amyloid plaques in transgenic mice', *Science,* 274(5284), 99-102.

Imhof, A., Charnay, Y., Vallet, P. G., Aronow, B., Kovari, E., French, L. E., Bouras, C. and Giannakopoulos, P. (2006) 'Sustained astrocytic clusterin expression improves remodeling after brain ischemia', *Neurobiol Dis,* 22(2), 274-83.

Inestrosa, N. C. and Varela-Nallar, L. (2014) 'Wnt signaling in the nervous system and in Alzheimer's disease', *J Mol Cell Biol,* 6(1), 64-74.

Ingelsson, M., Fukumoto, H., Newell, K. L., Growdon, J. H., Hedley-Whyte, E. T., Frosch, M. P., Albert, M. S., Hyman, B. T. and Irizarry, M. C. (2004) 'Early Abeta accumulation and progressive synaptic loss, gliosis, and tangle formation in AD brain', *Neurology,* 62(6), 925-31.

Iqbal, K., Liu, F., Gong, C.-X. and Grundke-Iqbal, I. (2010) 'Tau in Alzheimer Disease and Related Tauopathies', *Current Alzheimer research,* 7(8), 656-664.

Irizarry, M. C., McNamara, M., Fedorchak, K., Hsiao, K. and Hyman, B. T. (1997) 'APPSw transgenic mice develop age-related A beta deposits and neuropil abnormalities, but no neuronal loss in CA1', *J Neuropathol Exp Neurol,* 56(9), 965-73.

Israel, M. A., Yuan, S. H., Bardy, C., Reyna, S. M., Mu, Y., Herrera, C., Hefferan, M. P., Van Gorp, S., Nazor, K. L., Boscolo, F. S., Carson, C. T., Laurent, L. C., Marsala, M., Gage, F. H., Remes, A. M., Koo, E. H. and Goldstein, L. S. B. (2012) 'Probing sporadic and familial Alzheimer/'s disease using induced pluripotent stem cells', *Nature,* 482(7384), 216-220.

Jacobsen, J. S., Wu, C. C., Redwine, J. M., Comery, T. A., Arias, R., Bowlby, M., Martone, R., Morrison, J. H., Pangalos, M. N., Reinhart, P. H. and Bloom, F. E. (2006) 'Early-onset behavioral and synaptic deficits in a mouse model of Alzheimer's disease', *Proc Natl Acad Sci U S A,* 103(13), 5161-6.

Jinek, M., Chylinski, K., Fonfara, I., Hauer, M., Doudna, J. A. and Charpentier, E. (2012) 'A programmable dual-RNA-guided DNA endonuclease in adaptive bacterial immunity', *Science,* 337(6096), 816-21.

Jonsson, T., Atwal, J. K., Steinberg, S., Snaedal, J., Jonsson, P. V., Bjornsson, S., Stefansson, H., Sulem, P., Gudbjartsson, D., Maloney, J., Hoyte, K., Gustafson, A., Liu, Y., Lu, Y., Bhangale, T., Graham, R. R., Huttenlocher, J., Bjornsdottir, G., Andreassen, O. A., Jonsson, E. G., Palotie, A., Behrens, T. W., Magnusson, O. T., Kong, A., Thorsteinsdottir, U., Watts, R. J. and Stefansson, K. (2012) 'A mutation in APP protects against Alzheimer/'s disease and age-related cognitive decline', *Nature,* 488(7409), 96-99.

Jonsson, T., Stefansson, H., Steinberg, S., Jonsdottir, I., Jonsson, P.V., Snaedal, J., Bjornsson, S., Huttenlocher, J., Levey, A.I., Lah, J.J., Rujescu, D., Hampel, H., Giegling, I., Andreassen, O.A., Engedal, K., Ulstein, I., Djurovic, S., Ibrahim-Verbaas, C., Hofman, A., Ikram, M.A., van Duijn, C.M., Thorsteinsdottir, U., Kong, A. & Stefansson, K. 2013, "Variant of TREM2 associated with the risk of Alzheimer's disease", *The New England journal of medicine,* vol. 368, no. 2, pp. 107-116.

Kang, J., Lemaire, H.G., Unterbeck, A., Salbaum, J.M., Masters, C.L., Grzeschik, K.H., Multhaup, G., Beyreuther, K. & Muller-Hill, B. 1987, "The precursor of Alzheimer's disease amyloid A4 protein resembles a cell-surface receptor", *Nature,* vol. 325, no. 6106, pp. 733-736.

Karran, E., Mercken, M. and De Strooper, B. (2011) 'The amyloid cascade hypothesis for Alzheimer's disease: an appraisal for the development of therapeutics', *Nat Rev Drug Discov,* 10(9), 698-712.

Killick, R., Ribe, E. M., Al-Shawi, R., Malik, B., Hooper, C., Fernandes, C., Dobson, R., Nolan, P. M., Lourdusamy, A., Furney, S., Lin, K., Breen, G., Wroe, R., To, A. W. M., Leroy, K., Causevic, M., Usardi, A., Robinson, M., Noble, W., Williamson, R., Lunnon, K., Kellie, S., Reynolds, C. H., Bazenet, C., Hodges, A., Brion, J. P., Stephenson, J., Paul Simons, J. and Lovestone, S. (2014) 'Clusterin regulates [beta]-amyloid toxicity via Dickkopf-1-driven induction of the wnt-PCP-JNK pathway', *Mol Psychiatry,* 19(1), 88-98.

Killick, R., Scales, G., Leroy, K., Causevic, M., Hooper, C., Irvine, E. E., Choudhury, A. I., Drinkwater, L., Kerr, F., Al-Qassab, H., Stephenson, J., Yilmaz, Z., Giese, K. P., Brion, J. P., Withers, D. J. and Lovestone, S. (2009) 'Deletion of Irs2 reduces

amyloid deposition and rescues behavioural deficits in APP transgenic mice' in *Biochem Biophys Res Commun*, 257-62.

Kim, D. H., Inagaki, Y., Suzuki, T., Ioka, R. X., Yoshioka, S. Z., Magoori, K., Kang, M. J., Cho, Y., Nakano, A. Z., Liu, Q., Fujino, T., Suzuki, H., Sasano, H. and Yamamoto, T. T. (1998) 'A new low density lipoprotein receptor related protein, LRP5, is expressed in hepatocytes and adrenal cortex, and recognizes apolipoprotein E', *J Biochem,* 124(6), 1072-6.

Kim, J., Basak, J. M. and Holtzman, D. M. (2009) 'The role of apolipoprotein E in Alzheimer's disease', *Neuron,* 63(3), 287-303.

Kirszbaum, L., Bozas, S. E. and Walker, I. D. (1992) 'SP-40,40, a protein involved in the control of the complement pathway, possesses a unique array of disulphide bridges', *FEBS Letters,* 297(1), 70-76.

Komor, A. C., Kim, Y. B., Packer, M. S., Zuris, J. A. and Liu, D. R. (2016) 'Programmable editing of a target base in genomic DNA without double-stranded DNA cleavage', *Nature,* 533(7603), 420-424.

Kondo, T., Asai, M., Tsukita, K., Kutoku, Y., Ohsawa, Y., Sunada, Y., Imamura, K., Egawa, N., Yahata, N., Okita, K., Takahashi, K., Asaka, I., Aoi, T., Watanabe, A., Watanabe, K., Kadoya, C., Nakano, R., Watanabe, D., Maruyama, K., Hori, O., Hibino, S., Choshi, T., Nakahata, T., Hioki, H., Kaneko, T., Naitoh, M., Yoshikawa, K., Yamawaki, S., Suzuki, S., Hata, R., Ueno, S., Seki, T., Kobayashi, K., Toda, T., Murakami, K., Irie, K., Klein, W. L., Mori, H., Asada, T., Takahashi, R., Iwata, N., Yamanaka, S. and Inoue, H. (2013) 'Modeling Alzheimer's disease with iPSCs reveals stress phenotypes associated with intracellular Abeta and differential drug responsiveness', *Cell Stem Cell,* 12(4), 487-96.

Lambert, J.-C., Ibrahim-Verbaas, C. A., Harold, D., Naj, A. C., Sims, R., Bellenguez, C., Jun, G., DeStefano, A. L., Bis, J. C., Beecham, G. W., Grenier-Boley, B., Russo, G., Thornton-Wells, T. A., Jones, N., Smith, A. V., Chouraki, V., Thomas, C., Ikram, M. A., Zelenika, D., Vardarajan, B. N., Kamatani, Y., Lin, C.-F., Gerrish, A., Schmidt, H., Kunkle, B., Dunstan, M. L., Ruiz, A., Bihoreau, M.-T., Choi, S.-H., Reitz, C., Pasquier, F., Hollingworth, P., Ramirez, A., Hanon, O., Fitzpatrick, A. L., Buxbaum, J. D., Campion, D., Crane, P. K., Baldwin, C., Becker, T., Gudnason, V., Cruchaga, C., Craig, D., Amin, N., Berr, C., Lopez, O. L., De Jager, P. L., Deramecourt, V., Johnston, J. A., Evans, D., Lovestone, S., Letenneur, L., Morón, F. J., Rubinsztein, D. C., Eiriksdottir, G., Sleegers, K., Goate, A. M., Fiévet, N., Huentelman, M. J., Gill, M., Brown, K., Kamboh, M. I., Keller, L., Barberger-Gateau, P., McGuinness, B., Larson, E. B., Green, R., Myers, A. J.,

Dufouil, C., Todd, S., Wallon, D., Love, S., Rogaeva, E., Gallacher, J., St George-Hyslop, P., Clarimon, J., Lleo, A., Bayer, A., Tsuang, D. W., Yu, L., Tsolaki, M., Bossù, P., Spalletta, G., Proitsi, P., Collinge, J., Sorbi, S., Sanchez-Garcia, F., Fox, N. C., Hardy, J., Deniz Naranjo, M. C., Bosco, P., Clarke, R., Brayne, C., Galimberti, D., Mancuso, M., Matthews, F., European Alzheimer's disease, I., Genetic and Environmental Risk in Alzheimer's, D., Alzheimer's Disease Genetic, C., Cohorts for Heart and Aging Research in Genomic, E., et al. (2013) 'Meta-analysis of 74,046 individuals identifies 11 new susceptibility loci for Alzheimer's disease', *Nature genetics,* 45(12), 1452-1458.

Lambert, J. C., Heath, S., Even, G., Campion, D., Sleegers, K., Hiltunen, M., Combarros, O., Zelenika, D., Bullido, M. J., Tavernier, B., Letenneur, L., Bettens, K., Berr, C., Pasquier, F., Fievet, N., Barberger-Gateau, P., Engelborghs, S., De Deyn, P., Mateo, I., Franck, A., Helisalmi, S., Porcellini, E., Hanon, O., de Pancorbo, M. M., Lendon, C., Dufouil, C., Jaillard, C., Leveillard, T., Alvarez, V., Bosco, P., Mancuso, M., Panza, F., Nacmias, B., Bossu, P., Piccardi, P., Annoni, G., Seripa, D., Galimberti, D., Hannequin, D., Licastro, F., Soininen, H., Ritchie, K., Blanche, H., Dartigues, J. F., Tzourio, C., Gut, I., Van Broeckhoven, C., Alperovitch, A., Lathrop, M. and Amouyel, P. (2009) 'Genome-wide association study identifies variants at CLU and CR1 associated with Alzheimer's disease', *Nat Genet,* 41(10), 1094-9.

Lambert, M. P., Barlow, A. K., Chromy, B. A., Edwards, C., Freed, R., Liosatos, M., Morgan, T. E., Rozovsky, I., Trommer, B., Viola, K. L., Wals, P., Zhang, C., Finch, C. E., Krafft, G. A. and Klein, W. L. (1998) 'Diffusible, nonfibrillar ligands derived from Abeta1-42 are potent central nervous system neurotoxins', *Proc Natl Acad Sci U S A,* 95(11), 6448-53.

Leek, J. T., Scharpf, R. B., Bravo, H. C., Simcha, D., Langmead, B., Johnson, W. E., Geman, D., Baggerly, K. and Irizarry, R. A. (2010) 'Tackling the widespread and critical impact of batch effects in high-throughput data', *Nat Rev Genet,* 11(10), 733-739.

Lewis, T. L., Cao, D., Lu, H., Mans, R. A., Su, Y. R., Jungbauer, L., Linton, M. F., Fazio, S., LaDu, M. J. and Li, L. (2010) 'Overexpression of human apolipoprotein A-I preserves cognitive function and attenuates neuroinflammation and cerebral amyloid angiopathy in a mouse model of Alzheimer disease', *J Biol Chem,* 285(47), 36958-68.

Lidstrom, A. M., Bogdanovic, N., Hesse, C., Volkman, I., Davidsson, P. and Blennow, K. (1998) 'Clusterin (apolipoprotein J) protein levels are increased in hippocampus and in frontal cortex in Alzheimer's disease', *Exp Neurol,* 154(2), 511-21.

Lin, M., Pedrosa, E., Shah, A., Hrabovsky, A., Maqbool, S., Zheng, D. and Lachman, H. M. (2011) 'RNA-Seq of human neurons derived from iPS cells reveals candidate long non-coding RNAs involved in neurogenesis and neuropsychiatric disorders', *PLoS One,* 6(9), e23356.

Ling, I. F., Bhongsatiern, J., Simpson, J. F., Fardo, D. W. and Estus, S. (2012) 'Genetics of clusterin isoform expression and Alzheimer's disease risk', *PLoS One,* 7(4), e33923.

Liu, C.-C., Kanekiyo, T., Xu, H. and Bu, G. (2013) 'Apolipoprotein E and Alzheimer disease: risk, mechanisms, and therapy', *Nature reviews. Neurology,* 9(2), 106-118.

Liu, H. and Zhang, S.-C. (2011) 'Specification of neuronal and glial subtypes from human pluripotent stem cells', *Cellular and molecular life sciences : CMLS,* 68(24), 3995-4008.

Liu, L., Drouet, V., Wu, J. W., Witter, M. P., Small, S. A., Clelland, C. and Duff, K. (2012) 'Trans-synaptic spread of tau pathology in vivo', *PLoS One,* 7(2), e31302.

Lobo, A., Launer, L. J., Fratiglioni, L., Andersen, K., Di Carlo, A., Breteler, M. M., Copeland, J. R., Dartigues, J. F., Jagger, C., Martinez-Lage, J., Soininen, H. and Hofman, A. (2000) 'Prevalence of dementia and major subtypes in Europe: A collaborative study of population-based cohorts. Neurologic Diseases in the Elderly Research Group', *Neurology,* 54(11 Suppl 5), S4-9.

Lovestone, S., Davis, D. R., Webster, M. T., Kaech, S., Brion, J. P., Matus, A. and Anderton, B. H. (1999) 'Lithium reduces tau phosphorylation: effects in living cells and in neurons at therapeutic concentrations', *Biol Psychiatry,* 45(8), 995-1003.

Lynch, J. R., Tang, W., Wang, H., Vitek, M. P., Bennett, E. R., Sullivan, P. M., Warner, D. S. and Laskowitz, D. T. (2003) 'APOE genotype and an ApoE-mimetic peptide modify the systemic and central nervous system inflammatory response', *J Biol Chem,* 278(49), 48529-33.

Maccioni, R. B., Farias, G., Morales, I. and Navarrete, L. (2010) 'The revitalized tau hypothesis on Alzheimer's disease', *Arch Med Res,* 41(3), 226-31.

Makinen, P. I., Koponen, J. K., Karkkainen, A. M., Malm, T. M., Pulkkinen, K. H.,

Koistinaho, J., Turunen, M. P. and Yla-Herttuala, S. (2006) 'Stable RNA interference: comparison of U6 and H1 promoters in endothelial cells and in mouse brain', *J Gene Med,* 8(4), 433-41.

Mali, P., Yang, L., Esvelt, K. M., Aach, J., Guell, M., DiCarlo, J. E., Norville, J. E. and Church, G. M. (2013) 'RNA-guided human genome engineering via Cas9', *Science,* 339(6121), 823-6.

Mann, D. M. and Hardy, J. (2013) 'Amyloid or tau: the chicken or the egg?', *Acta Neuropathol,* 126(4), 609-13.

Marchetto, Maria C. and Gage, Fred H. (2012) 'Modeling Brain Disease in a Dish: Really?', *Cell Stem Cell,* 10(6), 642-645.

Matthews, F. E., Stephan, B. C., Robinson, L., Jagger, C., Barnes, L. E., Arthur, A. and Brayne, C. (2016) 'A two decade dementia incidence comparison from the Cognitive Function and Ageing Studies I and II', *Nat Commun,* 7, 11398.

Mattson, M. P., Partin, J. and Begley, J. G. (1998) 'Amyloid beta-peptide induces apoptosis-related events in synapses and dendrites', *Brain Res,* 807(1-2), 167-76.

May, P. C., Lampert-Etchells, M., Johnson, S. A., Poirier, J., Masters, J. N. and Finch, C. E. (1990) 'Dynamics of gene expression for a hippocampal glycoprotein elevated in Alzheimer's disease and in response to experimental lesions in rat', *Neuron,* 5(6), 831-839

Mayeux, R. and Stern, Y. (2012) 'Epidemiology of Alzheimer disease', *Cold Spring Harb Perspect Med,* 2(8).

McGeer, P. L., McGeer, E. G., Kawamata, T., Yamada, T. and Akiyama, H. (1991) 'Reactions of the Immune System in Chronic Degenerative Neurological Diseases', *Canadian Journal of Neurological Sciences / Journal Canadien des Sciences Neurologiques,* 18(Supplement S3), 376-379.

McManus, M. T. and Sharp, P. A. (2002) 'Gene silencing in mammals by small interfering RNAs', *Nat Rev Genet,* 3(10), 737-47.

Mertens, J., Paquola, Apuã C. M., Ku, M., Hatch, E., Böhnke, L., Ladjevardi, S., McGrath, S., Campbell, B., Lee, H., Herdy, Joseph R., Gonçalves, J. T., Toda, T., Kim, Y., Winkler, J., Yao, J., Hetzer, Martin W. and Gage, Fred H. (2015) 'Directly Reprogrammed Human Neurons Retain Aging-Associated Transcriptomic Signatures and Reveal Age-Related Nucleocytoplasmic Defects', *Cell Stem Cell,* 17(6), 705-718.

Mertens, J., Stüber, K., Wunderlich, P., Ladewig, J., Kesavan, Jaideep C., Vandenberghe, R., Vandenbulcke, M., van Damme, P., Walter, J., Brüstle, O. and Koch, P. (2013) 'APP Processing in Human Pluripotent Stem Cell-Derived Neurons Is Resistant to NSAID-Based γ-Secretase Modulation', *Stem Cell Reports,* 1(6), 491-498.

Mestas, J. and Hughes, C. C. (2004) 'Of mice and not men: differences between mouse and human immunology', *J Immunol,* 172(5), 2731-8.

Morales, I., Farias, G. and Maccioni, R. B. (2010) 'Neuroimmunomodulation in the pathogenesis of Alzheimer's disease', *Neuroimmunomodulation,* 17(3), 202-4.

Morgan, K. and Carrasquillo, M. M. (2013) *Genetic Variants in Alzheimer's Disease, SpringerLink : Bücher,* Springer New York.

Musunuru, K. (2013) 'Genome editing of human pluripotent stem cells to generate human cellular disease models', *Disease Models and Mechanisms,* 6(4), 896-904.

Namba, Y., Tomonaga, M., Kawasaki, H., Otomo, E. and Ikeda, K. (1991) 'Apolipoprotein E immunoreactivity in cerebral amyloid deposits and neurofibrillary tangles in Alzheimer's disease and kuru plaque amyloid in Creutzfeldt-Jakob disease', *Brain Res,* 541(1), 163-6.

Narayan, P., Orte, A., Clarke, R. W., Bolognesi, B., Hook, S., Ganzinger, K. A., Meehan, S., Wilson, M. R., Dobson, C. M. and Klenerman, D. (2012) 'The extracellular chaperone clusterin sequesters oligomeric forms of the amyloid-beta(1-40) peptide', *Nat Struct Mol Biol,* 19(1), 79-83.

Nieweg, K., Andreyeva, A., van Stegen, B., Tanriover, G. and Gottmann, K. (2015) 'Alzheimer's disease-related amyloid-[beta] induces synaptotoxicity in human iPS cell-derived neurons', *Cell Death Dis,* 6, e1709.

Nilselid, A. M., Davidsson, P., Nagga, K., Andreasen, N., Fredman, P. and Blennow, K. (2006) 'Clusterin in cerebrospinal fluid: analysis of carbohydrates and quantification of native and glycosylated forms', *Neurochem Int,* 48(8), 718-28.

Nishimasu, H., Ran, F. A., Hsu, P. D., Konermann, S., Shehata, S. I., Dohmae, N., Ishitani, R., Zhang, F. and Nureki, O. (2014) 'Crystal structure of Cas9 in complex with guide RNA and target DNA', *Cell,* 156(5), 935-49.

Nithianantharajah, J., McKechanie, A. G., Stewart, T. J., Johnstone, M., Blackwood, D. H., St Clair, D., Grant, S. G. N., Bussey, T. J. and Saksida, L. M. (2015) 'Bridging the translational divide: identical cognitive touchscreen testing in mice and humans carrying mutations in a disease-relevant homologous gene', *Scientific Reports,* 5, 14613.

Noble, W., Garwood, C., Stephenson, J., Kinsey, A. M., Hanger, D. P. and Anderton, B. H. (2009) 'Minocycline reduces the development of abnormal tau species in models of Alzheimer's disease', *Faseb j,* 23(3), 739-50.

Nuutinen, T., Suuronen, T., Kauppinen, A. and Salminen, A. (2009) 'Clusterin: A forgotten player in Alzheimer's disease', *Brain Research Reviews,* 61(2), 89-104.

Oddo, S., Billings, L., Kesslak, J. P., Cribbs, D. H. and LaFerla, F. M. (2004) 'Aβ Immunotherapy Leads to Clearance of Early, but Not Late, Hyperphosphorylated Tau Aggregates via the Proteasome', *Neuron,* 43(3), 321-332.

Oddo, S., Caccamo, A., Kitazawa, M., Tseng, B. P. and LaFerla, F. M. (2003a) 'Amyloid deposition precedes tangle formation in a triple transgenic model of Alzheimer's disease', *Neurobiol Aging,* 24(8), 1063-70.

Oddo, S., Caccamo, A., Shepherd, J. D., Murphy, M. P., Golde, T. E., Kayed, R., Metherate, R., Mattson, M. P., Akbari, Y. and LaFerla, F. M. (2003b) 'Triple-Transgenic Model of Alzheimer's Disease with Plaques and Tangles: Intracellular Aβ and Synaptic Dysfunction', *Neuron,* 39(3), 409-421.

Ohgidani, M., Kato, T. A., Setoyama, D., Sagata, N., Hashimoto, R., Shigenobu, K., Yoshida, T., Hayakawa, K., Shimokawa, N., Miura, D., Utsumi, H. and Kanba, S. (2014) 'Direct induction of ramified microglia-like cells from human monocytes:

Dynamic microglial dysfunction in Nasu-Hakola disease', *Scientific Reports,* 4, 4957.

Parachikova, A., Agadjanyan, M.G., Cribbs, D.H., Blurton-Jones, M., Perreau, V., Rogers, J., Beach, T.G. & Cotman, C.W. 2007, "Inflammatory changes parallel the early stages of Alzheimer disease", *Neurobiology of aging,* 28(12), 1821-1833.

Peineau, S., Bradley, C., Taghibiglou, C., Doherty, A., Bortolotto, Z. A., Wang, Y. T. and Collingridge, G. L. (2008) 'The role of GSK-3 in synaptic plasticity', *British Journal of Pharmacology,* 153(Suppl 1), S428-S437.

Perez, E. E., Wang, J., Miller, J. C., Jouvenot, Y., Kim, K. A., Liu, O., Wang, N., Lee, G., Bartsevich, V. V., Lee, Y.-L., Guschin, D. Y., Rupniewski, I., Waite, A. J., Carpenito, C., Carroll, R. G., Orange, J. S., Urnov, F. D., Rebar, E. J., Ando, D., Gregory, P. D., Riley, J. L., Holmes, M. C. and June, C. H. (2008) 'Establishment of HIV-1 resistance in CD4(+) T cells by genome editing using zinc-finger nucleases', *Nature biotechnology,* 26(7), 808-816.

Perez, M., Cuadros, R., Benitez, M. J. and Jimenez, J. S. (2004) 'Interaction of Alzheimer's disease amyloid beta peptide fragment 25-35 with tau protein, and with a tau peptide containing the microtubule binding domain', *J Alzheimers Dis,* 6(5), 461-7.

Pooler, A. M., Phillips, E. C., Lau, D. H., Noble, W. and Hanger, D. P. (2013) 'Physiological release of endogenous tau is stimulated by neuronal activity', *EMBO Rep,* 14(4), 389-94.

Purro, S. A., Dickins, E. M. and Salinas, P. C. (2012) 'The secreted Wnt antagonist Dickkopf-1 is required for amyloid beta-mediated synaptic loss', *J Neurosci,* 32(10), 3492-8.

Ran, F. A., Hsu, P. D., Wright, J., Agarwala, V., Scott, D. A. and Zhang, F. (2013) 'Genome engineering using the CRISPR-Cas9 system', *Nat. Protocols,* 8(11), 2281-2308.

Rapoport, M., Dawson, H. N., Binder, L. I., Vitek, M. P. and Ferreira, A. (2002) 'Tau is essential to beta -amyloid-induced neurotoxicity', *Proc Natl Acad Sci U S A,* 99(9), 6364-9.

Reitz, C. (2012) 'Alzheimer's Disease and the Amyloid Cascade Hypothesis: A Critical Review', *International Journal of Alzheimer's Disease,* 2012, 369808.

Ries, M. & Sastre, M. 2016, "Mechanisms of Aβ Clearance and Degradation by Glial Cells", *Frontiers in Aging Neuroscience,* 8, 10

Roberson, E. D., Halabisky, B., Yoo, J. W., Yao, J., Chin, J., Yan, F., Wu, T., Hamto, P., Devidze, N., Yu, G. Q., Palop, J. J., Noebels, J. L. and Mucke, L. (2011) 'Amyloid-beta/Fyn-induced synaptic, network, and cognitive impairments depend on tau levels in multiple mouse models of Alzheimer's disease', *J Neurosci,* 31(2), 700-11.

Roberson, E. D., Scearce-Levie, K., Palop, J. J., Yan, F., Cheng, I. H., Wu, T., Gerstein, H., Yu, G. Q. and Mucke, L. (2007) 'Reducing endogenous tau ameliorates amyloid beta-induced deficits in an Alzheimer's disease mouse model', *Science,* 316(5825), 750-4.

Rohani, L., Johnson, A. A., Arnold, A. and Stolzing, A. (2014) 'The aging signature: a hallmark of induced pluripotent stem cells?', *Aging Cell,* 13(1), 2-7.

Ross, C. A. and Akimov, S. S. (2014) 'Human-induced pluripotent stem cells: potential for neurodegenerative diseases', *Hum Mol Genet,* 23(R1), R17-26.

Sander, J. D. and Joung, J. K. (2014) 'CRISPR-Cas systems for editing, regulating and targeting genomes', *Nat Biotechnol,* 32(4), 347-55.

Schurmann, B., Wiese, B., Bickel, H., Weyerer, S., Riedel-Heller, S. G., Pentzek, M., Bachmann, C., Williams, J., van den Bussche, H., Maier, W. and Jessen, F. (2011) 'Association of the Alzheimer's disease clusterin risk allele with plasma clusterin concentration', *J Alzheimers Dis,* 25(3), 421-4.

Schöll, M., Lockhart, Samuel N., Schonhaut, Daniel R., O'Neil, James P., Janabi, M., Ossenkoppele, R., Baker, Suzanne L., Vogel, Jacob W., Faria, J., Schwimmer, Henry D., Rabinovici, Gil D. and Jagust, William J. (2016) 'PET Imaging of Tau Deposition in the Aging Human Brain', *Neuron,* 89(5), 971-982.

Shankar, G. M., Bloodgood, B. L., Townsend, M., Walsh, D. M., Selkoe, D. J. and Sabatini, B. L. (2007) 'Natural oligomers of the Alzheimer amyloid-beta protein

induce reversible synapse loss by modulating an NMDA-type glutamate receptor-dependent signaling pathway', *J Neurosci,* 27(11), 2866-75.

Shankar, G. M., Li, S., Mehta, T. H., Garcia-Munoz, A., Shepardson, N. E., Smith, I., Brett, F. M., Farrell, M. A., Rowan, M. J., Lemere, C. A., Regan, C. M., Walsh, D. M., Sabatini, B. L. and Selkoe, D. J. (2008) 'Amyloid-beta protein dimers isolated directly from Alzheimer's brains impair synaptic plasticity and memory', *Nat Med,* 14(8), 837-42.

Shepherd, C. E., Gregory, G. C., Vickers, J. C., Brooks, W. S., Kwok, J. B., Schofield, P. R., Kril, J. J. and Halliday, G. M. (2004) 'Positional effects of presenilin-1 mutations on tau phosphorylation in cortical plaques', *Neurobiol Dis,* 15(1), 115-9.

Sherrington, R., Rogaev, E.I., Liang, Y., Rogaeva, E.A., Levesque, G., Ikeda, M., Chi, H., Lin, C., Li, G., Holman, K., Tsuda, T., Mar, L., Foncin, J.F., Bruni, A.C., Montesi, M.P., Sorbi, S., Rainero, I., Pinessi, L., Nee, L., Chumakov, I., Pollen, D., Brookes, A., Sanseau, P., Polinsky, R.J., Wasco, W., Da Silva, H.A., Haines, J.L., Perkicak-Vance, M.A., Tanzi, R.E., Roses, A.D., Fraser, P.E., Rommens, J.M. & St George-Hyslop, P.H. 1995, "Cloning of a gene bearing missense mutations in early-onset familial Alzheimer's disease", *Nature,* vol. 375(6534), 754-760.

Shi, Y., Kirwan, P., Smith, J., MacLean, G., Orkin, S. H. and Livesey, F. J. (2012) 'A human stem cell model of early Alzheimer's disease pathology in Down syndrome', *Sci Transl Med,* 4(124), 124ra29.

Shi, Y., Kirwan, P., Smith, J., Robinson, H. P. C. and Livesey, F. J. (2012) 'Human cerebral cortex development from pluripotent stem cells to functional excitatory synapses', *Nat Neurosci,* 15(3), 477-486.

Shipton, O. A., Leitz, J. R., Dworzak, J., Acton, C. E., Tunbridge, E. M., Denk, F., Dawson, H. N., Vitek, M. P., Wade-Martins, R., Paulsen, O. and Vargas-Caballero, M. (2011) 'Tau protein is required for amyloid {beta}-induced impairment of hippocampal long-term potentiation', *J Neurosci,* 31(5), 1688-92.

Sofola, O., Kerr, F., Rogers, I., Killick, R., Augustin, H., Gandy, C., Allen, M. J., Hardy, J., Lovestone, S. and Partridge, L. (2010) 'Inhibition of GSK-3 ameliorates Abeta pathology in an adult-onset Drosophila model of Alzheimer's disease', *PLoS Genet,* 6(9), e1001087.

Stine, W. B., Jr., Dahlgren, K. N., Krafft, G. A. and LaDu, M. J. (2003) 'In vitro characterization of conditions for amyloid-beta peptide oligomerization and fibrillogenesis', *J Biol Chem,* 278(13), 11612-22.

Takahashi, K., Tanabe, K., Ohnuki, M., Narita, M., Ichisaka, T., Tomoda, K. and Yamanaka, S. (2007) 'Induction of pluripotent stem cells from adult human fibroblasts by defined factors', *Cell,* 131(5), 861-72.

Takahashi, K. and Yamanaka, S. (2006) 'Induction of pluripotent stem cells from mouse embryonic and adult fibroblast cultures by defined factors', *Cell,* 126(4), 663-76.

Takashima, A., Noguchi, K., Sato, K., Hoshino, T. and Imahori, K. (1993) 'Tau protein kinase I is essential for amyloid beta-protein-induced neurotoxicity', *Proc Natl Acad Sci U S A,* 90(16), 7789-93.

Takashima, A., Yamaguchi, H., Noguchi, K., Michel, G., Ishiguro, K., Sato, K., Hoshino, T., Hoshi, M. and Imahori, K. (1995) 'Amyloid β peptide induces cytoplasmic accumulation of amyloid protein precursor via tau protein kinase I/glycogen synthase kinase-3β in rat hippocampal neurons', *Neuroscience Letters,* 198(2), 83-86.

Tarczyluk, M. A., Nagel, D. A., Rhein Parri, H., Tse, E. H. Y., Brown, J. E., Coleman, M. D. and Hill, E. J. (2015) 'Amyloid β 1-42 induces hypometabolism in human stem cell-derived neuron and astrocyte networks', *Journal of Cerebral Blood Flow & Metabolism,* 35(8), 1348-1357.

Thambisetty, M., Simmons, A., Velayudhan, L., Hye, A., Campbell, J., Zhang, Y., Wahlund, L.-O., Westman, E., Kinsey, A., Güentert, A., Proitsi, P., Powell, J., Causevic, M., Killick, R., Lunnon, K., Lynham, S., Broadstock, M., Choudhry, F., Howlett, D. R., Williams, R. J., Sharp, S. I., Mitchelmore, C., Tunnard, C., Leung, R., Foy, C., O'Brien, D., Breen, G., Furney, S., Ward, M., Kloszewska, I., Mecocci, P., Soininen, H., Tsolaki, M., Vellas, B., Hodges, A., Murphy, D., Parkins, S., Richardson, J., Resnick, S. M., Ferrucci, L., Wong, D. F., Zhou, Y., Muehlboeck, S., Evans, A., Francis, P. T., Spenger, C., Lovestone, S. and AddNeuroMed, c. (2010) 'Association of plasma clusterin concentration with severity, pathology, and progression in Alzheimer disease', *Archives of general psychiatry,* 67(7), 739-748.

Tizon, B., Ribe, E. M., Mi, W., Troy, C. M. and Levy, E. (2010) 'Cystatin C protects neuronal cells from amyloid β-induced toxicity', *Journal of Alzheimer's disease : JAD,* 19(3), 885-894.

Toledo, E. M. and Inestrosa, N. C. (2010) 'Activation of Wnt signaling by lithium and rosiglitazone reduced spatial memory impairment and neurodegeneration in brains of an APPswe/PSEN1DeltaE9 mouse model of Alzheimer's disease', *Mol Psychiatry,* 15(3), 272-85, 228.

Trojanowski, J. Q., Arnold, S. E., Karlawish, J. H., Naylor, M., Brunden, K. R. and Lee, V. M. Y. (2012) 'A model for improving the treatment and care of Alzheimer's disease patients through interdisciplinary research', *Alzheimer's & Dementia,* 8(6), 564-573.

Valerie, K. and Povirk, L. F. (2003) 'Regulation and mechanisms of mammalian double-strand break repair', *Oncogene,* 22(37), 5792-812.

Vossel, K. A., Zhang, K., Brodbeck, J., Daub, A. C., Sharma, P., Finkbeiner, S., Cui, B. and Mucke, L. (2010) 'Tau reduction prevents Abeta-induced defects in axonal transport', *Science,* 330(6001), 198.

Walsh, D. M., Klyubin, I., Fadeeva, J. V., Rowan, M. J. and Selkoe, D. J. (2002) 'Amyloid-beta oligomers: their production, toxicity and therapeutic inhibition', *Biochem Soc Trans,* 30(4), 552-7.

Wang, J., Shou, J. and Chen, X. (2000) 'Dickkopf-1, an inhibitor of the Wnt signaling pathway, is induced by p53', *Oncogene,* 19(14), 1843-8.

White, F., Nicoll, J. A. R. and Horsburgh, K. (2001) 'Alterations in ApoE and ApoJ in Relation to Degeneration and Regeneration in a Mouse Model of Entorhinal Cortex Lesion', *Experimental Neurology,* 169(2), 307-318.

Wiedenheft, B., Sternberg, S. H. and Doudna, J. A. (2012) 'RNA-guided genetic silencing systems in bacteria and archaea', *Nature,* 482(7385), 331-338.

Wilcock, G. K. and Esiri, M. M. (1982) 'Plaques, tangles and dementia. A quantitative study', *J Neurol Sci,* 56(2-3), 343-56.

'World Alzheimer Report 2015: The Global Impact of Dementia' https://www.alz.co.uk/research/world-report-2015 [accessed online 12/05/16]

Wu, Z. C., Yu, J. T., Li, Y. and Tan, L. (2012) 'Clusterin in Alzheimer's disease', *Adv Clin Chem,* 56, 155-73.

Xie, Z., Harris-White, M. E., Wals, P. A., Frautschy, S. A., Finch, C. E. and Morgan, T. E. (2005) 'Apolipoprotein J (clusterin) activates rodent microglia in vivo and in vitro', *Journal of Neurochemistry,* 93(4), 1038-1046.

Xing, Y. Y., Yu, J. T., Cui, W. Z., Zhong, X. L., Wu, Z. C., Zhang, Q. and Tan, L. (2012) 'Blood clusterin levels, rs9331888 polymorphism, and the risk of Alzheimer's disease', *J Alzheimers Dis,* 29(3), 515-9.

Xu, X., Lei, Y., Luo, J., Wang, J., Zhang, S., Yang, X. J., Sun, M., Nuwaysir, E., Fan, G., Zhao, J., Lei, L. and Zhong, Z. (2013) 'Prevention of beta-amyloid induced toxicity in human iPS cell-derived neurons by inhibition of Cyclin-dependent kinases and associated cell cycle events', *Stem Cell Res,* 10(2), 213-27.

Yagi, T., Ito, D., Okada, Y., Akamatsu, W., Nihei, Y., Yoshizaki, T., Yamanaka, S., Okano, H. and Suzuki, N. (2011) 'Modeling familial Alzheimer's disease with induced pluripotent stem cells', *Hum Mol Genet,* 20(23), 4530-9.

Yahata, N., Asai, M., Kitaoka, S., Takahashi, K., Asaka, I., Hioki, H., Kaneko, T., Maruyama, K., Saido, T. C., Nakahata, T., Asada, T., Yamanaka, S., Iwata, N. and Inoue, H. (2011) 'Anti-Aβ Drug Screening Platform Using Human iPS Cell-Derived Neurons for the Treatment of Alzheimer's Disease', *PLoS ONE,* 6(9), e25788.

Yankner, B. A., Duffy, L. K. and Kirschner, D. A. (1990) 'Neurotrophic and neurotoxic effects of amyloid beta protein: reversal by tachykinin neuropeptides', *Science,* 250(4978), 279-82.

Yeh, F.L., Wang, Y., Tom, I., Gonzalez, L.C. & Sheng, M. 2016, "TREM2 Binds to Apolipoproteins, Including APOE and CLU/APOJ, and Thereby Facilitates Uptake of Amyloid-Beta by Microglia", *Neuron,* 91(2), 328-340.

Yu, J. T. and Tan, L. (2012) 'The role of clusterin in Alzheimer's disease: pathways, pathogenesis, and therapy', *Mol Neurobiol,* 45(2), 314-26.

Zahs, K. and Ashe, K. (2013) 'β-Amyloid oligomers in aging and Alzheimer's disease', *Frontiers in Aging Neuroscience,* 5, 28.

Zhang, Q. G., Wang, R. M., Khan, M., Mahesh, V. and Brann, D. W. (2008) 'Role of dickkopf-1, an antagonist of the Wnt/beta-catenin signaling pathway, in estrogen-induced neuroprotection and attenuation of tau phosphorylation', *Journal of Neuroscience,* 28(34), 8430-8441.

Appendix 1

Protocol for Qiagen Plasmid DNA Purification with QIAprep Spin Miniprep Kit

See Handbook link in Qiagen webpage 'QIAprep Spin Miniprep Kit [Accessed 16/08/2021]

https://www.qiagen.com/us/products/discovery-and-translational-research/dna-rna-purification/dna-purification/plasmid-dna/qiaprep-spin-miniprep-kit/

Protocol: DNA Purification from Cultured Cells Using the Gentra Puregene Cell Kit

See Handbook link in Qiagen webpage 'Gentra Puregene Kits' [Accessed 16/08/2021]

https://www.qiagen.com/us/products/discovery-and-translational-research/dna-rna-purification/dna-purification/genomic-dna/gentra-puregene-kits/

Appendix 2

Tables show up to 30 of the most significantly up- or down-regulated Molecular Functions (MF), Disease Pathways, KEGG pathways and Biological Processes (BP) for WT0 vs. WT48, WT0 vs. CLU0, and CLU0 vs. CLU48.

WT 0hr vs. WT 48hr – MF Upregulated

Pathway	p value	q value	Gene Count
chromatin binding	4.98E-06	4.38E-03	329
microtubule motor activity	1.73E-04	7.60E-02	73
DNA-dependent ATPase activity	4.49E-04	1.31E-01	69
microtubule binding	1.09E-03	2.38E-01	106
ubiquitin-protein ligase activity	2.08E-03	3.37E-01	251
small conjugating protein ligase activity	2.40E-03	3.37E-01	267
acid-amino acid ligase activity	2.68E-03	3.37E-01	294
histone-lysine N-methyltransferase activity	3.65E-03	4.00E-01	40
tubulin binding	5.18E-03	4.23E-01	156
histone deacetylase activity	5.75E-03	4.23E-01	19
structure-specific DNA binding	6.13E-03	4.23E-01	215
protein deacetylase activity	6.60E-03	4.23E-01	20
lysine N-methyltransferase activity	6.75E-03	4.23E-01	45
protein-lysine N-methyltransferase activity	6.75E-03	4.23E-01	45
ligase activity, forming carbon-nitrogen bonds	8.20E-03	4.39E-01	326
core promoter binding	9.27E-03	4.39E-01	55
transcription cofactor activity	1.05E-02	4.39E-01	469
histone methyltransferase activity	1.07E-02	4.39E-01	49
protein methyltransferase activity	1.07E-02	4.39E-01	68
DNA helicase activity	1.10E-02	4.39E-01	41
histone deacetylase activity (H3-K9 specific)	1.26E-02	4.39E-01	13
NAD-dependent histone deacetylase activity (H3-K9 specific)	1.26E-02	4.39E-01	13
histone deacetylase activity (H3-K14 specific)	1.27E-02	4.39E-01	11
NAD-dependent histone deacetylase activity (H3-K14 specific)	1.27E-02	4.39E-01	11
NAD-dependent histone deacetylase activity (H4-K16 specific)	1.27E-02	4.39E-01	11
histone deacetylase activity (H4-K16 specific)	1.40E-02	4.39E-01	12
NAD-dependent histone deacetylase activity (H3-K18 specific)	1.40E-02	4.39E-01	12
NAD-dependent histone deacetylase activity	1.50E-02	4.39E-01	15
NAD-dependent protein deacetylase	1.50E-02	4.39E-01	15

activity

WT 0hr vs. WT 48hr – MF Downregulated

Pathway	p value	q value	Gene Count
extracellular matrix structural constituent	5.46E-06	2.61E-03	76
actin binding	5.95E-06	2.61E-03	348
integrin binding	4.03E-05	1.18E-02	79
actin filament binding	5.56E-05	1.22E-02	69
ADP binding	9.95E-05	1.57E-02	23
fibronectin binding	1.07E-04	1.57E-02	16
growth factor binding	1.98E-04	2.35E-02	105
growth factor activity	2.14E-04	2.35E-02	149
carbohydrate binding	3.06E-04	2.99E-02	193
monosaccharide binding	3.78E-04	3.32E-02	59
antioxidant activity	5.33E-04	4.26E-02	63
metallopeptidase activity	1.04E-03	7.60E-02	172
platelet-derived growth factor receptor binding	1.42E-03	9.61E-02	13
enzyme inhibitor activity	1.65E-03	1.03E-01	290
structural constituent of muscle	1.99E-03	1.13E-01	46
metalloendopeptidase activity	2.06E-03	1.13E-01	111
collagen binding	2.41E-03	1.21E-01	45
lipase activity	2.48E-03	1.21E-01	102
cytokine binding	2.85E-03	1.24E-01	54
extracellular matrix binding	2.92E-03	1.24E-01	35
cytokine receptor binding	3.11E-03	1.24E-01	183
protein complex binding	3.24E-03	1.24E-01	315
carboxylic acid binding	3.25E-03	1.24E-01	170
growth factor receptor binding	3.56E-03	1.28E-01	89
phospholipase activity	3.70E-03	1.28E-01	85
serine-type endopeptidase inhibitor activity	3.79E-03	1.28E-01	83
structural constituent of ribosome	4.28E-03	1.36E-01	151
phosphatidylserine binding	4.33E-03	1.36E-01	15
rRNA binding	4.64E-03	1.41E-01	31
lipoprotein particle binding	5.19E-03	1.47E-01	22

WT 0hr vs. WT 48hr – KEGG Disease Upregulated

Pathway	p value	q value	Gene Count
Systemic lupus erythematosus	6.05E-03	2.84E-01	115

WT 0hr vs. WT 48hr – KEGG Disease Downregulated

Pathway	p value	q value	Gene Count
Amoebiasis	3.98E-05	1.87E-03	100
Hypertrophic cardiomyopathy (HCM)	1.57E-03	3.70E-02	81
Dilated cardiomyopathy	3.85E-03	4.55E-02	90
Rheumatoid arthritis	3.87E-03	4.55E-02	81
Bacterial invasion of epithelial cells	7.49E-03	5.93E-02	69
Arrhythmogenic right ventricular cardiomyopathy (ARVC)	7.57E-03	5.93E-02	74
Pathogenic Escherichia coli infection	1.14E-02	7.67E-02	53
Chagas disease (American trypanosomiasis)	1.74E-02	1.02E-01	96
Toxoplasmosis	2.22E-02	1.05E-01	124
Viral myocarditis	2.23E-02	1.05E-01	64
Malaria	2.70E-02	1.08E-01	49
Pathways in cancer	2.76E-02	1.08E-01	322
Leishmaniasis	3.01E-02	1.09E-01	64

WT 0hr vs. WT 48hr – KEGG Upregulated

Pathway	p value	q value	Gene Count
Ubiquitin mediated proteolysis	2.68E-03	4.23E-01	133
RNA degradation	8.25E-03	4.23E-01	71
Cell cycle	1.11E-02	4.23E-01	124
Progesterone-mediated oocyte maturation	1.19E-02	4.23E-01	86
Notch signaling pathway	1.29E-02	4.23E-01	46
Spliceosome	2.54E-02	6.96E-01	127
Oocyte meiosis	3.16E-02	7.40E-01	109
mRNA surveillance pathway	3.93E-02	8.06E-01	83

WT 0hr vs. WT 48hr – KEGG Downregulated

Pathway	p value	q value	Gene Count
Focal adhesion	1.03E-08	1.70E-06	200
ECM-receptor interaction	1.12E-06	9.18E-05	83
Regulation of actin cytoskeleton	2.85E-04	1.20E-02	209
Hematopoietic cell lineage	2.92E-04	1.20E-02	74
Protein digestion and absorption	8.17E-04	2.68E-02	77
Ribosome	2.56E-03	6.98E-02	88
Phagosome	5.77E-03	1.09E-01	139
Glutathione metabolism	6.46E-03	1.09E-01	46
Leukocyte transendothelial migration	7.18E-03	1.09E-01	113
Terpenoid backbone biosynthesis	7.20E-03	1.09E-01	15
Tight junction	8.60E-03	1.09E-01	130
Pentose phosphate pathway	8.60E-03	1.09E-01	27
Amino sugar and nucleotide sugar metabolism	8.68E-03	1.09E-01	48
Glycolysis / Gluconeogenesis	9.40E-03	1.09E-01	59
Lysosome	9.97E-03	1.09E-01	120
Endocytosis	1.45E-02	1.38E-01	196
Apoptosis	1.56E-02	1.38E-01	86
Cell adhesion molecules (CAMs)	1.60E-02	1.38E-01	125
Metabolism of xenobiotics by cytochrome P450	1.61E-02	1.38E-01	54
Porphyrin and chlorophyll metabolism	1.68E-02	1.38E-01	32
Steroid biosynthesis	1.91E-02	1.49E-01	19
One carbon pool by folate	2.49E-02	1.82E-01	18
MAPK signaling pathway	2.57E-02	1.82E-01	265
Tryptophan metabolism	2.66E-02	1.82E-01	42
Adherens junction	3.16E-02	2.07E-01	73
Osteoclast differentiation	3.54E-02	2.23E-01	118
Bile secretion	3.67E-02	2.23E-01	67
Fructose and mannose metabolism	3.91E-02	2.29E-01	36

WT 0hr vs. WT 48hr – BP Upregulated

Pathway	p value	q value	Gene Count
nuclear division	1.50E-13	3.05E-10	361
mitosis	1.50E-13	3.05E-10	361
M phase of mitotic cell cycle	2.11E-13	3.05E-10	372
organelle fission	4.02E-13	4.34E-10	386
microtubule-based process	3.09E-12	2.67E-09	428
mitotic prometaphase	4.49E-11	2.96E-08	85
chromosome segregation	4.79E-11	2.96E-08	145
cell division	1.39E-10	7.54E-08	477
microtubule cytoskeleton organization	5.38E-10	2.58E-07	284
DNA repair	2.24E-08	9.70E-06	391
sister chromatid segregation	4.46E-08	1.75E-05	53
chromatin modification	1.45E-07	5.23E-05	435
mitotic sister chromatid segregation	1.79E-07	5.96E-05	50
DNA conformation change	7.20E-07	2.22E-04	170
protein-DNA complex assembly	1.58E-06	4.56E-04	120
regulation of microtubule-based process	3.27E-06	8.84E-04	92
protein-DNA complex subunit organization	3.49E-06	8.88E-04	139
regulation of microtubule cytoskeleton organization	5.12E-06	1.23E-03	77
microtubule organizing center organization	7.91E-06	1.80E-03	67
centromere complex assembly	1.04E-05	2.24E-03	34
G2/M transition of mitotic cell cycle	1.10E-05	2.26E-03	147
DNA packaging	1.16E-05	2.27E-03	134
mitotic metaphase/anaphase transition	1.32E-05	2.48E-03	46
centrosome organization	1.38E-05	2.49E-03	63
mRNA processing	2.06E-05	3.49E-03	397
spindle organization	2.10E-05	3.49E-03	83
chromatin remodeling	3.37E-05	5.39E-03	95
forebrain development	3.83E-05	5.92E-03	281
centrosome cycle	4.89E-05	7.29E-03	42
RNA splicing	7.82E-05	1.12E-02	322

WT 0hr vs. WT 48hr – BP Downregulated

Pathway	p value	q value	Gene Count
extracellular matrix organization	1.04E-08	2.25E-05	202
extracellular structure organization	1.04E-08	2.25E-05	203
regulation of cell migration	3.57E-08	5.14E-05	385
angiogenesis	6.14E-08	6.64E-05	352
regulation of cellular component movement	1.10E-07	7.06E-05	457
regulation of cell motility	1.11E-07	7.06E-05	408
regulation of wound healing	1.14E-07	7.06E-05	78
platelet activation	1.77E-07	9.56E-05	209
positive regulation of cell migration	2.53E-07	1.14E-04	219
regulation of locomotion	2.81E-07	1.14E-04	440
platelet degranulation	2.94E-07	1.14E-04	76
cell-substrate adhesion	3.17E-07	1.14E-04	216
positive regulation of cell motility	4.06E-07	1.35E-04	224
muscle system process	5.27E-07	1.63E-04	279
positive regulation of cellular component movement	7.51E-07	2.16E-04	230
cytokine production	8.79E-07	2.26E-04	398
regulation of coagulation	9.54E-07	2.26E-04	63
muscle contraction	9.77E-07	2.26E-04	248
blood vessel development	9.93E-07	2.26E-04	487
response to steroid hormone stimulus	1.41E-06	3.04E-04	251
regulation of cytokine production	1.66E-06	3.17E-04	359
response to drug	1.66E-06	3.17E-04	327
positive regulation of locomotion	1.70E-06	3.17E-04	233
blood vessel morphogenesis	1.76E-06	3.17E-04	428
sterol biosynthetic process	2.02E-06	3.50E-04	50
response to oxidative stress	3.13E-06	5.21E-04	249
regulation of blood coagulation	3.53E-06	5.45E-04	58
regulation of hemostasis	3.53E-06	5.45E-04	58
reactive oxygen species metabolic process	6.30E-06	9.39E-04	122
response to alcohol	7.27E-06	1.05E-03	211

WT 0hr vs. CLU 0hr – MF Upregulated

Pathway	p value	q value	Gene Count
cytokine receptor binding	2.61E-15	1.40E-12	183
growth factor binding	3.18E-15	1.40E-12	105
cytokine activity	1.48E-14	4.32E-12	172
carbohydrate derivative binding	2.12E-14	4.66E-12	178
glycosaminoglycan binding	8.95E-14	1.32E-11	159
extracellular matrix structural constituent	9.03E-14	1.32E-11	76
enzyme inhibitor activity	2.61E-12	3.27E-10	290
growth factor activity	7.55E-12	8.29E-10	149
actin binding	9.38E-12	9.15E-10	348
heparin binding	7.53E-11	6.24E-09	120
peptidase regulator activity	7.82E-11	6.24E-09	182
sulfur compound binding	3.08E-10	2.26E-08	159
endopeptidase regulator activity	4.36E-09	2.94E-07	146
endopeptidase inhibitor activity	6.10E-09	3.77E-07	142
integrin binding	6.44E-09	3.77E-07	79
growth factor receptor binding	8.62E-09	4.73E-07	89
insulin-like growth factor binding	9.83E-09	5.08E-07	25
extracellular matrix binding	1.13E-08	5.53E-07	35
collagen binding	1.98E-08	9.13E-07	45
peptidase inhibitor activity	2.37E-08	1.04E-06	148
cytokine binding	1.18E-07	4.93E-06	54
cytokine receptor activity	1.58E-07	6.30E-06	75
protein complex binding	1.77E-07	6.75E-06	315
peptide binding	4.12E-07	1.51E-05	129
platelet-derived growth factor binding	5.26E-07	1.85E-05	11
structural constituent of ribosome	5.59E-07	1.89E-05	151
amide binding	1.48E-06	4.82E-05	133
GTPase activity	3.12E-06	9.77E-05	226
kinase regulator activity	5.40E-06	1.63E-04	132
platelet-derived growth factor receptor binding	6.21E-06	1.82E-04	13

WT 0hr vs. CLU 0hr – MF Downregulated

Pathway	p value	q value	Gene Count
helicase activity	3.01E-11	2.64E-08	145
DNA-dependent ATPase activity	2.77E-09	1.21E-06	69
histone binding	4.23E-09	1.24E-06	104
chromatin binding	7.73E-09	1.70E-06	329
microtubule motor activity	8.30E-08	1.46E-05	73
histone acetyltransferase activity	1.65E-07	2.42E-05	49
ATP-dependent helicase activity	3.70E-07	4.06E-05	107
purine NTP-dependent helicase activity	3.70E-07	4.06E-05	107
DNA helicase activity	7.16E-06	6.99E-04	41
S-adenosylmethionine-dependent methyltransferase activity	1.03E-05	9.03E-04	103
protein methyltransferase activity	1.29E-05	1.03E-03	68
transferase activity, transferring one-carbon groups	1.50E-05	1.04E-03	190
ubiquitin thiolesterase activity	1.58E-05	1.04E-03	76
methyltransferase activity	1.66E-05	1.04E-03	184
N-methyltransferase activity	2.81E-05	1.64E-03	67
nucleosome binding	3.04E-05	1.67E-03	16
lysine N-methyltransferase activity	4.95E-05	2.31E-03	45
protein-lysine N-methyltransferase activity	4.95E-05	2.31E-03	45
histone methyltransferase activity	5.13E-05	2.31E-03	49
ATP-dependent DNA helicase activity	5.26E-05	2.31E-03	31
histone acetyl-lysine binding	6.08E-05	2.54E-03	15
methylated histone residue binding	1.50E-04	5.97E-03	38
mRNA binding	1.91E-04	7.31E-03	93
N-acetyltransferase activity	2.42E-04	8.72E-03	75
histone-lysine N-methyltransferase activity	2.48E-04	8.72E-03	40
nucleocytoplasmic transporter activity	3.57E-04	1.20E-02	13
motor activity	3.93E-04	1.28E-02	128
N-acyltransferase activity	5.61E-04	1.76E-02	89
microtubule binding	6.17E-04	1.87E-02	106
small conjugating protein-specific protease activity	7.33E-04	2.14E-02	51

WT 0hr vs. CLU 0hr – KEGG Disease Upregulated

Pathway	p value	q value	Gene Count
Systemic lupus erythematosus	6.05E-03	2.84E-01	115
Amoebiasis	2.67E-16	1.26E-14	100
Rheumatoid arthritis	3.35E-12	7.86E-11	81
Pathways in cancer	3.95E-09	6.18E-08	322
Hypertrophic cardiomyopathy (HCM)	1.02E-07	1.19E-06	81
Dilated cardiomyopathy	1.39E-07	1.25E-06	90
Alzheimer's disease	1.59E-07	1.25E-06	163
Chagas disease (American trypanosomiasis)	2.74E-07	1.84E-06	96
Bacterial invasion of epithelial cells	9.51E-07	5.59E-06	69
Small cell lung cancer	2.90E-06	1.52E-05	85
Malaria	5.50E-06	2.58E-05	49
Toxoplasmosis	8.92E-06	3.81E-05	124
Leishmaniasis	1.61E-05	6.31E-05	64
Arrhythmogenic right ventricular cardiomyopathy (ARVC)	6.73E-05	2.43E-04	74
Epithelial cell signaling in Helicobacter pylori infection	1.09E-04	3.44E-04	67
Glioma	1.10E-04	3.44E-04	62
Pathogenic Escherichia coli infection	1.43E-04	3.99E-04	53
Hepatitis C	1.44E-04	3.99E-04	125
Melanoma	1.86E-04	4.87E-04	70
Chronic myeloid leukemia	4.91E-04	1.21E-03	72
Shigellosis	6.05E-04	1.42E-03	61
Viral myocarditis	6.90E-04	1.52E-03	64
Huntington's disease	7.10E-04	1.52E-03	181
Vibrio cholerae infection	1.11E-03	2.26E-03	53
Renal cell carcinoma	1.87E-03	3.67E-03	70
Primary immunodeficiency	2.73E-03	5.13E-03	30
Pancreatic cancer	3.25E-03	5.87E-03	70
Parkinson's disease	4.16E-03	7.25E-03	129
Prion diseases	5.39E-03	9.04E-03	32
Bladder cancer	6.32E-03	1.02E-02	42
Graft-versus-host disease	7.45E-03	1.17E-02	28

WT 0hr vs. CLU 0hr – KEGG Upregulated

Pathway	p value	q value	Gene Count
Focal adhesion	4.43E-22	7.26E-20	200
ECM-receptor interaction	2.23E-18	1.83E-16	83
p53 signaling pathway	3.28E-12	1.80E-10	68
Lysosome	3.37E-11	1.38E-09	120
Endocytosis	8.80E-11	2.89E-09	196
Osteoclast differentiation	1.99E-10	5.05E-09	118
Phagosome	2.16E-10	5.05E-09	139
Protein digestion and absorption	6.88E-09	1.41E-07	77
Apoptosis	2.22E-08	4.05E-07	86
Hematopoietic cell lineage	2.96E-08	4.85E-07	74
Complement and coagulation cascades	4.75E-08	7.09E-07	60
Leukocyte transendothelial migration	8.63E-08	1.18E-06	113
Regulation of actin cytoskeleton	7.17E-07	8.53E-06	209
MAPK signaling pathway	7.28E-07	8.53E-06	265
Protein processing in endoplasmic reticulum	1.61E-06	1.76E-05	163
Ribosome	6.48E-06	6.64E-05	88
Jak-STAT signaling pathway	2.05E-05	1.98E-04	137
Natural killer cell mediated cytotoxicity	2.25E-05	2.05E-04	113
Mucin type O-Glycan biosynthesis	7.71E-05	6.66E-04	29
Cardiac muscle contraction	8.50E-05	6.97E-04	76
B cell receptor signaling pathway	9.89E-05	7.72E-04	75
Glycosaminoglycan biosynthesis - chondroitin sulfate	1.31E-04	9.76E-04	22
Tight junction	2.05E-04	1.44E-03	130
TGF-beta signaling pathway	2.10E-04	1.44E-03	84
Chemokine signaling pathway	2.88E-04	1.89E-03	168
Oxidative phosphorylation	3.35E-04	2.11E-03	131
Bile secretion	4.01E-04	2.43E-03	67
Porphyrin and chlorophyll metabolism	5.90E-04	3.46E-03	32
Amino sugar and nucleotide sugar metabolism	7.29E-04	4.12E-03	48
Antigen processing and presentation	8.20E-04	4.48E-03	62

WT 0hr vs. CLU 0hr – KEGG Downregulated

Pathway	p value	q value	Gene Count
Spliceosome	3.61E-10	5.91E-08	127
RNA transport	1.34E-06	1.10E-04	150
mRNA surveillance pathway	6.04E-06	3.30E-04	83
Notch signaling pathway	6.12E-04	2.32E-02	46
DNA replication	7.08E-04	2.32E-02	36
Taste transduction	1.12E-03	3.07E-02	45
Cysteine and methionine metabolism	4.25E-03	9.97E-02	36
Homologous recombination	8.48E-03	1.74E-01	28
RNA degradation	1.26E-02	2.29E-01	71
Progesterone-mediated oocyte maturation	2.36E-02	3.87E-01	86
Lysine degradation	2.94E-02	4.28E-01	44
Non-homologous end-joining	3.13E-02	4.28E-01	13
Oocyte meiosis	3.53E-02	4.45E-01	109
beta-Alanine metabolism	3.83E-02	4.48E-01	22
Ubiquitin mediated proteolysis	4.24E-02	4.63E-01	133
Base excision repair	4.66E-02	4.77E-01	33

WT 0hr vs. CLU 0hr – BP Upregulated

Pathway	p value	q value	Gene Count
blood vessel development	1.31E-37	5.68E-34	487
blood vessel morphogenesis	1.14E-34	2.04E-31	428
angiogenesis	1.42E-34	2.04E-31	352
extracellular structure organization	5.47E-34	4.92E-31	203
extracellular matrix organization	5.69E-34	4.92E-31	202
regulation of cellular component movement	3.01E-32	2.17E-29	457
regulation of cell motility	9.30E-29	5.52E-26	408
regulation of cell migration	1.02E-28	5.52E-26	385
regulation of locomotion	1.54E-28	7.38E-26	440
response to oxygen levels	5.92E-24	2.56E-21	239
inflammatory response	1.07E-23	4.19E-21	447
tissue morphogenesis	3.85E-23	1.39E-20	476
hemostasis	2.66E-22	8.86E-20	475
coagulation	4.31E-22	1.33E-19	474
blood coagulation	7.95E-22	2.20E-19	471
response to decreased oxygen levels	8.13E-22	2.20E-19	226
regulation of response to external stimulus	1.24E-21	3.15E-19	360
negative regulation of multicellular organismal process	1.42E-21	3.41E-19	340
response to hypoxia	1.66E-21	3.61E-19	224
immune effector process	1.67E-21	3.61E-19	418
response to cytokine stimulus	5.36E-21	1.10E-18	477
positive regulation of cell death	5.88E-21	1.16E-18	436
positive regulation of programmed cell death	3.58E-20	6.73E-18	418
muscle structure development	6.75E-20	1.22E-17	459
positive regulation of intracellular protein kinase cascade	1.03E-19	1.79E-17	483
cytokine production	1.69E-19	2.81E-17	398
positive regulation of apoptotic process	1.80E-19	2.88E-17	413
positive regulation of cellular component movement	1.89E-19	2.92E-17	230
positive regulation of cell motility	2.66E-19	3.96E-17	224
response to steroid hormone stimulus	6.03E-19	8.69E-17	251

WT 0hr vs. CLU 0hr – BP Downregulated

Pathway	p value	q value	Gene Count
RNA splicing	1.15E-24	4.96E-21	322
mRNA processing	1.55E-23	3.34E-20	397
chromatin modification	9.43E-19	1.36E-15	435
RNA splicing, via transesterification reactions	1.29E-18	1.40E-15	214
chromosome segregation	1.68E-18	1.46E-15	145
RNA splicing, via transesterification reactions with bulged adenosine as nucleophile	2.94E-18	1.82E-15	209
mRNA splicing, via spliceosome	2.94E-18	1.82E-15	209
microtubule-based process	1.05E-17	5.69E-15	428
nuclear division	1.95E-17	8.44E-15	361
mitosis	1.95E-17	8.44E-15	361
microtubule cytoskeleton organization	3.56E-17	1.37E-14	284
organelle fission	3.80E-17	1.37E-14	386
M phase of mitotic cell cycle	5.88E-17	1.96E-14	372
mitotic prometaphase	9.98E-15	3.08E-12	85
DNA conformation change	1.43E-14	4.12E-12	170
DNA repair	1.13E-13	3.05E-11	391
sister chromatid segregation	1.77E-13	4.49E-11	53
cell division	1.92E-13	4.62E-11	477
mitotic sister chromatid segregation	4.29E-12	9.76E-10	50
DNA packaging	4.80E-12	1.04E-09	134
chromatin remodeling	1.19E-11	2.45E-09	95
protein-DNA complex subunit organization	3.09E-11	6.07E-09	139
RNA localization	8.48E-11	1.59E-08	137
chromatin assembly or disassembly	2.94E-10	5.30E-08	123
nucleic acid transport	7.82E-10	1.25E-07	130
RNA transport	7.82E-10	1.25E-07	130
establishment of RNA localization	7.82E-10	1.25E-07	130
mRNA transport	8.16E-10	1.26E-07	112
nucleosome organization	1.39E-09	2.08E-07	110
protein-DNA complex assembly	2.21E-09	3.18E-07	120

CLU 0hr vs. CLU 48hr – MF Upregulated

Pathway	p value	q value	Gene Count
voltage-gated cation channel activity	3.70E-04	1.93E-01	128
helicase activity	4.40E-04	1.93E-01	145
DNA-dependent ATPase activity	9.82E-04	2.88E-01	69
motor activity	1.75E-03	3.16E-01	128
ATPase activity	2.55E-03	3.16E-01	351
gated channel activity	3.30E-03	3.16E-01	295
ion gated channel activity	3.30E-03	3.16E-01	295
metal ion transmembrane transporter activity	3.56E-03	3.16E-01	368
microtubule motor activity	3.56E-03	3.16E-01	73
taste receptor activity	3.60E-03	3.16E-01	15
voltage-gated potassium channel activity	6.12E-03	4.89E-01	77
substrate-specific channel activity	1.11E-02	6.38E-01	364
ATP-dependent helicase activity	1.13E-02	6.38E-01	107
purine NTP-dependent helicase activity	1.13E-02	6.38E-01	107
potassium channel activity	1.13E-02	6.38E-01	107
cation channel activity	1.22E-02	6.38E-01	263
ion channel activity	1.44E-02	6.38E-01	357
voltage-gated ion channel activity	1.51E-02	6.38E-01	174
voltage-gated channel activity	1.51E-02	6.38E-01	174
ATPase activity, coupled	1.62E-02	6.38E-01	277
neurexin family protein binding	1.75E-02	6.38E-01	13
small GTPase regulator activity	1.76E-02	6.38E-01	289
histone acetyl-lysine binding	1.87E-02	6.38E-01	15
ligand-gated ion channel activity	1.89E-02	6.38E-01	130
ligand-gated channel activity	1.89E-02	6.38E-01	130
nucleocytoplasmic transporter activity	1.97E-02	6.38E-01	13
mannosidase activity	2.02E-02	6.38E-01	13
glutamate receptor activity	2.03E-02	6.38E-01	26
histone binding	2.16E-02	6.45E-01	104
alpha-mannosidase activity	2.28E-02	6.45E-01	12

CLU 0hr vs. CLU 48hr – MF Downregulated

Pathway	p value	q value	Gene Count
structural constituent of ribosome	3.70E-29	3.25E-26	151
hydrogen ion transmembrane transporter activity	1.02E-06	4.48E-04	96
rRNA binding	1.46E-05	4.29E-03	31
GTP binding	2.93E-05	6.44E-03	352
GTPase activity	5.16E-05	9.07E-03	226
oxidoreductase activity, acting on a heme group of donors	7.72E-05	1.08E-02	27
oxidoreductase activity, acting on NAD(P)H	8.61E-05	1.08E-02	98
oxidoreductase activity, acting on the CH-OH group of donors, NAD or NADP as acceptor	9.87E-05	1.08E-02	111
enzyme inhibitor activity	1.22E-04	1.12E-02	290
guanyl nucleotide binding	1.68E-04	1.12E-02	366
guanyl ribonucleotide binding	1.68E-04	1.12E-02	366
cytochrome-c oxidase activity	1.79E-04	1.12E-02	26
heme-copper terminal oxidase activity	1.79E-04	1.12E-02	26
oxidoreductase activity, acting on a heme group of donors, oxygen as acceptor	1.79E-04	1.12E-02	26
carboxylic ester hydrolase activity	2.40E-04	1.41E-02	103
oxidoreductase activity, acting on CH-OH group of donors	3.43E-04	1.88E-02	123
NAD binding	3.65E-04	1.88E-02	44
carbohydrate binding	5.21E-04	2.54E-02	193
cytokine receptor binding	5.80E-04	2.68E-02	183
beta-tubulin binding	7.40E-04	3.25E-02	26
oxidoreductase activity, acting on NAD(P)H, quinone or similar compound as acceptor	9.05E-04	3.73E-02	58
G-protein coupled receptor binding	9.34E-04	3.73E-02	178
cofactor binding	1.14E-03	4.33E-02	252
NADH dehydrogenase activity	1.42E-03	4.79E-02	44
NADH dehydrogenase (ubiquinone) activity	1.42E-03	4.79E-02	44
NADH dehydrogenase (quinone) activity	1.42E-03	4.79E-02	44
coenzyme binding	1.76E-03	5.73E-02	178
monosaccharide binding	2.47E-03	7.76E-02	59
macromolecule transmembrane transporter activity	2.96E-03	8.87E-02	17
cytokine activity	3.06E-03	8.87E-02	172

CLU 0hr vs. CLU 48hr – KEGG Disease Upregulated

No pathways significantly upregulated

CLU 0hr vs. CLU 48hr – KEGG Disease Downregulated

Pathway	p value	q value	Gene Count
Parkinson's disease	5.85E-11	2.75E-09	129
Huntington's disease	1.10E-08	2.60E-07	181
Alzheimer's disease	5.84E-07	9.15E-06	163
Pathogenic Escherichia coli infection	5.26E-04	6.18E-03	53
Rheumatoid arthritis	2.48E-03	2.34E-02	81
Vibrio cholerae infection	3.40E-03	2.66E-02	53
Hepatitis C	4.09E-03	2.74E-02	125
Shigellosis	7.53E-03	4.42E-02	61
Bladder cancer	9.86E-03	4.98E-02	42
Systemic lupus erythematosus	1.06E-02	4.98E-02	115
Epithelial cell signaling in Helicobacter pylori infection	1.33E-02	5.34E-02	67
Toxoplasmosis	1.41E-02	5.34E-02	124
Malaria	1.62E-02	5.34E-02	49
Pathways in cancer	1.68E-02	5.34E-02	322
Bacterial invasion of epithelial cells	1.73E-02	5.34E-02	69
Primary immunodeficiency	1.82E-02	5.34E-02	30
Chagas disease (American trypanosomiasis)	2.19E-02	5.85E-02	96
Leishmaniasis	2.24E-02	5.85E-02	64
Autoimmune thyroid disease	2.37E-02	5.85E-02	38
Amoebiasis	2.84E-02	6.66E-02	100
Allograft rejection	3.54E-02	7.93E-02	30
Thyroid cancer	4.25E-02	9.07E-02	29
Acute myeloid leukemia	4.68E-02	9.56E-02	57

CLU 0hr vs. CLU 48hr – KEGG Upregulated

Pathway	p value	q value	Gene Count
Taste transduction	3.66E-02	1.00E+00	45

CLU 0hr vs. CLU 48hr – KEGG Downregulated

Pathway	p value	q value	Gene Count
Ribosome	1.19E-26	1.94E-24	88
Oxidative phosphorylation	1.24E-11	1.02E-09	131
Lysosome	2.16E-07	1.18E-05	120
Phagosome	6.55E-06	2.69E-04	139
Endocytosis	6.48E-05	2.13E-03	196
Glycolysis / Gluconeogenesis	8.51E-05	2.33E-03	59
Porphyrin and chlorophyll metabolism	1.73E-04	4.05E-03	32
Proteasome	2.13E-04	4.36E-03	44
Glutathione metabolism	2.59E-04	4.56E-03	46
Purine metabolism	2.78E-04	4.56E-03	160
Fructose and mannose metabolism	5.64E-04	8.42E-03	36
Antigen processing and presentation	6.98E-04	9.53E-03	62
Galactose metabolism	7.78E-04	9.82E-03	26
Arginine and proline metabolism	8.96E-04	1.05E-02	53
Cardiac muscle contraction	1.12E-03	1.23E-02	76
Pyrimidine metabolism	1.35E-03	1.30E-02	98
Pentose phosphate pathway	1.35E-03	1.30E-02	27
Citrate cycle (TCA cycle)	1.53E-03	1.39E-02	29
Protein processing in endoplasmic reticulum	2.55E-03	2.20E-02	163
Tight junction	2.88E-03	2.36E-02	130
Leukocyte transendothelial migration	3.17E-03	2.41E-02	113
Sulfur relay system	3.23E-03	2.41E-02	10
Aminoacyl-tRNA biosynthesis	6.57E-03	4.51E-02	41
Biosynthesis of unsaturated fatty acids	6.60E-03	4.51E-02	21
Neurotrophin signaling pathway	7.16E-03	4.69E-02	124
Collecting duct acid secretion	7.84E-03	4.95E-02	27
Amino sugar and nucleotide sugar metabolism	8.15E-03	4.95E-02	48
Fc gamma R-mediated phagocytosis	9.23E-03	5.33E-02	92
Tryptophan metabolism	9.42E-03	5.33E-02	42
Osteoclast differentiation	1.03E-02	5.49E-02	118

CLU 0hr vs. CLU 48hr - BP Upregulated

Pathway	p value	q value	Gene Count
cilium assembly	2.01E-06	8.67E-03	79
cilium morphogenesis	1.81E-05	3.92E-02	107
cellular component assembly involved in morphogenesis	1.06E-04	1.53E-01	145
regulation of centrosome duplication	2.73E-04	2.18E-01	15
centrosome cycle	2.94E-04	2.18E-01	42
regulation of RNA splicing	3.02E-04	2.18E-01	62
centrosome duplication	4.55E-04	2.81E-01	30
microtubule organizing center organization	6.18E-04	3.17E-01	67
establishment of protein localization to Golgi	6.70E-04	3.17E-01	14
mRNA processing	7.33E-04	3.17E-01	397
RNA splicing	1.00E-03	3.94E-01	322
protein targeting to Golgi	1.12E-03	4.05E-01	13
alternative mRNA splicing, via spliceosome	1.27E-03	4.24E-01	25
retrograde transport, vesicle recycling within Golgi	1.40E-03	4.31E-01	14
microtubule-based process	1.78E-03	4.99E-01	428
centrosome organization	1.85E-03	4.99E-01	63
microtubule cytoskeleton organization	2.07E-03	5.26E-01	284
regulation of mRNA splicing, via spliceosome	2.22E-03	5.34E-01	36
centriole replication	2.69E-03	5.90E-01	13
protein localization to Golgi apparatus	2.73E-03	5.90E-01	18
regulation of centrosome cycle	3.00E-03	6.19E-01	19
sister chromatid cohesion	3.59E-03	7.05E-01	34
regulation of mRNA processing	4.15E-03	7.53E-01	48
histone lysine methylation	4.18E-03	7.53E-01	46
regulation of alternative mRNA splicing, via spliceosome	4.92E-03	8.34E-01	19
homophilic cell adhesion	5.02E-03	8.34E-01	137
mRNA transport	9.01E-03	1.00E+00	112
centromere complex assembly	9.83E-03	1.00E+00	34
recombinational repair	1.13E-02	1.00E+00	57
double-strand break repair via homologous recombination	1.18E-02	1.00E+00	56

CLU 0hr vs. CLU 48hr – BP Downregulated

Pathway	p value	q value	Gene Count
translational termination	6.15E-26	2.66E-22	91
SRP-dependent cotranslational protein targeting to membrane	3.41E-25	7.37E-22	105
protein targeting to ER	1.29E-24	1.85E-21	107
translational elongation	2.96E-24	2.85E-21	106
cotranslational protein targeting to membrane	3.29E-24	2.85E-21	107
establishment of protein localization to endoplasmic reticulum	7.38E-24	5.32E-21	108
protein localization to endoplasmic reticulum	1.50E-22	9.29E-20	121
viral genome expression	4.81E-22	2.31E-19	152
viral transcription	4.81E-22	2.31E-19	152
cellular protein complex disassembly	6.45E-19	2.79E-16	155
viral infectious cycle	1.39E-18	5.46E-16	226
protein complex disassembly	4.62E-18	1.56E-15	160
nuclear-transcribed mRNA catabolic process, nonsense-mediated decay	4.68E-18	1.56E-15	118
protein targeting to membrane	7.43E-17	2.29E-14	154
macromolecular complex disassembly	9.19E-17	2.65E-14	180
translational initiation	1.12E-15	3.03E-13	153
translation	3.47E-15	8.82E-13	460
cellular component disassembly	6.04E-14	1.45E-11	287
establishment of protein localization to organelle	2.95E-13	6.72E-11	210
nuclear-transcribed mRNA catabolic process	1.99E-11	4.31E-09	171
mRNA catabolic process	2.22E-10	4.57E-08	183
RNA catabolic process	1.23E-09	2.35E-07	210
symbiosis, encompassing mutualism through parasitism	1.31E-09	2.35E-07	433
interspecies interaction between organisms	1.31E-09	2.35E-07	433
interaction with host	2.38E-09	4.05E-07	402
positive regulation of cell death	2.43E-09	4.05E-07	436
positive regulation of programmed cell death	6.29E-09	9.92E-07	418
generation of precursor metabolites and energy	6.42E-09	9.92E-07	444
protein targeting	6.89E-09	1.03E-06	474
response to oxygen levels	8.83E-09	1.27E-06	239

Appendix 3

Dendogram showing relationships between all gene expression. The greatest difference is between the WT line and the CLU knockout line. Differences between the three biological replicates are small in both lines. In the WT line the 48hr treated samples are closely grouped, with a large difference between the WT0_0 sample and other WT0 samples. In the CLU line the CLU0_1 and CLU48_0 lines differ from the rest of the samples. The other samples are grouped closely by treatment: CLU0_0 with CLU0_2, and CLU48_1 with CLU48_2.